PALAEOCEANOGRAPHY AT THE JUNCTURE BETWEEN THE INDIAN AND SOUTH ATLANTIC OCEANS DURING THE LATE QUATERNARY

RUTH ACHESON

Thesis submitted to the University of Edinburgh
in accordance with the requirements of the degree of
Doctor of Philosophy.

2001

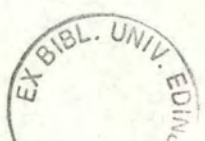

ABSTRACT

This study uses planktonic foraminifera assemblage and SST proxy (transfer function and alkenone) data from the Southern Benguela System, offshore the Cape of Good Hope to examine palaeoceanographic change at this important juncture of the thermohaline circulation. The records of watermass characteristics and variation thus derived are used to understand further climatic mechanisms and feedbacks within the southern hemisphere and globally.

Various modes of surface circulation are associated with particular climatic intervals through statistical and ecological analysis of faunal census data. Transitions and early interglacials are associated with watermasses including a significant Indian Ocean component. The main feature of glacials is an eutrophic ocean environment interval (OEI) linked to increased upwelling and filament projection into the Cape Basin. Cooler stadials of interglacials are marked by increased abundance of transitional and oligotrophic species associated with the South Atlantic gyre. These environments are seen in a characteristic order through a typical glacial–interglacial cycle as watermasses respond to insolation changes and thermohaline and atmospheric reorganisations. These are driven by northern hemisphere summer insolation cycles through trade wind strength, ITCZ position, and the position of the Agulhas Retroflection. The South Atlantic gyre signal is determined by austral summer insolation, however.

SST reconstructions provide a direct record of the changing temperature characteristic of regional watermasses and are thus a second constraint on the interpretations derived from planktonic foraminiferal assemblages. Two techniques are used in this study: faunal-based transfer functions; and alkenones ($U^{k'}_{37}$). Past interglacials were at least as warm as today

ACKNOWLEDGEMENTS

Great thanks are due to Prof. Dick Kroon for, above all his exuberant and wholehearted enthusiasm, supervision and support! To Kate Darling for many stimulating discussions, and Ralph Schneider for his insight, access to data, and welcoming me during my stay in Bremen.

This work was completed during a NERC scholarship at the Geology and Geophysics Department in Edinburgh University. This research results from a collaboration with the Geosciences Department in the University of Bremen, Germany. I thank Prof. Gerold Wefer for inviting me to spend three months in 1998 experiencing palaeoceanography Bremen-style! Special thanks are due to Elena Perez (Scripps), Laurence Vidal, Elenora Uliana, Lydie Dupont, Torsten Bickert, Barbara Donner, Peter Müller, and last but by no means least, Stefan Niebler.

Jacques Giraudeau (Bordeaux), Laurence Vidal (Bremen), Richard Washington (Oxford), Mark Chapman (UEA), Min-te Chen (Taiwan), Emma Durham (UCL), Lydie Dupont (Bremen), Amanda Rau and John Rogers (UCT) for discussions, opinions, and perspectives on fauna, flora, oceans, and climates of the southern African region.

Many thanks to friends and colleagues in Edinburgh in particular, Conor Snowden, Bridget Wade, Iain Stewart, Rachel Oxburgh, Bryne Ngwenya, Sandy Tudhope, and Raja Ganeshram.

Thanks to Dave Anderson and Steve Stokes for sparking my interest in Quaternary palaeo-environments.

I also thank Gillian Hamilton for being a fantastic friend and story teller. The only linguist I know who can be so easily persuaded into attending a palaeoceanography conference!

Very special thanks to my original Quaternary buddies Justin Taylor (now husband!) and Matt Higginson (Best Man!). You are both heroes to me. It has been quite a journey from the Mansfield Road and we seem to have drunk rather a lot of gin along the way! I look forward to many, many more challenges, adventures, debates, and laughter!

Immense thanks and gratitude are reserved for my family. Mum, Dean, and Robert, thank you all for the happy times, allowing me to be myself, and showing me what's important in life. Justin, thank you again for being wonderful and generous in every way. This thesis would not have been completed with out your support, encouragement, advice, and great sense of humour!

Finally, I dedicate this thesis in fondest memory of my inspirational and brilliant Dad, William.

TABLE OF CONTENTS

LIST OF FIGURES

CHAPTER 1: INTRODUCTION

CHAPTER 2: METHODS

CHAPTER 3: CHRONOSTRATIGRAPHY

CHAPTER 4: OCEANOGRAPHY

CHAPTER 5: PLANKTONIC FORAMINIFERAL ASSEMBLAGES

CHAPTER 6: SEA SURFACE TEMPERATURES

CHAPTER 7: CLIMATE CONNECTIONS

List of Tables

Chapter 2: Methods

Chapter 3: Chronostratigraphy

Chapter 5: Planktonic Foraminiferal Assemblages

Chapter 7: Climate Connections

LIST OF PLATES

LIST OF ABBREVIATIONS

A1/2/3	Arid period 1/2/3
ACC	Antarctic Circumpolar Current
AABW	Antarctic Bottom Water
AAIW	Antarctic Intermediate Water
AE	Agulhas Eddy
APF	Antarctic Polar Front
AR	Agulhas Retroflection
BC	Benguela Current
BOC	Benguela Oceanic Current
B.P.	Before Present
CLIMAP	Climate: Long Range Investigations, Mapping, and Prediction.
cmbsf	Centimetres below sea-floor
CPDW	Circumpolar Deep Water
CWR	Cold Water Route
DB1/2/3/4	Dune Building phase 1/2/3/4
DSDP	Deep Sea Drilling Project
E	Equitability (diversity)
Ga.	*Globigerinita*
Ge.	*Globigerinella*
GeoB	Geowissenschaften Bremen
Gr.	*Globorotalia*
Gs.	*Globigerinoides*
G-ST	Sediment trap (Giraudeau *et al.*, 2000)
H	Shannon-Weaver (diversity)
IMAGES	International Marine Global Change Study
ITCZ	Inter-Tropical Convergence Zone
ka	Thousand years (date)
k.y.	Kiloyear (interval)
LDeo	Lamont Doherty
LGM	Last Glacial Maximum
MAT	Modern Analog Aechnique (method of palaeo-SST reconstruction)
mbsl	Metres below sea-level
MD	RV Marion-Dufresne
MIS	Marine Isotope Stage
MST	Mixed Subtropical – Tropical assemblage (an OEI)
Ma	Million years (date)
N.	*Neogloboquadrina*
NADW	North Atlantic Deep Water
NAUSICAA	Namibia Angola Upwelling System and Indian Connection to the Austral Atlantic (= IMAGES II)
NBS	Northern Benguela upwelling System
O.	*Orbulina*
ODP	Ocean Drilling Project
OEI	Ocean Environment Interval

P.	*Pulleniatina*
PDI	*N. pachyderma* Intergrades (Kipp, 1976)
P-moll	Middle Shelf Molluscs (Pether, 1994)
PS	RV Polarstern
PSP	Pretoria Salt Pan
S	Simple (diversity)
S.	*Sphaeroidinella*
SAAC	South Atlantic Anticyclone
SAC	South Atlantic Current
SAF	Subantarctic Front
SBS	Southern Benguela upwelling System
SC	Spliced Cape Basin Core
SST (s)	Sea Surface Temperature (s)
SSST	Summer Sea Surface Temperature
STC	Subtropical Convergence Zone
STF	Subtropical Front
T.	*Turborotalita*
TFT	Transfer Function Technique (method of palaeo-SST reconstruction)
UCT	University of Cape Town
$U^{k'}_{37}$	Alkenone unsaturation Ratio
WSST	Winter Sea Surface Temperature
WWR	Warm Water Route

Chapter 1: Introduction

CHAPTER 1: INTRODUCTION

1.1 INTRODUCTION

The earth's climate has, for at least the past two million years, been characterised by cyclical glaciations and retreats (interglacials). This period of geological history, which extends to the present day, is known as the Quaternary. The frequency and intensity of Quaternary climatic oscillations, leading to at least fifty glacial-interglacial cycles (Ruddiman *et al.*, 1989; Shackleton *et al.*, 1990), distinguishes it from earlier periods in geological time. These climatic fluctuations are related to changes occurring in the earth's orbital parameters, whereby the shape of the earth's orbit around the sun varies slightly due to gravitational and planetary effects (Milankovitch, 1930; Hays *et al.*, 1976; Imbrie *et al.*, 1992; 1993). The periodicity of orbital eccentricity is ~100 k.y. The tilt of the earth's axis varies over a period of ~41 k.y., whilst the equinox, the time when the earth is nearest the sun (perihelion), progresses once around the sun every ~21 to 23 k.y. The reason these variables affect the earth's climate system lies in their regulation of the varying amount of solar radiation that the earth receives through time. The total amount of insolation received is determined by eccentricity, whilst the distribution of this energy and seasonal contrast is determined by obliquity and precession. Obliquity effects are greatest at higher latitudes and are the same for the northern and southern hemispheres. In contrast, precession effects are seen in opposing hemispheres, i.e. when the contrast is greatest in the northern hemisphere, it will be least in the southern hemisphere. However, the climate cycles of the Quaternary have not been constant and are superimposed on a long-term global cooling trend. Prior to ~800 ka B. P. the 41 k.y. cycle predominated, after which the 100 k.y. cycle became the prevalent periodicity. This change in rhythm was accompanied by the intensification of global glaciations and rapid large-scale growth and decay of northern hemisphere ices masses (Ruddiman *et al.*, 1989).

1.2 Oceanic Context

1.2.1 Evolution of ocean circulation

Although insolation cycles are thought to explain the overall pattern of Quaternary climate change (Imbrie *et al.*, 1984), it is clear that other factors act to modulate and/or amplify global climatic change. The most important additional forcing mechanisms are ocean circulation and global ice volume (Broecker and Denton, 1989), as well as carbon dioxide concentration (Shackleton, 2000). Distribution of energy throughout the ocean is controlled by variations in salinity and heat, the so-called 'thermohaline circulation'. Deep-sea sediments form particularly important reservoirs of information about these modulators of past climatic change. Glacial and interglacial cycles are defined stratigraphically by the marine isotopic record preserved in the shells of calcareous marine plankton that compose a relatively undisturbed sequence of sediments in the deep ocean. Furthermore, the identifiable species that make up these oozes can themselves provide a record of past ocean circulation, sea surface temperatures and, by implication, atmospheric changes throughout the Quaternary.

The evolution of present climate and oceanography commenced during the Jurassic, with the break-up of Pangea and the Tethys Ocean. Early rifting lead to the formation of the proto-Atlantic. Most other oceans developed during the Mesozoic and the Southern Ocean was formed around 50 Ma B.P. The redistribution of land mass was associated with alteration of ocean circulation, from a globally coherent pattern to smaller, constrained gyres, contained within relatively isolated basins (Williams *et al.*, 1993). One of the most important events in this evolution was the thermal isolation of Antarctica by the Antarctic Circumpolar Current (ACC). This was the result of a northern movement of Australia away from Antarctica and the formation of Southern Ocean Passages (Shackleton and Kennett, 1975). The ACC was enhanced by the opening of the Drake Passage ~30 Ma B.P. and by the early Oligocene India was approaching the Eurasian landmass, effectively sealing off the remaining equatorial currents (Williams *et al.*, 1993). The closure of the Paratethys and formation of the

Himalayas lead to the enhancement of the Asian Monsoon (Ramstein *et al.*, 1997), a further key feature of the present day global climate.

A final stage in the development of the modern thermohaline circulation was the closure of the Isthmus of Panama in the Pliocene, ~3.0 to 3.5 Ma B.P., (Keigwin, 1978; Burton *et al.*, 1997). The onset of northern hemisphere glaciation was partly as a result of the subsequent establishment of the Gulf Stream and the advection of warm, watermasses to high northern latitudes. With this closure, the modern thermohaline system was established and is critical in understanding weather and climate today.

1.2.2 The Benguela System

The Benguela region, on the continental shelf and slope offshore southern Africa (Figure 1.1), is one of the four major coastal upwelling regions now established in the world ocean. These areas are associated with greatly enhanced productivity and therefore, play a crucial role in controlling the oceanic carbon budget and atmospheric CO_2 levels (Sarnthein *et al.*, 1988). The Benguela System also forms the eastern branch of the South Atlantic subtropical gyre and is strongly involved in the mechanisms of heat and salt exchange between the Indian and Atlantic Oceans (Gordon, 1986). It has therefore been the focus of a number of hydrological and palaeoceanographic investigations aiming at understanding its complex present and past dynamics (Wefer and Fisher, 1993; Garzoli and Gordon, 1996; Wefer and Berger, 1996; Bertrand *et al.*, 1997; Boebel *et al.*, 1998; Wefer *et al.*, 1999).

The evolution of the Benguela upwelling systems started in the Mid-Miocene (~15 My B.P.) and is associated with the establishment of ice-sheets on Antarctica, following its isolation by the ACC. Upwelling was enhanced in the Pliocene when deep water formation in the North Atlantic commenced (Diester-Haas *et al.*, 1992). The Quaternary record of the Benguela and other upwelling systems is marked by cycles of upwelling. Upwelling is intense during cold periods and less intense in warm periods. Oscillations in upwelling have been observed on both glacial – interglacial scales (Diester-Haas *et al.*, 1988a; 1988b; McIntyre *et al.*, 1989; Oberhansli, 1991; Imbrie *et al.*, 1992; Schneider *et al.*, 1994; Giraudeau *et al.*, 2001) and shorter interval (sub-

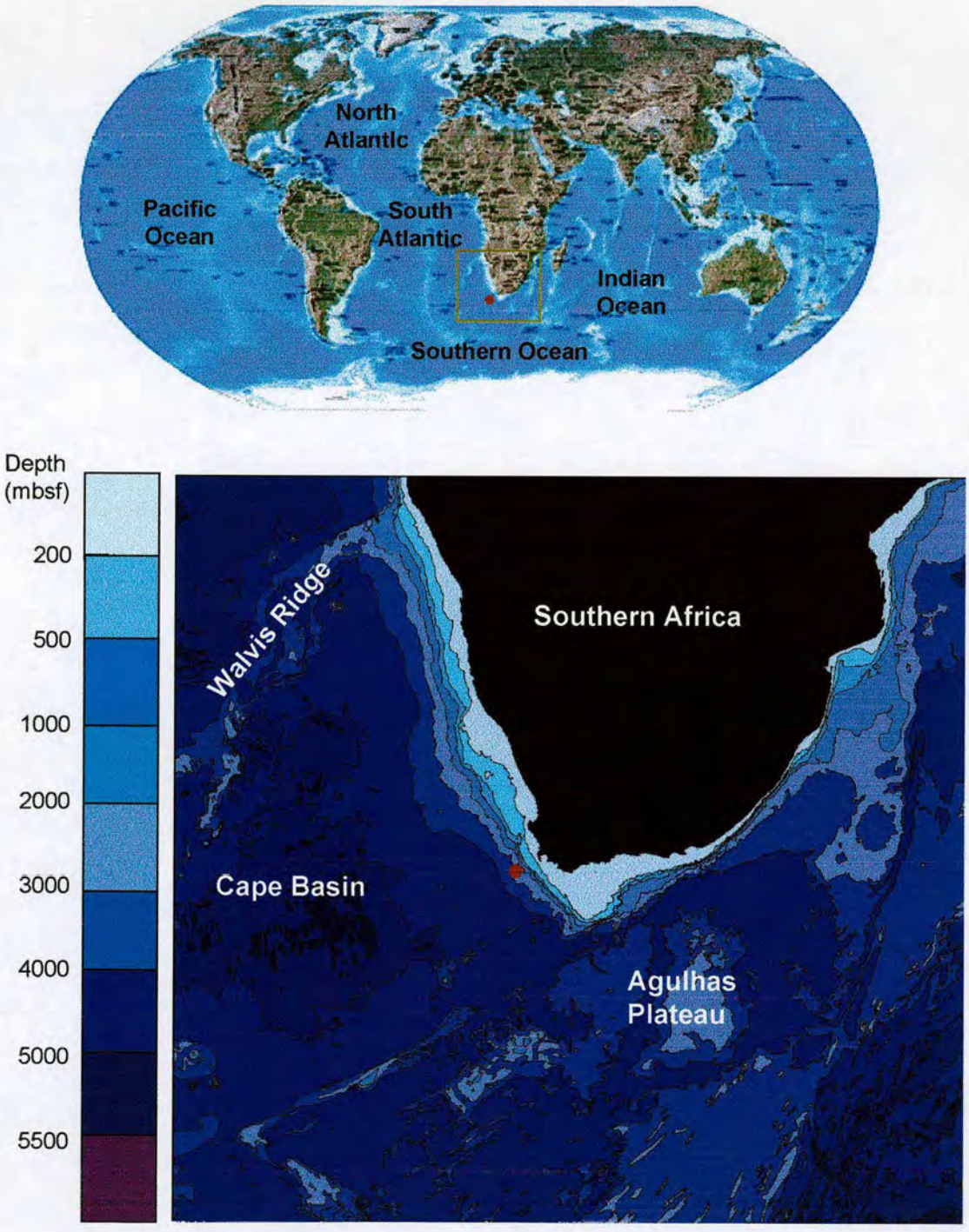

Figure 1.1 Bathymetry of the juncture between the Indian and Atlantic Oceans. Red dot signifies location of marine sediment cores used in this study.

Milankovitch) time-scales (Kennett and Venz, 1995; Mix and Morey, 1996; Little *et al.*, 1997a; 1997b).

1.2.3 Significance of the Cape Basin

In order to unravel climates of the past, so that they may enlighten us as to the possible course of future climate change, we must understand interactions within the ocean as well as the influence they have on the climate. The Cape Basin, located near the tip of southern Africa, is a key location during the Quaternary in terms of understanding variations in oceanic heat flux and thermohaline circulation. The southern hemisphere is maritime compared to the northern hemisphere, with over 80% of the austral hemisphere being ocean. To the south of Africa the ocean is characterised by a high degree of variability due to the mesoscale variations in the input of Indian Ocean water through the retroflection of the Agulhas Current and the generation of eddies. The position of the retroflection displays a high degree of variability and a substantial component of Agulhas waters may enter the Benguela region (Shannon *et al.*, 1990a, Lutjeharms, 1996). Situated at this 'hotspot' in the ocean's climate conveyor belt (Broecker *et al.*, 1985; Gordon, 1986; Gordon, 1996a; 1996b), the region's oceanography is important. In addition, the productivity of the Benguela upwelling system and the Southern Ocean frontal zones are potentially important carbon dioxide sinks. Changes in primary production and circulation south of Africa will therefore not just have regional consequences but implications for global climate change as well. Records of sea surface temperature are particularly important to studies of global climate change because much of the residual heat which drives atmospheric anomalies is stored in the upper ocean. At the same time, it is also an indicator of the dynamic processes occurring in the ocean. Therefore, the Cape Basin record is particularly sensitive to changes in regional and global climate because of its location at the margin of several oceanic and associated climatic systems.

1.3 SCIENTIFIC APPROACH

Several stages must be observed in addressing questions of climatic change in a marine setting Firstly, proxy records relating to water-mass evolution must be retrieved. Secondly, these must be analysed in relation to energy (heat) parameters of the system. Finally, the water mass dynamics and sea surface temperature characteristics should be interpreted at a variety of scales to understand both the mechanisms and processes of palaeoceanographic and climatic variability.

Reconstructing the linkages and heat transport of the surface return flow of the thermohaline circulation at the juncture between the Indian and Atlantic Oceans will focus on utilizing the information held in planktonic foraminifera assemblages. Two sediment cores, spanning the past 700 k.y. B.P., will create a long-term, high-resolution, multi-proxy, palaeoceanographic record of water mass, productivity, and sea surface temperature variability.

1.4 SCOPE OF THE RESEARCH

This research aims to address several issues on several scales.

GLOBAL-SCALE:

- ► Will it be possible to unravel the planktonic foraminiferal assemblages to identify and distinguish a signal of the advection of Indian Ocean water into the South Atlantic Ocean?

IF SO:

- ► What is the record of advection, i.e. surface return flow of the thermohaline circulation? Is it a continuous or variable feature? Or does it cease during glacials?
- ► What is the influence of this warm water advection on the Southern Benguela System?

- Is early warming at glacial terminations observed in the Cape Basin? What mechanisms appear to control deglacial patterns of climate change?
- How do the Quaternary dynamics of the Benguela region fit with other palaeoclimatic records from the southern hemisphere, and how are the mechanisms of these changes related?
- Are the interglacials of the late Quaternary distinct in character? Did advection occur at the same rate and intensity? Which interglacial is the best analogue for scenarios of future climate change?

REGIONAL SCALE:

- Aim to construct the first faunal-based sea surface temperature record from the Benguela System.
- Upwelling in the Southern Benguela System is currently seasonal. Is this intensified during glacials, similar to the Northern Benguela System, does it become perennial?
- Examination of southern African climate modes and their distribution in time throughout the late Quaternary. Is it possible to understand continental records of aridity in relation to regional records of sea surface temperature?

1.5 THESIS STRUCTURE

The thesis is divided into four sections:

1) BACKGROUND AND CONTEXT

The theoretical and practical background to the techniques used in this research are described in **Chapter 2**. The oxygen and carbon isotopic results for the sediment cores are described in **Chapter 3** and are used to form the chronostratigraphy. **Chapter 4** outlines the oceanographic context of the research, in terms of global circulation,

regional South Atlantic oceanography, the Benguela upwelling system and the Agulhas Current and Retroflection.

2) RESULTS AND INTERPRETATION

Planktonic foraminiferal assemblage results and watermass interpretations are described in **Chapter 5**. These lead to long-term records of upwelling and Indian Ocean advection. Records of sea surface temperature change offshore south west Africa, generated from planktonic foraminiferal transfer functions and the alkenone technique, are then presented and analysed in **Chapter 6**. Together these results and interpretations constrain more fully the interactions of the different oceanographic systems present in the Benguela region.

3) DISCUSSION

Chapter 7 analyses further these changes in a global context throughout the late Quaternary. In particular, issues relating to the conditions and instability within interglacials especially MIS 11, southern hemisphere connections, and ocean-terrestrial linkages are addressed.

4) SUMMARY AND CONCLUSIONS

The findings of the thesis and major results are outlined in **Chapter 8**, together with a summary of suggested further work.

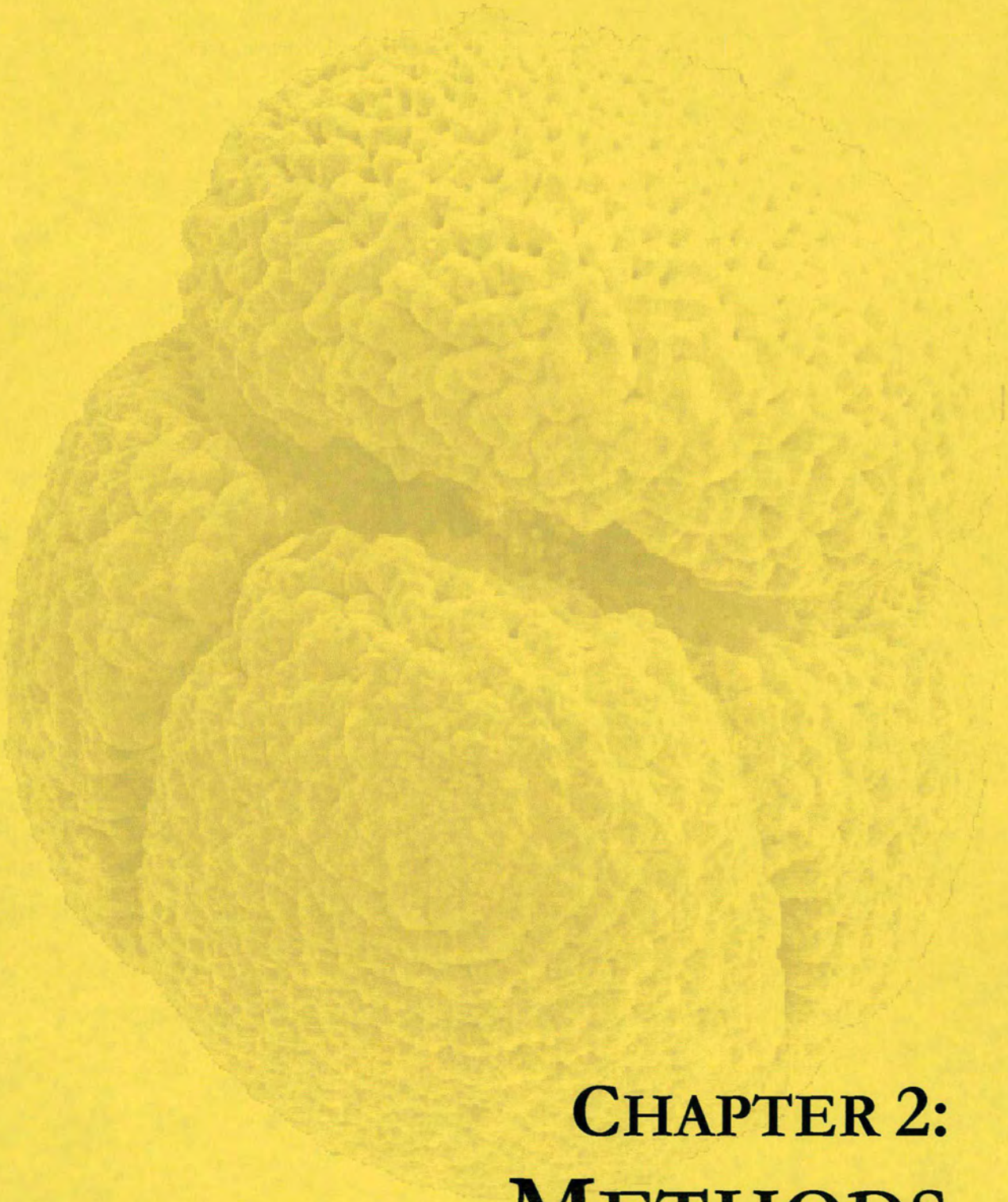

Chapter 2: Methods

CHAPTER 2: METHODS

2.1 PLANKTONIC FORAMINIFERA

2.1.1 Climate change proxies from assemblage data

Planktonic foraminifera are carbonate shelled protists that float in the surface waters of the oceans. Although they generally constitute a minor proportion of the total living zooplankton, they form the bulk of the sediment of the ocean floor, as most zooplankton are not composed of fossilisable minerals. The first significant descriptions of foraminifera were published by d'Orbigny (1826; 1839) and, together with other early workers (Ehrenberg, 1861; Parker and Jones, 1865), assumed that all foraminiferal species were benthic. It was not until the 1872-1875 Challenger expedition (Brady, 1884) that it became accepted that some foraminifera had a pelagic lifestyle, being readily gathered from the surface waters. This expedition was the first of its kind, and has come to be regarded as the birth of oceanography. Never before had an expedition been organised with the express purpose of making observations of the physics, chemistry, geology, and particularly the biology of the deep ocean. At each of the 362 official stations, water depth was measured and a small sample of the bottom sediment collected. Murray (1897) noted that 'Globigerina ooze' formed the bulk of sediment material and that differences in species composition contain clues to the temperature of the water masses in which they lived. He noted that they appeared to be distributed in global belts and grouped the foraminifera into faunal assemblages, which acknowledged the influence of temperature and climate on their distributions. However, Schott (1935) was the first to apply quantitative methods to the study of planktonic foraminifera. He counted species in the fossil assemblages gathered during the Meteor Expedition (1925-1927). He realised that as global climate changed from glacial to interglacial, so too did the temperatures of the surface ocean, and this was reflected in the foraminiferal assemblages he recorded.

2.1.2 Past climate reconstruction from present day distribution patterns

From the earliest investigations, planktonic foraminifera have been used to reconstruct climates of the past (Schott, 1935; Emiliani, 1954; Imbrie and Kipp, 1971; Shackleton and Opdyke, 1973; Imbrie *et al.,* 1973; Ruddiman and McIntyre, 1976; Bé, 1977; Brummer, 1988; Ravelo *et al.,* 1990; Oberhänsli, 1991; Kroon *et al.,* 1993; Murray, 1995; Little *et al.,* 1997a, b). The general geographical and geological distribution patterns of planktonic foraminifera are governed by the environmental interactions between temperature, salinity, ocean currents, seasonality, and nutrient distributions, which together form ecosystems to which specific planktonic foraminiferal species are associated.

Bé and Tolderlund (1971) grouped planktonic foraminifera into five faunal provinces: 'polar', 'subpolar', 'transitional', 'subtropical', and 'tropical'. These divisions reflected the nature of habitat niches, and distinct faunas were described as living in particular latitudinal zones. Initially it was suggested that their distribution was determined by the temperature regime, but later studies questioned this assumption. For instance, *Globigerina bulloides* (d'Orbigny, 1826), a cool-water species (Bé and Tolderlund, 1971), is also found in tropical upwelling areas (Thiede, 1975; Prell and Curry, 1981; Kroon, 1991) and in nutrient rich surface waters (Kemle-von Mücke and Oberhänsli, 1999; Ufkes *et al.,* 1998). Further work has emphasised the importance of nutrient levels and productivity on distribution in addition to temperature (Reynolds and Thunnel, 1985; Kroon and Ganssen, 1989). The relative combination of over thirty species in most sediment samples, from the transitional and subtropical/tropical regions, can potentially provide a huge amount of environmental information (Hale and Pflaumann, 1999).

Studies of living planktonic foraminifera have shown that their distributions reliably trace environmental conditions in the surface water masses (Bé and Tolderlund, 1971; Bé, 1977), currents and frontal systems (Ottens, 1991; Ottens and Nederbragt, 1992; Ufkes *et al.,* 1998), and upwelling zones (Auras-Schudnagies *et al.,* 1989; Kroon, 1991; Oberhänsli *et al.,* 1992). These studies also tell us much about the ecology of the foraminifera, such as life cycle dynamics, thermocline, and habitat preferences.

However, plankton tow and net data only sample the planktonic foraminifera status at a moment in time and, therefore, cannot reflect the temporal effects of seasonality or reproductive cyclicity (Reynolds and Thunnell, 1985; Bijma *et al.*, 1990). However, data on the seasonal variations in assemblages can now be gathered in sediment traps, allowing the investigation of temporal influences on fossil assemblages. (Berger and Wefer, 1990; Fischer and Wefer, 1996; Marchant *et al.*, 1998).

Planktonic foraminifera can be divided into two morphological groups based on wall structure: spinose and non-spinose. Spinose species, first observed by Murray (1897), are associated with algal symbionts (predominantly dinoflagellates), which are held within the rhizopodial system and sequestered in the cytoplasm. Environmental factors influence the relative distributions of these groups (Ortiz *et al.*, 1995). Spinose species with a relatively high zooplankton diet are more abundant in the oligotrophic central water masses where copepods predominate (Hemleben *et al.*, 1989). However, omnivorous spinose species may be found together with the omnivorous and herbivorous non-spinose species in abundance in eutrophic waters with high phytoplankton productivity, e.g. upwelling areas, or the nutrient and diatom rich sub-Antarctic waters of the Southern Ocean. Plankton tow data from the southeastern Atlantic showed that in order to fully understand the relationship between species distribution and habitat, a knowledge of the food web is required (Kemle-von Mücke and Oberhänsli, 1999). Food availability controls the blooming of species of foraminifera in addition to the hydrological and biological factors previously discussed. Prey preferences also have a seasonal effect on the assemblage. In the Sargasso Sea, where phytoplankton blooms occur in the winter, the non-spinose species *Globorotalia inflata* (d'Orbigny, 1839) and *Globorotalia truncatulinoides* (d'Orbigny, 1839) occur in abundance during these months. During other times of the year, the spinose species *Globigerinoides sacculifer* (Brady, 1877), *Orbulina universa* (d'Orbigny, 1839), and *Globigerinella siphonifera* (d'Orbigny, 1839) predominate (Bé and Tolderlund, 1971; Tolderlund and Bé, 1971). All planktonic foraminifera spend at least part of their life cycle in the photic zone (Bé, 1967; Bé and Tolderlund, 1971; Fairbanks *et al.*, 1982; Oberhänsli *et al.*, 1992; Kemle-von Mücke and Oberhänsli, 1999) and, therefore, accurate counts of relative abundance in an assemblage allow us to investigate past conditions of the surface waters

of the ocean. Figure 2.1 demonstrates the potential consequences of this by showing the differences between living and fossil assemblages in the Indian Ocean. It is evident that there are latitudinal trends in the distribution of planktonic foraminifera in the living and fossil assemblages. The factors governing these large-scale differences in distribution patterns between living and fossil assemblages are complex. The distribution of the living plankton is only a snapshot of the annual production and sediment trap data show seasonal production patterns and intermittent production (Berger and Wefer, 1990). Surface and core sediments represent a long-term average of production in the surface waters. How well these values correspond to actual production depends on other factors e.g. dissolution in the water column and on the sea floor. Variations in dissolution occur with depth, water temperature and climate changes that may, for example, raise or lower the calcium carbonate compensation depth at any particular site. However, there are ways to examine the possible influence of dissolution of sediments in samples (Le and Shackleton, 1994). A dissolution index was calculated for the sediments of this study and is examined in Chapter Five. Planktonic foraminiferal assemblages and their respective watermasses in the southern Atlantic and south western Indian Oceans will be introduced in Chapter Five.

2.1.3 Sediment Core Material

This study is based in the southern Cape Basin to investigate the late Quaternary history of the Benguela Current and to detect possible influences of the Agulhas Current, from the Indian Ocean. The sediment cores we selected are located at the juncture between the Indian and Atlantic Oceans (Figure 2.2), and have a time-resolution which enables reconstruction of significant changes in ocean circulation and Indian Ocean input and productivity fluctuation during the time frame stated. This is the first study using multiple sediment cores recovered from the area offshore the Cape of Good Hope, focusing on late Quaternary inter-ocean communication in addition to examining the upwelling history of the area.

In 1975 the Deep Sea Drilling Project (DSDP) drilled this margin to investigate the upwelling history of the region (Bolli *et al.,* 1978). However, the Cape Basin Sites, 360 and 361, did not contain sediments of late Quaternary age. The youngest material

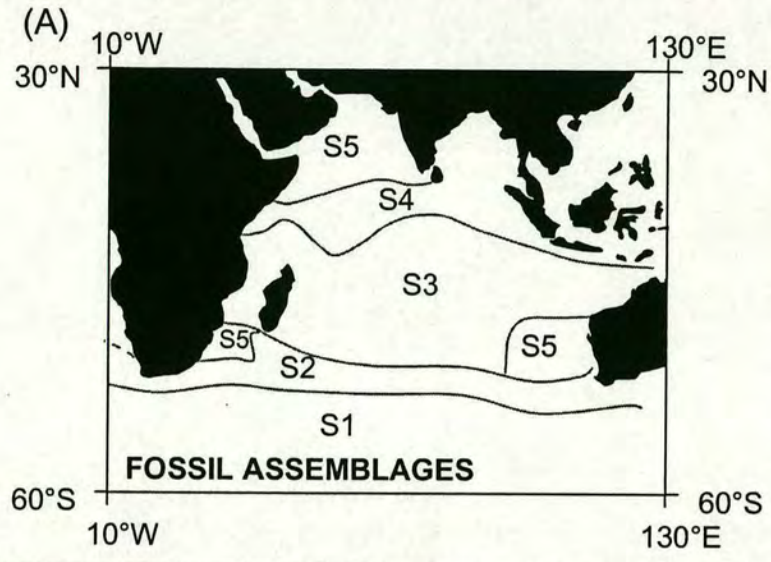

Key:
S1 -Polar- Subpolar, **S2** - Transitional, **S3** - Tropical-subtropical, **S4** - Tropical, **S5** - Tropical-subtropical boundary current.

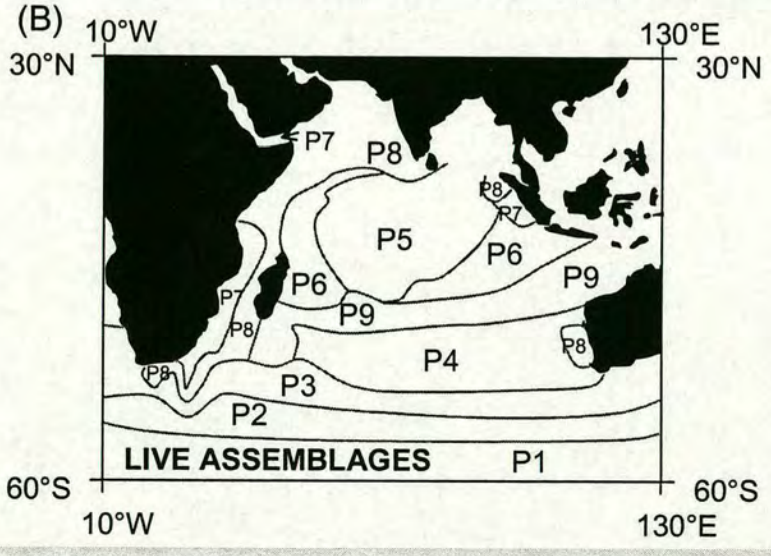

Key: **P1** -Polar, **P2** -Subpolar, **P3** -Transitional, **P4** -Southern subtropical, **P5** -Tropical, **P6** -Tropical-subtropical "a", **P7** -Tropical-subtropical "b", **P8** -Tropical-subtropical boundary current, **P9** -Northern subtropical.

Figure 2.1 Composite maps of regional dominance of foraminifera in the Indian Ocean, **(A)** fossil assemblages (190 samples); **(B)** live assemblages (154 plankton tows). After Bé and Hutson (1977).

available from Site 360 was from the lower Pliocene, whilst upper Eocene and upper Palaeocene sediments were identified in Site 361 (Bolli *et al.,* 1978).

Two sediment cores have been sampled and examined in this study and these are shown in Figure 2.2. The first, gravity core GeoB 3603-2, was collected in January 1996 on Meteor cruise 34/1 (Bleil *et al.,* 1996). One of the purposes of this cruise was to carry out an ODP pre-site survey of the southwest African continent, in preparation for the ODP Leg 175. Core GeoB 3603-2 (35°S 07.5′ - 17°E 32.6′), located in the Southern Cape Basin, was the southernmost core retrieved on the cruise. Four cores were recovered from the upper slope of the southern Cape Basin (31 to 35°S) during the cruise and the sediment characteristics for each were similar. The sediment cores consisted mainly of nannofossil ooze (>60% from smear slide analysis) with varying amounts of foraminifera (Bleil *et al.,* 1996). The core was taken at 2840m water depth and the core length was 1133 cm. The core was sampled every 5cm which produces an average temporal interval of 1600 years per sample.

The International Marine Global Change Study (IMAGES) was designed to examine, firstly, the history of surface and deep ocean circulation, secondly, the record of ocean productivity and carbon exchange between the ocean and the atmosphere, and, finally, how these are related to global climates over the past 300,000 years. A project of IMAGES, the Namibia Angola Upwelling System and Indian Connection to Austral Atlantic (NAUSICAA- IMAGES II), focused on these aims within the geographical context of the South Atlantic, namely, links with the Indian Ocean and coastal upwelling. The second sediment core used in this study, MD96 2081, was collected during the NAUSICAA IMAGES II (cruise105) onboard the RV Marion-Dufresne (Bertrand *et al.,* 1996). Twenty three cores were collected during the cruise on a transect from Madagascar round the horn of Africa to the Angola Basin. Prior to this cruise no piston cores had been recovered in the South Atlantic longer than twenty metres. Piston core MD 96-2081 is located in the southern Cape Basin at 35°S 20.7′ - 17°E 24.7′, parallel to but south of Cape Canyon. It is in close proximity to core GeoB 3603-2. Core MD96 2081 was recovered from 3164m water depth and its total length was 3032cm. The lithology of the core is dominantly nannofossil ooze with variable

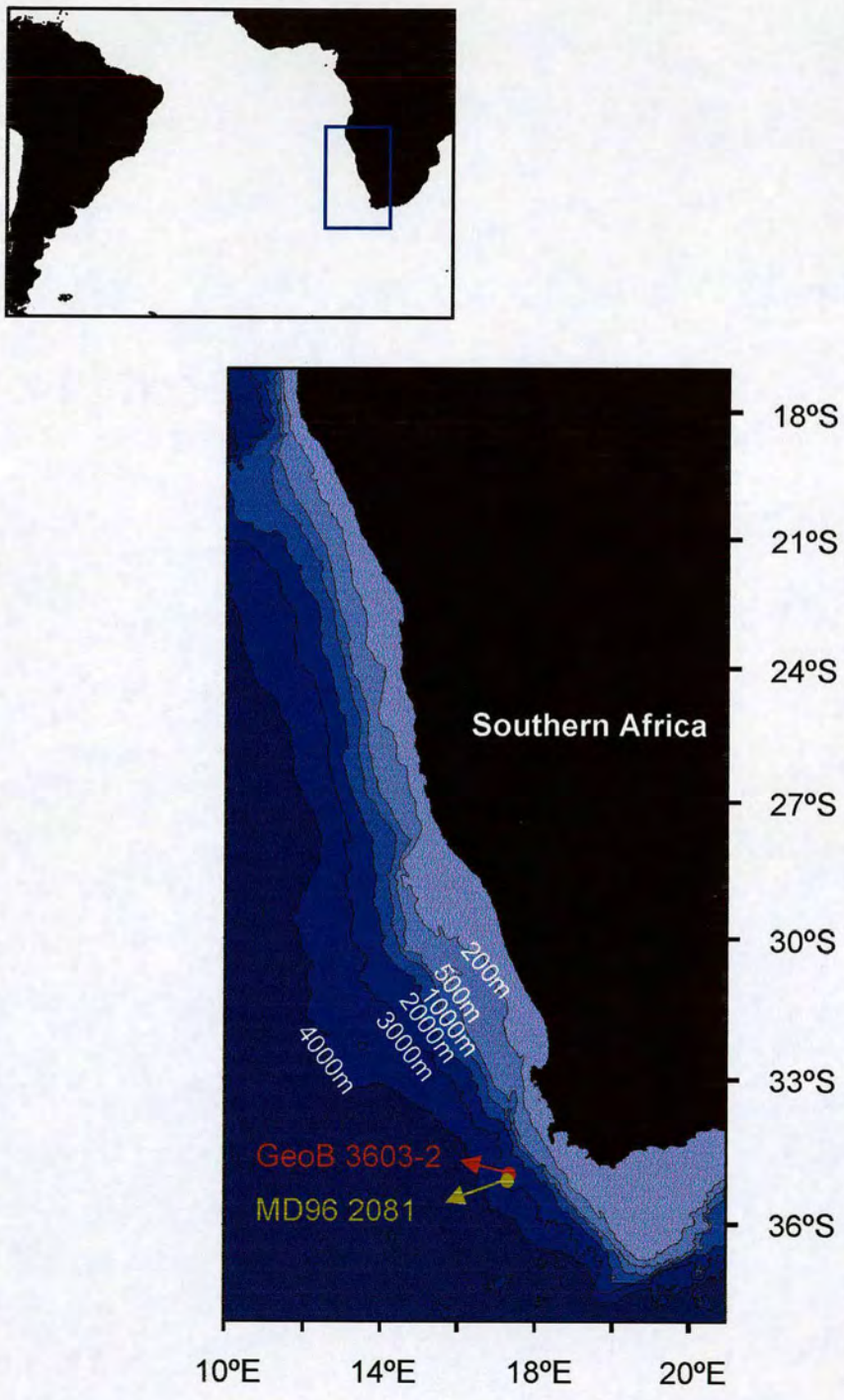

Figure 2.2 Locations of sediment cores sampled from the continental slope of the southern Cape Basin offshore the Cape of Good Hope. Inset shows the position of the Benguela region in relation to the South Atlantic. Bathymetry depth contours are indicated.

amounts of foraminifera (Bertrand *et al.*, 1996). The core was sampled at intervals every five cm in the middle section of the core, from 963 to 2113 cmbsf, giving an average temporal interval of 1600 years per sample.

2.1.4 Sample preparation for planktonic foraminiferal analysis

The same procedure was used on both sediment cores. Core samples ($10cm^3$) were washed, and sieved through a >63 µm screen. Planktonic foraminiferal counts were carried out on the >150µm size fraction. As one of the purposes of this study is to calculate past sea surface temperatures, the >150µm size fraction was chosen to be consistent with the core top reference datasets that are being used in transfer functions. Furthermore, the relative proportion of species in the South Atlantic water assemblages throughout this region (north of 40°S) does not change significantly when using a smaller >125µm mesh (Niebler, 1995). To facilitate examination and counting, the fraction was divided using a microsplitter until approximately 400 specimens remained for counting. All faunal counts were based on at least 300 tests per sample. The resulting species percentages were used for sea surface temperature (SST) reconstruction in addition to planktonic foraminifera assemblage analysis. Core materials for the GeoB cores and core MD96 2081 are archived in Fachbereich Geowissenschaften, University of Bremen, Germany. Micropalaeontological samples are archived in the Faculty of Earth Sciences, Vrige Universiteit, Amsterdam, The Netherlands, and the University of Bremen.

2.1.5 Taxonomy

Planktonic foraminiferal species identification followed the taxonomic concepts of Bé (1967; 1977), Hemleben *et al.* (1989), and Kennett and Srinivasan (1983). Classification is given in Appendix 1. For the purpose of this study the transitional forms between *Neogloboquadrina pachyderma* dextral coiling (Ehrenberg, 1861) and *Neogloboquadrina dutertrei* (d'Orbigny, 1839) were combined with the right coiling *N. pachyderma* (Giraudeau 1993; Pflaumann *et al.*, 1996). This method was used to overcome the *N. pachyderma* intergrade (PDI) category of morphological intergrades

between *N. dutertrei* and *N. pachyderma* (d) of Kipp (1976). In fact, phylogenetics, based on molecular biology, now calls into question the close relationship between *N. dutertrei* and *N. pachyderma* (d). Recent work on the DNA of specimens collected from plankton nets shows that *N. dutertrei* is, in fact, more related to *N. pachyderma* (sinistral coiling) than to the morphologically similar *N. pachyderma* (d) (Darling *et al.*, 2000). *Globorotalia menardii* (Parker, Jones, and Brady, 1865; d'Orbigny, 1865) and *Globorotalia tumida* (Brady, 1882) were combined together to form a single group, *G. menardii* (Dowslett and Poore 1990). The modern temperature range of both single taxa and their combination shows only minor differences within their temperature ranges (Pflaumann *et al.*, 1996). Plates 1 to 5 illustrate the planktonic foraminiferal species identified in this study.

2.2 SEA SURFACE TEMPERATURE RECONSTRUCTION USING PLANKTONIC FORAMINIFERA

2.2.1 Introduction

Estimates of ocean palaeotemperature are a vital component in the development of integrated models of past global climates. These models are powerful tools that can be used to predict the possible course of future climate change. The ocean plays a major role in the modulation and modification of climate. The characteristics of watermasses are defined principally by mean temperature and temperature ranges. Early attempts at ocean palaeotemperature reconstruction were mainly based on the presence or absence of certain planktonic foraminiferal species, such as *G. menardii* (Schott, 1935). High percentages of *G. menardii* were interpreted to indicate warmer, perhaps interglacial periods, while the absence, or reduced presence of the species, indicated cooler, or glacial periods. Other methods used to estimate palaeotemperature include utilising the relationship between foraminiferal calcite precipitation and the ambient water temperature (Urey, 1947; Epstein *et al.*, 1953; Emiliani, 1955). However, this technique has some uncertainties surrounding the effect of salinity on the temperature equations in some parts of the world ocean (Hale and Pflaumann, 1999). Additional robust proxies for SST, which attempt to overcome the problems of salinity variations and seasonal temperature fluctuations, have been developed based on census-based transfer function techniques, and organic geochemical techniques.

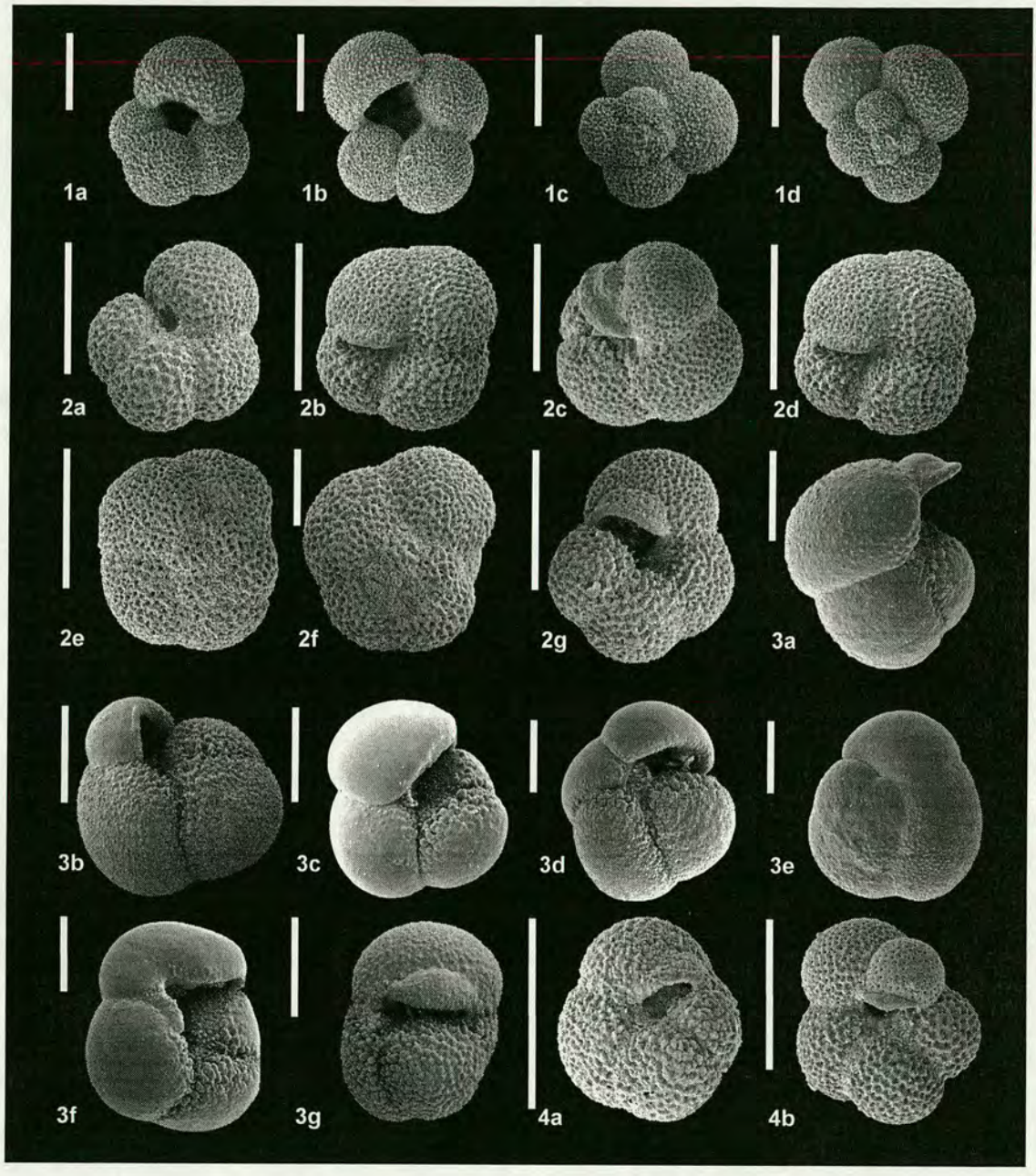

Plate 1: Scanning Electron Microscope photographs of planktonic foraminifera from the southern Benguela System, offshore Cape Town.
Scale bars represent 200 µm.

1a - d:	*Globigerina bulloides* d'Orbigny, 1826
2a - g:	*Neogloboquadrina pachyderma* (Ehrenberg), 1861 (dextral coiling)
3a - g:	*Globorotalia inflata* (d'Orbigny), 1839
4a - b:	*Neogloboquadrina pachyderma* (Ehrenberg), 1861 (sinistral coiling)

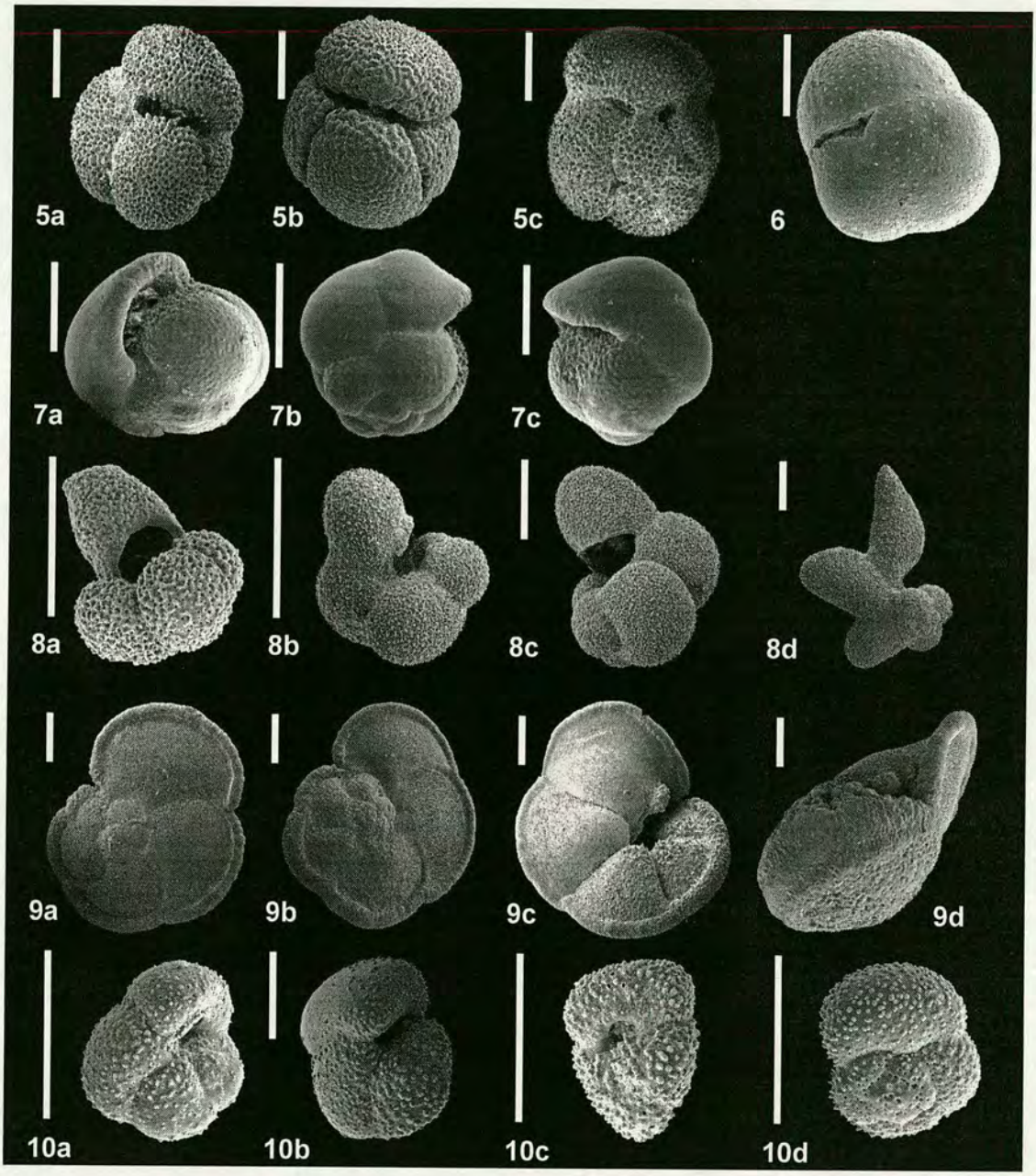

Plate 2: Scanning Electron Microscope photographs of planktonic foraminifera from the southern Benguela System, offshore Cape Town. Scale bars represent 200 µm.

5a - c:	*Globigerinoides conglobatus* (Brady), 1879
6:	*Sphaeroidinella dehiscens* (Parker and Jones), 1865
7a - c:	*Pulleniatina obliquiloculata* (Parker and Jones), 1865
8a - d:	*Globigerina digitata* (Brady), 1879
9a - d:	*Globorotalia menardii* (Parker, Jones, and Brady), 1865
10a - d:	*Globorotalia crassaformis* ssp. (Galloway and Wissler), 1927

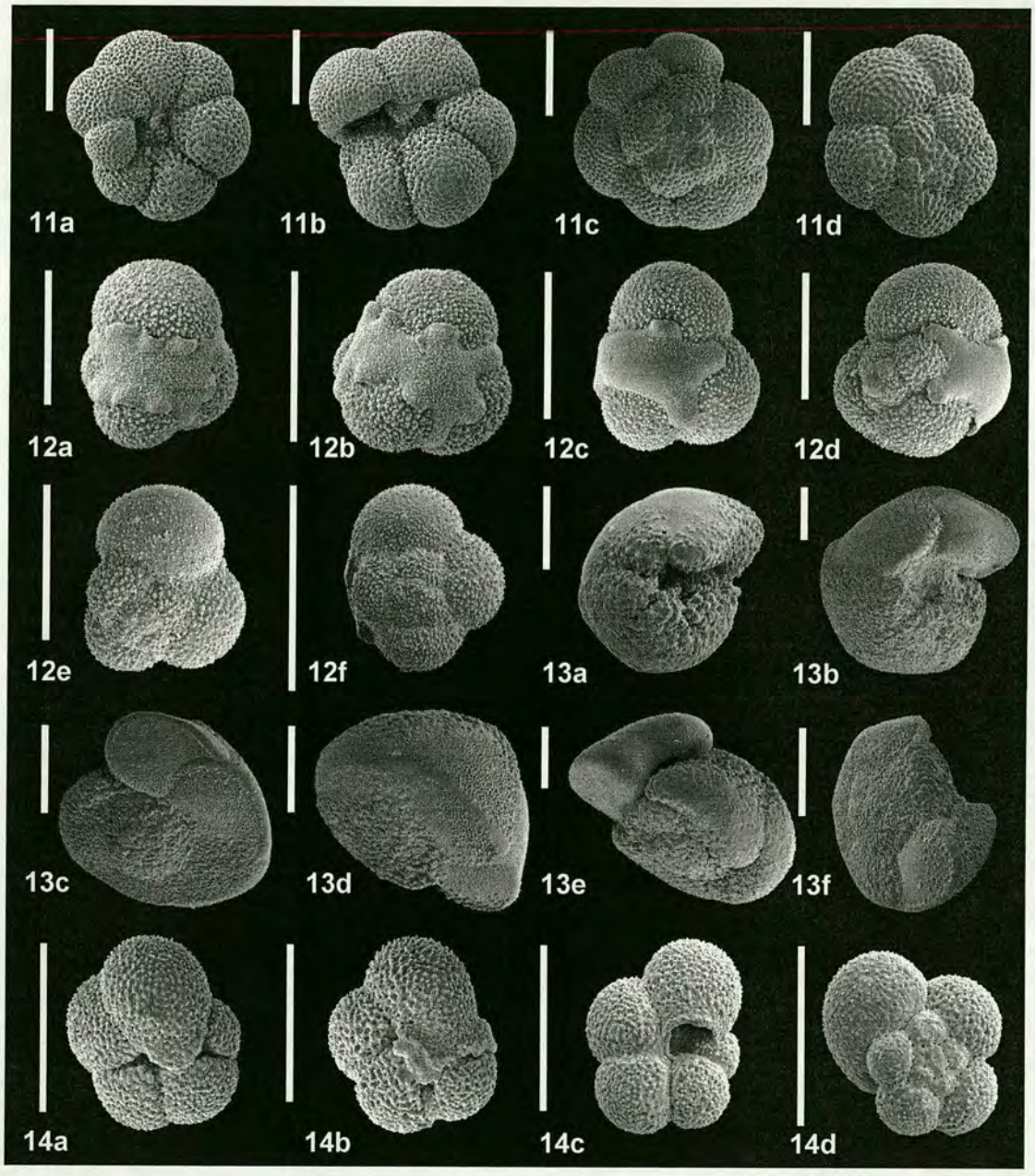

Plate 3: Scanning Electron Microscope photographs of planktonic foraminifera from the southern Benguela System, offshore Cape Town. Scale bars represent 200 µm.

11a - d: *Neogloboquadrina dutertrei* (d'Orbigny), 1839 [=*Globigerina eggeri* (Rhumbler)]
12a - f: *Globigerinita glutinata* (Egger), 1895
13a - f: *Globorotalia truncatuliniodes* (d'Orbigny), 1839
14a - d: *Turborotalita quinqueloba* (Natland), 1938

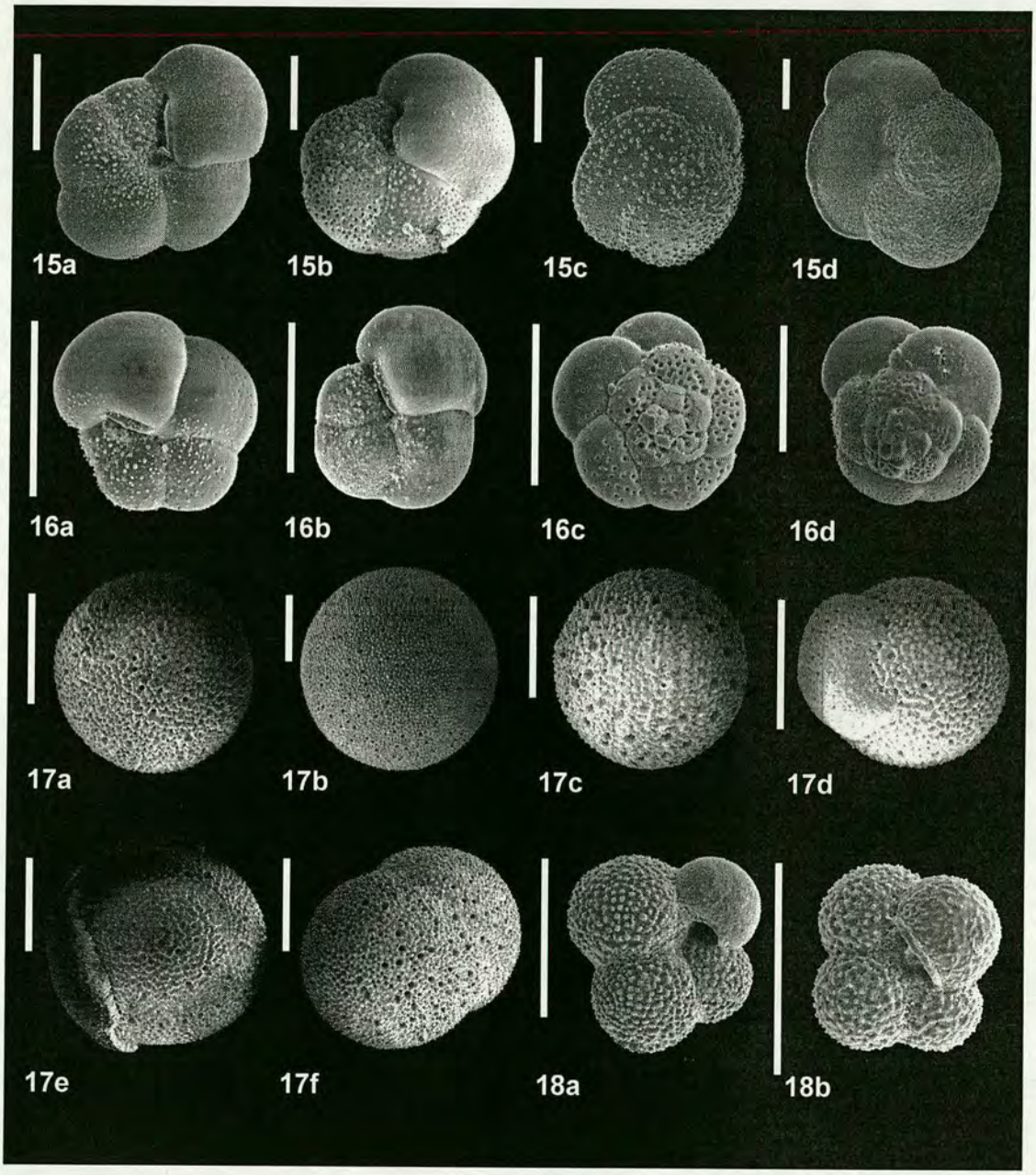

Plate 4: Scanning Electron Microscope photographs of planktonic foraminifera from the southern Benguela System, offshore Cape Town. Scale bars represent 200 µm.

15a - d: *Globorotalia hirsuta* (d'Orbigny), 1839
16a - d: *Globorotalia scitula* (Brady), 1882
17a - f: *Orbulina universa* (d'Orbigny), 1839
18a - b: *Globigerina falconensis* Blow, 1959

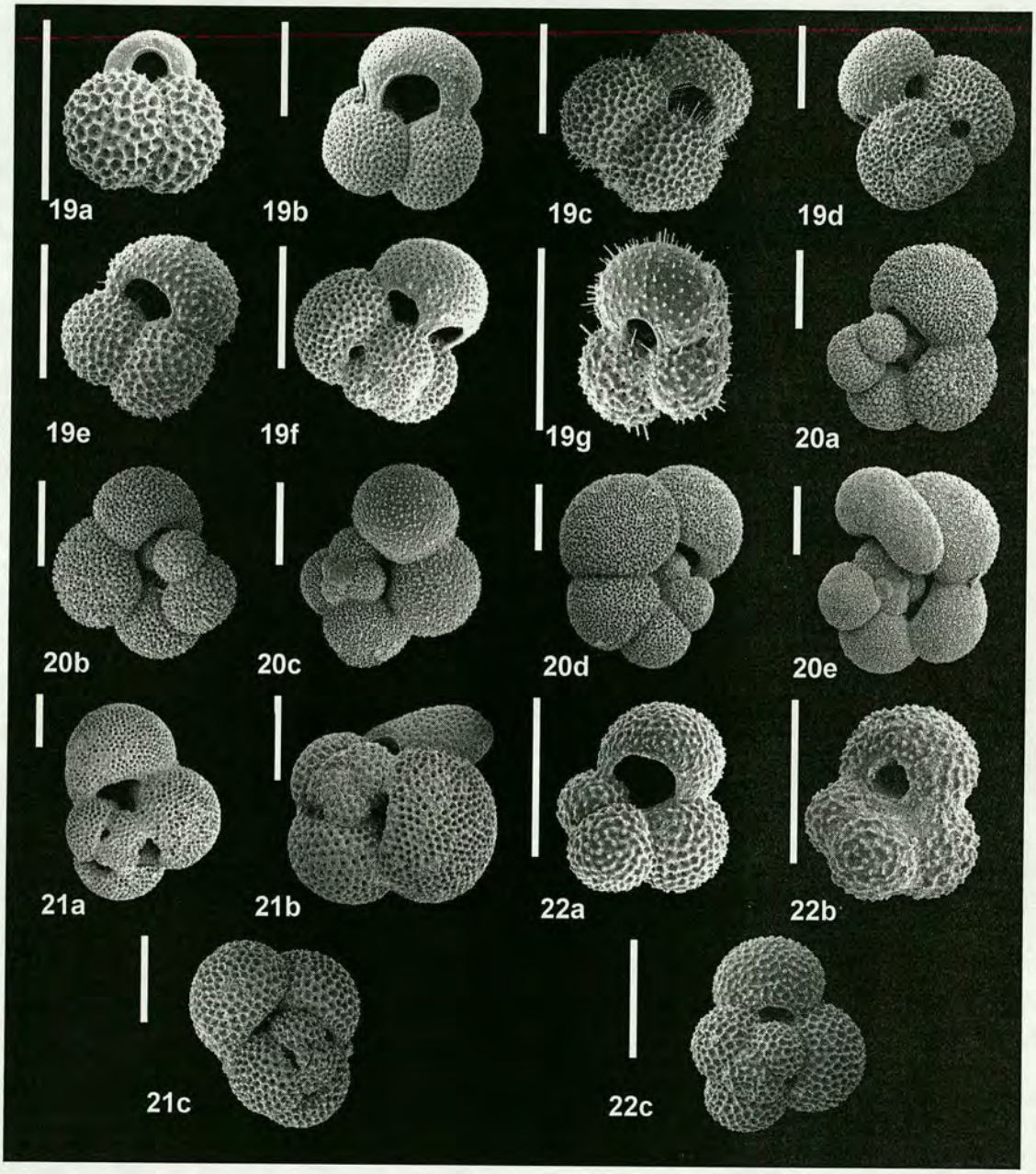

Plate 5: Scanning Electron Microscope photographs of planktonic foraminifera from the southern Benguela System, offshore Cape Town. Scale bars represent 200 µm.

19a - g:	*Globigerinoides ruber* (d'Orbigny), 1839
20a - e:	*Globigerinella siphonifera* (d'Orbigny), 1839
	[*Globigerinella aequilateralis* (Brady), 1839]
21a - c:	*Globigerinoides sacculifer* (Brady), 1877
	[=*Globigerinoides trilobus* (Reuss) form]
22a - c:	*Globigerinoides tenellus* (Parker), 1958

2.2.2 Planktonic foraminifera based transfer functions

Transfer functions are essentially variants on multiple linear regression models. They are used to establish quantitative relationships between biological data and environmental variables for palaeoecological analysis. The technique is based on the assumption that an assemblage of organisms will be related to its environment by a complex set of relations (the transfer function). If these relationships, or by definition the function, can be determined in the modern environment, then multivariate numerical analysis should allow that function to be applied to fossil assemblages, enabling the quantitative reconstruction of past environmental parameters (Birks and Birks, 1980).

The first attempt to use transfer functions to reconstruct palaeo-sea surface temperatures (SSTs) was made by Imbrie and Kipp (1971). Their method takes modern planktonic foraminiferal distributions from core top samples and calibrates these to present day ocean SST parameters using transfer functions. These relationships can then be used to infer palaeoceanographic conditions from fossil planktonic foraminiferal assemblage data. A similar method, the modern analog technique or MAT, proposed by Hutson (1980), also relies on the comparison of ancient assemblages to large reference sets of core top assemblages. However, rather than extracting factor relationships and applying them to fossil datasets, this principle employs a similarity index whereby fossil assemblages are matched to modern assemblages and, by implication, sea surface temperature associated with those assemblages (Pflaumann *et al.*, 1996). The assumptions that underlie both techniques are discussed in some detail by Imbrie and Kipp (1971), Prell (1985), and Pflaumann *et al.*, (1996). Briefly these are: stable ecology of the organisms through time; equilibrium in the relationship between fauna, sediment, and SST; as well as globally comparable ecological responses to changing conditions. The transfer function technique was employed by CLIMAP (1976; 1981) to produce the first large scale maps of inferred SSTs at the last glacial maximum (LGM). The CLIMAP method (Imbrie and Kipp, 1971; Imbrie *et al.*, 1973; Mix *et al.*, 1986a; 1986b) was highly successful in generating a SST database that revolutionised concepts of global climate change (Pflaumann *et al.*, 1996), not only describing the state of the oceans at the LGM, but also showing that some parts of the ocean experienced much greater temperature change than others.

It should be noted that as the technique assumes a steady relationship between the biota and the environment, times of disequilibrum may produce fossil assemblages which are not observed in the modern fauna. These may either reflect past conditions with extremes beyond the ranges experienced today or some core top assemblages may not be a true ecological assemblage (Mix *et al.,* 1999). As a result, some sediment samples from certain periods will not fit into a modern SST regression model. This is known as the 'non-analogue sample problem' (Hutson, 1977; Pflaumann *et al.,* 1996; Mix *et al.,* 1999).

2.2.3 Transfer function calculations

The transfer functions (F81-25-5: Niebler and Gersonde, 1998; F279-24-5: *unpublished;* and F271-24-5: Niebler *et al.,* submitted) used in this study were calculated using the CABFAC program of Imbrie and Kipp (1971). Calculations were made during two secondments in the University of Bremen and are the result of collaborations with Dr. Stefan Niebler. The modern species assemblage reference datasets used in these calculations were varied for each transfer function used, and included core top samples from 55°S to 20°S in the South Atlantic (Niebler and Gersonde, 1998), and samples ranging to 10°N in the North Atlantic, in addition to core tops from the southwestern Indian Ocean (Niebler, unpublished data). The core top reference datasets used document a close relationship between the species distribution and austral summer surface temperature (Donner and Wefer, 1994; Niebler and Gersonde, 1998; Niebler *et al.,* submitted; King and Howard, 2001), which is significant to the reliability of the inferred palaeo-temperature estimations. To calibrate the assemblages to environmental parameters, the core top assemblages were related by multiple linear regression to modern SSTs from meteorological datasets of Levitus and Boyer (1994). The core top database and reference details of each transfer function are given in Table 2.1. Le and Shackleton (1994) and Mix *et al.,* (1999) have shown that regional calibrations, such as those employed in this study, are more accurate than global datasets.

Transfer Function	Core Top Data	Reference
F81-25-5	South Atlantic Ocean only (55°S to 20°S)	Niebler and Gersonde (1998)
F227-24-5	South Atlantic (55°S to 20°S) samples from F81-25-5 above. Indian Ocean (10°S to 55°S) coretop samples included. F81-25-5 cold samples removed.	unpublished preliminary equation
F279-24-5	F227-24-5 Atlantic database expanded (55°S to 10°N) to include non-PDI-data, Indian Ocean core top samples as for F227-24-5 above.	unpublished preliminary equation
F271-24-5	55°S to 10°N Atlantic Ocean (as above), plus southwestern sector of the Indian Ocean, and F81-25-5 cold samples.	Niebler et al., submitted

Table 2. 1 Details of the modern core top reference datasets used in the transfer function calculations used in this study. Transfer functions are listed in the order that they were developed and used.

The standard error for the SST estimation for each transfer function is 1.2°C for summer and winter, and 1.1°C for annual mean temperatures. For each depth a communality measure is calculated, which indicates how well the specific faunal composition is explained by the transfer function used. SSTs for core depths with a communality lower than 0.7 are not reliable because of the large margin of error.

Three different transfer functions were used in this study. The first SST reconstructions were made using function F81-25-5 (Niebler and Gersonde, 1998). This is a localised transfer function based on core tops solely from the southern sector of the South Atlantic. However, the large number of very low communality values in interglacial periods for the core samples offshore Cape Town, indicated that the geographical extent was too limited to encompass warmer conditions experienced during interglacial intervals. The results of this experiment are a good example of the

'non-analogue sample problem' as described above, and reflect the difficulties in employing the transfer function technique successfully.

In order to overcome this difficulty we decided to expand the core top reference database to include some subtropical and tropical samples. The reasoning behind this decision is based on the locations of sediment cores GeoB 3603-2 and MD96 2081 in an area under the influence of warm tropical waters of the Indian Ocean via the Agulhas Current. If, during interglacial periods, Indian Ocean input to the South Atlantic was higher than present, these warmer core tops samples could reflect these extremes. The results from the second transfer function F227-24-5 were more robust than those of F81-25-5. Nevertheless, communality problems still remained but this time in the glacial periods. The core tops used in the reference data set included samples whose assemblages included a PDI category. The fossil assemblages from the Cape Basin sediment cores did not (see Section 2.1.5 for discussion). Subsequently, a third transfer function was used on the planktonic foraminifera assemblages of this study, F279-24-5. This transfer function was constructed from an expanded coretop database into the North Atlantic to 10°N to include a suitable diverse number of non-PDI categorised samples. This transfer function produced an SST curve with similarities to the $\delta^{18}O$ curve for core GeoB 3603-2 but communality values were still not sufficiently robust because of the remaining PDI core top samples in the database.

In the final transfer function of this study, F271-24-5, the PDI category samples were completely removed from the database in order that it would be absolutely consistent with the normal counting procedures employed in the Cape Basin sediment cores. The results of transfer function calculations are only meaningful if the environmental input factors are those which control the species distributions. Temperature is a dominant control, but there are other environmental influences on the assemblages, discussed in Section 2.1.2, which may act independently, or in combination. The SST results of these transfer functions are presented and discussed in Chapter six.

2.3 ALKENONE PALAEOTHERMOMETRY

2.3.1 Technique

An organic geochemical technique for palaeo SST reconstruction has been developed based on C_{37} alkenones ($U^{k'}_{37}$ index), which is independent of species relative abundance data. Alkenones are a biomarker found in marine autotrophic coccolithophores (Prahl *et al.*, 1995). They were first detected in sediments in the northern Benguela System (Boon *et al.*, 1978). The dominant coccolithophore species are *Emiliani huxleyi* (Lohmann, Hay and Mohler) and *Geophyrocapsa oceanica* (Kamptner). The method employs unsaturation ratios of long chain ketones ($U^{k'}_{37}$ index, Brassell *et al.*, 1986) that are linearly related to water temperature (Sikes and Keigwin, 1994; Rosell-Melé *et al.*, 1995a; Schneider *et al.*, 1995). The alkenones have C_{37}, C_{38}, and C_{39} chain lengths and two or three double bonds (De Leeuw *et al.*, 1980). The ratios of these di- and tri- unsaturated bonds vary as a function of growth temperature (Brassell, *et al.*, 1986; Prahl and Wakeman, 1987; Prahl *et al.*, 1988; Sikes *et al.*, 1991; Rosell-Melé *et al.*, 1995b; Müller *et al.*, 1998). One of the main assumptions is that this ratio does not change within the sediment. Studies in the South Atlantic calibrating alkenone derived temperatures to modern SST values in surface and downcore sediment samples support this relationship and show a temperature range of 29° to 5°C for the past 400 k.y. (Müller *et al.*, 1997; Müller *et al.*, 1998). Calibration of core top samples (Müller *et al.*, 1998), and lab culture experiments of the coccolithophore *Emiliani huxleyi* (Prahl and Wakeman, 1987), to SST/growth temperature have resulted in almost identical regression equations to calculate palaeo-SST (Schneider *et al.*, 1999).

(1) $U^{k'}_{37} = 0.044 + 0.033 \times SST\ (°C)$ (Müller *et al.*, 1998)

(2) $U^{k'}_{37} = 0.043 + 0.033 \times SST\ (°C)$ (Prahl and Wakeman, 1987)

The results of global core top calibration suggest that the $U^{k'}_{37}$ ratio is not significantly affected by changes in ocean productivity. The standard error of using the calibration from the South Atlantic is ±1°C, and from the global compilation 1.5°C (Wefer *et al.*, 1999). This technique has been used on the sediments of core GeoB

3603-2 to provide an independent temperature proxy. In Chapter Six, I will make a comparison of the results of the two methods.

2. 3. 2 Alkenone analysis procedure

Samples were taken at 5cm intervals along the length of core GeoB 3603-2. Alkenone analysis followed the method described in Schneider *et al.* (1995). Alkenones were extracted from 0.5 to 5g aliquots of freeze-dried sediment by a modified flow bending technique (Radke *et al.*, 1978) using an Ultra Turrax T25 centrifuge at 24,000 rpm and successively less polar solvent mixtures (MeOH, MeOH/$CHCl_3$ 1:1, $CHCl_3$), each for 5 minutes. The three extracts were combined, desalted, and dried over Na_2SO_4, concentrated under N_2, and finally taken up in 25µl of a 1:1 MeOH/$CHCl_3$ mixture. A 2µl aliquot of this extract was analysed by capillary gas chromatography using a HP 5890A gas chromatograph equipped with a 50-m x 0.32 mm ID HP Ultra 1 fused silica column, split injection, and flame ionisation detection. Helium was used as a carrier gas. The oven temperature was programmed from 50 -150°C at 30°C/min, 150 - 230°C at 8°C/min, and 230 -320°C at 6°C/min. The final temperature was then maintained for 37 minutes. Quantification of di- and tri- unsaturated C_{37} alkenones was achieved by an internal standard method using the relative response factor of the C_{38} n-alkane for both alkenones. The alkenone unsaturation index was calculated from the concentrations of di- and tri- unsaturated C_{37} alkenones using the expression $U^{k'}_{37}$ = [37:2]/[37:3+37:2] and translated into temperature using calibration (1) above. Sampling and analysis were carried out at the Fachbereich Geowissenschaften, University of Bremen, Germany.

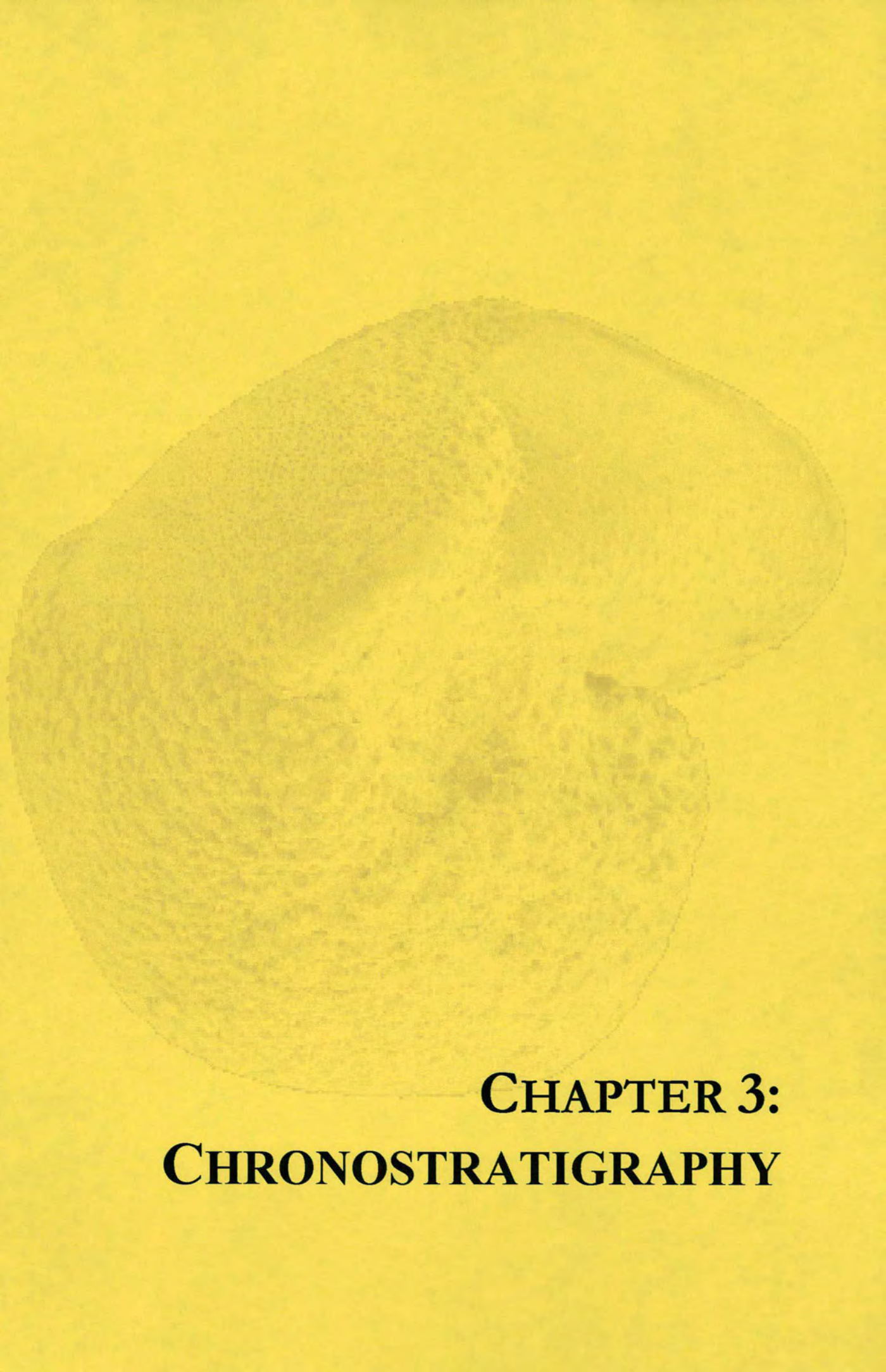

CHAPTER 3: CHRONOSTRATIGRAPHY

CHAPTER 3: CHRONOSTRATIGRAPHY

3.1 TIMING CLIMATE CHANGE

3.1.1 Stable Isotope Theory

Variations in the isotopic composition of carbonate shells, belonging to marine organisms, reveal a fossil record of the Earth's changing climate that was first exploited by Emiliani (1955). The ratio of oxygen isotopes ^{18}O and ^{16}O (expressed ^{18}O:^{16}O), which is incorporated into the shells at the time of formation, is controlled by the temperature and the isotopic composition of the sea water in which the organism lived. The ratio of ^{18}O:^{16}O in ocean waters has varied on glacial – interglacial timescales as a result of the natural fractionation of oxygen isotopes during the evaporation of sea water. Oxygen isotope ratios are measured as relative deviations ($\delta^{18}O$ per mil) from a laboratory standard (Shackleton and Opdyke, 1973). PDB (Pee Dee Belemnite) standard was obtained from carbonate from the belemnite *Belemnitella americana* from the Upper Cretaceous Pee Dee Bee Formation from South Carolina (Epstein and Urey, 1951). A $\delta^{18}O$ value of close to 0‰ is recorded at times of minimal ice cover and a 0.11‰ change in the $\delta^{18}O$ represents a ~10m change in sea level.

$$\delta\ ^{18}O = 1000 \times \left[\frac{^{18}O/^{16}O \text{ sample} - {}^{18}O/^{16}O \text{ standard}}{^{18}O/^{16}O \text{ standard}} \right]$$

EQUATION 1: Oxygen isotope ratios are expressed as positive or negative values relative to the standard (δ= zero).

The lighter ^{16}O isotope is taken up during evaporation in preference to ^{18}O; thus rainwater is isotopically lighter than the ocean from which it originated (Williams *et al.*, 1998). Consequently, the oxygen isotopic composition of the global ocean is mainly controlled by evaporation in the tropics. However, another factor, the ice volume effect, becomes important during periods of climatic change. While polar ice caps become enriched by precipitation-derived ^{16}O, the oceans become relatively ^{18}O

enriched (Shackleton, 1987). This process is temperature dependent and the amplitude of change is more marked in colder latitudes. During glacial periods of the Quaternary, the expansion of ice sheets over much of the northern hemisphere and Antarctica resulted in the oceans becoming relatively enriched in ^{18}O (i.e. isotopically heavier or more positive). An inverse situation existed during interglacial periods, when melting of the polar ice sheets released $H_2{}^{16}O$ enriched waters into the oceans resulting in lighter isotopic values. Thus, in most parts of the oceans an isotopic shift is the result of a combination of temperature and the ice volume effect (Mix and Ruddiman, 1985). Down-hole records of oxygen isotope ratios of both benthic and planktonic foraminifera species show a remarkable similarity throughout the oceans. Furthermore, they have revealed a far greater number of glacial – interglacial cycles than was previously known. A common forcing mechanism, global insolation cycles so-called 'Milankovitch cycles', based upon the fluctuations of the Earth's orbit, is now accepted (Milankovitch, 1930; Imbrie *et al.*, 1984; 1992).

While foraminifera are assumed to precipitate calcium carbonate in approximate equilibrium with the surrounding sea water (Urey, 1947, Epstein *et al.*, 1953), slight variations dependent on species have been documented. For instance, changes in depth habitat, local water chemistry, temperature, nutrients, and light all have small effects which must be considered when interpreting such data (Kahn 1979; Fairbanks, *et al.*, 1982; Kroon and Ganssen 1989; Sautter and Thunnell, 1991; Ravelo and Fairbanks 1992; Spero *et al.*, 1997).

3.1.2 Oxygen and carbon stable isotope analysis

Samples were taken at 5cm intervals along GeoB core 3603-2 and the IMAGES II core MD96 2081 for a high resolution analysis. $\delta^{18}O$ and $\delta^{13}C$ ratios were measured on both cores using the epibenthic foraminifer *Cibicidoides wuellerstorfi* (Schwager). In addition, tests of the planktonic taxa *Globorotalia inflata* (d'Orbigny) from core MD96 2081 were analysed. The foraminifers (2-3 specimens for *Cibicidoides*, and 8 – 10 specimens for *G. inflata*) were picked from the >250 μm fraction to achieve an analytical weight of 0.05 – 0.1 μg. Stable isotope analysis was made on a Finnigan MAT 251 mass

spectrometer, using an automatic sampling line. The isotopic composition of the tests was measured from the CO_2 released by the treatment of the carbonate with orthospheric acid at a constant temperature of 75°C. Isotope data are calibrated to the Pee Dee Belemnite (PDB) standard in δ notation (Epstein *et al.*, 1953) using the NBS 18, 19, and 20 standards. The analytical precision for the $\delta^{18}O$ and $\delta^{13}C$ was ±0.08 ‰ and ±0.04, respectively. Sampling and analysis were carried out at the Isotope Laboratory, University of Bremen, Germany.

3.2 Dating and Correlation

3.2.1 Age model Construction

Oxygen isotope analysis not only provides one of the principal indices of global environmental change during the Quaternary, but also serves as the basis for global stratigraphic division and correlation. Stratigraphic frameworks for the $\delta^{18}O$ and $\delta^{13}C$ records of cores GeoB 3603-2 (Figure 3.1A) and MD96 2081 (Figure 3.1B) were constructed using the time scales of Imbrie *at al.* (1984) and Martinson *et al.* (1987). Stable isotope age control points for core GeoB 3603-2 are given in Table 3.1A and Table 3.1B for core MD96 2081. The age control points from both cores were extrapolated using the ARAND 'Ager' software (Dr. P. Howell, Brown University, Connecticut) to calculate an age estimation for each depth in the core. The benthic and planktonic isotope records display the familiar sequence of glacial and interglacial Marine Isotope Stages (MIS) of the standard orbital chronostratigraphy (Emiliani, 1955; Imbrie *et al.*, 1984; Martinson *et al.*, 1987; Shackleton *et al.*, 1990). Using this method, MIS 5.5, 9, and 11 are the isotopically lightest, thus the 'most' interglacial. MIS 2, 6, and 10 have similarly high $\delta^{18}O$ values and MIS 12, with the heaviest values of all is, in isotopic terms, the most extreme glacial of the time period studied. The benthic $\delta^{18}O$ glacial-interglacial amplitudes at the Cape Basin site are consistently larger (2.0‰) than the expected 1.1‰ based on ice volume changes. This indicates that the deep waters offshore the Cape of Good Hope experienced large temperature changes during glacial-interglacial cycles relative to the global deep ocean during the past 700 kyr.

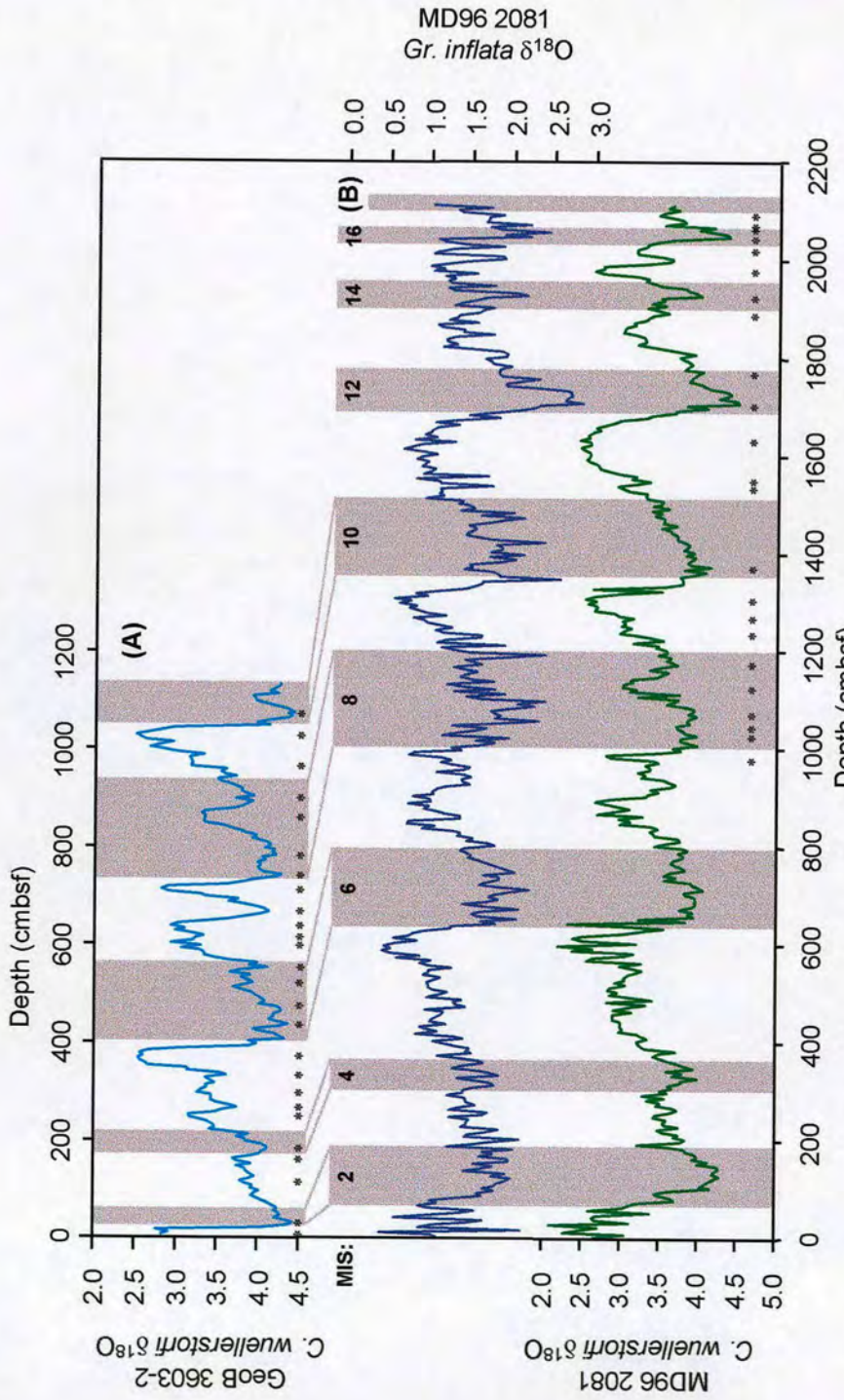

Figure 3.1 Oxygen isotope depth profiles for **A)** GeoB 3603-2 and **B)** MD96 2081 (planktonic and benthic). Both cores are plotted to the same depth scale. Marine oxygen isotope stages (MIS) are given for comparison between cores (glacials are shaded). Age control points are indicated by * after Imbrie *et al.* (1984).

Depth (cmbsf)	Age (k.y.)	Marine Isotope Stage (MIS)
8	4	(top)
33	19	2.2
63	28	3.1
153	53	3.3
193	65	4.2
248	80	5.1
268	87	5.2
303	99	5.3
328	107	5.4
373	122	5.5
413	135	6.2
448	146	6.3
463	151	6.4
523	171	6.5
558	183	6.6
588	194	7.1
613	205	7.2
638	216	7.3
673	228	7.4
708	238	7.5
743	249	8.2
803	269	8.4
863	287	8.5
908	299	8.6
958	310	9.1
1028	331	9.3
1063	342	10.2

Table 3.1A (above) Stable isotope age control points for *C. wuellerstorfi* oxygen isotope data from core GeoB 3603-2. These points correspond to the stars marked on Figure 3.1A).

Depth (cmbsf)	Age (k.y.)	Marine Isotope Stage (MIS)
988	238	7.5
993	245	8
1008	249	8.2
1048	257	8.3
1073	269	8.4
1133	287	8.5
1173	299	8.6
1238	310	9.1
1268	320	9.2
1308	331	9.3
1373	341	10.2
1538	368	11.1
1548	375	11.2
1633	40`5	11.3
1708	434	12.2
1773	471	12.4
1893	513	13.2
1928	563	14.4
1978	574	15.1
2018	617	15.5
2048	628	16.22
2053	631	16.23
2058	641	16.3
2063	656	16.4
2073	668	17.1
2078	679	17.2
2093	689	17.3

Table 3.1B (above) Stable isotope age control points for *C. wuellerstorfi* oxygen isotope data from core MD96 2081. These points correspond to the stars marked on Figure 3.1B.

3.2.2 Sedimentation rates

A further way to examine the chronostratigraphical properties of a sediment core is to examine the sedimentation rates. Figure 3.2 illustrates the age – depth profiles for cores GeoB 3603-2 and MD96 2081. Furthermore, it shows the variability in

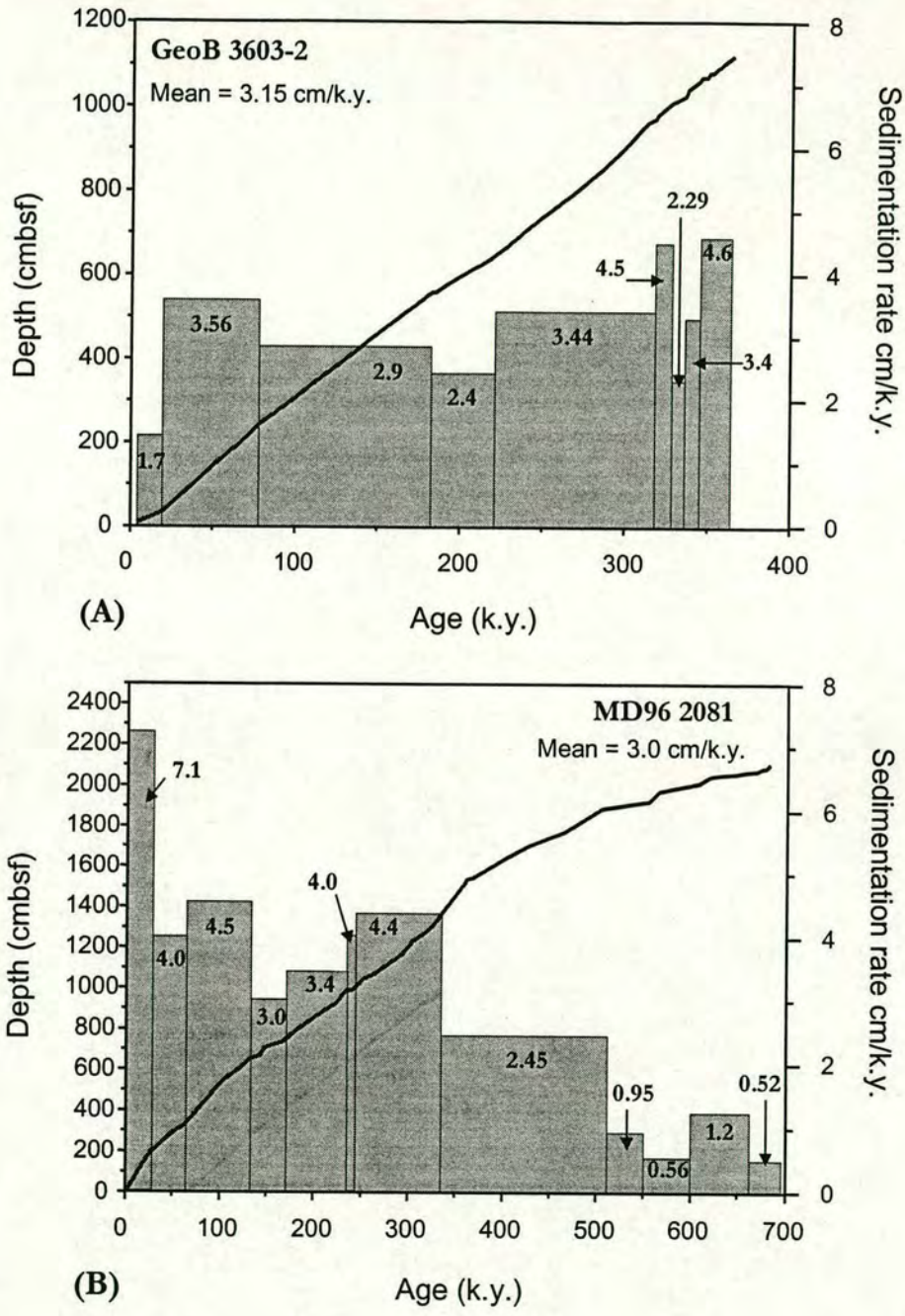

Figure 3.2 Age depth profiles and sedimentation rates in Cape Basin cores **A)** GeoB 3603-2 and **B)** MD96 2081.

sedimentation rate in the cores over time. The mean sedimentation rate for both cores is similar between 3.0 and 3.15 cm/k.y. Core GeoB 3603-2 shows a fairly consistent rate of sediment accumulation throughout the length of the core. However, MD96 2081 displays several distinct phases of sedimentation. Prior to 340 ka B.P sedimentation rates were below 2.45 cm/k.y. and had a mean of 1.1 cm/k.y. After that time sedimentation rates were higher with a mean of 3.9 cm/k.y. The highest sedimentation rate (7.1. cm/k.y.) is observed during the past 20,000 years.

3.2.3 Splicing the cores: developing a common time scale

In order to analyse the long term trends in the data from offshore the Cape of Good Hope the data from the two cores, GeoB 3603-2 and MD96 2081, was spliced to form one time-series covering a continuous period of ~700 k.y. The rationale behind this 'splicing' is explained below. The cores are located in very close proximity to each other, at similar depths, within the southern Cape Basin. Core GeoB 3603-2 was retrieved from 35°S 07.5′ - 17°E 32.6′ (2840m depth), whilst core MD96 2081 is located at 35°S 20.7′ - 17°E 24.7′ (3164m depth). The cores are positioned on the upper slope, parallel to but south of Cape Canyon (Figure 2.2). As the cores are adjacent to each other the oceanic environmental conditions that they record should be identical. The bulk core descriptions, summarised in Section 2. 1. 3, reveal that the cores are composed of similar material.

Extensive analysis of the data from both cores reveals that in the period of temporal overlap, 238 to 365 k.y., there are consistent trends across all proxy records. Benthic isotope records from cores GeoB 3603-2 and MD96 2081 are shown in Figure 3.3. The considerable period of overlap is illustrated. If the similarity in the overlapped portion of the sediment cores was only observed in the benthic $\delta^{18}O$ records then it would not be possible to justify splicing the cores. The overlapping section was also analysed at species level using planktonic foraminiferal census data and the dissolution proxy based on the degree of fragmentation of sediment samples (Le and Shackleton, 1992). The consistent patterns observed in these other proxies in the two Cape Basin cores are summarised in Figure 3.4. The correspondence of the percentage

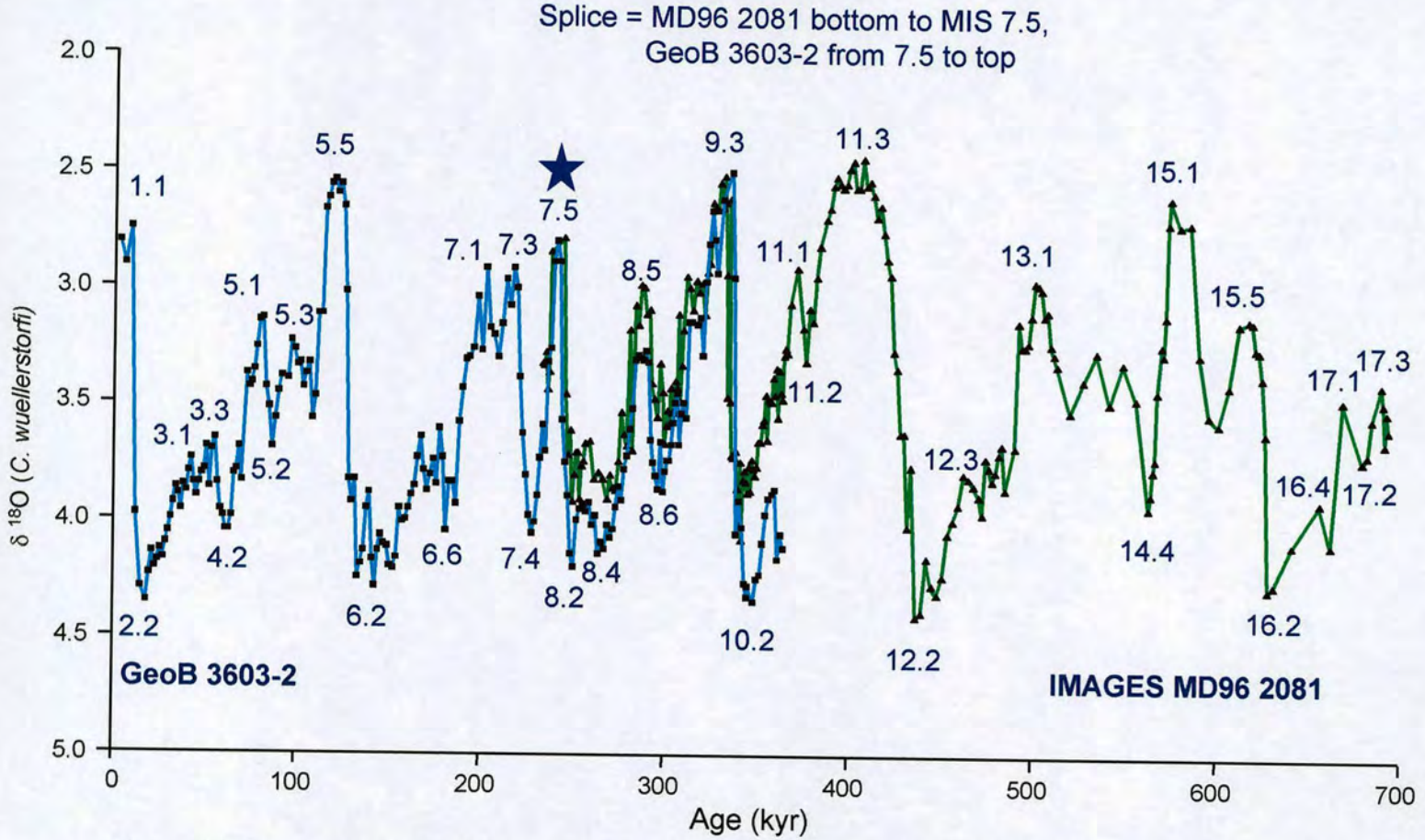

Figure 3.3 Benthic oxygen isotope age model core splice between cores GeoB 3603-2 (blue) and MD96 2081 (green). The age control points for each core are labelled. The core overlap is shown and the splice point is indicated by a star.. The same stratigraphy is applied to the carbon isotope data and planktonic isotope profiles for MD96 2081.

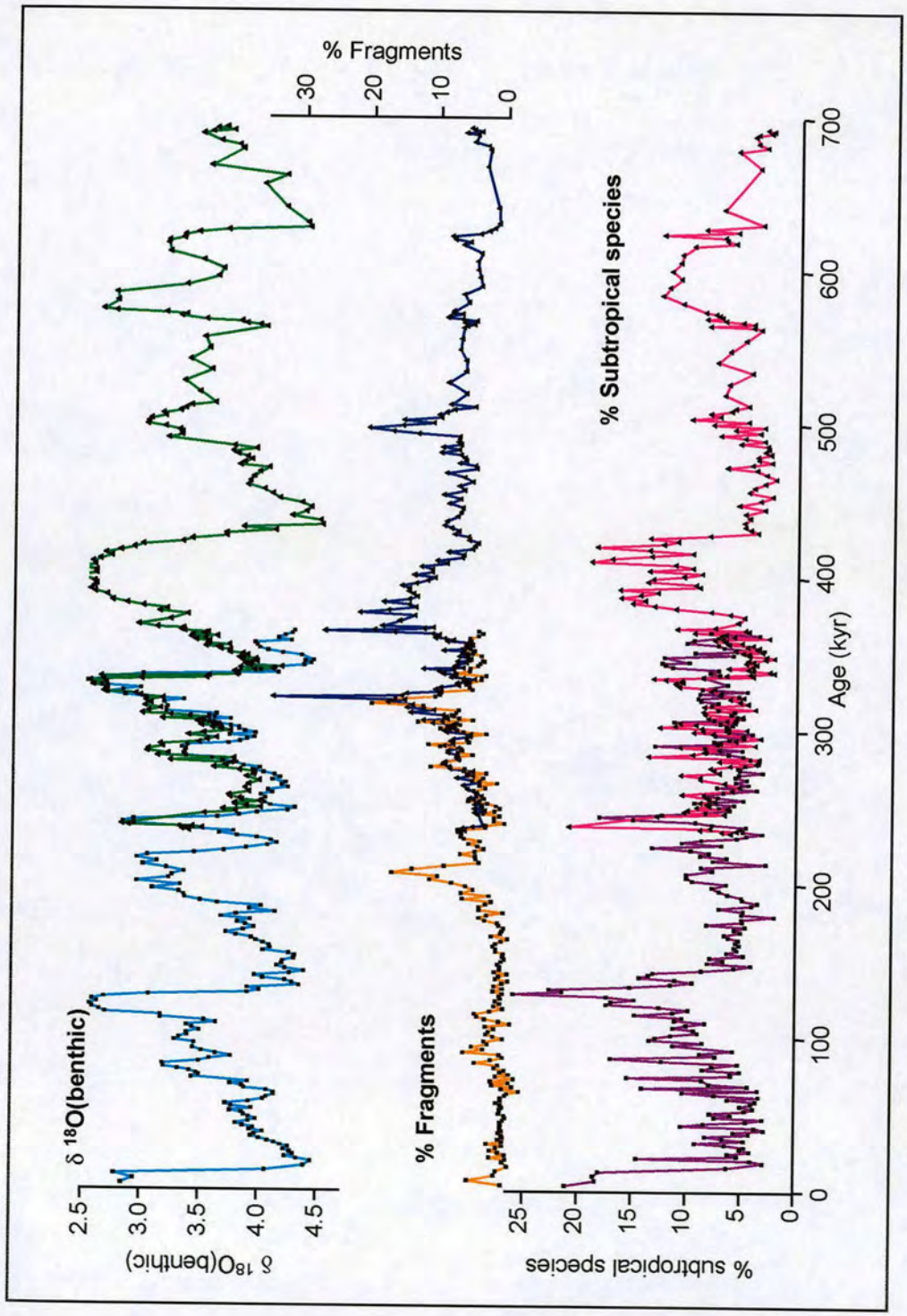

Figure 3.4 Overlapping $\delta^{18}O$ (benthic), % fragments, and % subtropical records for cores GeoB 3603-2 and MD96 2081.

fragments per sample in the two records in the overlap is striking. There are many processes governing fluctuations in dissolution and the relative abundance of planktonic foraminiferal species. The matching trends of the multivariate data set are relatively independent of the forcing mechanisms for the isotopes, in as much as local oceanic conditions play an significant role in addition to global climate changes. These observations support the action to splice the two cores together to create a long time series.

The joining point was taken at the peak of MIS 7.5. Samples in the overlapping section were removed to produce a single record which covers a continuous period of c. 700 kyr. The splice point at MIS 7.5 was selected for several reasons. Firstly, both cores had a $\delta^{18}O$ value of 2.8‰ at the peak of MIS 7.5 (Figure 3.3). Secondly, as discussed above, the trends in the different records correspond along the overlapped section of the two cores. More importantly, however, the sedimentation rates of MD96 2081 were greater (Figure 3.2), allowing a higher resolution analysis of the interval between 238 k.y. and 365 k.y. than would be possible using the samples from GeoB 3603-2 for this same interval. Neither core has an hiatus. The upper portion of the spliced record uses samples from core GeoB 3603-2 and the lower section is core MD96 2081. Eighty six of the samples from the bottom of core GeoB 3603-2 (708 cm to 1133 cmbsf) are not included in the spliced Cape Town record, whilst the top four samples (963 to 978 cmbsf) were removed from the IMAGES II core MD96 2081. Hereafter, unless otherwise indicated, the records described in this work relate to this spliced core combining cores GeoB 3603-2 and MD96 2081, and is referred to as the Cape Basin spliced record.

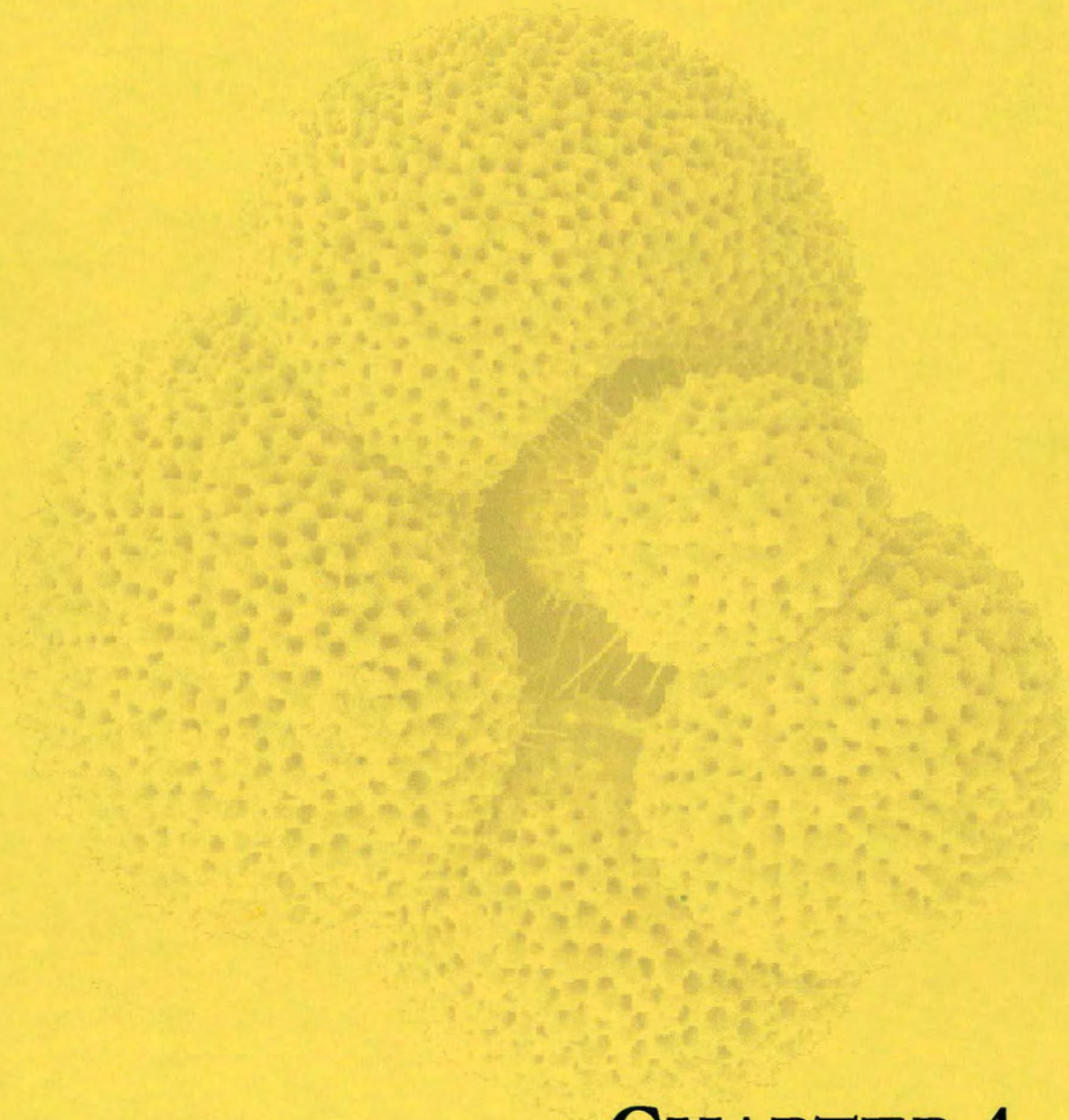

Chapter 4:
Oceanography

CHAPTER 4: OCEANOGRAPHY

4.1 ROLE OF THE SOUTH ATLANTIC IN CONTEXT OF GLOBAL CIRCULATION

4.1.1 Overview of global circulation

Ocean circulation links the energy of the ocean volume to climate (Gordon, 1996). Heat and water are transferred between different climatic regions and from low to high latitudes and vice versa. This is known as the thermohaline circulation. Each ocean basin has a distinct chemistry, stratification and atmospheric forcing. The North Pacific has excess precipitation over evaporation, resulting in very low salinity and little overturning. In contrast, the Indian and Atlantic Oceans are strongly evaporative. Convective overturning in the subpolar North Atlantic causes cold, dense, surface waters to sink and form North Atlantic Deep Water (NADW). Consequently, warm waters are drawn north (North Atlantic Drift), causing a relative latitudinal warming of the western European climate. As this deep water formation is not compensated for within the North Atlantic basin, inter-ocean exchange must occur to balance the circulation. In short, the thermohaline circulation is thought to be mainly driven by temperature and salinity differences, in comparison to principally wind-driven basin scale flow (Figure 4.1).

4.1.2 The 'conveyor'

The large-scale thermohaline circulation (Figure 4.2) is a simplified model stating that the deep layers of the South Atlantic are a conduit for the transport of NADW, which is formed in the northern North Atlantic and joins the Antarctic Circumpolar Current (ACC) in the South Atlantic, from where it spreads through the Indian and Pacific oceans. Water masses at all depths (Reid, 1996) are transferred to the North Atlantic to compensate for the NADW outflow, thus closing the global thermohaline circulation cell (Broecker, 1991). Schmitz (1995) reviews the literature concerning the transfer of surface waters which are required to compensate for the export of NADW. Much controversy exists concerning the origin of waters which eventually form deep water in the northern North Atlantic (Gordon, 1986; Gordon *et al.,* 1992; Rintoul, 1991;

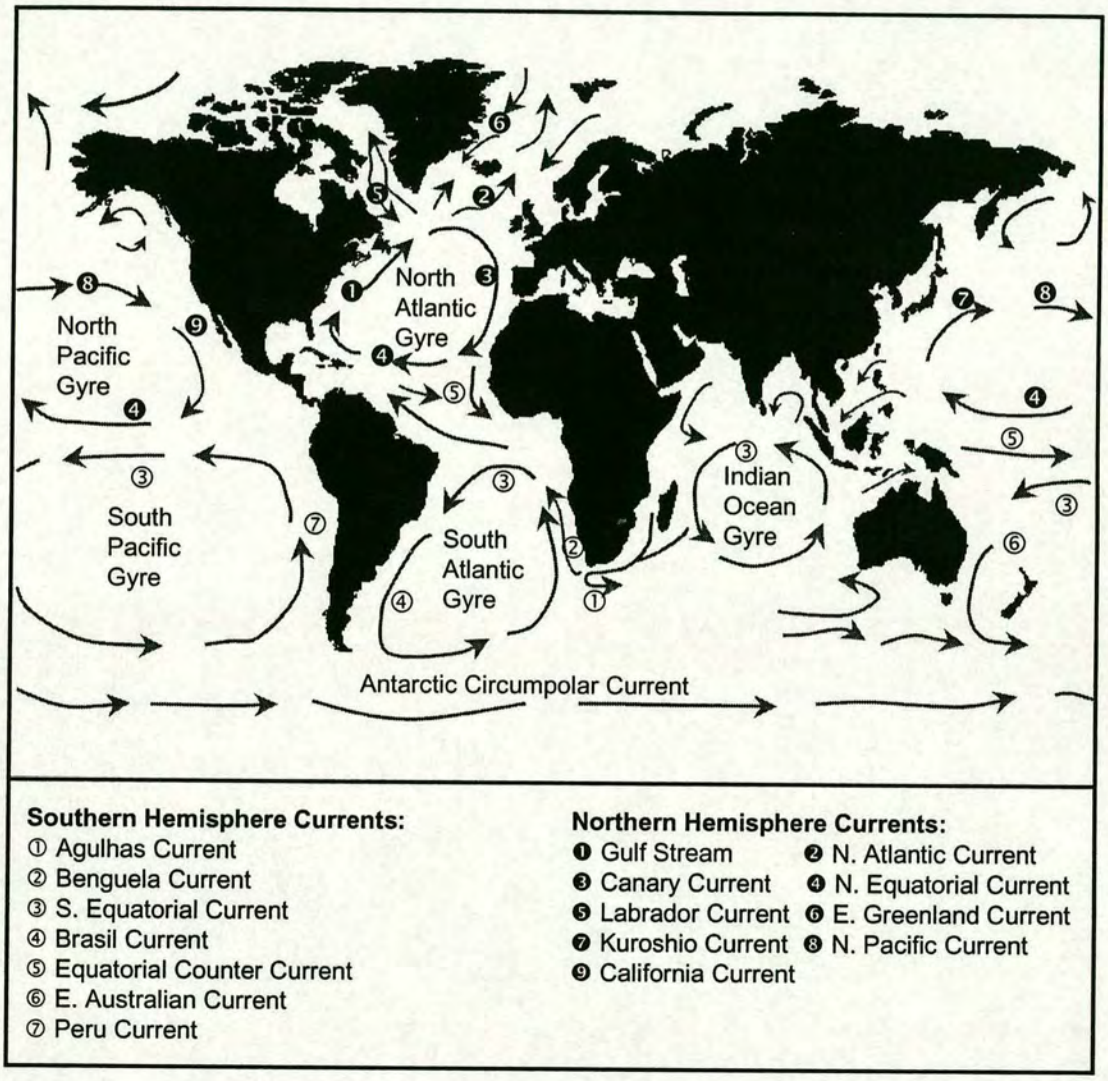

Figure 4.1 World ocean surface circulation.

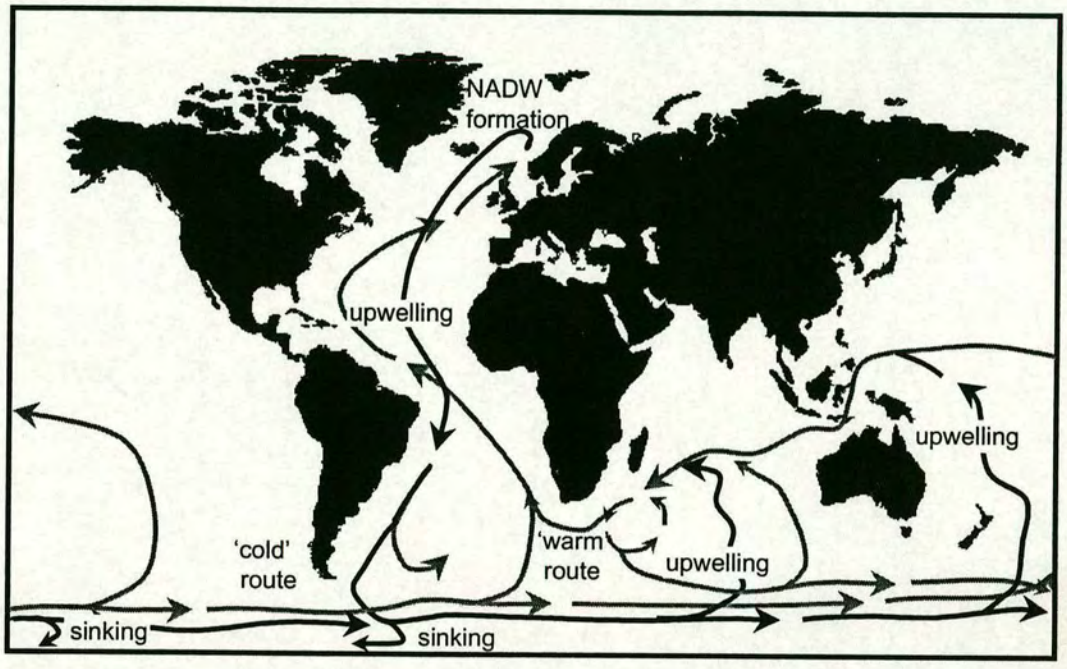

Figure 4.2 Global thermohaline circulation, a simplified scheme to show inter-ocean circulation driven by sinking of surface water in the North Atlantic to form deep water (NADW). Grey lines are surface waters warmer than 3.5°C, black lines are deep waters (< 3.5 ° C). After Gordon *et al.* (1992).

Garzoli and Gordon, 1996; Macdonald and Wunsch, 1996). Two theories have been proposed to explain this compensation, and both have received support from modelling experiments.

- **Warm Water Route** (WWR) proposed by Gordon (1986).
  NADW is carried within the ACC to the Indian and Pacific Oceans where it is upwelled into surface waters. These thermocline waters then flow west via the Indonesian throughflow and the Agulhas Current into the South Atlantic and eventually to the North Atlantic.
- **Cold Water Route** (CWR) proposed by Rintoul (1991).
  Intermediate water transport by the ACC via the Drake Passage is the most significant contribution to northward heat transport. It does so by gaining heat from the atmosphere in outcrop regions of AAIW within the South Atlantic. This effect surpasses the heat import of Indian Ocean thermocline water from the Agulhas Current.

Various modelling experiments have been set up to test these theories and have shown that both pathways possibly co-exist. Stutzer and Krauss (1998) found that the warm water route (WWR) dominated the heat flux and that the cold water route (CWR) had a strong influence on the salt balance. Macdonald and Wunsch (1996) found that there was no single overturning cell but two almost independent cells. They interpreted their results to suggest that the two routes are important sources for deep water formation, however, but possibly dominant at different time periods. Thus, the circulation of the South Atlantic is governed by a wide range of interacting processes from local wind driven eddies to long term thermohaline circulation.

4.1.3 Surface water circulation in the South Atlantic

As the South Atlantic connects the North Atlantic with the South Pacific and the South Indian oceans, it plays a major role in the global ocean system. The large-scale, upper water circulation of the South Atlantic is schematically represented in Figure 4.3. The circulation is characterised by complex features that result from water

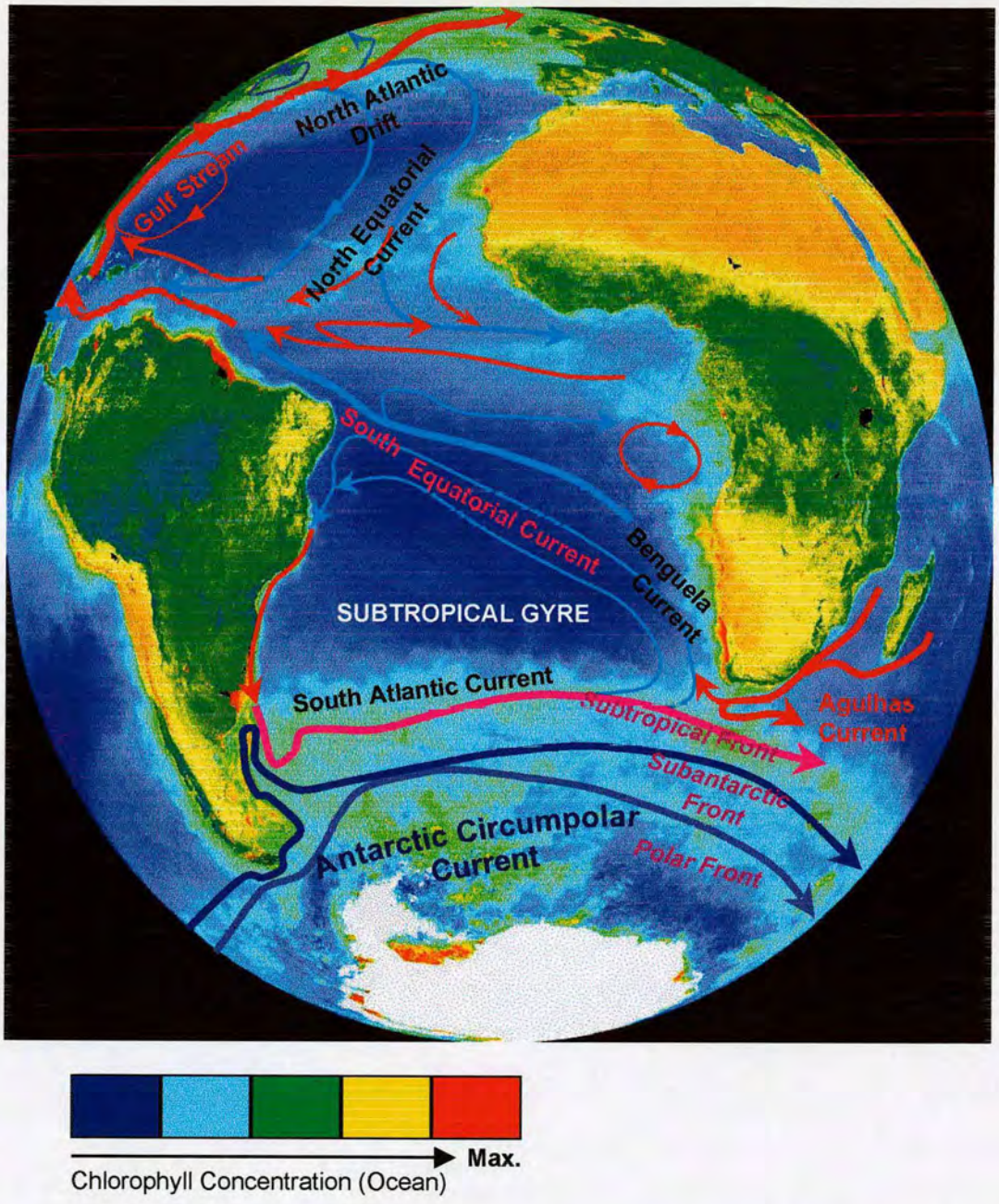

Figure 4.3 Surface water circulation in the Atlantic Ocean. Adapted from Peterson and Stramma (1991). Satellite image showing ocean productivity courtesy of NOAA.

exchange with adjacent oceans. Much of the basin scale circulation is dominated by the wind driven Subtropical Gyre and the ACC. The eastern boundary current is the Benguela Current, where the prevailing trade winds drive an offshore surface drift and coastal upwelling of cold, nutrient rich water. The western boundary current associated with the Subtropical Gyre is the southward Brasil Current. It meets a branch of the ACC, the northward Falkland Current, in a zone distinguished by high spatial and temporal variability (Gordon, 1981). The ACC links the Pacific with the Atlantic through the narrow Drake Passage. In contrast, the boundary between the South Atlantic and South Indian Ocean is wide (Figure 4.3). The southern hemisphere is dominated by maritime environments with relatively little landmass. As the African continent does not extend further than 35°S, the western boundary current of the Indian Ocean, the Agulhas Current, interacts and mixes with the eastern boundary current of the South Atlantic, a situation unique in the world ocean. The Agulhas Current contributes heat to the South Atlantic in surface, thermocline, and intermediate depths in almost equal parts (Stutzer and Krauss, 1998). Another aspect of the circulation in the South Atlantic not observed in other ocean basins is equatorward transport of heat across 30°S (Gordon, 1988). Normally, heat transport is from tropical to polar regions. The anomaly in the South Atlantic is accounted for by the feedback system set in place by the formation of NADW, termed 'North Atlantic Heat Piracy' by Berger and Wefer (1996), whereby cold deep water is exchanged for warm upper waters. This results in several other differences in the circulation of the South Atlantic. The Brasil Current is not a strong poleward jet comparable to the Gulf Stream of the North Atlantic. In contrast to the weak Brasil Current the Benguela Current is very strong and dominates much of the tropical and subtropical flow in the basin.

4.1.4 South Atlantic water mass structure

Antarctic Bottom Water (AABW), Circumpolar Deep Water (CPDW), and NADW drive the abyssal circulation in the South Atlantic (Figure 4.4). Before dealing with the distribution and sources of these watermasses, the vertical water types are defined according to Gordon *et al.* (1992). Thermocline waters are those warmer than 9°C and are confined to the upper 1500m. The intermediate water encompasses the water depth range between the 1500m isobath and the 9°C isotherm or the sea surface,

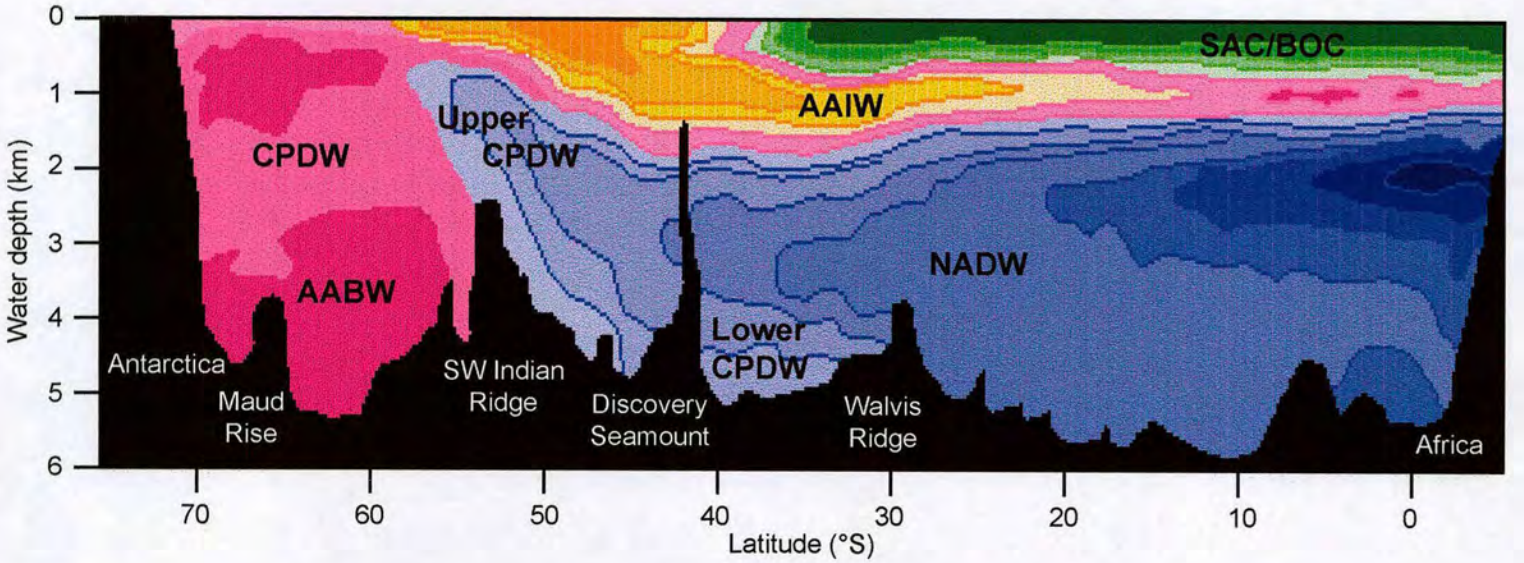

Figure 4.4 Present day stratification of main ocean water masses in the South Atlantic as displayed by salinity isopycnals (‰) at a north-south transect along the Greenwich Meridian. Drawn from Reid (1989).
AABW - Antarctic Bottom Water, **CPDW** - Circumpolar Deep Water, **AAIW** - Antarctic Intermediate Deep Water, **NADW** - North Atlantic Deep Water, **SAC/BOC** - South Atlantic Current/ Benguela Oceanic Current.

respectively, if there is no water warmer than 9°C. Finally, all water below 1500m is called deep water. The definition is somewhat arbitrary because, for example, intermediate water includes the whole upper ocean south of the subtropical front. The stratification of the water masses in the South Atlantic is shown in Figure 4.4. AABW is the lowest water mass and is characterised by a low potential temperature (1 to 0.7°C) and moderate salinity (Reid, 1989). Its source is the Weddell Sea at the margin of the Antarctic continent. AABW only occurs in the deepest parts of the basins below 4000m (Diekmann *et al.*, 1996). NADW is of convective origin in the subpolar North Atlantic, and is the most important deep water mass to this study (Figure 4.4).

4.2 Benguela Region

4.2.1 Physical oceanography of upwelling

Wind systems blow in response to differential heating of the Earth's surface and the effect of the earth's rotation, the Coriolis force. Along most of the ocean's eastern boundaries, the mean winds blow equatorward at low to mid latitudes. The wind stress on the ocean surface, which is proportional to wind speed, causes a divergence in the near surface currents. As a result, sea-level drops at the coast, creating a cross-shelf pressure gradient filled by upwelling of subsurface waters into the surface layers (Figure 4.5). In the southern hemisphere, this wind stress causes a net transport to the left of the wind direction (Ekman, 1905), in the northern hemisphere the movement is deflected to the right. Ekman transport is a phenomenon that is important to the intensity of eastern boundary current upwelling. This principle states that there is increasing deflection of currents with increasing depth away from the direction of the initial wind. A spiraling current is the result of the current deepening and increasing deflection. Volume transport calculations have shown that surface currents move at 45° from the wind direction while net transport is 90° from the generating wind. This transport is limited to the thickness of the surface mixed layer and has a magnitude (per unit width) equal to the wind stress divided by the Coriolis forcing. The boundary between upwelled water and warmer surface waters is often sharp. The strong density gradient across this upwelling front established a strong geostrophic current along the

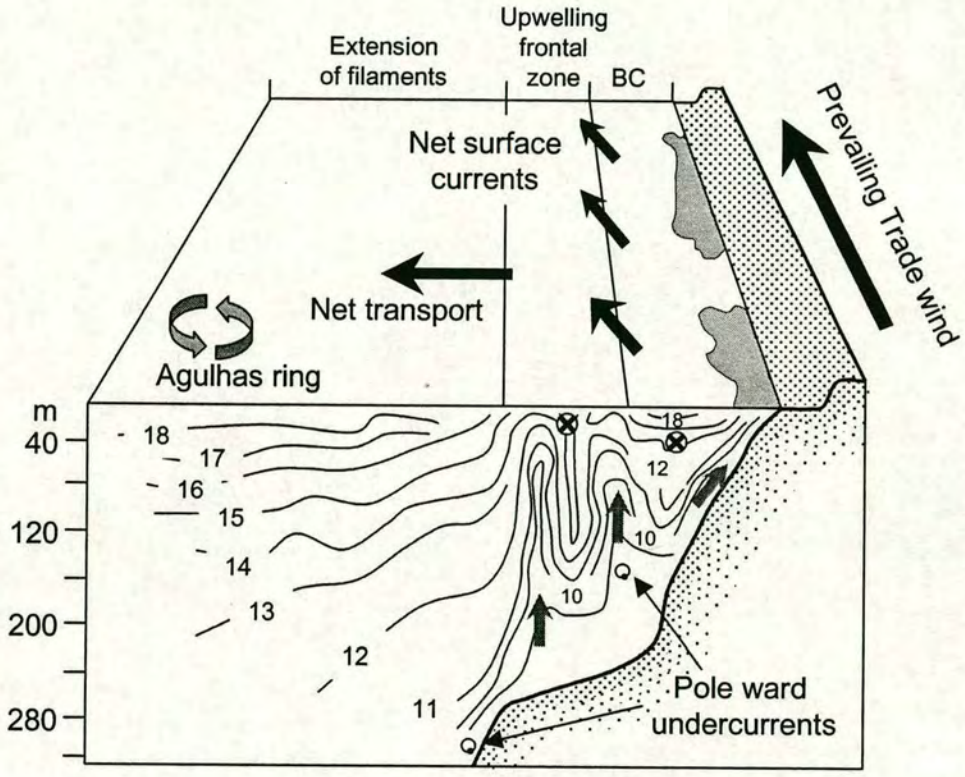

Figure 4.5 Conceptual cross section of the Benguela upwelling system (adapted from Little, 1997; data from Bang, 1971; Barange and Pillar, 1992; Summerhayes *et al.*, 1995). Isotherms in °C, depth in metres. Surface water expressions of upwelling cells are shown in grey and grey arrows represent upwelling. Crossed circles indicate equator ward transport and dotted circles indicate pole ward undercurrents. BC denotes the Benguela Current.

front, the 'coastal jet' (Mooers *et al.*, 1976). This current flows roughly parallel to the coast and the upwelling generating winds.

4.2.2 The Benguela Current Systems

The Benguela region is unique in that it is flanked to the equator and poleward ends by warm water systems. It is the pulsing of these boundaries that give the Benguela much of its character (Shannon *et al.*, 1990). The water mass sources of the Benguela Current (BC) include: Indian and South Atlantic thermocline water; relatively saline, low oxygen tropical Atlantic water; and cooler, fresher subantarctic waters (Gordon *et al.*, 1992). The South Atlantic thermocline and subantarctic inflow is derived mainly from a component of the eastward flowing South Atlantic Current (SAC), which breaks off and flows northward with the BC, thus linking the South Atlantic subtropical gyre (Figure 4.3) to the southern high latitudes (Stramma and Peterson, 1989; Peterson and Stramma, 1991). The BC is confined at 30°S by the topography of the Walvis Ridge and is channelled between this feature and the African coast (Reid, 1989). Within the BC there are eddies mostly derived from the Agulhas retroflection (Shannon, 1985a). The combination of equatorward BC and prevailing south east trade winds results in a voluminous upwelling of cold, nutrient rich subsurface water off the west coast of South Africa and Namibia. This system, referred to as the Benguela upwelling system, extends from 35°S to 17°S, the southern and northern boundaries being controlled by the opposing warm water flow of the Agulhas Current and the Angola Current, respectively.

Research on the coastal upwelling offshore southwest Africa has a long history. A number of detailed reviews on the upwelling systems (Figure 4.6) have been published (Nelson and Hutchings, 1983; Shannon, 1985; Shannon and Pillar, 1986; Shannon, 1996). Broadly, the system can be divided into two according to the duration and timing of upwelling, although each part is composed of a number of upwelling cells (e.g. Dingle, 1995). In the Northern Benguela upwelling System (NBS), north of 27°S, the wind field exhibits relatively little seasonal variation (Shannon, 1985) and upwelling occurs all year round. The zonal wind flow, producing trade winds, is directed south-

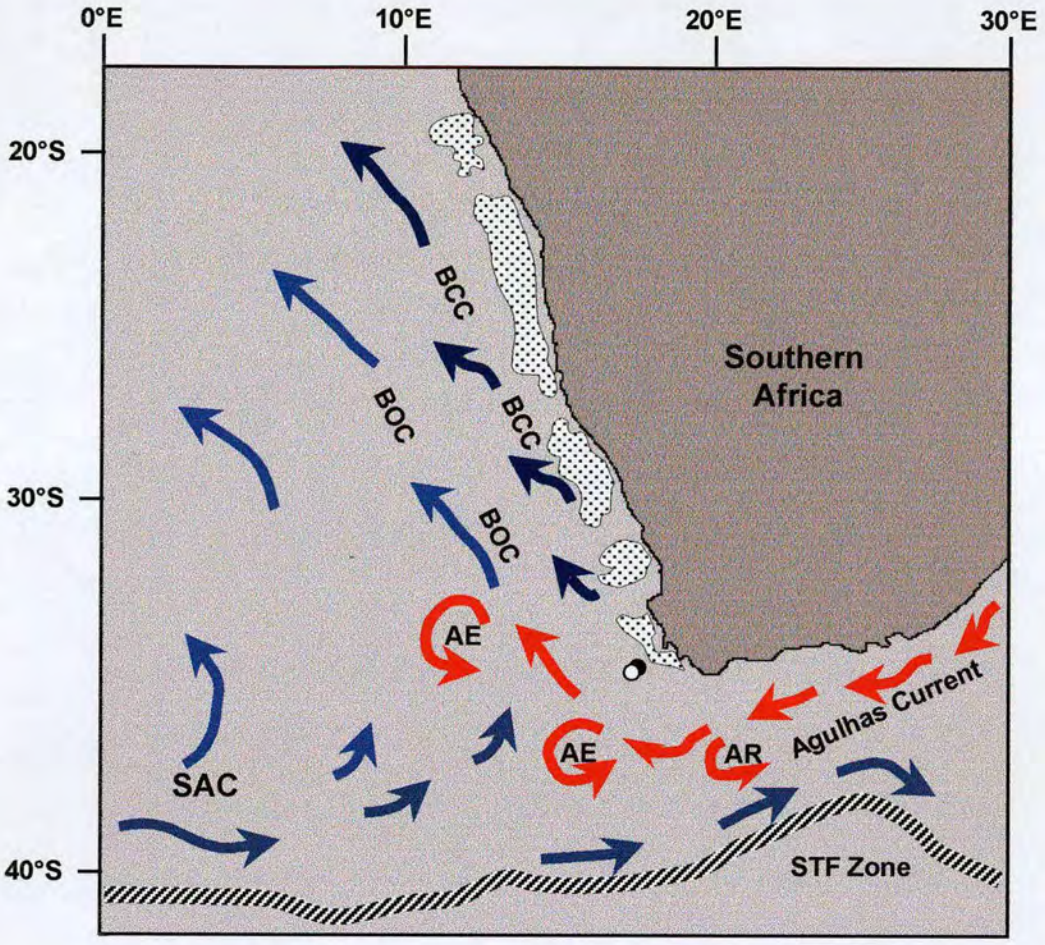

Figure 4.6 Regional surface water circulation (after Stramma and Peterson, 1989; Lutjeharms, 1996). Dotted areas represent individual upwelling cells (after Dingle, 1995). Subtropical convergence (STF) zone average position is indicated after Shannon *et al.* (1990). SAC - South Atlantic Current; BOC - Benguela Oceanic Current; BCC – Benguela Coastal Current (upwelling); AR – Agulhas Retroflection; AE – Agulhas Eddy.
Sediment core locations: O - MD96 2081 (IMAGES); ● - GeoB 3603-2.

east to north-west (i.e. equatorwards) for much of the year. However, to the south, the oceanography of the Southern Benguela upwelling System (SBS) is dominated by the seasonal wind cycle of predominant south-easterly winds in summer and north-westerly winds in winter. Upwelling is highly seasonal as well and more intense than in the NBS, lasting from September to March (Figure 4.7). This implies a strong thermal front and lower sea surface temperatures (SSTs) on the inner shelf during the upwelling season.

4.2.3 Volume transport in the Benguela Region

The first estimates of transport in the Benguela Current were given by Sverdrup *et al.* (1942), who estimated a relative northward transport of 18.7 Sverdrups (Sv) at 1200m at 30°S. Using historical data, Stramma and Peterson (1991) calculated the geostrophic transport of the BC at 32°S to be 21 Sv. Near to where the current separates from the coast at 30°S this transport is 18 Sv. In the 1990s, studies of the magnitude and variability of the large-scale transports in the area were undertaken by Garzoli and Gordon (1996). Their inverted echo sounder data, collected over a period of 16 months, revealed some important results concerning the origin and transport of the waters of the Benguela Current. This time series study showed that, on average, 50% of the BC is derived from the central Atlantic (mainly South Atlantic waters), 25% comes from the Indian Ocean (primarily Agulhas waters), and the remaining 25% is a mixture of Agulhas and subtropical Atlantic waters (Figure 4.8). However, Gordon (1996) states that other water mass studies indicate that Indian Ocean water masses contribute to transport that Garzoli and Gordon (1996) attribute solely to South Atlantic sources.

4.2.4 Upwelling filaments in the Benguela System

It has been shown that productivity in upwelling areas is greatest at the frontal edge of the systems (Dengler, 1985; Lutjeharms *et al.*, 1985), resulting in areas of maximum productivity and biomass outside the coastal upwelling region. Furthermore, Shannon *et al.* (1983) have shown that in the Benguela System phytoplankton blooms occur at the fringes of the active upwelling cell. Satellite pictures of the transition zone

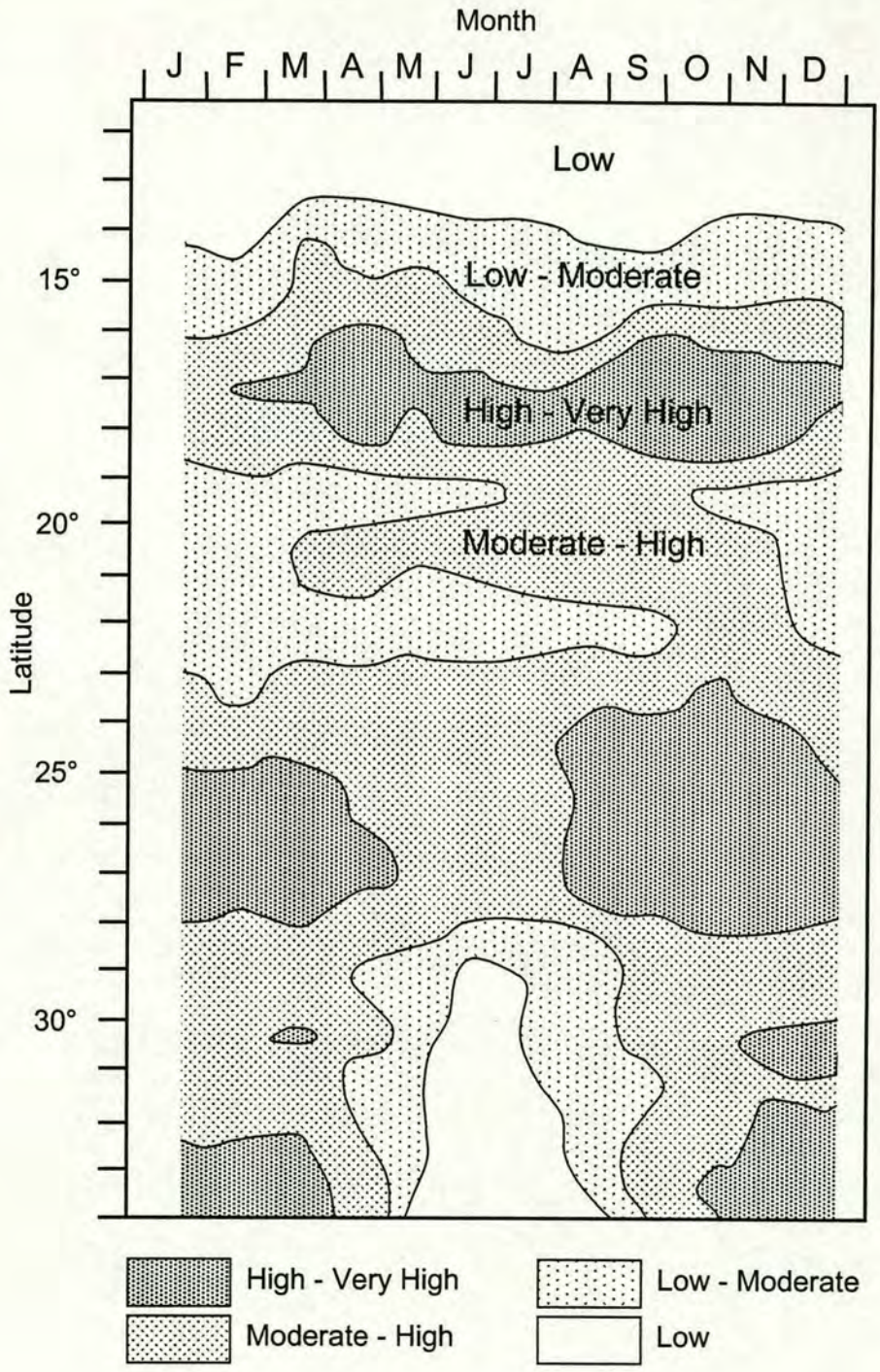

Figure 4.7 Monthly wind stress along the west coast of Africa, centred 40 nautical miles offshore at whole degrees of latitude. After Boyd (1987). Shading (dynes.cm^{-2}): low< 0.2; low-moderate 0.2 - 0.4; moderate - high 0.4 - 0.8; high >0.8.

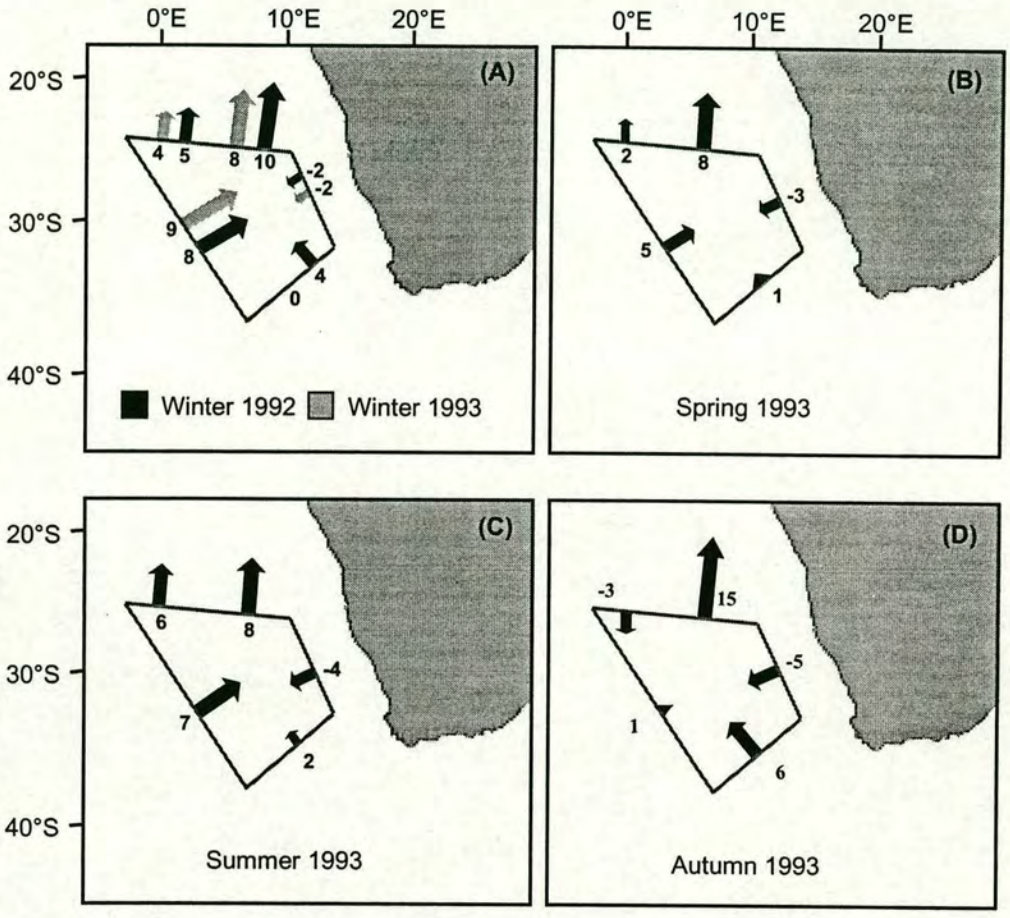

Figure 4.8 Mean surface water seasonal transports in the Benguela System in Sverdrups by austral hemisphere seasons:
A) winters of 1992, 1993, **B)** spring 1993, **C)** summer 1993, **D)** autumn 1993. Drawn from Garzoli and Gordon (1996).

(e.g. Figure 4.9) show that filaments and plumes are an extremely important aspect of coastal upwelling. While the coastal upwelling regime may extend as far as 250km offshore, filaments of cold, high chlorophyll water may extend from the coastal zone up to 750 km offshore (Van Foreest *et al.,* 1984). A filament is a narrow protruberence extending at least 50km from the main thermal upwelling front and is generally narrower than 50km. When filaments coalesce to form a larger feature this is referred to as a plume. The concept of such filaments and plumes originating in the southern Benguela amalgamating to form an extensive plume off the Cape Peninsula has been put forward by Nelson and Hutchings (1983). These features have also been described by a number of authors (Jury, 1985; Shannon *et al.,* 1985b; Taunton-Clark, 1985). Filaments are more extensive off the Cape in summer when upwelling is strongest (Taunton-Clark, 1985). Conditions for plankton growth are ideal, with nutrient rich waters coming to the surface in the summer when light conditions are good. Figure 4.10 illustrates the modern average extent of the main upwelling area and the full extent of upwelling filaments. The sediment cores used in this study lie within the influence of these features in the system. Lutjeharms and Stockton (1987), in detailed investigation of the kinematics of the Benguela upwelling front, concluded that the extensive area seawards of and parallel to the coastal upwelling zone is an extremely important component of the total productivity of the total upwelling regime. In addition, they observed eddies in the frontal zone between the southern Benguela system and the Agulhas Current. The catalyst for the shedding of these upwelling eddies is the presence of warm Agulhas water which is preferentially advected along the western shelf edge of the Agulhas Bank into the southern reaches of the upwelling zone.

4.2.5 Input of subantarctic waters into the Benguela

Intrusions of subantarctic waters in the southern Benguela region, such as that described by Shannon *et al.* (1989), are associated with 'cold wedges' that develop occasionally as a perturbation in the subtropical front in the vicinity of the Agulhas Ridge (Figure 4.11). The 'cold wedge' has also been noted by Lutjeharms and Meeuwis (1987) and Lutjeharms and Ballegooyen (1984), who suggested that it is caused by a baroclinic instability in the circumpolar front induced by the topography of the Agulhas Ridge. Cool events, while potentially as important as warm ones, have received

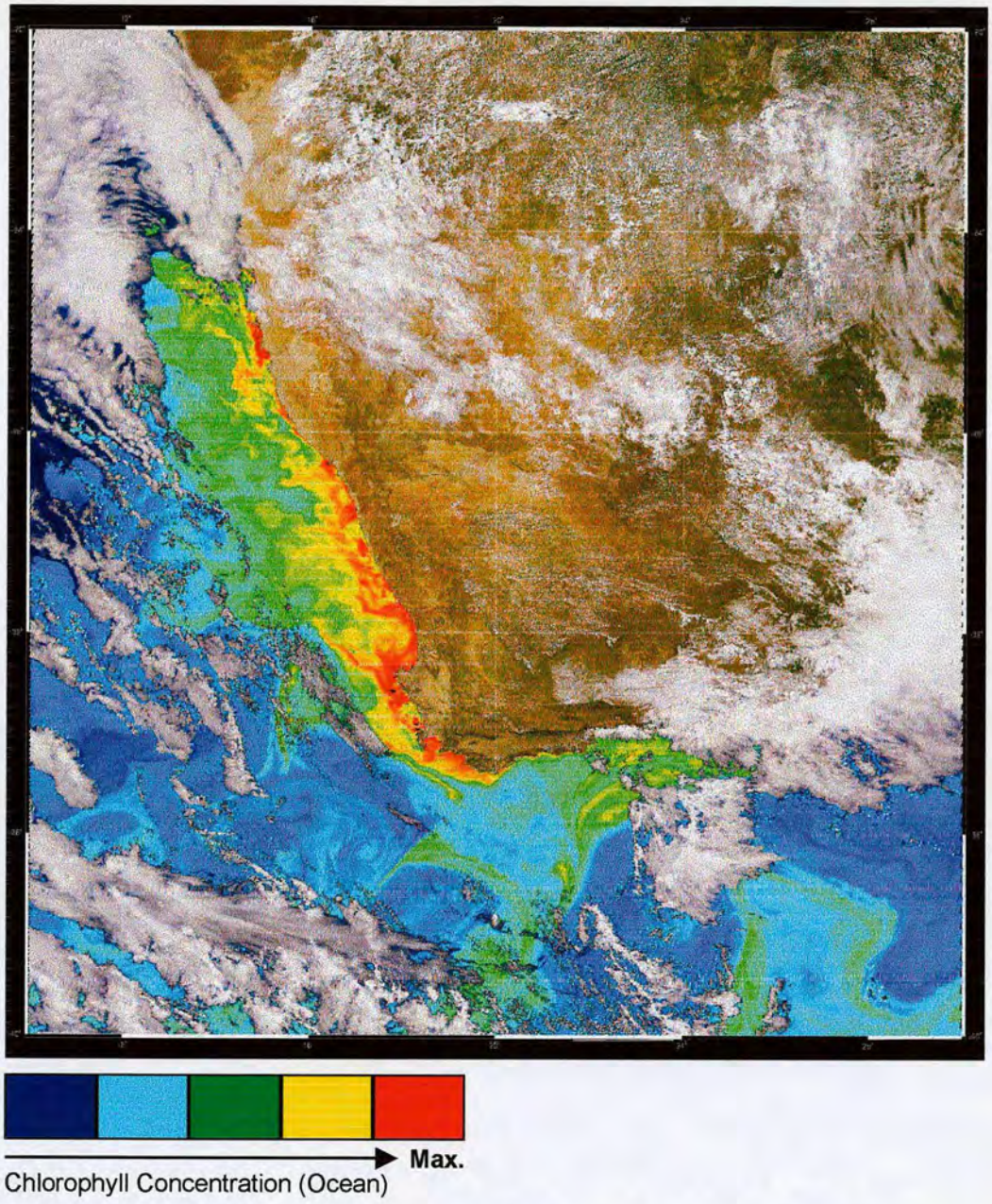

Figure 4.9 SeaWiFs image of chlorophyll concentrations in the south-east Atlantic. Coastal upwelling and upwelling filaments clearly visible. Agulhas eddies can also be seen entering the system from the south-west. Image provided by SeaWiFS Project, NASA/Goddard Space Flight Center and ORBIMAGE.

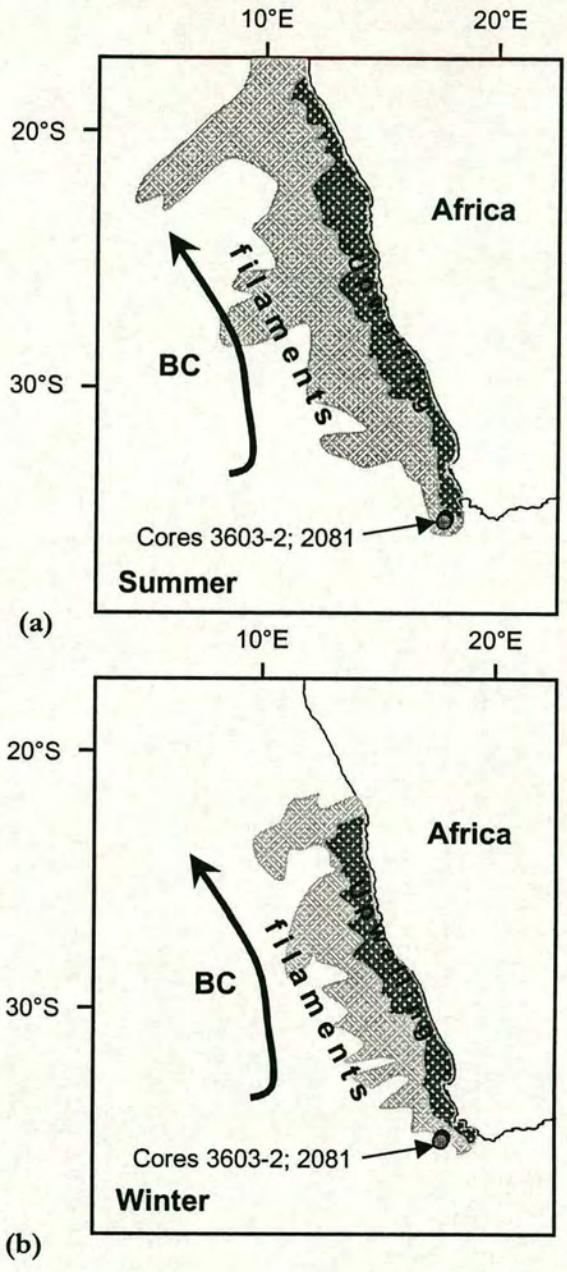

Figure 4.10 Modern extent of upwelling and filaments in the Benguela System. Average borders to the main upwelling area (dark shading) and the full extent of upwelling filaments (lighter shading) for a) February and b) August. Based on METEOSAT II data after Lutjeharms and Stockton (1987). Sediment cores denoted by dots. MD96 2081 (grey) and GeoB 3603-2 (black).

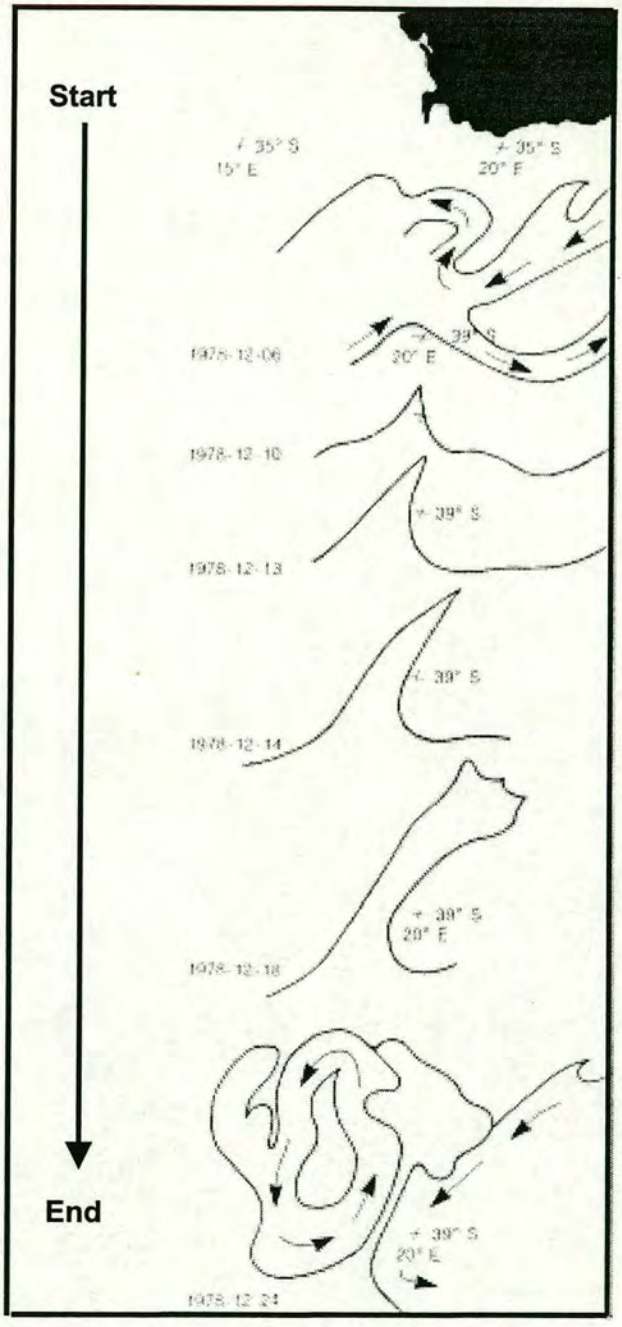

Sequence of events over 17 days in December 1978:

1. 6th Dec. 1978

Perturbation between STC and AR, embryo wedge of cold water (shaded) forms.

2.

3.

Wedge becomes more pronounced.

4. 14th December 1978

Cold wedge (shaded) of subantarctic water fully formed .

5. 18th December 1978

Subantarctic waters are pushed northward into the wedge between two warm eddies.

6. Christmas Eve 1978

Input of cold, subantarctic water eddy into Benguela region, As the wedge is pinched off from source waters by Agulhas rings.

Figure 4.11 Development of a perturbation in the Subtropical Convergence (STC) and Agulhas Retroflection (AR) resulting in an injection of subantarctic water (shaded) between Agulhas eddies into the Benguela region (after Shannon *et al.*, 1989). Dates are shown in the following format: year-month-date.

relatively little attention (Shannon *et al.*, 1990). Taunton-Clark (1990) commented that the cooling observed in 1928 and 1955 may have been associated with changes in the Subtropical Front (STF) and in the easterly winds.

4.3 THE AGULHAS CURRENT

4.3.1 An ocean 'hotspot'

The SBS is located at the gateway for inter-ocean exchange between the Indian and Atlantic Oceans. This exchange of water masses, heat, and salt, and the processes which govern it, has been the subject of numerous studies (Gordon, 1985, 1986; Lutjeharms, 1996; Garzoli *et al.* 1996). Changes in the magnitude and intensity of the transport flux between these two regions were linked with climate related issues by Gordon (1996). It is possible that this 'inter ocean exchange' forms a junction in the global thermohaline circulation ('conveyor belt'; Broecker *et al.* 1985; Broecker, 1991; Gordon *et al.*, 1992, Macdonald and Wunsch, 1996). Input to the Benguela from the Agulhas System seems to be controlled by small changes in the wind field in the Indian Ocean and south of Africa (Lutjeharms and van Ballegooyen, 1988). Together with watermasses from the South Atlantic, the warm, saline waters of the Agulhas Current advect northward with the Benguela Current. Changes in the circulation south of Africa have important implications both for and global climate change. Section 4.1.2 reviews the literature which deals with the transfer of surface waters from the Pacific and Indian Oceans to the Atlantic which are required to compensate for the export of NADW.

4.3.2 Significance of Agulhas input

Through a process of rings, eddies, and filaments detaching from the Agulhas Retroflection (Lutjeharms, 1981; Shannon *et al.*, 1990; Lutjeharms and van Ballegooyen, 1984; Gordon and Haxby, 1990; van Ballegooyen *et al.*, 1994) pulses of warm, saline water enter the Atlantic (Figure 4.12). As previously stated, the thermohaline fluxes of the BC are an important feature of the meridional circulation of the South Atlantic, as they more or less balance the poleward flow of warm, saline water in the Brasil Current. Garzoli *et al.* (1996), using the 10°C isotherm as a proxy for the thermocline, found

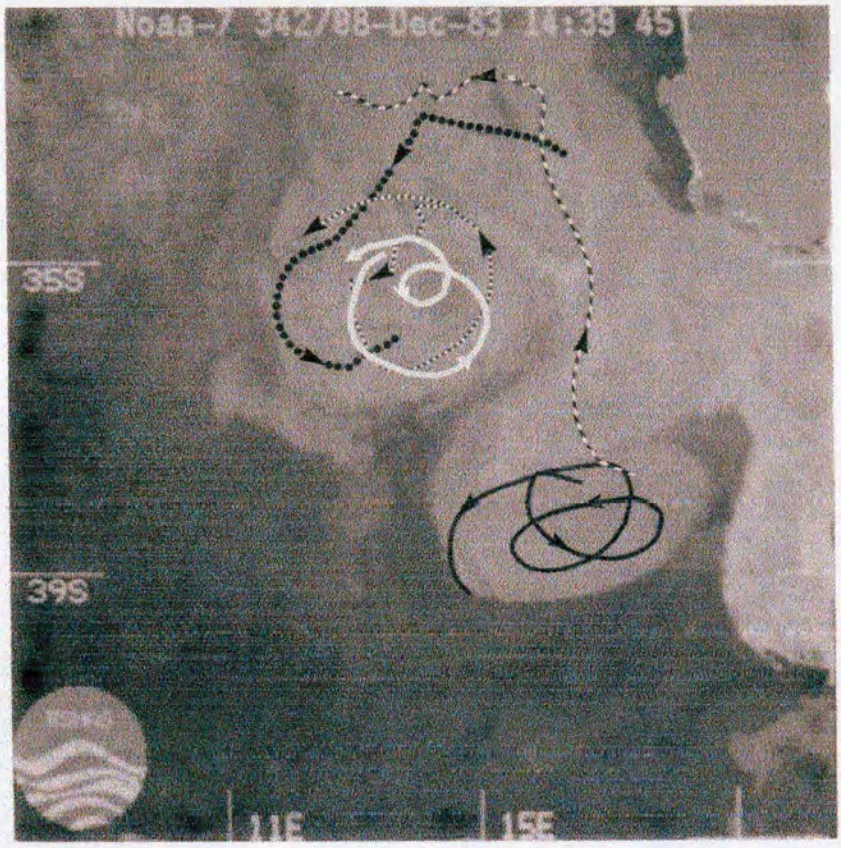

Figure 4.12 Sea surface temperature images showing the extent of Agulhas eddies in the south east Atlantic. Image is derived from a NOAA-7/AVHHR with superimposed ARGOS drifter trajectories on a Mercator projection. The image is a composite of images from 7 and 9 December, 1983. The enhancement used in the image is coded such that warmer waters are light and colder temperatures are darker shades of grey. The trajectories of the five drifters for ±10 days centred on the mean date of the image, 8 Dec 1983. The coastline of Africa is shown in the top right (after Olson and Evans, 1983).

some very significant results. When they compared the transport of the BC and the salinity at the thermocline level they found a positive correlation. In general, when northward transport is increasing the thermocline salinity also increases. This indicates that the BC increases in strength by incorporating more subtropical water. Agulhas input is the most effective factor in increasing the salinity of the upper thermocline in the Benguela region. South Atlantic Current water, the other main source, being lower in salinity (Gordon *et al.*, 1992; Olson *et al.*, 1992) than the Agulhas Current. Garzoli *et al.* (1996) suggested that variations in the BC transport are related to Agulhas water input. This input is determined by the eddy field generated at the Agulhas Retroflection (Byrne *et al.*, 1995).

4.3.3 Physical oceanography of the Agulhas Current

The Agulhas Current is a major western boundary current in the Indian Ocean (Figure 4.6) which flows poleward along the continental shelf off eastern Africa. The original survey by Rennell (1778) of the Agulhas Current is one of the pioneering works in oceanography. At the Agulhas retroflection, the main stream of the Agulhas periodically pinches and sheds rings (Lutjeharms and Gordon, 1987; Olson and Evans 1986; Shannon *et al.*, 1990). The Agulhas is unique compared to the other ring formation regions (Olson and Evans, 1986), due to the termination of the continent prior to boundary current separation from it (cp. Benguela Current). The Agulhas makes an elongated retroflection loop into the South Atlantic before returning back into the Indian Ocean, (Figure 4.6; Lutjeharms, 1981; Olson and Evans, 1986; Lutjeharms and Gordon, 1987; Lutjeharms and Valentine, 1988).

4.3.4 Agulhas Rings and eddies

The frequency of Agulhas ring and eddy shedding is uncertain. Lutjeharms and Valentine (1988) estimate that an average of 9 rings per year are produced. Byrne *et al.* (1995) estimate an average of 6 per year. The discrepancy may be the result of some Agulhas eddies returning eastward and not entering the region of study of Byrne *et al.* (1995). Figure 4.13 shows the persistent nature of this feature as it pulses into the southeastern Atlantic. The energy flux a ring contributes to the South Atlantic is 7% of the annual wind input over the entire basin (Olson and Evans, 1986). Each Agulhas

eddy that enters the South Atlantic will contribute not only energy but heat and salt to the thermocline waters. Figure 4.14 shows an 'eddy corridor' produced by Garzoli and Gordon (1996) which summarises the mean route taken by the rings in the south-east Atlantic. Van Ballegooyen *et al.* (1994) calculated that one well sampled eddy produced a salt flux of 2.5 x 10^6 kg s^{-1} with a corresponding heat influx of 0.045 PW (for six eddies per year). Agulhas rings are thus a significant component of the Indian/South Atlantic interbasin exchange and of the South Atlantic thermohaline flux.

4.3.5 The Agulhas Retroflection

Several attempts to model the Agulhas Retroflection have been published (de Ruijter and Boudra, 1985; de Ruijter, 1982; Lutjeharms and Ballegooyen, 1988). In summary, this work reveals that the volume transport of the Agulhas Current itself may determine the actual position of the retroflection and leakage into the southeastern Atlantic. Observations of the position of the retroflection have been measured by satellite and from ships. The strong thermal gradients in the retroflection area (which can exceed 4°C in 10km in some cases) mean that establishing the location of this feature is not difficult. The model of Lutjeharms and van Ballegooyen (1988) predicts greater westward penetration of the current for low volume transports before retroflecting, and further eastward positions for larger transports. De Ruijter (1982) and de Ruijter and Boudra (1985) modelled the Agulhas system in relation to the large-scale wind circulation. This work demonstrates that the leakage into the Atlantic is largely controlled by the 'wind stress curl'. A southward shift of the westerlies of less than 120km was shown to decrease transport in the Current and at the same time to decrease the isolation of the subtropical gyres in both the South Atlantic and Indian Oceans. In addition, there could be a seasonal dimension, Gründlingh (1978) proposed that westernmost retroflections could take place during the summer months when the flow of the Agulhas Current is assumed to be weakest. Furthermore, Lutjeharms and Ballegooyen (1984) observed a westward penetration of the Agulhas Current in the summer months from satellite images, but noted that observations were severely hampered by the amount of cloud cover. However, the results of the inverted echo sounder survey presented by Garzoli and Gordon (1996) suggest that the BC receives a

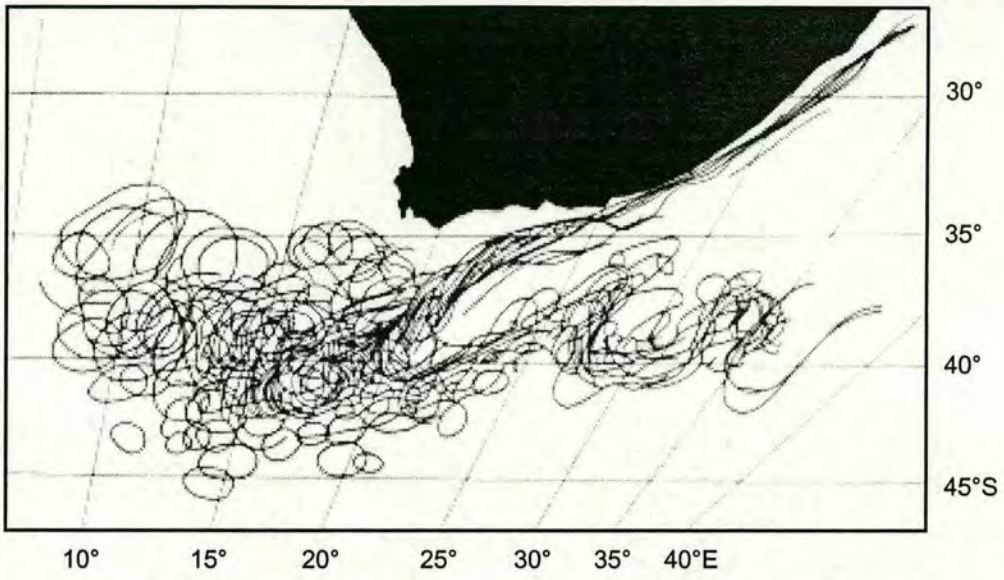

Figure 4.13 Boundaries of the Agulhas Current during one year from December 1984 to December 1985. Data are derived from METEOSAT images in the thermal infrared. One image per 12 day period was used. (After Lutjeharms and Ballegooyen, 1988).

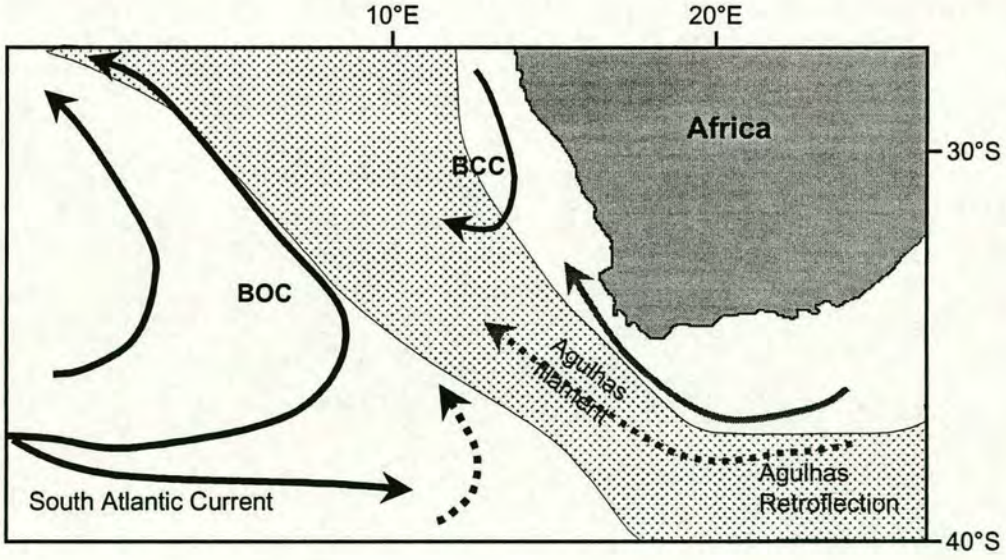

Figure 4.14 Corridor (shaded) along which Agulhas Eddies migrate into the Atlantic. BOC = Benguela Oceanic Current, BCC = Benguela Coastal Current. (After Garzoli and Gordon, 1998).

greater Agulhas input during the autumn. In summer and winter there is a mainly South Atlantic input to the BC (Figure 4.8). Furthermore, transport to the BC from the coastal region is at a maximum during the summer months (-4 Sv) and autumn (-5 Sv), when the upwelling winds favour this offshore circulation. In the Agulhas retroflection area maximum transport to the BC, during the period studied, is during the autumn (6 Sv) and minimum during the summer (2 Sv) (Garzoli and Gordon, 1996). The difficulty in establishing a seasonal picture of the retroflection lies in the complexity of eddies as ocean features. It may be that an early retroflection in the summer weakens the link with the Benguela with the result of less Agulhas water input into the BC.

4.3.6 Conditions for strong (modern) intrusion of Agulhas waters into the Benguela System: case study of 1986

It is well established that there is a flow of surface water in the form of rings and eddies from the Indian to the South Atlantic Ocean around the Cape of Good Hope (section 4.3.4). The water is generally modified rather than pure Agulhas water. Less frequently observed is the movement of a large mass of pure Agulhas water close to Cape Town into the Benguela region. These were termed Agulhas intrusions by Shannon *et al.* (1990). In 1986 there was a progressive weakening of the trade winds, i.e. a substantial relaxation in the driving force of the Agulhas Current (Shannon *et al.*, 1990). It should thus follow that there would have been a corresponding decrease on the supply of water to the Agulhas Current and a decrease in its volume transport. The extended period of reduced westerly currents in 1986 was a consequence of abnormally strong circulation south east of Africa and poleward displacement of the atmospheric circumpolar Westerlies (Shannon *et al.* 1990). Satellite images reveal that there was widespread (240 km wide zone), and persistent influx of Agulhas waters into the Benguela region in winter (austral) 1986, which contrasted sharply with that of other years (Shannon *et al.*, 1990). In the same paper, SST profiles at 34°S (offshore Cape Town), show an intense temperature front (4°C in 20 km) and reveal the SST increase associated with the intrusion. The recorded SSTs of 19 to 20°C approximate ambient summer SST in the area (Levitus and Boyer, 1994). Shannon *et al.* (1990) suggest that the 1986 shift in wind patterns, and the associated reduction in Agulhas volume

transport, provided suitable conditions for increased flow of Agulhas Current waters around the Cape of Good Hope into the southeastern Atlantic. This finding is consistent with model predictions. For example, the significance of the location of the retroflection is revealed by modelling experiments of Lutjeharms and van Ballegooyen (1988). This work shows that the most westerly retroflections occur for lower volume transports of the Agulhas Current. The strong Agulhas intrusion described above was the cause of 1986 being the warmest year on record in the twentieth century in the extreme south east Atlantic. The extensive SST anomaly in the region was followed by monthly rainfall anomalies 200 – 600% above normal over much of central and western Africa, statistical analyses of available data confirm this positive association (Walker, 1990).

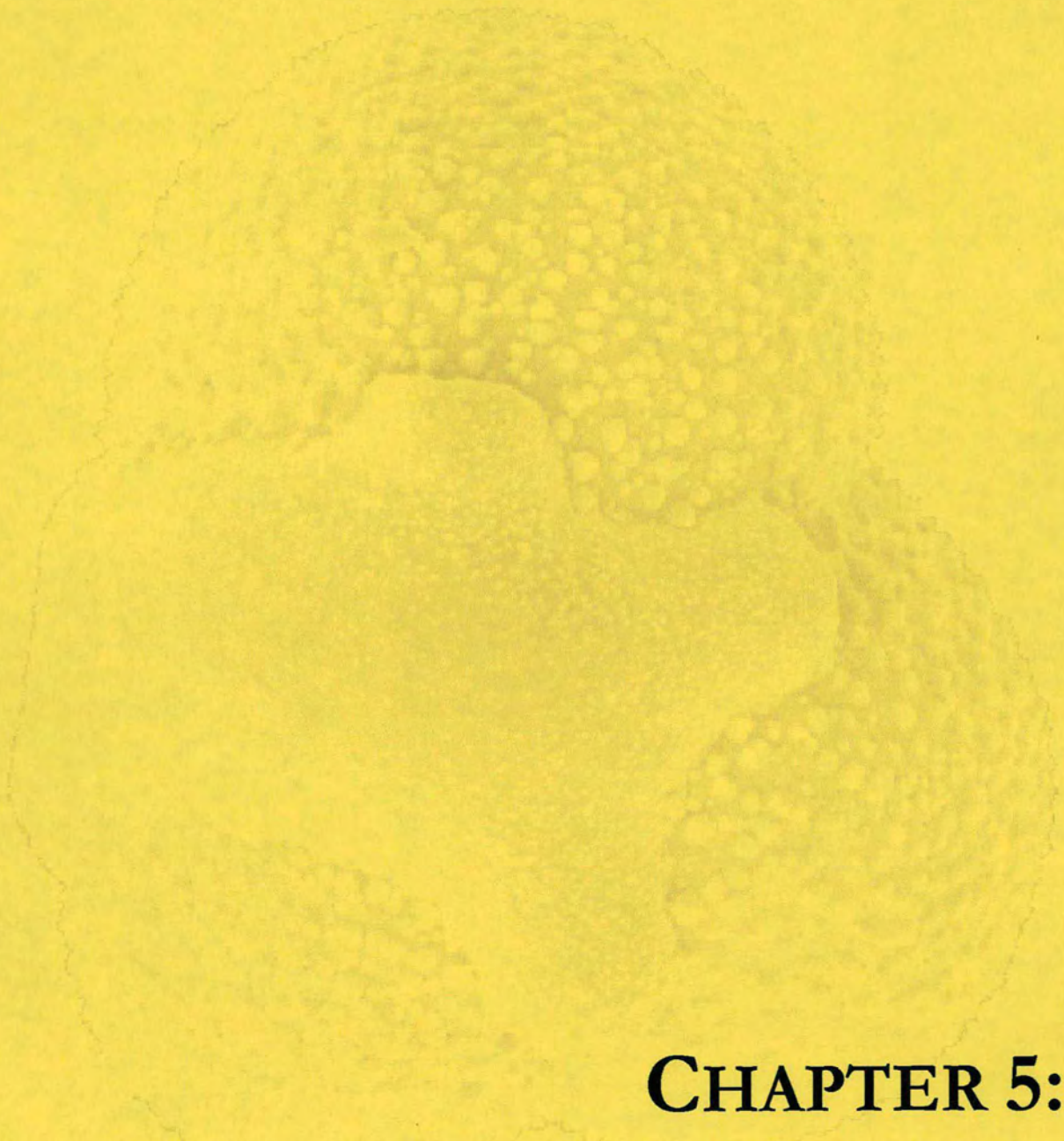

CHAPTER 5: FORAMINIFERAL ASSEMBLAGES

CHAPTER 5: PALAEOCEANOGRAPHY OF THE SOUTHERN CAPE BASIN BASED ON PLANKTONIC FORAMINIFERAL ASSEMBLAGE WATER MASS INDICATORS

5.1 PLANKTONIC FORAMINIFERA RECORD FROM THE CAPE BASIN SPLICED RECORD (CORES GEOB 3603-2/MD96 2081)

5.1.1 Observed planktonic foraminifera taxa

The preservation of the highly abundant planktonic foraminifera contained in cores GeoB 3603-2/MD96 2081, which constitute the spliced Cape Basin record, is very good. The excellent condition of the calcareous microfossils of this study, coupled with the results of recent studies that document the reliability of planktonic foraminifers as tracers of present water masses in the Southeast Atlantic (Giraudeau, 1993; Niebler and Gersonde 1998; Ufkes *et al.*, 1998), suggest that the downcore distribution of species assemblages may allow for precise reconstructions of surface circulation changes around the tip of southern Africa.

The planktonic foraminifera census data are described below and presented in Appendix 3. Core GeoB 3603-2 was examined at 5cm intervals from 8 to 1133 cmbsf. Core MD96 2081 was sampled at 5cm intervals in the middle section of the core, from 963 to 2113 cmbsf. The methods used are described in Section 2.1.3. The data from these two cores were examined and spliced to produce a long record from the Cape Basin. The method and procedures used to splice the records are described in section 3.2.2. The splice-point, where the cores were joined, is at the peak of MIS 7.5 (Figure 3.2). Eighty six of the samples from the bottom of core GeoB 3603-2 (708 cm to 1133cm) are not included in the spliced Cape of Good Hope record, whilst the top four samples (963 to 978 cmbsf) were removed from the IMAGES core MD96 2081.

Thirty species (Table 5.1) were identified throughout the 453 samples used for planktonic foraminiferal census counts. Species diversity is high, reflecting the hydrography of the southern Cape Basin, which is an area of the South Atlantic where several major watermasses converge (described in Chapter 2). The planktonic foraminifera assemblages of cores GeoB 3603-2 and MD96 2081 are dominated by six species, viz *Neogloboquadrina pachyderma* (dextral coiling) (Ehrenberg); *Globorotalia inflata* (d'Orbigny); *Globigerina bulloides* d'Orbigny; *Globigerinita glutinata* (Egger); *Globigerinoides*

ruber (d'Orbigny); and *Globorotalia truncatuliniodes* (d'Orbigny). These species constitute ~90% of the total assemblage and their down core abundances are shown in Figure 5.1. The dominance of these taxa down core is consistent with the distribution of planktonic foraminifera in surface sediments in the vicinity of the spliced cores (Giraudeau, 1993). Cores GeoB 3603-2 and MD96 2081 are located seaward of the boundary of active coastal upwelling, and below the main Benguela Drift, within a mixing zone of old, upwelled and oligotrophic waters (Figure 4.6). Twenty four further species are found with average frequencies lower than 3%. Summary statistics describing each species observed are listed in Table 5.1.

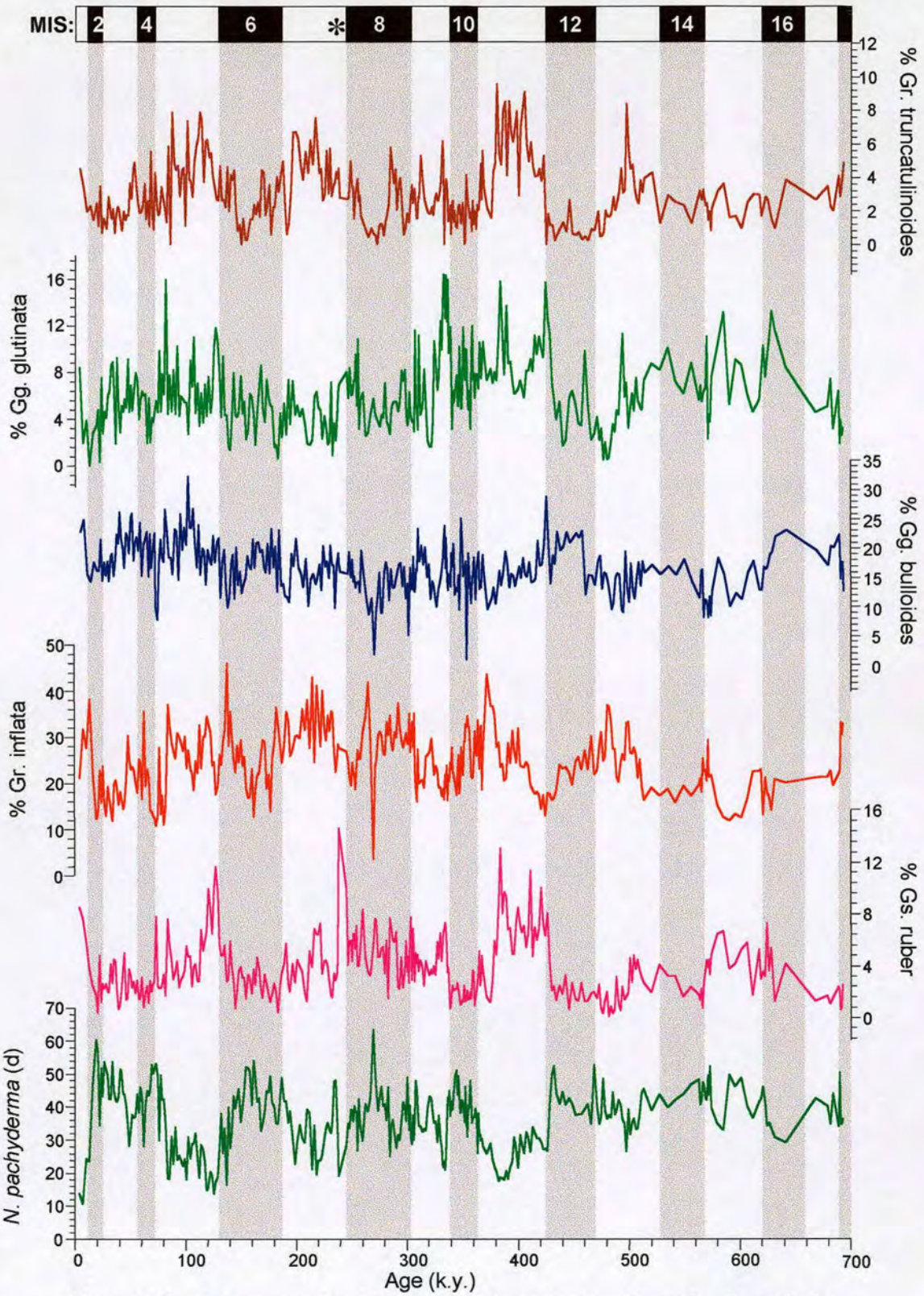

Figure 5.1: Downcore adundance of the six major taxa from the Cape Basin spliced record. Splice-point indicated by asterisk. Glacial periods are shaded. Planktonic foraminifera census data are presented in Appendix 3.

	Spliced Record		GeoB 3603-2		MD96 2081	
	Mean %	Max %	Mean %	Max %	Mean %	Max %
C. nitida	-	. 25	-	. 25	-	-
Gg. bulloides	16. 4	32. 2	17. 2	32. 2	15. 3	28. 8
Gg. calida	0. 1	2. 6	0. 1	2. 6	-	0. 8
Gg. digitata	-	1. 2	-	0. 3	0. 1	1. 2
Gg. falconensis	0. 7	4. 0	0. 5	3. 1	0. 8	4. 0
Gg. rubescens	0. 1	2. 8	0. 1	0. 7	0. 1	2. 8
Ge. siphonifera	0. 8	3. 8	1. 0	4. 2	0. 6	2. 6
Ga. glutinata	6. 2	16. 4	5. 1	16. 0	6. 9	16. 4
Ga. uvula	-	0. 7	-	0. 4	-	0. 7
Gs. conglobatus	0. 1	2. 1	0. 1	2. 1	0. 1	2. 0
Gs. ruber	3. 7	14. 5	3. 5	11. 6	3. 9	14. 5
Gs. ruber (pink)	-	0. 9	-	0. 3	-	0. 9
Gs. sacculifer	1. 0	6. 5	1. 0	6. 5	0. 8	3. 6
Gs. tenellus	-	1. 5	-	1. 5	-	1. 0
Gr. cavernula	-	0. 6	-	0. 6	-	0. 3
Gr. crassaformis	0. 9	4. 8	0. 9	4. 9	0. 9	4. 7
Gr. hirsuta	0. 3	3. 7	0. 4	3. 7	0. 2	1. 7
Gr. inflata	24. 5	45. 9	26. 4	45. 9	24. 5	43. 6
Gr. menardii	0. 2	1. 7	0. 1	1. 7	0. 2	1. 7
Gr. scitula	1. 0	4. 0	0. 9	3. 9	1. 0	4. 0
Gr. theyeri	-	0. 5	-	-	-	0. 5
Gr. truncatulinoides	2. 9	9. 6	3. 1	7. 9	2. 8	9. 6
G. hexagonus	0. 3	2. 3	0. 3	2. 5	0. 3	2. 1
N. dutertrei	1. 3	6. 1	1. 0	6. 1	1. 4	5. 7
N. pachyderma (d)	36. 4	63. 3	36. 6	60. 2	36. 6	63. 3
N. pachyderma (s)	1. 2	13. 3	0. 3	2. 5	1. 7	13. 3
O. universa	1. 1	6. 3	1. 3	6. 3	1. 0	6. 0
P. obliquiloculata	-	1. 1	0. 1	1. 1	-	0. 6
S. dehiscens	-	0. 3	-	0. 3	-	-
T. quinqueloba	0. 6	5. 1	0. 3	5. 1	0. 7	3. 3

Table 5. 1 Planktonic foraminifera abundance for cores GeoB 3603-2, MD96 2081, and Cape Basin spliced record. Full species descriptions and references are given in Appendix 1, assemblage data is presented in Appendix 3.

5.2 DOWNCORE DISTRIBUTION OF DOMINANT AND SUBORDINATE TAXA

For comparison, the observed planktonic foraminiferal species are divided into the basic water mass types (cold and warm) according to Bé and Tolderlund (1971). However, the distribution of planktonic foraminifera is not governed by temperature regime alone. Studies such as those of Thiede (1975), Prell and Curry (1981) and Kroon (1991) brought the dominance of temperature into question, with typically subpolar and polar species such a *Gg. bulloides* and *N. pachyderma* (sinistral coiling) being found in tropical upwelling areas. The results described below reinforce the idea that species distribution is governed by nutrient levels and not temperature alone (Reynolds and Thunnell, 1985; Kroon and Ganssen, 1989). The general geographical and geological distribution patterns of planktonic foraminifera are in fact governed by the environmental interactions between temperature, salinity, ocean currents, seasonality, and nutrient distributions which together form ecosystems to which specific planktonic foraminiferal species are associated. The relative combination of the thirty species identified in the sediment core samples from the southern Cape Basin will provide a huge amount of environmental information (Hale and Pflaumann, 1999), providing an insight into the past palaeoceanography of the area.

5.2.1 'Cold water' forms

According to the classification of Bé and Tolderlund (1971), the following species are characteristic of subpolar environments: *N. pachyderma* (d); *Gg. bulloides*; *Turborotalita quinqueloba* (Natland); *Globorotalia scitula* (Brady); and *Globorotalia cavernula* (Bé); the latter is a rare species which is found only in subantarctic waters of the southern hemisphere. *N. pachyderma* (s) is described as a polar species (Figure 5.2). All these species are identified in the Cape Basin spliced record, but not all can be described as a distinct 'cold' species. The planktonic foraminifera identified are illustrated in Plates 1, 3 and 4.

N. pachyderma (d), illustrated in Plate 1, constitutes the largest average fraction of the fossil record. It is recorded in every sample downcore and has a mean abundance of 36.4% in the spliced record, and 36.6% in both core GeoB 3603-2 and MD96 2081. *N. pachyderma* (d) exhibits frequency oscillations that switch abruptly between two extremes: <25% to >50%. This species is the dominant form during cold intervals represented by

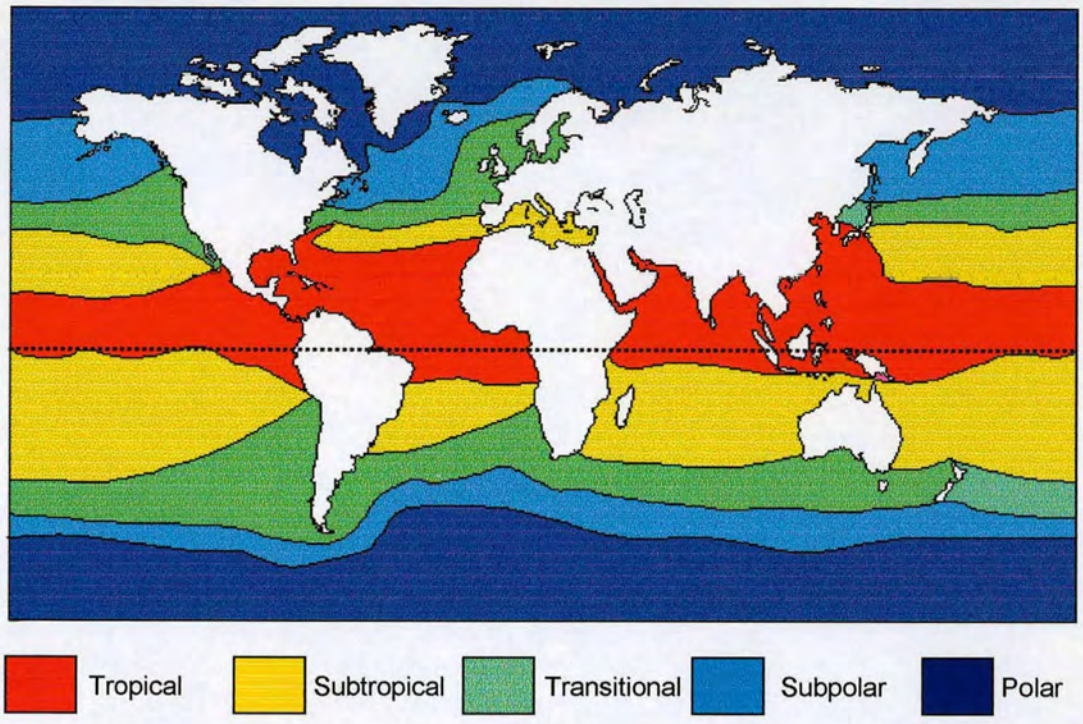

Figure 5.2 Five world distribution zones of planktonic foraminifera according to Bé and Tolderlund (1971). Dashed line represents the geographical equator.

MIS 2/4, 6, 8, 10, 12, and 14 (Figure 5.1). During these intervals *N. pachyderma* (d) makes up between 40% and ~63% of the assemblage. During warm intervals *N. pachyderma* (d) generally exhibits frequencies lower than 30%. The two highest values are recorded at 269 ka B.P. during MIS 8, (63. 3%) and at 19 ka B.P. in MIS 2 (60.2%). After MIS 12, the record of % *N. pachyderma* (d) shows clear glacial – interglacial variations. Prior to MIS 12, the differences between glacial and interglacial stages are not as extreme. MIS 16 records very low values of *N. pachyderma* (d), whilst the interglacials of this time period show values that are comparable to subsequent glacial periods.

According to the classification of Bé and Tolderlund (1971), *N. pachyderma* (d) is characteristic of subpolar environments, but it is also significant in transitional waters (Bé, 1969). *N. pachyderma* (d) flourishes in cold surface waters with a poorly developed or shallow thermal stratification (Chapman *et al.,* 1996). The preferred temperature range is between 10 and 18°C (Bé and Tolderlund, 1971). Distribution maps of living planktonic foraminifera (Bé and Tolderlund, 1971) show this species maximum occurrence in the southern hemisphere along the southwest African continental margin, with highest numbers in the NBS (Northern Benguela System). The relative abundance in surface sediments of the SBS (Southern Benguela System) is high relative to its presence in the water column (Giraudeau, 1993). Sinistral coiled *N. pachyderma* dominates over dextral in modern assemblages of the seasonal upwelling regime of the SBS. The planktonic foraminifera distribution of planktonic foraminifera in core top sediments of the Benguela region is illustrated in Figure 5.3, which has been generated from Giraudeau (1993). This map shows that *N. pachyderma* (d) exhibits highest abundance in the frontal zone between coastal upwelling cells and the oligotrophic waters of the South Atlantic Subtropical Gyre.

Gg. bulloides (Plate 1) exhibits high variability in relative abundance, with maximum frequencies of ~30% (Figures 5.1 and 5.4). Average abundance for the spliced record is 16.4% and reaches a maximum of 32.2% at 101 ka B.P. during interglacial MIS 5. No clear relationships exist between this variability and the climatic oscillations based on oxygen isotopic changes. *Gg. bulloides* is typically a subpolar species, with maximum abundance in the South Atlantic occurring in a latitudinal belt between 55°S and 40°S (Bé and Tolderlund, 1971). According to Ottens and Nederbragt (1992), *Gg. bulloides* is a nutrient opportunistic species characteristic of spring blooms. *Gg. bulloides* is the

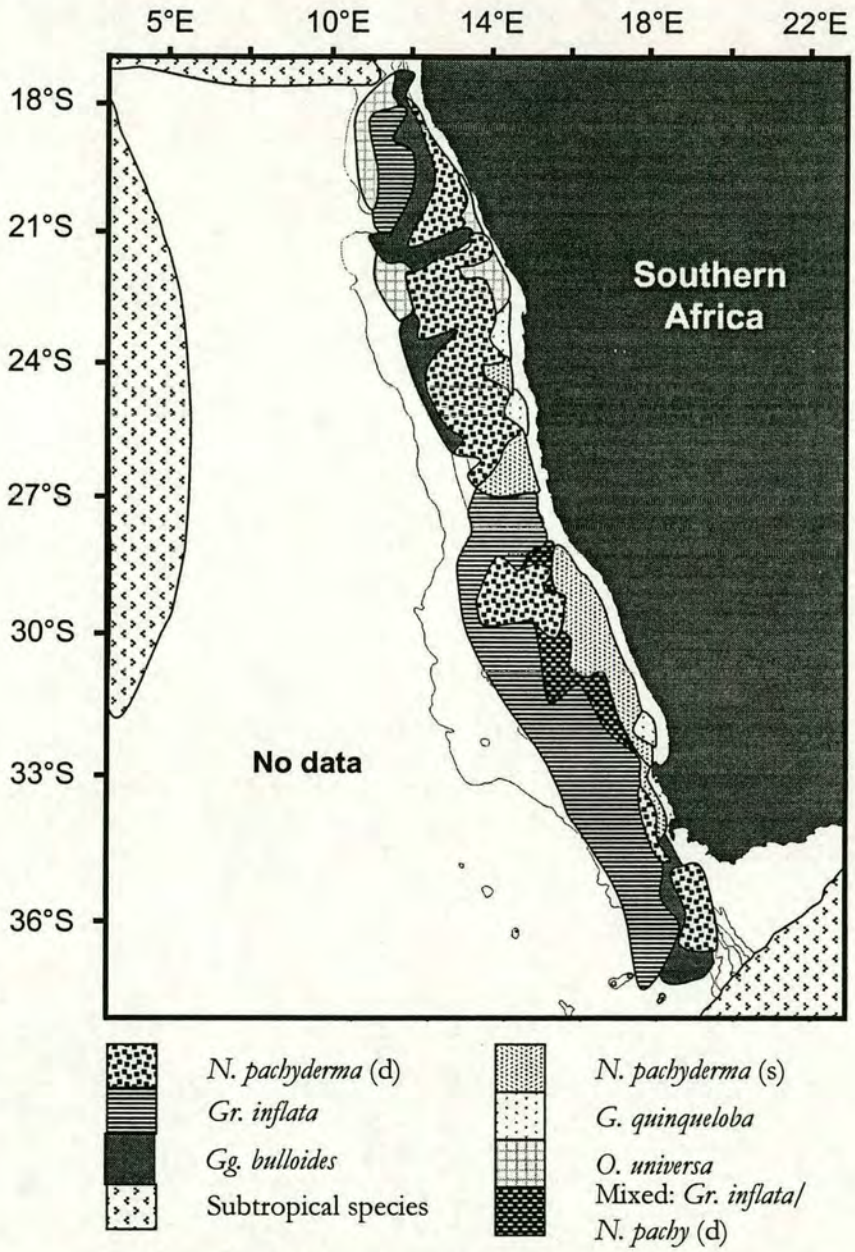

Figure 5.3: Distribution map of key planktonic foraminifera taxa (>20% total) in the south east Atlantic, Giraudeau (1993). Subtropical species after Van Leeuwen (1989); Schmidt (1992); and Ufkes *et al.* 1998). There is no published foraminiferal data for the unshaded area.

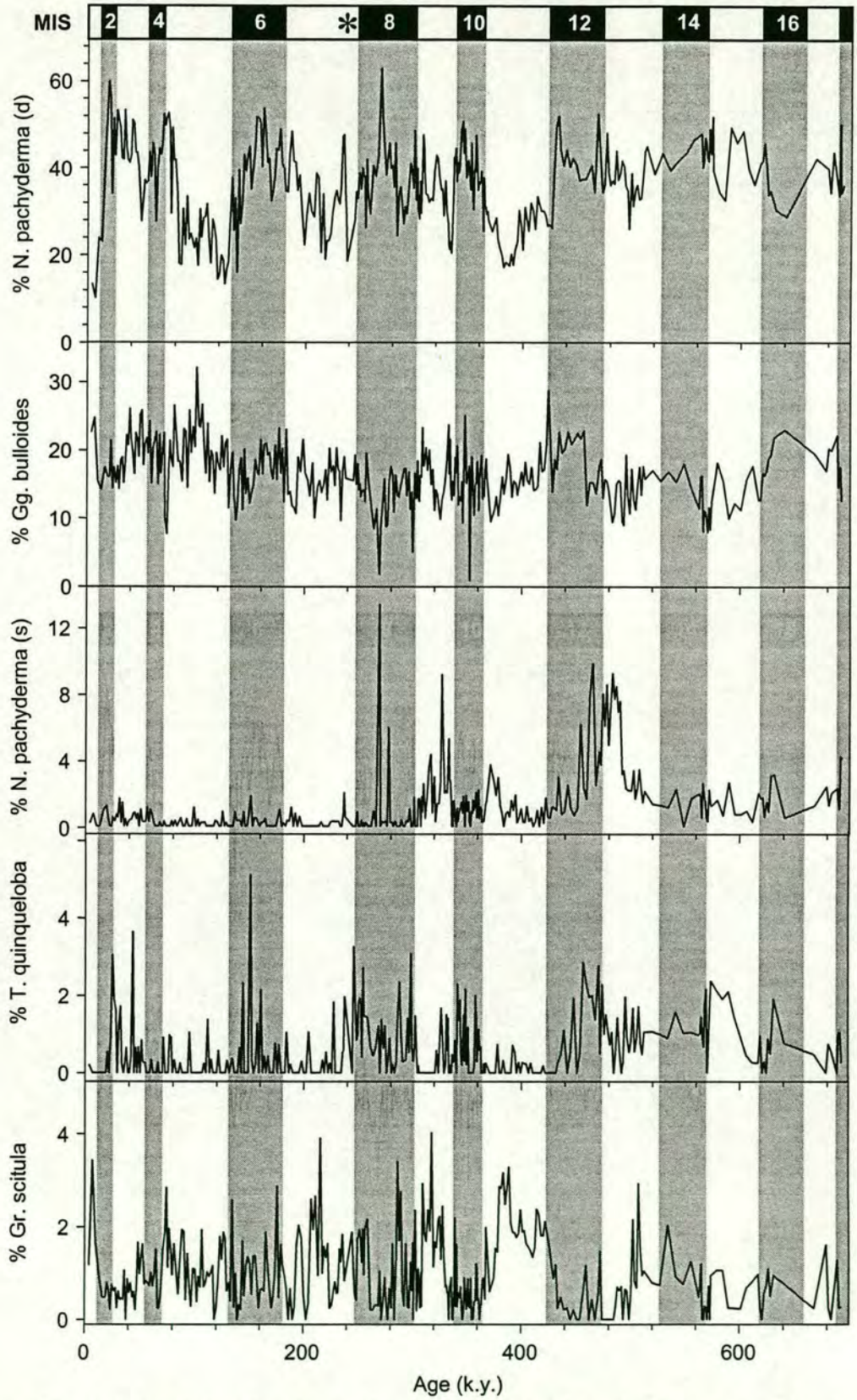

Figure 5.4: Relative abundance of 'subpolar' species from the Cape Basin spliced record. Glacial periods are shaded grey.

dominant species (> 50%) in the modern day living foraminiferal plankton in the Benguela Current system (Bé and Tolderlund, 1971). Kemle-von Mücke and Oberhänsli (1999) observed *Gg. bulloides* in plankton tows and recorded greatest abundance near the coastal upwelling cells where phosphate and nitrate levels are higher than the surrounding ocean.

N. pachyderma (s), is the cold end member of the planktonic foraminifera assemblage (Figure 5.4, Plate 1). During most periods this species is unimportant in the assemblage (<2%). However, some intervals exhibit elevated relative abundances (>5%, maximum ~13%) which may reflect oceanographic change in the southern Benguela system. Peaks of abundance occur in interglacial MIS 9 and the transition between MIS 13/12. In the present South Atlantic, this species generally reflects cool and highly productive waters and is found in waters south of the STF. The species is also found in the NBS and SBS (Bé and Tolderlund, 1971; van Leeuwen, 1989; Schmidt, 1992; Giraudeau, 1993), where it is dominant in surface sediments of the inner and middle shelf below coastal upwelling cells (Giraudeau and Rogers, 1994) as shown in Figure 5.3. The changes in relative abundance of sinistrally coiled *N. pachyderma* are not related clearly to the isotopic palaeo-temperature changes. Intervals of glacial extremes are not associated with higher relative abundance of this form, nor are the warmest intervals marked by the lowest abundances.

T. quinqueloba (Plate 3) is a minor component of the assemblage (mean 0.6%) throughout the Cape Basin record, achieving a maximum of 5.1% during MIS 6 (Table 5.1). Highest values of this species occur during glacial periods (Figure 5.4). Average relative values for *T. quinqueloba* are higher during the early portion of the record. *T. quinqueloba* is mainly found in subpolar waters and predominantly in waters colder than 12°C. The northern distribution limit is the transition zone, which separates the subpolar regions from the subtropical, but *T. quinqueloba* also occurs in small percentages in the Benguela and Agulhas Currents (Bé and Tolderlund, 1971).

Gr. scitula (Plate 4) occurs sporadically in low frequencies (<4%) throughout the Cape Basin record (Figure 5.4). Despite being usually described as a subantarctic/ transitional species (Giraudeau, 1993) *Gr. scitula* shows a down core pattern that

resembles other warm water forms in the record. The most consistent occurrences of this species are in MIS 11 and 9.

5.2.2 'Warm water' form

Gr. inflata (Plate 1), is the only endemic species of the transitional zone between 35°S and 45°S (Bé and Tolderlund (1971). This zone extends equatorwards (Figure 5.2) from the Benguela system along the Benguela Current (Niebler and Gersonde, 1998). *Gr. inflata* is also present in the main South Atlantic Gyre waters and favours warm, oligotrophic conditions (Giraudeau, 1993). *Gr. inflata* exhibits frequency variations generally opposite to those of dextral coiled *N. pachyderma.* Average abundance is 24. 5% and reaches a maximum of 45. 9% at 137 ka B. P. during interglacial MIS 6 (Table 5.1). The general temporal distribution of *Gr. inflata* shows glacial – interglacial variation with highest abundance being in interglacial periods (Figure 5.1). Lowest values are recorded in MIS 2, 4 and 12. In the earlier portion of the record, until the onset of MIS 6, the lowest values of *Gr. inflata* occur around termination events. During interglacials the relative abundance of *Gr. inflata* increases steadily and falls sharply before the onset of the subsequent glaciation. The decreasing trend continues gradually during glacial stages 14, 12, 10, and 8, only increasing post termination. These trends are reversed in the upper portion of the record with highest percentage *Gr. inflata* values recorded around the terminations of MIS 6, 4, and 2.

Bé and Tolderlund (1971) describe the following species as living in tropical waters (Figure 5.2, Plates 2, 3, 4, and 5): *Globigerinoides sacculifer* (Brady), *Gr. menardii, Pulleniatina obliquiloculata* (Parker and Jones), *Globigerina digitata* (Brady), *Sphaeroidinella dehiscens* (Parker and Jones), *Globorotaloides hexagonus* (Natland). Subtropical species typically found in oligotrophic waters listed by the same authors are: *Globorotalia hirsuta* (d'Orbigny), *Gr. truncatulinoides, Gs. ruber, Globigerina rubescens* (Hofker), *Globigerina falconensis* (Blow), *Globigerinoides conglobatus* (Brady), *Globorotalia crassaformis* (Galloway and Wissler), *N. dutertrei, Globigerinella siphonifera* (d'Orbigny), and *Orbulina universa* (d'Orbigny). *Ga. glutinata* is included in the warm water region between 20°S and 40°S and 20°N and 40°N. Despite this species being ubiquitous, its greatest abundance is found in subtropical waters (Bé and Tolderlund; 1971).

Gr. truncatulinoides (Plate 3) is recorded in the Cape Basin spliced record and displays glacial – interglacial variation. Relative abundance of this species is higher during interglacial periods and the overall down core distribution patterns are similar to those of *Gr. inflata* (Figure 5.1). The maximum percentage peaks of *Gr. truncatulinoides* are centred around the mid- to late stages of interglacial periods MIS 13, 11, 9, 7, and 5. *Gr. truncatulinoides* constitutes on average 3% of the total assemblage, reaching a maximum of 10% during MIS 11. The similarity between the records of *Gr. truncatulinoides* and *Gr. inflata* reflects their similar environmental preferences. *Gr. truncatulinoides* inhabits the central water masses of the subtropical gyres. The highest frequencies occur between May and June in the southern hemisphere (Bé and Tolderlund, 1971). The distribution of *Gr. truncatulinoides* in the surface sediments of the Benguela system is similar to the patterns of *Gr. inflata* (Figure 5.1). However, as observed in the fossil record of the Cape Basin spliced record, the frequencies of *Gr. truncatulinoides* in water column and surface sediments of the Benguela region are lower by 12 and 25% than *Gr. inflata. Gr. truncatulinoides* is a deep dwelling species and the association with *Gr. inflata* corresponds with the recorded association of these species as representing oligotrophic offshore waters (Giraudeau and Rogers, 1994).

Gs. ruber (Plate 5) is the dominant subtropical species of the planktonic foraminifera assemblage. *Gs. ruber* occurs in varying numbers throughout the core, mean abundance is 3.7% and the maximum abundance is 14. 5% (Table 5.1). This species is the warm end member of the most dominant species in the planktonic foraminifera assemblages of the Cape Basin spliced record. The downcore distribution of *Gs. ruber* is fairly straightforward. Like *Gr. truncatulinoides*, maximum occurrences of *Gs. ruber* are during interglacial periods (Figure 5.1). In contrast to other subtropical and tropical species in MIS 11 (Figure 5.5), *Gs. ruber* is notable for the sustained high values, relative to other interglacial stages where values are highest immediately following the termination of the preceding glacial period. *Gs. ruber* usually does not exceed 2% in the Benguela region faunal community (Giraudeau, 1993). Therefore, the higher abundances observed in the Cape Basin record may be connected to Indian Ocean input from the Agulhas Current.

N. dutertrei (Plate 3) displays a glacial – interglacial pattern that is also common to *Gs. ruber* and *Gr. truncatulinoides* and is opposite to that of *N. pachyderma* (d). The average

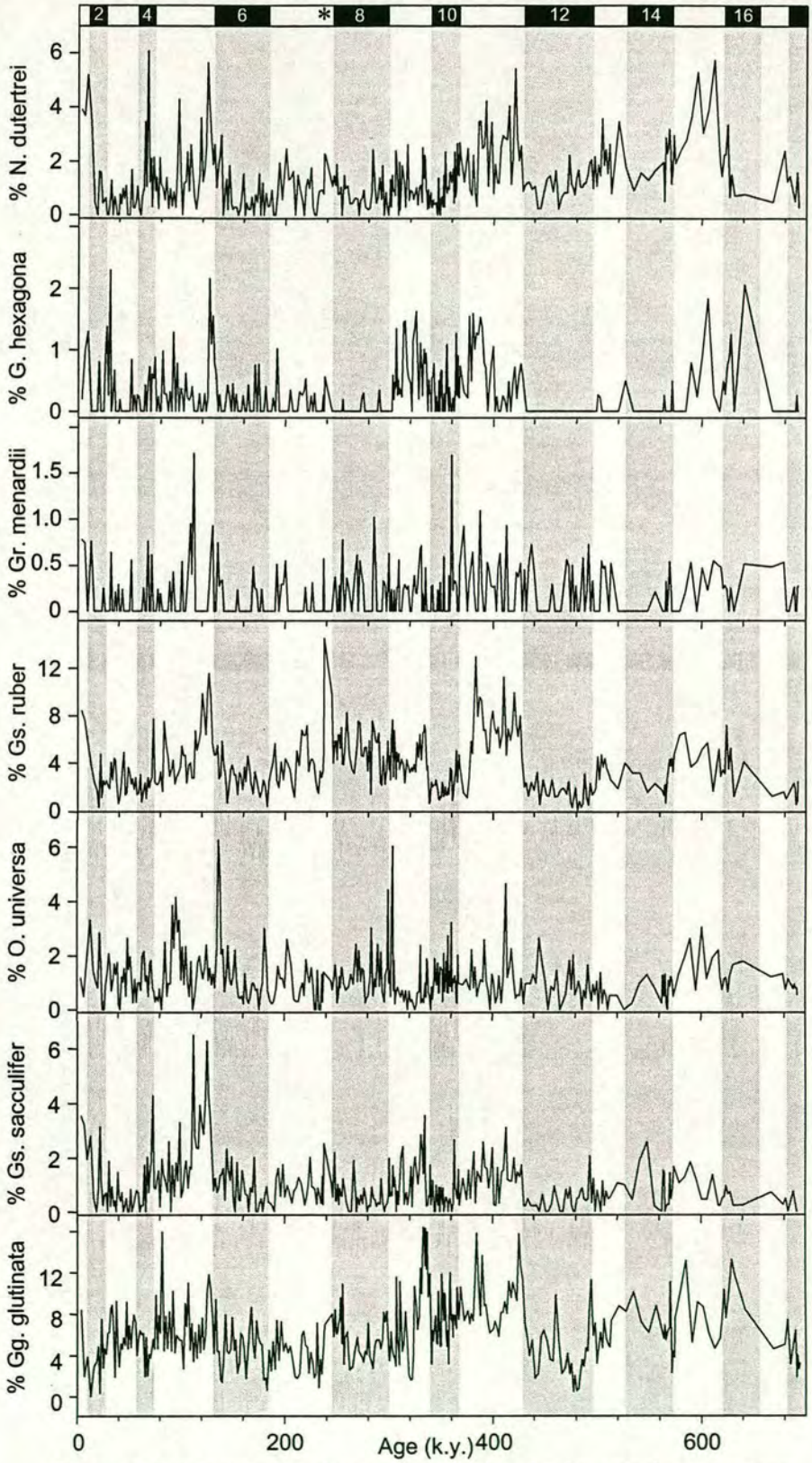

Figure 5.5 Relative abundance of tropical and subtropical species from the Cape Basin spliced record.

abundance of *N. dutertrei* is 1.3% and reaches a maximum occurrence of 6.1% in MIS 15. As with the other subtropical species shown in Figure 5. 5 the peak shown by *N. dutertrei* during MIS 9 is in general less distinct than the other interglacial periods. *N. dutertrei* is a subtropical – tropical species that is particularly abundance in current systems along continental margins (Giraudeau, 1993). *N. dutertrei* is often referred to as an upwelling indicator because of its occurrence in upwelling regions in the tropics (Kroon and Ganssen, 1989; Sautter and Thunnell, 1991; Kemle-von Mücke and Oberhänsli, 1999). Studies have shown that *N. dutertrei* reaches a maximum concentration where the thermocline is shallow and the deep chlorophyll is between 20 and 50 m (Fairbanks and Wiebe, 1980). Average relative abundance of this species in surface sediments reaches 20% directly under upwelling cells. However, abundance decreases to around 3% beyond these cells (Giraudeau, 1993), which confirms earlier observations by Thiede (1975) and Kroon (1991).

The Cape Basin record of *Gs. sacculifer* (Plate 5) documents the changes from glacial to interglacial periods very clearly (Figure 5.5). MIS 5 is particularly distinct. *Gs. sacculifer* is a tropical species and is only found in relatively low concentrations in surface sediments in this part of the Benguela System (Giraudeau, 1993). *Gs. sacculifer* occurs at a maximum abundance where the annual mean water temperatures are >24°C (Bé and Tolderlund, 1971). The occurrence of this species in the Benguela Current corresponds to well oxygenated surface water conditions (Kemle-von Mücke and Oberhänsli, 1999). Increased abundance of this species is indicative of increased advection from the Indian Ocean which causes surface water eddies of the Agulhas Current to mix with the Benguela Current.

The *Ga. glutinata* (Plate 3) record of relative abundance is complex (Figure 5.5). It broadly displays two modes, with a switch around MIS 8. Prior to MIS 8 this species displays a typically subtropical pattern of abundance, with higher concentrations during interglacial periods. The younger section of the core shows high frequency variations which appear to be unrelated to glacial – interglacial changes. *Ga. glutinata* is described as a subtropical species with a cosmopolitan distribution in the oceans and tolerates a temperature range of 3 to 30°C with peak abundance occurring between 24 and 30°C (Bé and Tolderlund, 1971). Hale and Pflaumann (1999) categorise this species as tropical which supports the downcore patterns of this species in the Cape Basin. *Ga. glutinata* has

an affinity for high nutrient content and high salinity environments (Kemle-von Mücke and Oberhänsli, 1999). Normally this species rarely occurs with frequencies above 5%. However, in a broad belt from Brazil to the Cape of Good Hope it occurs in relatively high frequencies between 5 and 10% (Bé and Tolderlund, 1971).

Certain tropical species present in the planktonic foraminifera assemblages in negligible amounts are perhaps more significant than their abundance would initially suggest. For instance, *G. hexagonus* in the present day only inhabits the Indian and Pacific Oceans and is only found in Pleistocene sediments in the Atlantic. The relative abundance record shown in Figure 5.5 reveals concentrations only during interglacial periods. There are distinct abundance peaks of *G. hexagonus* in MIS 5.5 and MIS 11, both thought to be periods when circulation in the BC was strongly affected by advection from the Indian Ocean. The presence of a species that is strongly associated with the Indian Ocean would support this argument. Conversely, *G. ruber* (pink) is now only found in the Atlantic Ocean and is restricted to Pleistocene age sediments in the Indian Ocean and is only present in the Cape Basin fossil record during MIS 11, 9, 7, and 5 (data in Appendix 3). The dynamics of these trace and other rare species could throw additional light onto connections between the oceans over the period of study.

The percentages of the warm water species in the Cape Basin (*Gs. sacculifer, Gr. menardii, P. obliquiloculata, Gg. digitata, S. dehiscens, G. hexagonus, Gr. hirsuta, Gr. truncatulinoides, Gs. ruber, Gg. rubescens, Gs. conglobatus, Gr crassaformis, N. dutertrei, Ge. siphonifera,* and *Orbulina universa*) are summed as a single group in Figure 5.6. Frequency variation of this group reveals peaks during all warm interglacial stages.

5.3 STATISTICAL ANALYSIS AND ECOLOGICAL SIGNIFICANCE OF PLANKTONIC FORAMINIFERA DATA

5.3.1 Diversity

In order to further reconstruct the palaeoceanographic trends in the planktonic foraminifera assemblage time series, a statistical analysis of the data set was undertaken. Diversity is independent of individual species composition, and changes in diversity through time can yield information on ecological and thus palaeoceanographic change

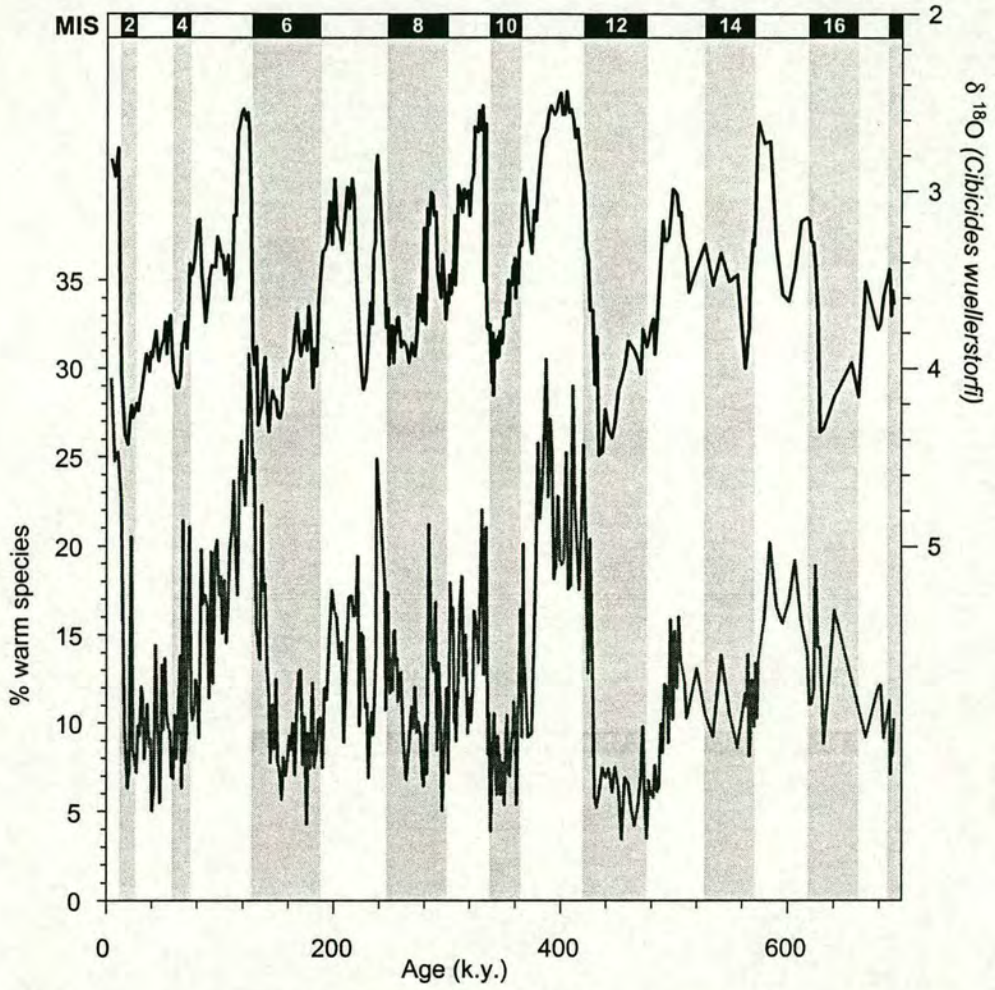

Figure 5.6 Percentage frequency change with age (k.y.) of the sum of warm water species (*Gs. sacculifer, Gr. menardii, P. obliquiloculata, Gg. digitata, S.dehiscens, G. hexagonus, Gr. hirsuta, Gr. truncatulinoides, Gs. ruber, Gg. rubescens, Gs. conglobatus, Gr. crassaformis, N. dutertrei, Ge. siphonifera,* and *Orbulina universa*) within the planktonic foraminiferal assemblages in the Cape Basin record.

(Ottens and Nederbragt, 1992). A suite of diversity equations were employed: Simple Diversity is the number of species in each sample; Shannon-Weaver Diversity takes into account the relative proportion of species within samples (Shannon, 1949):

$$H' = -\sum p_i \ln p_i$$

where p_i is the proportion of each species.

Equitability is a measure of evenness of species distribution within a sample (Buzas and Gibson, 1969). Equitability equals one if all species are present in the same proportion and approaches zero if one species dominates the fauna.

$$E' = e^{H'} / s$$

where s is the number of species in a sample.

The diversity indices were calculated from the faunal count data (Appendix 3). Simple Diversity variations in the Cape Basin spliced record are large, from nine to twenty species per sample, and highly variable reflecting the cores position in a transitional zone that is influenced by upwelling and by input from Agulhas rings. In general, peak diversity values are associated with interglacial periods (Figure 5.7). Shannon-Weaver diversity shows fluctuations between 1.4 and 2.3 (Figure 5.7). The curve reflects glacial – interglacial oscillations and higher values are typical of interglacial periods. Equitability variations show similarities to the Shannon-Weaver diversity index, recording higher values, and thus more mixed assemblages, in interglacial stages.

The diversity data of this study are supplemented by water mass characteristics defined by environmental properties (temperature and salinity) and planktonic foraminifera assemblages (Ottens, 1991). Diversity maps based on core top data from the Benguela System (Giraudeau, 1993) are used to define the environmental parameters of the system (Figure 5.8). Williams and Johnson (1975) showed that at high latitudes in the southern hemisphere diversities of planktonic foraminifera in surface sediments decrease with increasing latitude and secondly, that there is a strong correlation between decreasing diversity and decreasing sea surface temperature. Giraudeau (1993) showed diversity patterns in the BS that were consistent with these findings.

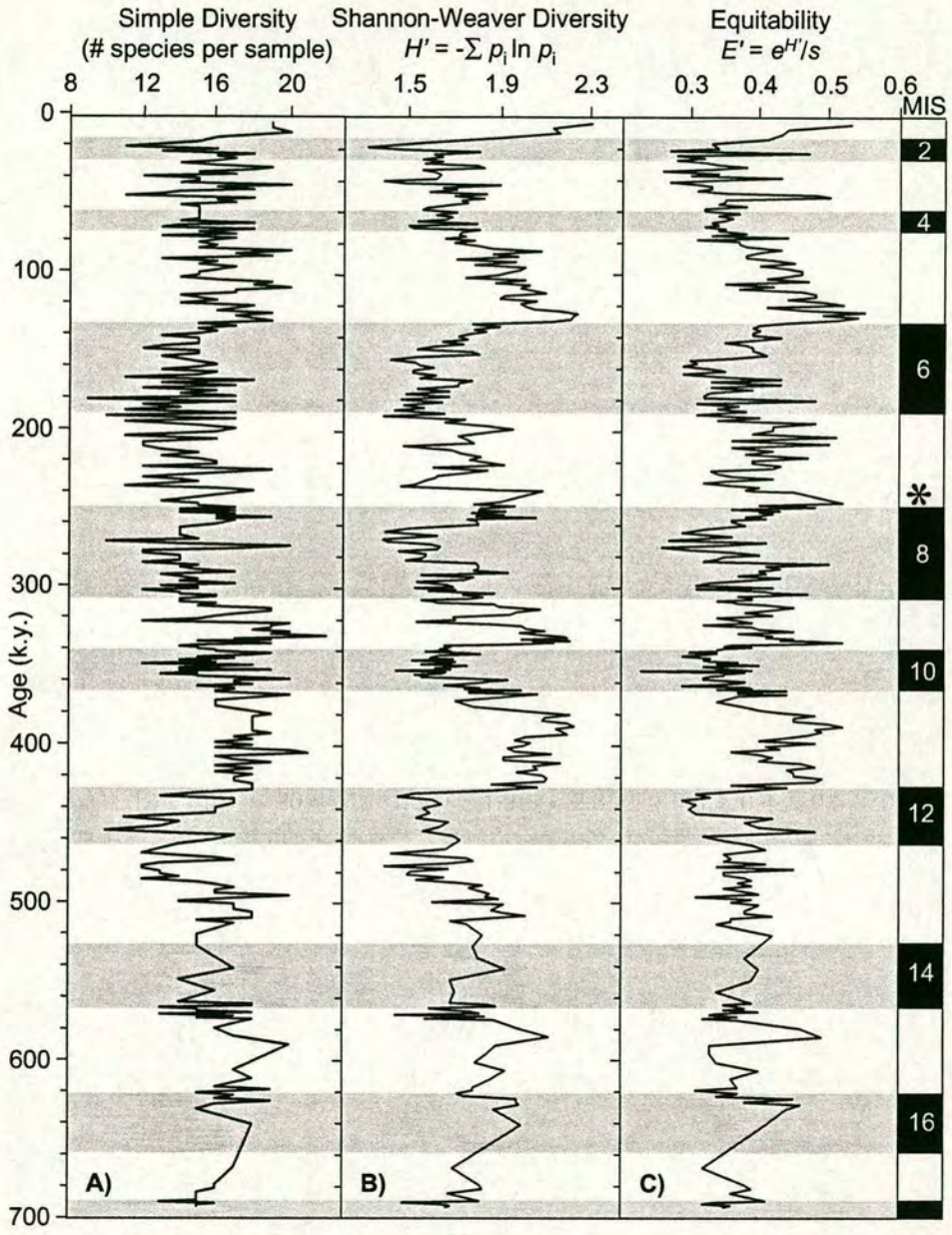

Figure 5.7 Diversity Statistics for spliced Cape Basin record. **A)** Simple Diversity, **B)** Shannon-Weaver Diversity, **C)** Equitability.
Diversity data is shown in Appendix 3.

High diversity and low equitability characterise frontal zones and water mass boundaries as mixing enhances frequencies of those species that occur in both water masses, while species unique to one water mass are scarce (Giraudeau, 1993). Eddy centres and upwelling cells show low values in all three indexes. Areas affected by upwelling plumes, (low temperatures and high nutrient levels in surface waters) reveal a Simple Diversity that is the same as surrounding areas, i.e. same overall number of species, but a relatively low Shannon-Weaver diversity Figure. Equitability also shows a decrease in these areas. Extremely oligotrophic ocean environments, such as the Red Sea, yield low diversity and low species numbers. Periods experiencing high variability in environmental parameters will be characterised by relatively low diversity and equitability faunas in comparison to the surrounding environment (Ottens and Nederbragt, 1992). These conditions are summarised in Table 5.2 below:

OCEAN ENVIRONMENT:	DIVERSITY CONDITIONS		
Oligotrophic (gyre) environments	Simple (S), Shannon-Weaver(H), and Equitability (E) intermediate - high		
Frontal zones and water mass boundaries	High diversity (S & H)	Low equitability	
Eddy centres and upwelling cells	Low diversity (S & H)	Low equitability	
Upwelling plumes and filaments	S - similar to surrounding waters (intermediate to high)	H - low	Equitability decreases
Mixing zone with warm current inflow	High diversity (S & H)	Equitability similar to surrounding waters	
Subpolar water	Low diversity (S & H)	Intermediate equitability	
Periods of change and high variability in environmental parameters	Low diversity (S & H)	Low equitability	

Table 5.2 Ocean environments and descriptive diversity statistics, information from Ottens and Nederbragt (1992); and Giraudeau (1993).

5.3.2 Cluster Analysis

To associate, statistically, planktonic foraminifera forms with similar temporal distribution patterns, a standard correlation analysis (Pearson r correlation) was used to generate a matrix of correlation coefficients from the original data of relative species frequencies. Cluster analysis was performed on the species percentage data, based on the

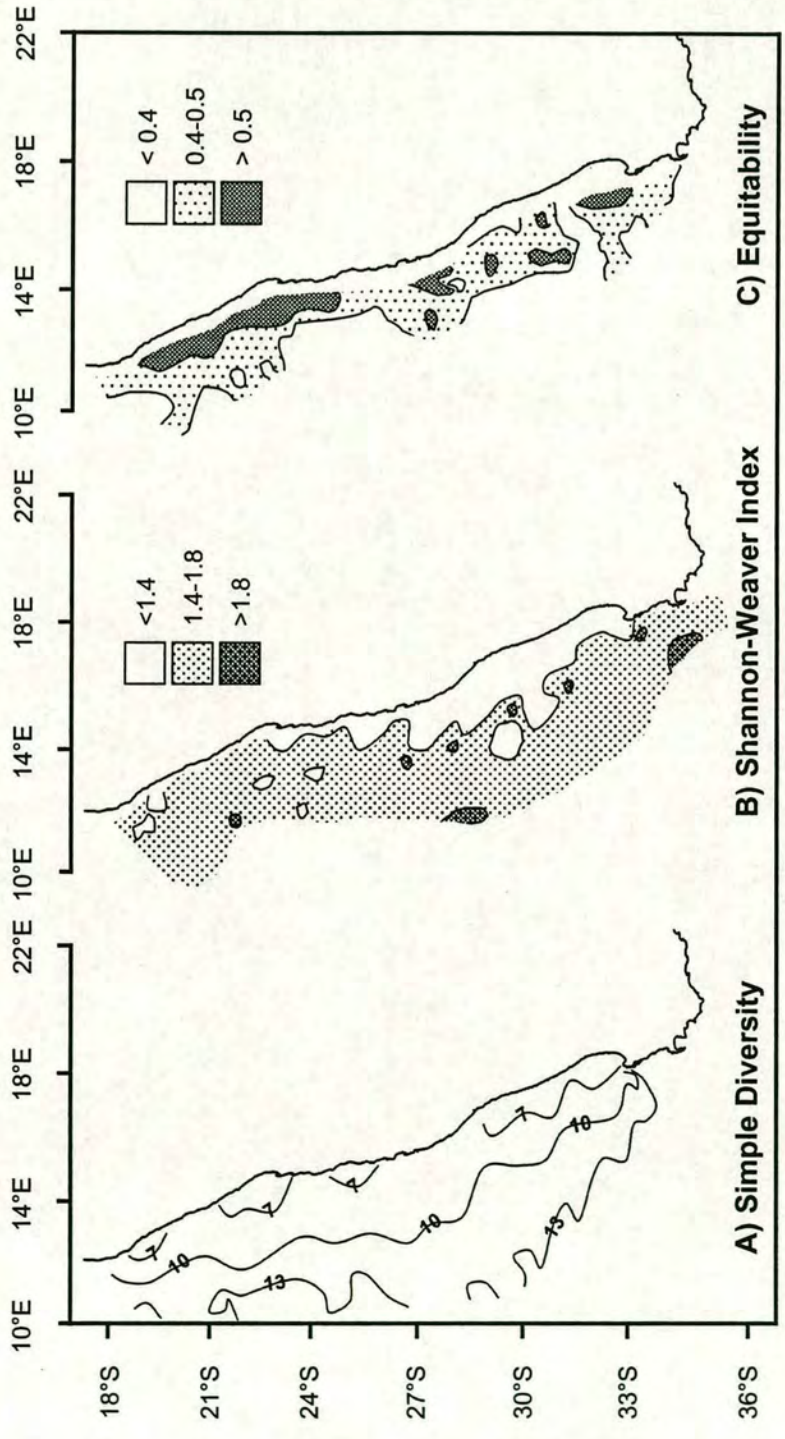

Figure 5.8 Contoured maps of planktonic foraminifera diversity indices: **A)** Simple Diversity (# species), **B)** Shannon-Weaver Index, **C)** Equitability. Adapted from Giraudeau (1993).

Pearson correlation matrix described above. For this analysis the SYSTAT program was used (SYSTAT 5.2.1; Wilkinson, 1989).

Cluster analysis of downcore planktonic foraminifera data produces four clusters (Figure 5.9). The clusters are based on a 5% confidence interval. The clusters can be defined as: Oligotrophic (mixed subtropical-tropical); Oligotrophic (gyre); Mesotrophic; and Eutrophic. Such clusters largely reflect the modern distribution of planktonic foraminifera in the south east Atlantic, as defined by Giraudeau (1993). The species of the first and largest cluster, containing *Gs. ruber*, *Gr. scitula*, *Gs. sacculifer*, *Gr. hirsuta*, *N. dutertrei*, *Gr. truncatulinoides*, and *Ga. glutinata*, occur within the South Atlantic subtropical gyre and in the Southern Indian subtropical gyre and Agulhas Current (Bé and Tolderlund, 1971; Bé and Hutson, 1977; Van Leeuwen, 1989; Schmidt, 1992; Giraudeau, 1993; Ufkes *et al.* 1998). This cluster thus represents warm conditions with substantial leakage of Indian tropical water past the southern tip of Africa, via advection from the Agulhas Current. The distribution of these species is illustrated in Figure 5.3. The second group, consisting of *Gr. crassaformis*, *Gr. inflata*, and *O. universa*, represents the oligotrophic watermasses of the subtropical gyre transition with the Benguela Oceanic Current (Bé and Tolderlund, 1971; Van Leeuwen, 1989; Schmidt, 1992; Giraudeau, 1993; Ufkes *et al.* 1998, Ufkes *et al.* 2000). This group is linked to the Mixed Subtropical-Tropical (Oligotrophic) group. The third cluster, comprising *Ge. siphonifera* and *Gg. bulloides*, reflects the relatively warm water mesotrophic zone along the thermal front between the coastal upwelled water and the offshore, oligotrophic water (Bé, 1977; Oberhänsli, 1991; Schmidt, 1992; Giraudeau, 1993; Pflaumann *et al.*, 1996). Kemle-von Mücke and Oberhänsli (1999) recorded greatest abundance of *Gg. bulloides* in fertile transitional areas south of 30°S near the coastal upwelling area off Namibia. Bé and Tolderlund (1971) found that *Ge. siphonifera* was rare in the central waters of the South Atlantic, preferring the outermost margins of the subtropical gyre into the transitional zone and areas of upwelling. Highest concentrations of this form were found in the Benguela Current and neighbouring waters (Bé and Tolderlund, 1971). Bradshaw (1959) showed in the Pacific that the preferred habitat of *Ge. siphonifera* is around current systems along continental margins. The association of *Ge. siphonifera* and *Gg. bulloides* has been observed in the Arabian Sea and was attributed to the influence of nearby upwelling cells (Auras-Schudnagies *et al.*, 1989). The final cluster of *N. pachyderma* (d), *N. pachyderma* (s), *Gg. quinqueloba*, and *Gg. falconensis* reflects upwelling cells and filaments of the BCS

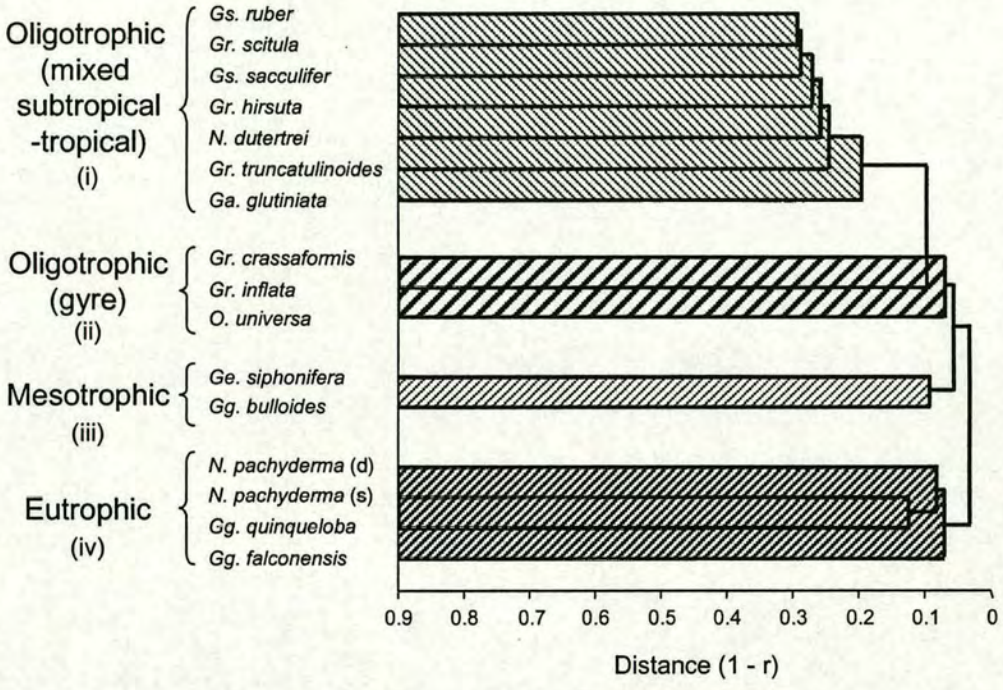

Figure 5.9 Dendrogram showing four environmentally-interpreted species groupings based on the planktonic foraminiferal percentages of the 16 most abundant species, all with a mean of >4%, for the Cape Basin spliced record.

(Oberhänsli, 1991; Schmidt, 1992; Ufkes and Zachariasse, 1993; Giraudeau, 1993; Little *et al.*, 1997a). The geographical distribution of these forms is illustrated in Figure 5.4. Studies of living planktonic foraminifera show that upwelling filaments are dominated by >60% *N. pachyderma* (d) (Ufkes and Zachariasse, 1993, Giraudeau *et al.*, 2000). *N. pachyderma* (s) and *Gg. quinqueloba* are identified as opportunistic species which thrive in cold surface waters that are affected by upwelling processes (Giraudeau, 1993; Giraudeau and Rogers, 1994; Giraudeau *et al.*, 2000).

5.4 Discussion

5.4.1 Nutrient availability and planktonic foraminifera distribution

The response of the planktonic foraminiferal fauna, taken as a whole, describes the effects of climatic fluctuations over the past eight glacial – interglacial cycles. It is important to examine the distribution of temperate and subtropical species, as well as upwelling species, in order to accurately constrain the extent of upwelling variability in the southern Benguela System throughout the time period studied. The planktonic foraminifera records for the Cape Basin spliced core are subdivided into intervals characterised by specific types of foraminiferal groupings. Figure 5.10 illustrates the five different types of Ocean Environmental Intervals (OEIs) identified in the time period under examination. Each OEI is defined using a combination of planktonic foraminifera census data and statistical analyses of the Cape Basin spliced record data. Firstly, 'diversity episodes' were identified within the diversity data (Figure 5.7). The 'high' values were defined by comparison with typical modern ocean values (Giraudeau, 1993) and the diversity conditions defined by Ottens and Nederbragt (1992), described in Table 5.2 Secondly, the relative abundance of planktonic foraminifera during each 'diversity episode' was examined. The significant species were equated to the habitats defined during cluster analysis. This ensured that both types of environmental descriptions concur and make ecological sense in order to finally provide an environmental character for each OEI. Table 5.3 details the parameters that contribute to each type of OEI.

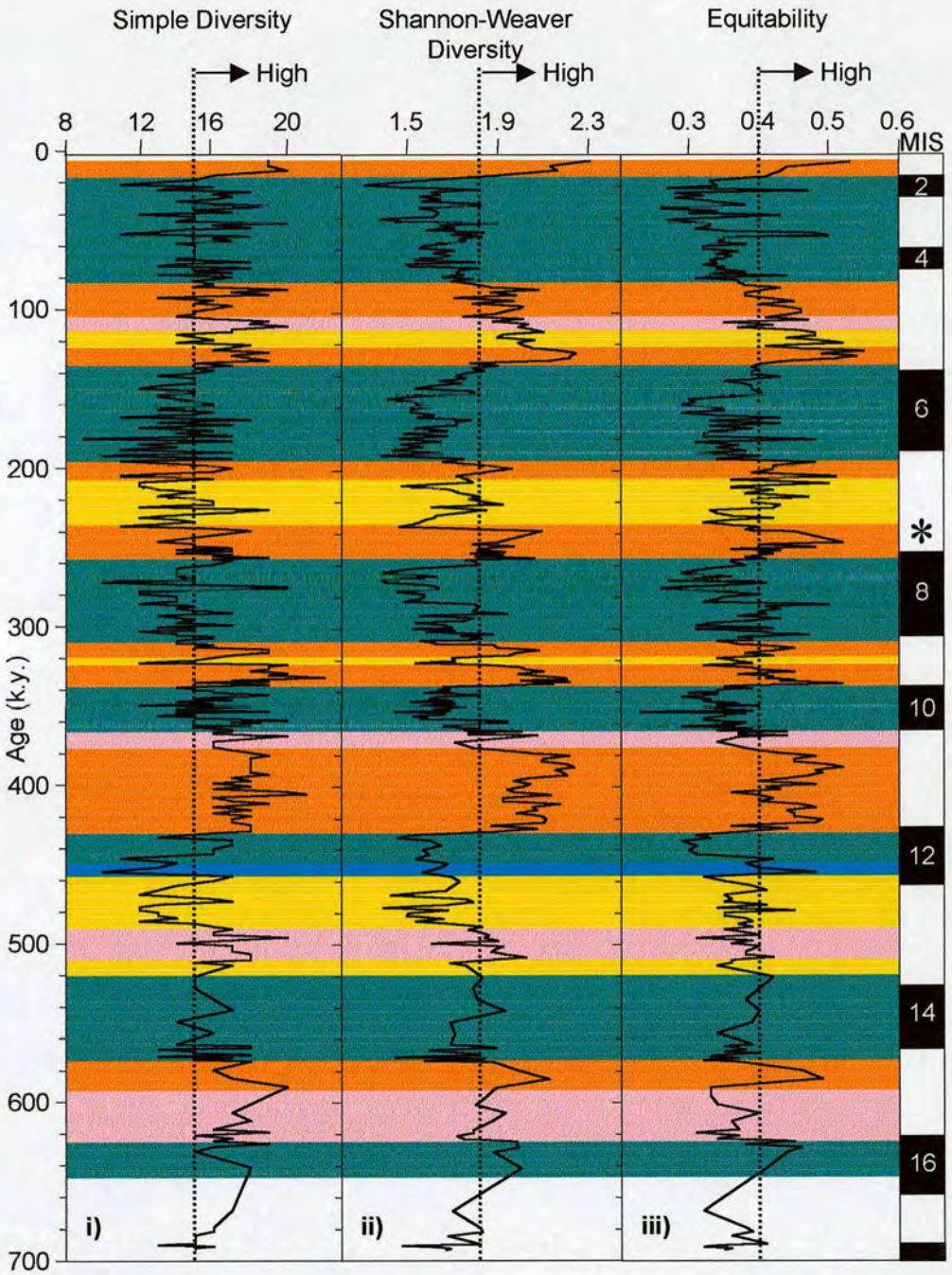

Figure 5.10 Ocean environment intervals, defined by diversity statistics and planktonic foraminiferal data, observed in the spliced Cape Basin record for the past 700 k.y. 'High' diversity values are defined from Giraudeau (1993).

OEIs	DIVERSITY PATTERN			INDICATOR FORAMINIFERAL SPECIES
	Simple	*Shannon-Weaver*	*Equitability*	
Eutrophic	Intermediate	Low	Low	*N. pachyderma* (d)
Oligotrophic (gyre)	Intermediate	Intermediate	Intermediate	*Gr. inflata* and *O. universa*
Mixed subtropical - tropical (oligotrophic)	Very High	Very High	Very High	Mixed subtropical with significant contribution of tropical species and Indian Ocean taxa.
Mesotrophic	High	High	Low	*Gg. bulloides,* transitional and subtropical species
Subpolar	Low	Low	High	*N. pachyderma* (s)

Table 5.3 Overview of the five different OEIs that are identified from deviations in diversity (Simple and Shannon-Weaver) and equitability of planktonic foraminifera assemblages in the southern Cape Basin during the past 700 kyr. The descriptors, e.g. 'high', are developed from Giraudeau (1993). The distribution of these zones through time are shown in Figure 5.10.

The varying abundance of subtropical and tropical species have a strong effect on the outcome of this analysis and the significance of this will be described in Section 5.4.3. The oscillations of the warm species complement the general glacial-interglacial pattern as described by *N. pachyderma* (d). Figure 5.11 illustrates the relationship of the two dominant planktonic foraminifera species, *N. pachyderma* (d) and *Gr. inflata*, along with the total percentage surface dwelling warm species observed in the core to the OEIs described above. Previous investigations in the Benguela region have revealed a good relationship between the distribution patterns of planktonic foraminifera, nutrient levels and surface water hydrography (Giraudeau, 1993; Ufkes and Zachariasse, 1993; Kemle-von Mücke and Oberhänsli, 1999). The modern day distribution of nutrient levels corresponds well to the distribution of planktonic foraminifera (Giraudeau, 1993; Giraudeau and Rogers, 1994). This implies a relationship between species type and relative abundance of foraminiferal taxa and nutrient levels within the Benguela System that is similar to those observed in other areas (Reynolds and Thunnell, 1985a; Kroon and Ganssen, 1989; Kroon, 1991; Kennettt and Venz, 1995; Hebbeln *et al.,* 2000). The fossil foraminiferal assemblages are thus best interpreted in terms of nutrient availability. The five OEIs identified characterise observed modern day nutrient – foraminiferal relationships.

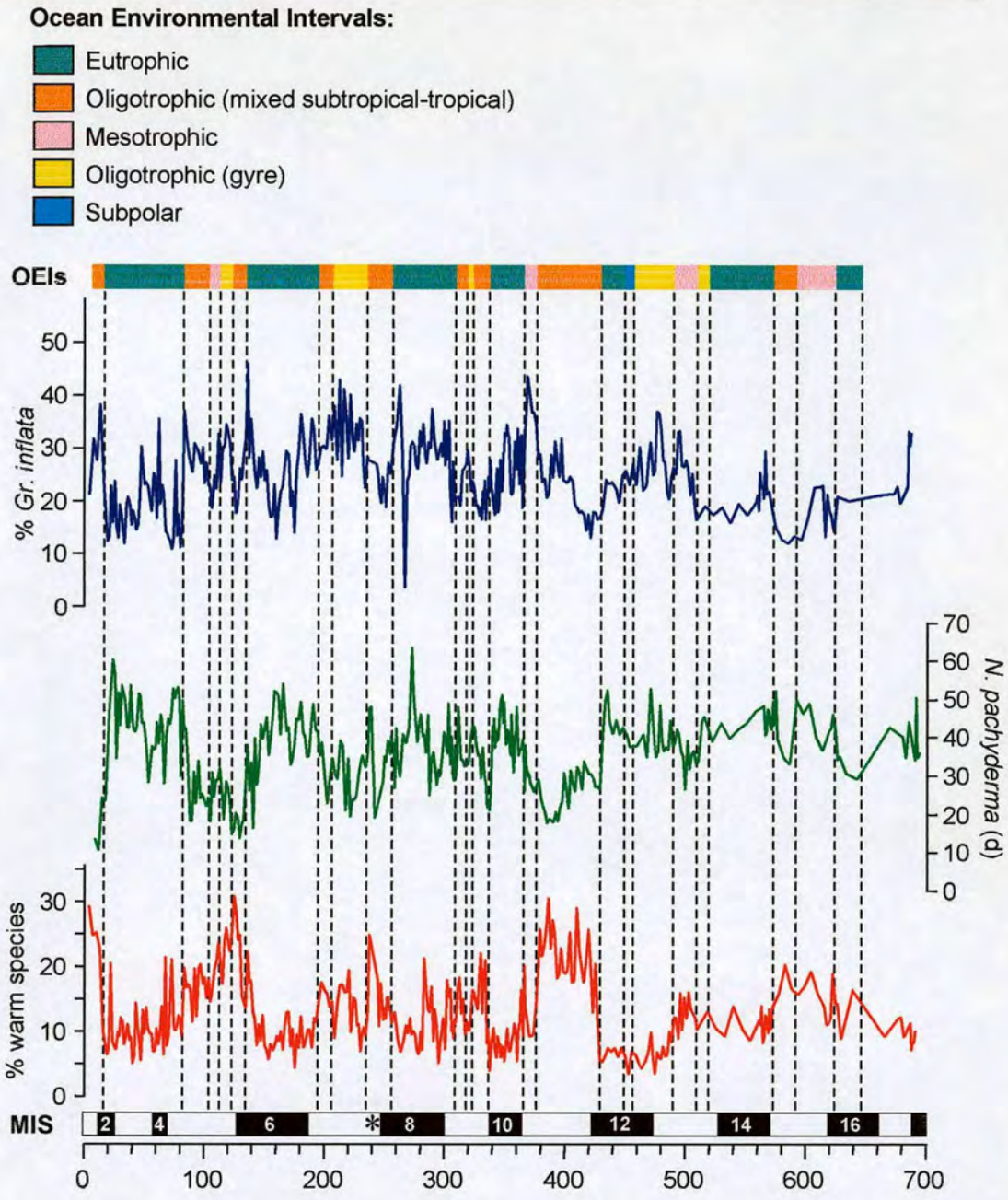

Figure 5.11 Relative abundance of percentage warm species, *N. pachyderma* (d), and *Gr. inflata* in relation to the Ocean Environmental Intervals (OEIs) and Marine Isotope Stages (MIS) identified in the Cape Basin spliced record.

5.4.2 Eutrophic Ocean Environmental Interval

In the Cape Basin spliced record glacial periods broadly correspond with the 'eutrophic' OEI and intervals of high relative abundance of *N. pachyderma* (d). The glacial-interglacial downcore pattern of *N. pachyderma* (d) is determined primarily by changes in the water masses affecting the core site. *N. pachyderma* (d) favours watermasses that are nutritionally enriched and poorly stratified (Giraudeau, 1993; Chapman *et al.,* 1996). Therefore, it can be inferred that during times when this species dominates surface water foraminiferal assemblages, hydrographic and climatic changes must bring nutrient rich water masses to the locality. The presence of eutrophic water masses in glacial periods back to MIS 12 may be due to:

- enhanced upwelling strength and an associated seaward extension of mature upwelled waters;
- advection of subantarctic waters from south of the STF;
- increased mixing of the water column due to greater storminess associated with intensified atmospheric Westerlies;
- increased input into the region from the South Atlantic Current;
- or a combination of these four.

The spliced core is located too far offshore, and is too deep (Figure 2.2), to ever be directly under the southernmost Benguela coastal upwelling cell, the Peninsula cell (Dingle *et al.,* 1996). Coastal upwelling is concentrated in a small number of cells that show only a limited change in position (Lutjeharms and Meeuwis, 1987). The strength of upwelling cells is related to wind stress. In the SBS maximum upwelling takes place in summer (Dingle and Nelson, 1993). Due to advection of Antarctic Intermediate Waters (AAIW) to the South Atlantic Central Water, the water that upwells in the SBS is cooler than those of the NBS. Shoaling of the top of the nutrient rich AAIW is strongest in the SBS and this influences the fertility of the upwelling cells. Thus, the highest nutrient levels are found in the SBS (Dingle and Nelson, 1993) and the southern Benguela upwelling cells are dominated by *N. pachyderma* (s) (Giraudeau and Rogers, 1994; Niebler, 1995). In the Northern Benguela System, Little *et al.* (1997a) observed intensified upwelling during glacial periods (MIS 2, 4, and 6) because of strengthened trade winds. The resulting 'productivity events' were recorded by increases in the abundance of *N. pachyderma* (s), a species not normally associated with upwelling in the NBS. The cores (GeoB 1711, GeoB 1706, PG/PC12) used in that study were located on the edge of the

zone of influence of the Lüderlitz upwelling cell (Figure 5.12). Little *et al.* (1997a) argued that the expansion and intensification of upwelling due to climatic changes brought much colder, deeper waters to the surface, a process of upwelling that is more analogous to the seasonal intense upwelling of the SBS which, during the upwelling phase is characterised by a dominance of *N. pachyderma* (s) (Giraudeau and Rogers, 1994). However, *N. pachyderma* (s) is not present throughout most of the glacial periods in the spliced core. Therefore, the increased productivity observed in glacials cannot be due to an expanded upwelling cell influencing the area, or newly upwelled waters, which would contain this species in high numbers. Nonetheless, more upwelling and or increased filament projection could result in greater nutrient availability. The seaward extension of mature upwelled waters in the form of plumes and filaments is an important feature of the hydrography of the area and is described in Section 4.2.4. Figure 4.10 shows the modern average extent of these upwelling filaments, based on satellite imaging, and the relative location of the sediment cores. The oceanward penetration of upwelled waters normally extend as far as 750 km, and occasionally 1200 km offshore (van Foreest *et al.,* 1984; Lutjeharms and Meeuwis, 1987; Lutjeharms and Stockton, 1987; Lutjeharms *et al.,* 1991), and could certainly reach the location of the spliced core. *N. pachyderma* (d) thrive in the mixed, filamentous environment, preferring higher nutrient availability than e.g. *Gg. bulloides* (Giraudeau, 1993). Following Pether (1994), it is possible to argue that northward movement of the STF (Prell *et al.,* 1979; 1980; Howard and Prell, 1992) would increase summer atmospheric regional pressure gradients, creating more or stronger easterly winds, driving water offshore and causing upwelling.

Furthermore, the distinct lack of *N. pachyderma* (s) during virtually all glacial periods (Figure 5.3) in the sediment cores of this study (GeoB 3603-2, MD96 2081) and others in the region (Little, 1997; Flores *et al.,* 1999; Chang *et al.,* 1999; Giraudeau *et al.,* 2000; Giraudeau *et al.,* 2001; Chen *et al.,* submitted; Rau *pers. comm.*) suggests that advection from subantarctic waters south of the STF is also unlikely to be the source of the high nutrient watermasses observed during the eutrophic OEIs. *N. pachyderma* (s) is by far the dominant species in planktonic foraminifera assemblages south of the STF in the Southern Ocean. Clearly any advection of Southern Ocean watermasses across the STF, or an expansion of the subpolar zone into the southern Cape Basin, would include a clear and significant abundance of *N. pachyderma* (s).

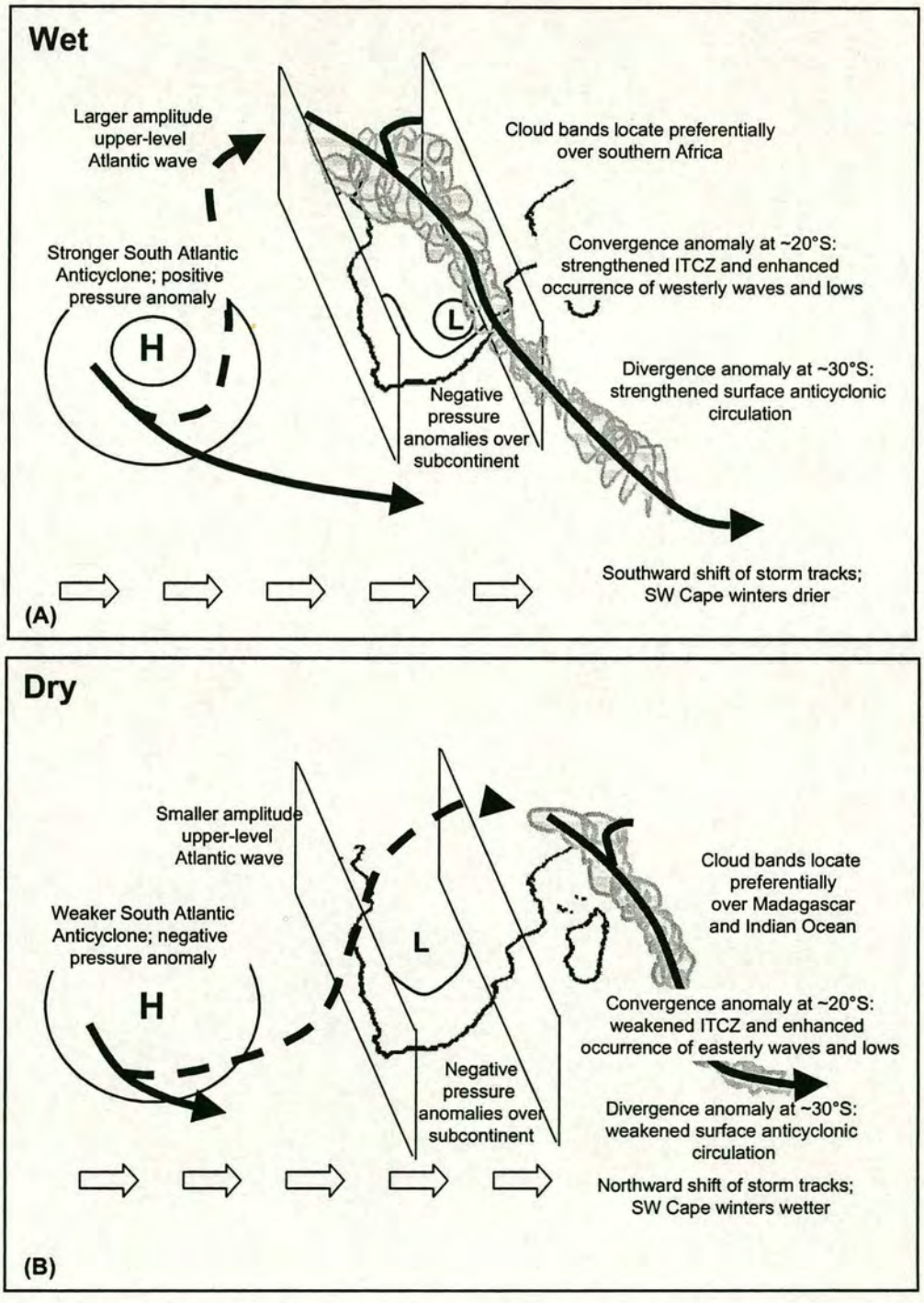

Figure 5.12 Models of anomalous meridional atmospheric circulation over southern Africa during spells of predominantly **A)** wet and **B)** dry conditions. The oligotrophic (gyre) OEI may prevail under situation **A)**. After Mason and Jury (1997)and Tyson (1986).

In interpreting the source of this eutrophic water it is thus fundamentally important that links between atmospheric and oceanic circulation are addressed. The most dominant feature of South Atlantic atmospheric circulation is the anticyclonic flow around the Subtropical High. However, the trade winds and westerly wind belts experience latitudinal changes during the Quaternary, which have important effects on the Benguela Systems. The NBS experienced increased upwelling (Little *et al.,* 1997a) due to the intensification of the Southeast Trades consistent with the increased meridional thermal gradient during glacials (Gardiner and Hays, 1976; Morley and Hays, 1979) in the late Quaternary. However, upwelling in the SBS is seasonal and is strongly modulated, i.e. subdued, by the passage of frontal systems embedded in the Westerlies (Shannon, 1985*).* It is possible that the frequency of Westerlies increased during glacial periods, given that an enhanced circumpolar circulation is a major feature of glacial climate. An equatorward shift of the influence of the zone of Westerlies has been proposed as a major determinant of glacial climates (Van Zinderen Bakker, 1976; Tankard and Rogers, 1978; Harrison *et al.,* 1984; Salinger, 1984; Tyson, 1986; Cockroft *et al.,* 1987; Heusser, 1989; Partridge *et al.,* 1990; Partridge, 1997; Mason and Jury, 1997).

At present Westerlies predominate during the austral winter season, suppressing upwelling in the SBS. If, as a result of atmospheric changes, Westerlies blew during glacial summers upwelling offshore Cape Town may have been significantly reduced. Newell *et al.,* (1981) estimated that the general increase in the intensity of the last Glacial circulation of the Southern Hemisphere was about 17%. Greater mixing of the water column and a raising of the nutricline might also be expected due to the increased incidence of storms associated with the intensified Westerlies.

A further effect of the increased importance of Westerlies in the region is the amount of input in the Benguela System from the South Atlantic Current (SAC). At present, seasonal transports in the Benguela system are dominated by the SAC during the winter period (Garzoli and Gordon, 1996; Figure 4.8). In glacials the source waters for the SAC, the confluence of the Falkland Current and the Brazil Current (Peterson and Stramma, 1991), may be colder. Palaeo SST estimates for 18,000 B.P., based on radiolarian transfer functions, indicate that subantarctic waters were 2–5 ° colder than today (Morley and Hays, 1979). Intensified circulation, due to a northward shift of the Antarctic Polar front (APF) towards the STF (ibid.), may have resulted in a mixing

induced nutrient-enriched SAC. In the Cape Basin, part of the SAC turns north to feed the BC, while the remainder follows the STF into the Indian Ocean. Increased incidence of westerly winds result in greater ocean transport in a northeasterly direction, thereby entraining more SAC waters into the BC. Relict mollusc data support the theory of increased transport from the SAC into the Benguela area during glacial periods. Pether (1993) reported beds of locally extinct molluscs of subantarctic origin, from the Southern Ocean Islands of Tristian da Cunha, Gough, and South Georgia, on the Orange Shelf during the last Glacial. Pether (ibid.) described the probable method of transport to the Benguela region as drift within an enhanced SAC.

The sum effects of glacial atmospheric circulation changes on the palaeoceanography of the SBS would appear to result in an increased overall nutrient budget, regardless of whether productivity was concentrated in the summer. Assuming that Westerlies remained seasonal (i.e. winter, but enhanced), summer upwelling could be induced by winds associated with the increased summer atmospheric pressure gradient caused by the northward movement of the STF. Without other proxy data concerning the western position of STC, the strength of Westerlies in the summer during glacials, and cores from directly beneath upwelling cells, it is not possible to distinguish the causes of enhanced productivity during eutrophic OEIs, other than to say that it is a probable result of enhanced water mass mixing. It may also transpire that productivity is enhanced throughout the year as a result of the combination of several of the above factors through both summer and winter seasons. Given the extremely high (<60%) proportion of *N. pachyderma* (d) (Figures 5.4 and 5.11), such a combination of factors seems likely.

5.4.3 Oligotrophic (Gyre) Ocean Environmental Intervals

Analysis of the down core diversity and warm water species abundance patterns in the Cape Basin spliced record reveals that interglacial periods consist of two distinct types of OEI. The first, discussed here, is termed oligotrophic (gyre). The diversity results are consistent with the findings of Ottens and Nederbragt (1992) showing mainly intermediate values in all three diversity scales (Figure 5.10). Examination of the planktonic foraminiferal assemblages during these intervals show that *Gr. inflata* rises to relatively high percentages during these intervals (Figure 5.11), with the exception of one oligotrophic (gyre) interval in glacial MIS 13. Intermediate levels of warm species

abundance contribute to the oligotrophic South Atlantic gyre watermasses but peaks in percentage warm species are only observed in 'warmer' intervals, i.e. the mixed subtropical – tropical OEI (Section 5.4.4). In the cluster analysis, *Gr. inflata* clustered with *Gr. crassaformis* and *O. universa*, and together they comprise the oligotrophic (gyre) group. This group is consistent with modern surface water and core top distributions of planktonic foraminifera in the Benguela Oceanic Current and the South Atlantic Subtropical Gyre (Giraudeau, 1993). The oligotrophic (gyre) OEI occurs in cooler stadials of interglacial stages 5, 7, 9, and 13. The gyre OEI is absent throughout MIS 11. The oligotrophic (gyre) OEI is interpreted as representing times when the South Atlantic Subtropical Gyre strongly influences planktonic foraminiferal assemblages at the core site. In the Southern and Southern Indian Oceans meridional shifts of the STF have been suggested as the major determinant of planktonic assemblages (Hays *et al.*, 1976; Morley and Hays, 1979; Prell *et al.*, 1979; 1980; Howard and Prell, 1984; Howard and Prell, 1992, Layberie *et al.*, 1996). It has been established that the STF lay south of 42°S during MIS 7, 9, and 11 and in a position poleward of present in the early stages of MIS 1 and 5 (Prell *et al.*, 1979; Howard and Prell, 1992). Little (1997) showed through shifts in planktonic foraminifera species abundance that movement of the STF was recorded in core GeoB 3602 in the Cape Basin. He argued that in addition to the poleward shifts observed in interglacial stages 11, 9, 5, and 1 (Howard and Prell, 1992) the STF in MIS 13 also occupied a southerly position. Flores *et al.*, (1999), examining a core sited in the Agulhas Retroflection region, also demonstrated that the STF was furthest south during interglacial periods. Terrestrial records of rainfall, primarily from the Pretoria Saltpan (Partridge *et al.*, 1997) and the Cango Cave $\delta^{13}C$ stalagmite data (Talma and Vogel, 1991), also support a southerly position of the STC during interglacials, by recording wetter conditions in these locations at these times. 'Wet-spell' scenarios (Tyson, 1986) occur during interglacial periods (Partridge, 1993; Mason and Jury, 1997) because of a strengthened Walker circulation and greater tropical modulation of the atmospheric systems (Tyson, 1986). These conditions are associated in turn with a poleward position for the STF, leading to an overall increase in summer rainfall over the southern African continent. At the same time, a weaker Westerly circulation would have occurred, leading to drier conditions in the southwestern Cape (Cockcroft *et al.*, 1987). Climate reconstructions show that greater insolation during interglacials would lead to a positive pressure anomaly between the African subcontinent and the South Atlantic Anticyclone strengthening the anticyclone (Harrison, 1984; Mason and Jury, 1997). Therefore, during

interglacials, the margins of the South Atlantic Subtropical Gyre may expand due to the changes in atmospheric pressure and winds, resulting in a more easterly position of the Agulhas Retroflection. As described in Section 4.3.5, a stronger Agulhas Current volume transport results in an eastern Agulhas Retroflection which powerfully directs almost all of the AC back into the Indian Ocean. The Agulhas Retroflection will be located further west when the AC is weaker. This results in greater advection from the Indian Ocean into the South Atlantic as the retroflection loop is looser and the AC 'slips' into the South Atlantic. De Ruijter and Boudra (1985), in an oceanographic modelling study, showed that a southerly shift in the Westerlies of just 120 km was enough to decrease transport from the Agulhas Current into the south east Atlantic and decrease isolation of the Subtropical Gyres in the Indian and South Atlantic Oceans. This concept is illustrated in Figure 5.12. Thus, increased insolation in interglacials in fact *limits* advection from the Indian Ocean. The climate mechanisms which expand the subtropical gyres simultaneously cause a reduction in advection from the Indian Ocean, but clearly explain the increased influence of the oligotrophic (gyre) OEI in the Cape Basin during interglacial periods in the late Pleistocene.

5.4.4 Mixed subtropical-tropical Ocean Environmental Intervals

The second interglacial OEI is a mixed subtropical – tropical group (MST). Comparison of the OEI scale with the marine isotope divisions (Figure 5.11) reveals that the MST intervals are associated with the warmer interstadials of interglacial periods MIS 1, 5, 7, and 9. MST intervals only occur in the early and terminal portions of these interglacial stages apart from MIS 11 when it dominates the entire period. The duration of the MST intervals clearly influenced the % warm species (Figure 5.11). Although the proportion of warm species is high during the oligotrophic (gyre) OEIs, peak values of subtropical and tropical taxa are only associated with the MST intervals (Figure 5.11).

There are clear differences between the oligotrophic (gyre) and MST OEIs, based on the planktonic foraminifera species present in interglacial stadials and interstadials, changes in the diversity profiles, and the environmental implications of these factors. That the character of the water masses in the southern Cape Basin change *within* interglacial periods cannot then be disputed. Given the location of the sediment cores at the juncture between the Indian and Atlantic Oceans it seems likely that changes in the Agulhas Current may account for observed shifts to 'warmer' species assemblages and

ocean environments. The high values of 'warm water' species (25 to 30%) occurring during interglacials of the Quaternary exceed levels observed today (Giraudeau, 1993). Currently, the Cape Basin spliced core is located in transitional water masses that are strongly influenced by filaments of old, upwelled waters from the nearby southern Benguela upwelling cell and from passing Agulhas eddies. The high concentration of tropical and subtropical species observed during some climatic stages of the past 650 kyr are more representative of assemblages from the Agulhas Current (Hutson, 1980). This suggests that the MST intervals may indicate times of enhanced direct input Agulhas Current water masses into the Benguela region. Flores *et al.,* (1999), examining coccoliths and planktonic foraminifera in a core located in the Agulhas retroflection area, proposed enhanced Agulhas Current influence in interglacial periods. However, in addition to ecological support, the validation of this theory must also come from oceanographic and climatological evidence.

Presently, the majority of the transport from the Agulhas Current into the Benguela System is in the form of rings and eddies (Lutjeharms, *et al.,* 1981; Lutjeharms and van Ballegooyen, 1984; Shannon *et al.,* 1990a). These are a persistent and important feature of the region (discussed in Section 4.3.4). One ring can contribute an energy flux equivalent to 7% of the annual wind input over the entire basin (Olson and Evans, 1986). Furthermore, the majority of the rings follow an observed path into the Benguela System and South Atlantic (Figure 4.14). Therefore, an increase in Agulhas transport would have a major impact on the system and on thermohaline flux. A generation mechanism for an increase in Agulhas advection, or Agulhas 'warm events', exists. Strong easterly winds, which would be generated by an increased pressure gradient in interglacials, blowing across the southwest Indian Ocean (Agulhas source area) would enhance the poleward flow of the Agulhas Current. Modelling studies have shown the importance of changing atmospheric circulation to changes in oceanography and SST characteristics (de Ruijter and Boudra, 1985). A poleward shift in the Westerlies, as would be expected in interglacials, south of the African subcontinent, would facilitate westward penetration of the Agulhas Current into the southeast Atlantic (de Ruijter, 1982; de Ruijter and Boudra, 1985). These studies indicate that the Agulhas Current could flow directly into the South Atlantic because of the lack of a latitudinal variation in the wind stress curl. De Ruijter (1982) suggested that a latitudinal shift of just 1° could double the transport from the Indian Ocean. De Ruijter and Boudra (1985) again showed how little the wind stress curl

needed to shift, just 120 km, in order to both increase Agulhas advection and decrease the isolation of the Subtropical Gyres. Flores *et al.,* (1999) showed that north/south movements of the STF were linked to the east/west displacement of the Agulhas retroflection, resulting in a western position for the Agulhas Retroflection during Quaternary interglacials which is consistent with the results of this study. Increased advection of the Agulhas Current waters within the southeast Atlantic Ocean could alter the heat content of the surface waters considerably (Walker, 1990). Agulhas 'warm events', when large quantities of relatively warm water are observed northwest of the Agulhas Retroflection area in the southern and central Benguela area, do occur (Shannon *et al.,* 1990b) and are a possible analogue for times of greater Indian Ocean connection as described in the peaks of Quaternary interglacial periods (Figure 5.11). The generation of Agulhas 'warm events' depends upon intensification of the prevailing easterlies across the southwest Indian Ocean and a poleward displacement of the Westerlies. A positive ocean-atmosphere feedback may evolve, whereby the presence of abnormally warm waters south of the African subcontinent induces a southward shift of the major SST fronts in the region. Consequently, the meridional gradients of temperature, wind, and humidity would alter and further facilitate poleward displacement of the zonal Westerlies (Walker, 1990).

5.4.5 Mesotrophic Ocean Environmental Intervals

The planktonic foraminiferal composition and diversity profiles of the mesotrophic OEI indicate that it is an intermediate stage between eutrophic events and oligotrophic (gyre) intervals. The foraminifera species associated with this group (Figure 5.9) are characteristic of the mixing zone that lies between the upwelling influenced Benguela waters and the oligotrophic waters of the South Atlantic Subtropical Gyre (Giraudeau, 1993).

5.4.6 Subpolar Ocean Environmental Intervals

N. pachyderma (s), a species typical of newly upwelled waters in the Southern Benguela System and of subantarctic waters, is present in very small concentrations during most of the past 700 kyr. However, there are several intervals of peak abundance, in MIS 13/12 and MIS 9 (Figure 5.3). These *N. pachyderma* (s) peaks have been observed in other sediment cores in the region (Ufkes *et al.,* 2000; Giraudeau *et al.,* 2000; Chen *et*

al., submitted; Rau *pers. comm.*) confirming the reality of these signals in terms of water mass changes. The *N. pachyderma* (s) peaks in MIS 9 and 13 appear to be distinct in character from that identified as a unique OEI in MIS 12. This OEI, described as 'subpolar' in character, shows low values in each diversity index and a peak in *N. pachyderma* (s) consistent with observations of subpolar waters (Ottens and Nederbragt, 1992). Climate conditions in glacial MIS 12 would permit and would favour advection from subantarctic watermasses into the region as a result of perturbations in the STF. Indeed, this is an observed phenomena in the Benguela area, described in Section 4.2.5, and the mechanism illustrated in Figure 4.11. However, it is difficult to explain why this is only observed in one glacial period. Furthermore, equatorward advection of cold subantarctic waters, along the southwest margin of the African subcontinent, cannot be inferred as a mechanism for the abundance peak of *N. pachyderma* (s) in MIS 9 and 13. Previous studies of the palaeoceanography of the Southern Ocean indicate that MIS 9 was one of the warmest stages of the past half million years with extreme southward positions of the STF and SPF (Howard and Prell, 1992; Hodell, 1993; Niebler, 1995). This process would seriously prohibit the presence of subpolar waters in the SBS during these interglacials. The factors influencing *N. pachyderma* (s) peak abundance in interglacial MIS 9 and 13, as well as glacial MIS 12 (the unique OEI), do not appear to be related to the forcing mechanisms which drive glacial – interglacial cycles.

5.5 Summary

The planktonic foraminifera assemblage data from the spliced Cape Basin records reveal that the area was subject to extreme oceanographic and climatic change over the past 700 kyr. The core is located at the juncture of three oceanographic regimes: the South Atlantic, the Indian Ocean, and the Southern Ocean, together with upwelling of the Benguela system, all of which have shown varying degrees of influence on the surface mixed layer of the Southern Benguela region according to the nature of the prevailing climate conditions. It is also evident that given the complexity of the system, this data alone cannot provide firm answers on the mechanisms that drive the oceanographic changes recorded by the planktonic foraminifera. Nevertheless, this work will contribute to subsequent and ongoing studies in the area.

Firstly, it is shown that glacial periods are associated with enhanced productivity, most probably due to the oceanward penetration of filaments of old upwelled waters from the main coastal upwelling cells and increased mixing of surface waters due to enhanced Westerlies. However, it is difficult to draw any firm conclusions about the seasonality of such production given the lack of additional data concerning the strength of the Westerlies, the western position of the STF and the strength and position of the main upwelling cell. Nevertheless, given the dominance of eutrophic planktonic foraminifera *N. pachyderma* (d) in these intervals (Figure 5.11) it is likely that productivity is enhanced throughout the year as a result of the combination of the above factors.

Secondly, interglacial periods describe two distinct types of surface water regimes that appear to be driven by climatic processes. Greatest Agulhas transport into the South Atlantic appears to be shown in the planktonic foraminifera assemblage record as high relative abundance of subtropical and tropical species. These MST intervals are associated with periods of glacial – interglacial transition and peak interglacial stadials (Figure 5.11). Enhanced advection from the Indian ocean may be driven by intensified ocean-atmosphere feedbacks. Cooler interglacial intervals show greater influence of the South Atlantic Subtropical Gyre on the area as indicated by the foraminiferal species *Gr. inflata* (Figure 5.11). Insight into the timing and forcing mechanisms behind enhanced input of warm, saline watermasses from the Indian Ocean are important to furthering understanding of the thermohaline circulation and global climate patterns.

Chapter 6: Sea Surface Temperatures

CHAPTER 6: MULTI-PROXY RECORDS OF SEA SURFACE TEMPERATURE OSCILLATIONS OFFSHORE THE CAPE OF GOOD HOPE

6.1 INTRODUCTION

6.1.1 Importance of SSTs to palaeo-environmental research

The primary objective of this chapter is to present and discuss the results of the palaeo-sea surface temperature calculations from the spliced Cape Basin record and examine whether there is a meaningful relationship between the planktonic foraminiferal assemblage water mass indicators that coincide with observed temperature variations. The monitoring of past changes in SST and associated surface water mass circulation changes is crucial to understanding past climate change. Palaeo-SSTs should enable reconstruction of the past surface circulation at the juncture between the Indian and Atlantic Ocean. Understanding the changes in this region are important because the major climatic features of the area are linked closely to global climate through the thermohaline circulation (Gordon, 1986; Gordon *et al.* ,1992; Macdonald and Wunsch, 1996). Analysis of the SST data from the southern Cape Basin will focus on the timing and causation of early warming of SSTs at deglaciations during the late Quaternary.

The ability to accurately reconstruct SST through time is important to the study of global climate change because much of the residual heat which drives atmospheric anomalies is stored in the upper ocean. As described in chapter two, planktonic foraminifera have been used extensively in palaeo-environmental research because of their widespread geographical and geological occurrence, and more specifically, their sensitivity to environmental conditions. These qualities, coupled with the fact that all extant species spend at least a portion of their time in the upper waters of the photic zone (Bé, 1967; Bé and Tolderlund, 1971; Oberhänsli *et al.*, 1992; Kemle-von Mücke and Oberhänsli, 1999), make them an ideal tool for studying past sea surface temperature changes. However, as also stated in chapter two and illustrated in chapter five, interpretation of planktonic foraminiferal assemblage data is not as simple as evaluating the temperature ranges of the species present. Many species are sensitive to other environmental factors such as nutrient levels, salinity, thermocline depth and upwelling

conditions (Reynolds and Thunnell, 1985; Kroon and Ganssen, 1989; Giraudeau, 1993; Ufkes and Zachariasse, 1993, Kemle-von Mücke and Oberhänsli, 1999). Nevertheless, it is assumed that all species contribute some information relating to the temperature of the water they inhabited.

In this chapter, two independent methods of temperature determination are used. Firstly, transfer functions based on the planktonic foraminifera census data analysed in chapter five, and secondly, the alkenone $U^{k'}_{37}$ index, which employs unsaturation ratios of long chain ketones that are linearly related to water temperature (Sikes and Keigwin, 1994; Rosell-Melé *et al.*, 1995a; Schneider *et al.*, 1995). Both of these methods rely on extensive calibration to core top reference datasets and meteorological SST data. The assumptions behind the methods are described in chapter two.

6.1.2 Review of SST records in the SE Atlantic

During the Quaternary, climate and environmental change in southern Africa have been determined by a combination of the following factors: sea surface temperatures; ocean currents; atmospheric pressure and winds; and expansion and contraction of the Antarctic ice sheets. Palaeoceanographic research has shown that in general, SSTs were cooler than present during glacial periods over most of the Atlantic, Indian, and Antarctic Oceans (Hays *et al.*, 1976; Morley and Hays, 1979; Prell *et al.*, 1986; Mix *et al.*, 1986a), and warmer during interglacial MIS 5 and 1 (Summerhayes *et al.*, 1995; Labeyrie *et al.*, 1996; Kirst *et al.*, 1999). Present knowledge of the late Quaternary history of the surface circulation and upwelling in the Benguela Current System is based on sediment core material and most workers have focussed on the northern part of the system that experiences year-round upwelling. Oberhänsli (1991), Summerhayes *et al.* (1995), Little *et al.* (1997 a, b), Ufkes *et al.* (2000), and Shi *et al.* (2001) propose enhanced glacial upwelling and cooler associated SSTs, whilst Diester-Haas (1985) and Schmidt (1992) argue that upwelling in glacials was less intense. In the SBS upwelling appears to have been more intense during glacial periods and, associated with this, SSTs during glacials are lower than present (Chang *et al.*, 1999; Giraudeau *et al.*, 2000, 2001; Chen *et al.*, submitted). Flores *et al.* (1999), working in the Agulhas Retroflection area, found an increase in cold-eutrophic coccolithophorid species as well as a reduction in warm and

stratified water indicators during glacial periods. Schneider *et al.* (1999) presented the first alkenone based SST record in the southern Benguela System. This work showed lowest SSTs during glacial periods 2/4, 6, and 8, with MIS 6 being slightly warmer than the preceding and subsequent glacials.

A further feature of SST records from the South Atlantic and the Atlantic/Indian sector of the Southern Ocean are early warming and cooling signals in palaeo-SST records (Howard and Prell, 1992; Waelbroeck *et al.*, 1995; Labeyerie *et al.*, 1996; Schneider *et al.*, 1999; Mulitza and Rühlemann, 2000). Proposed explanations link this to north – south shifts in the location of the main frontal zones (Howard and Prell, 1992; Laybeyerie *et al.*, 1996), meltwater-induced reductions in northward heat transport (Mulitza and Rühlemann, 2000), and CO_2 forcing (Shackleton, 2000; Mudelsee 2001).

6.2 Initial attempts at generating palaeo- SST estimates from faunal assemblage data

6.2.1 Transfer function F81-25-5

Generation of robust SST estimates in the SBS is challenging because of the possibility of upwelling related variability. Upwelling in the SBS is strongly seasonal and a pulse of upwelling associated foraminifera could skew the temperature estimates. The fist attempt at generating SSTs on the gravity core GeoB 3603-2 was made using the transfer function 'F81-25-5', which was generated for use in the southern South Atlantic Ocean(Niebler and Gersonde, 1998). The summer and winter season SSTs are illustrated in Figure 6.1. The temperature range is from 18°C to 24°C in summer and 14°C to 21. 5°C in winter. Peak palaeo-SST is generated in the MIS 5/4 transition. Sample communality is high (Figure 6.2), especially during glacial periods, when colder water planktonic foraminifera assemblages prevailed (Figure 5.3). Non-analogue samples were common in interglacial periods, especially MIS 1, 5, and 7. The downcore F81-25-5 SST profiles (Figure 6.1) do not show any strong glacial – interglacial variations, in contrast to the variations in planktonic foraminifera species described in Chapter five (e.g. Figure 5.1). Explanation of the F81-25-5 SSTs in the context of

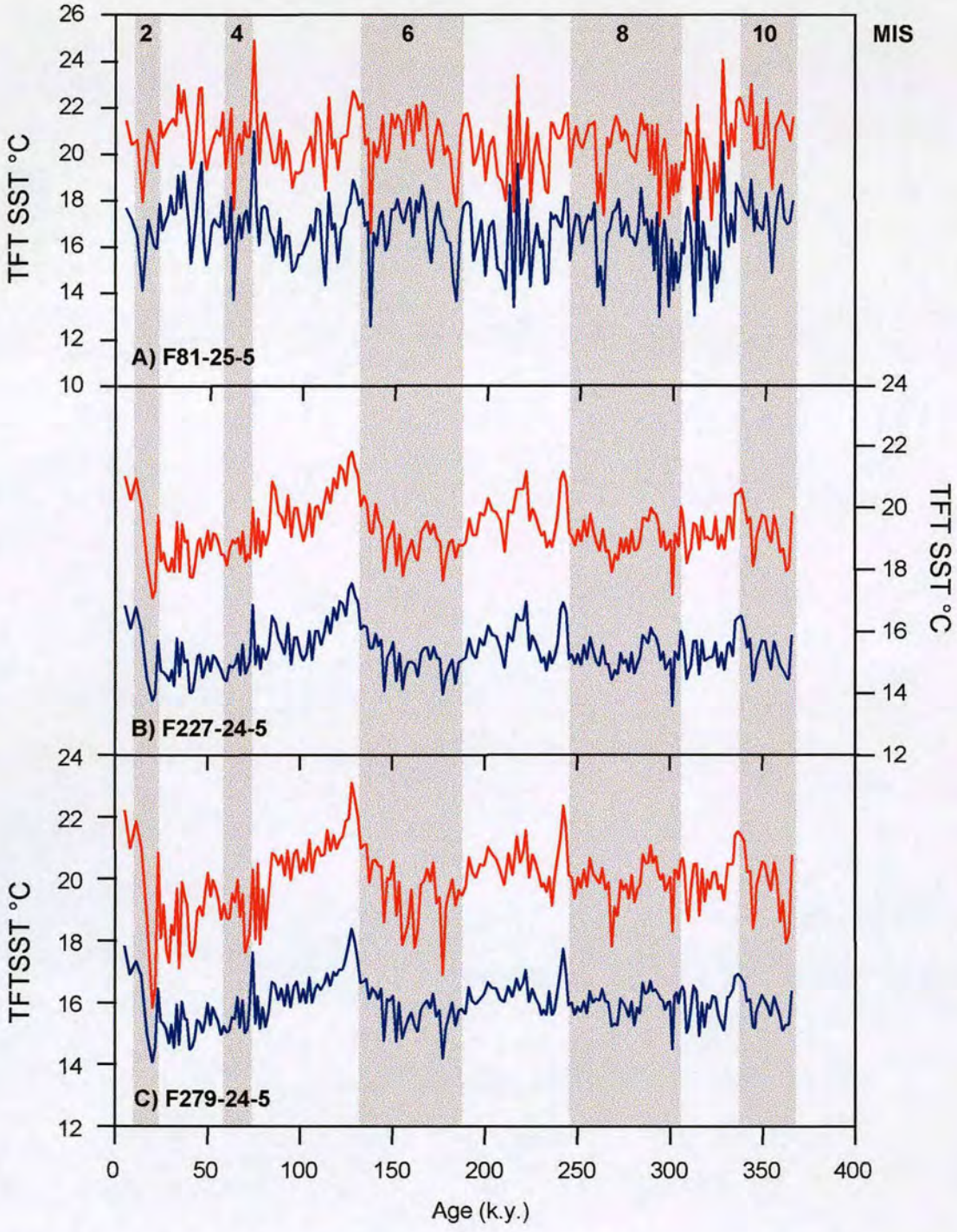

Figure 6.1 Preliminary transfer function results showing summer (red) and winter (blue) temperatures for core GeoB 3603-2. Descriptions of each transfer function are given in Table 2.1. The SST data are presented in Appendix 4.

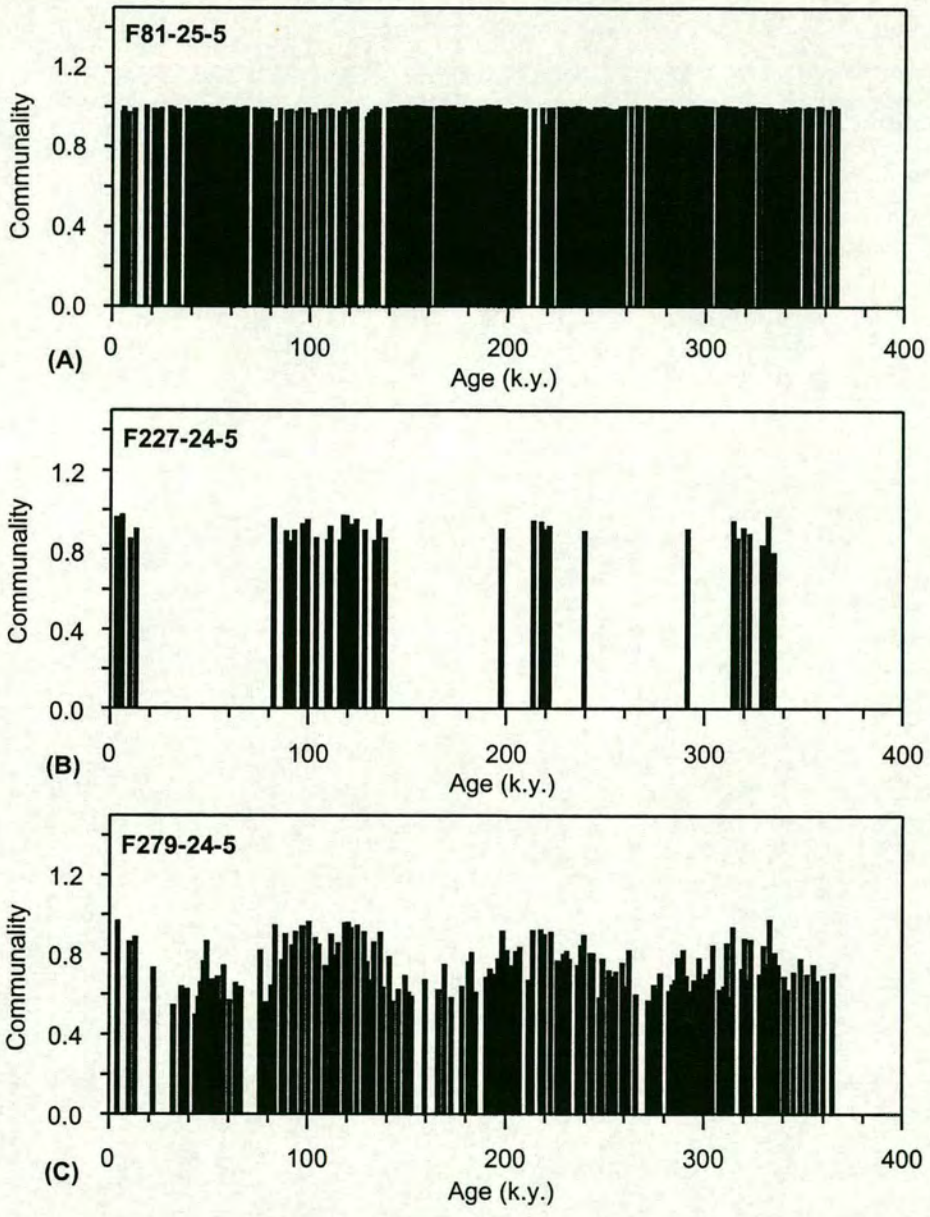

Figure 6.2: Communality results for preliminary transfer functions: **A)** F81-25-5 (Niebler and Gersonde, 1998); **B)** F227-24-5; **C)** F279-24-5.

oceanographic and climatic change is difficult, given the environmental information generated by the planktonic foraminifera. The core top database used in this transfer function is relatively small and geographically concentrated. The majority of the core tops are in the subantarctic southern South Atlantic, well south of the Cape Basin, and the Benguela System coretop samples are from the centres of upwelling in the NBS, where the upwelling regime is very different to that prevalent at the location of the Cape Basin spliced core. Examination of the data revealed that nine coretop samples from the NBS were forcing much of the palaeo-SST estimates. Factor 1 of the transfer function linked the relative abundance of *N. pachyderma* (d) in the spliced core to similar values in the NBS. The NBS coretops are located under upwellling cells and the *N. pachyderma* (d) in the Cape Basin spliced core are most probably related to upwelling filaments. Most planktonic foraminiferal species can tolerate a wide band of temperature but the F81-25-5 transfer function appears to be biased towards the cold-end of the *N. pachyderma* (d) range. Furthermore, the peaks in tropical and subtropical species seen in the spliced core (Figure 5.6) were causing non-analogue samples in interglacials. The SSTs estimates generated from F81-25-5 were thus rejected in favour of a wider coretop database. This was necessary as the location of the core, at the juncture of several distinct oceanographic regimes, requires coretop samples from areas that can describe these oceanographic conditions and thus explain oceanographic variance throughout the late Quaternary.

6.2.2 Transfer function F227-24-5

The aim of this transfer function equation was to address the interglacial non-analogue sample problem revealed by F81-25-5. F227-24-5 was essentially a stage in the development of a new transfer function that would be applicable to sites of the ocean area in the juncture between the Indian and Atlantic Oceans. In the past it has been extremely difficult to generate reliable faunal based SST estimates for this area, as the example F81-25-5 above illustrates. The coretop database was expanded to include sites in the Indian Ocean, in order to provide analogues for interglacial periods when advection from the Agulhas Current may have been greater. The SSTs generated by this transfer function are shown in Figure 6.1. The summer temperature range is 17°C to 22°C and winter is 13.5°C to 17.5°C. The seasonal temperature records show glacial –

interglacial variation with warmer conditions during interglacial periods. Coldest SSTs were reached in MIS 2 and warmest in MIS 5.5. Temperature changes show a gradual saw-tooth pattern of change across transitions in sharp contrast to foraminiferal abundance changes, e.g. *N. pachyderma* (d) (Figure 5.1) and the planktonic and benthic oxygen isotope profiles for the core illustrated in Figure 6.3. Communality values for this transfer function are shown in Figure 6.2. The results are poor, showing good communality only in interglacial periods and non-analogue samples throughout the glacial periods. Therefore, the temperature estimates produced by the F227-24-5 equation are also not reliable.

6.2.3 Transfer function F279-24-5

One further transfer function was used in an attempt to circumvent the problems of the previous two equations. F279-24-5 incorporated coretop samples from sites in the Atlantic Ocean from 10°N to 55°S and sites in the Indian Ocean to provide suitable analogue data for the Cape Basin spliced record. The SST data for F279-24-5 are shown in Figure 6.1. The profile of the summer and winter temperatures resembles the oxygen isotopes more closely than any of the previous transfer functions of the study. Interglacial stages 5.5, 7.3, and 9.3 are easily distinguished as intervals of peak sea surface temperatures. The temperature range of 8°C, calculated for the summer season, extends from a minimum of 15.5°C in MIS 2 to a maximum temperature of 23.5°C in MIS 5.5. The winter temperature curve shows much smaller temperature range of 4.5°C (minimum of 14°C and maximum 18.5°C). Apart from the interglacial peaks of MIS 9.3, 7.3, and 5.5, the SST profiles are relatively flat, showing cyclic variations in temperature during glacials and interglacials that are not explained by changes in global climate. The communality profile for F279-24-5 shows much fewer non-analogue samples than F271-24-5 but the communality values are not consistent and many values are below the 0.7 lower confidence level. The communality figures show that F279-24-5 is not a strong enough transfer function to provide robust SST estimates for the Cape Basin spliced record.

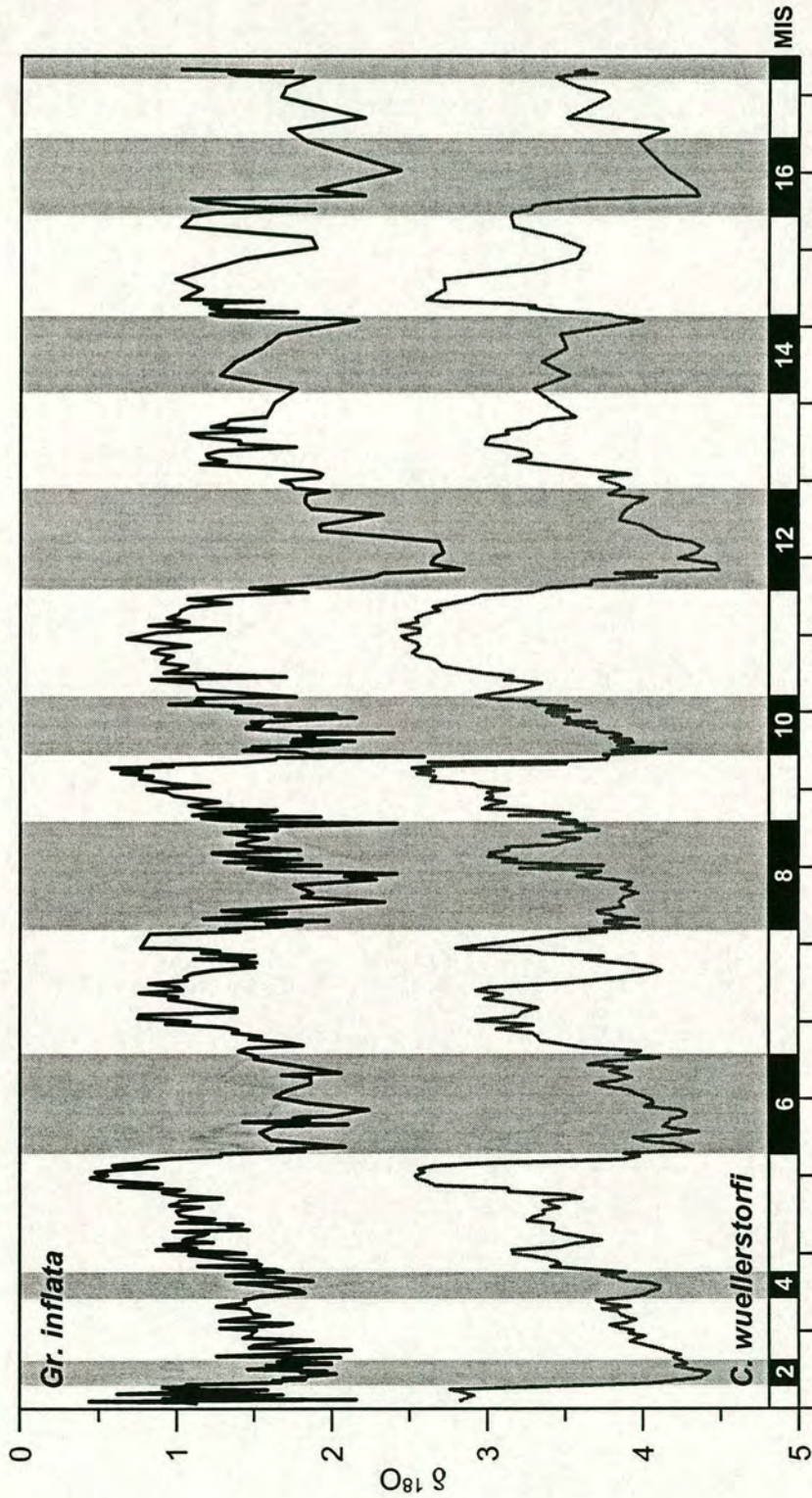

Figure 6.3: Benthic and planktonic $\delta^{18}O$ data from the Cape Basin site. Benthic data from spliced Cape Basin record, planktonic $\delta^{18}O$ from MD96 2081 only.

6.3 Robust attempts at generating SST records for the southern Cape Basin by using a new transfer function F271-24-5

6.3.1 Seasonal SST records from the Cape Basin spanning the past 700 kyr

The final transfer function F271-24-5 (Niebler *et al.*, submitted) incorporated the most extensive suite of coretop samples from the Benguela area, the Atlantic Ocean from 10°N to 55°S, and the south-western Indian Ocean. The results for warm and cold season SSTs are illustrated in Figure 6.4. Also included on this figure is the benthic oxygen isotope curve, which provides a general stratigraphic profile of global boundary conditions, with the glacial periods depicted by shading. The summer and winter SST records are typical for the pelagic ocean, displaying clear glacial – interglacial variations, with warmest temperatures during MIS 5.5 and 1 and coldest temperatures at full-glacial periods. Interglacial warming is more pronounced in the early parts of the stages. The amplitude per mil variation between glacials and interglacials is fairly constant, except for a significant excursion to cooler temperatures recorded during the transition from MIS 13 to MIS 12. This interval is clearly the coldest glacial period throughout the core length. The *C. wuellerstorfi* $\delta^{18}O$ data show that the MIS 12 glacial has the heaviest isotope values than any other climatic period of the past 700 kyr. Including this cold excursion, an extra 4°C cooling, the temperature range in the summer season spans 8.5°C from 14°C to 22.5°C. The maximum temperatures are similar to those generated by transfer function F227-24-5, which focused on interglacial analogues. MIS 1, 5, and 11 are the warmest interglacial periods over the past 700 kyr. Peak SSTs are reached in MIS 5.5 and MIS 11 is the longest sustained warm interglacial of this time period. The unique conditions of MIS 11 in the context of the Cape Basin record and globally will be a focus of discussion in Chapter seven. The average difference between cold and warm season values is 4°C.

Winter season SSTs have a smaller temperature range from 11°C to 17.5°C. The TFT SSTs show much variability superimposed on the broad glacial – interglacial patterns so far described. In this they are similar to the foraminifera species profiles described in chapter five. Communality for F271-24-5 is illustrated in Figure 6.5. The values are consistently high throughout the length of the core and there are very few

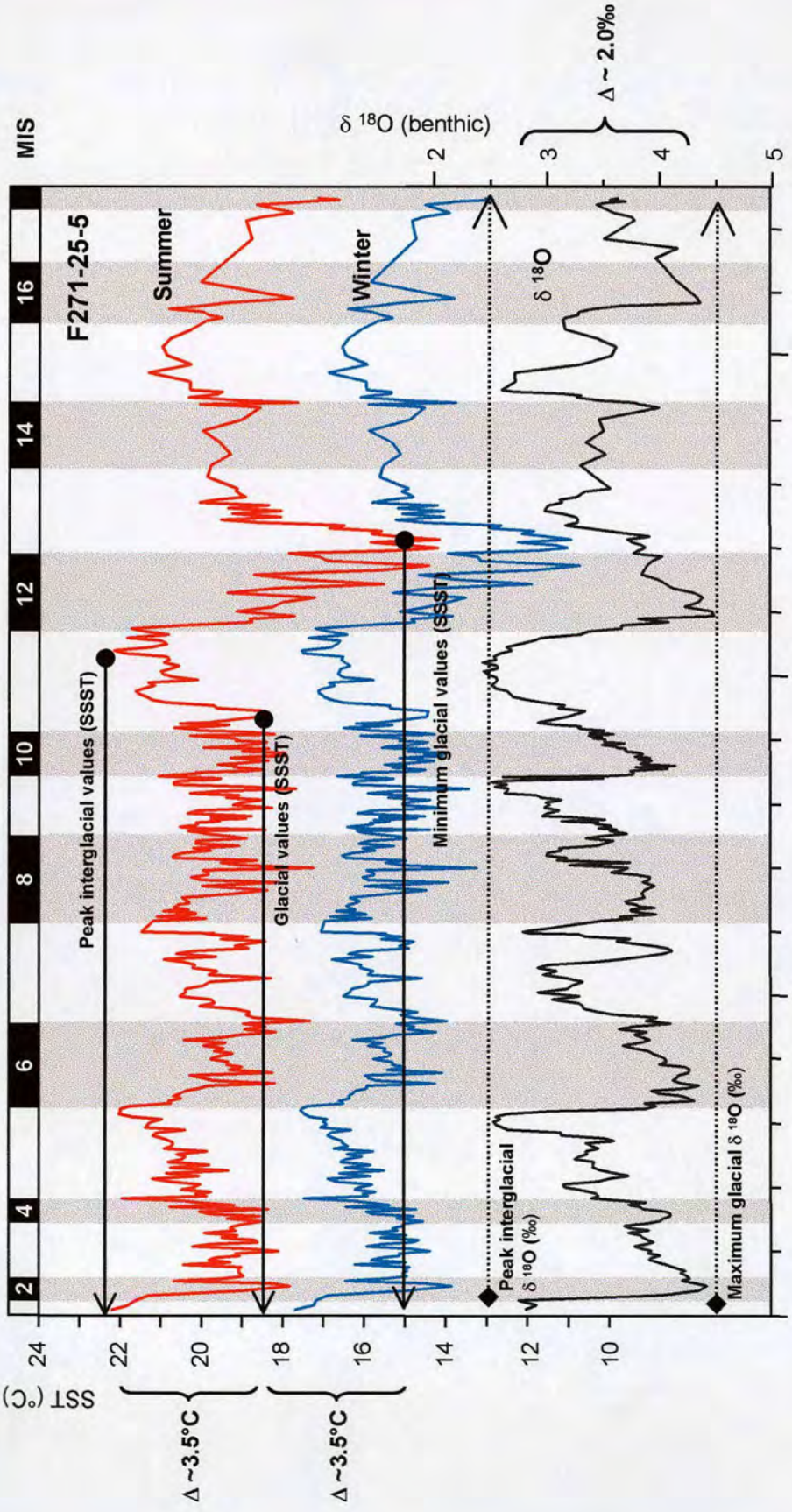

Figure 6.4: F271-24-5 summer and winter SSTs offshore Cape Town. Solid black arrows indicate the amplitude of glacial - interglacial summer SST (SSST) variations. The $\delta^{18}O$ (*C. wuellerstorfi*) stratigraphy is shown to indicate the amplitude of global climate variations during the same period.

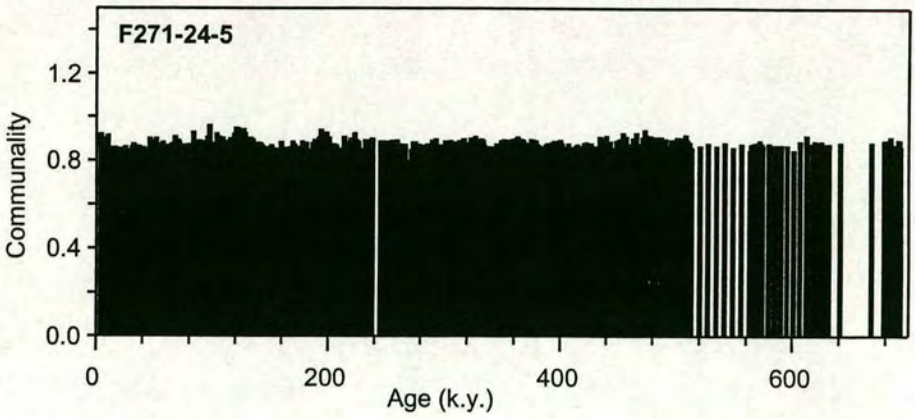

Figure 6.5: Communality statistics from transfer function F271-24-5 (Niebler *et al.*, in prep.) for the Cape Basin spliced record.

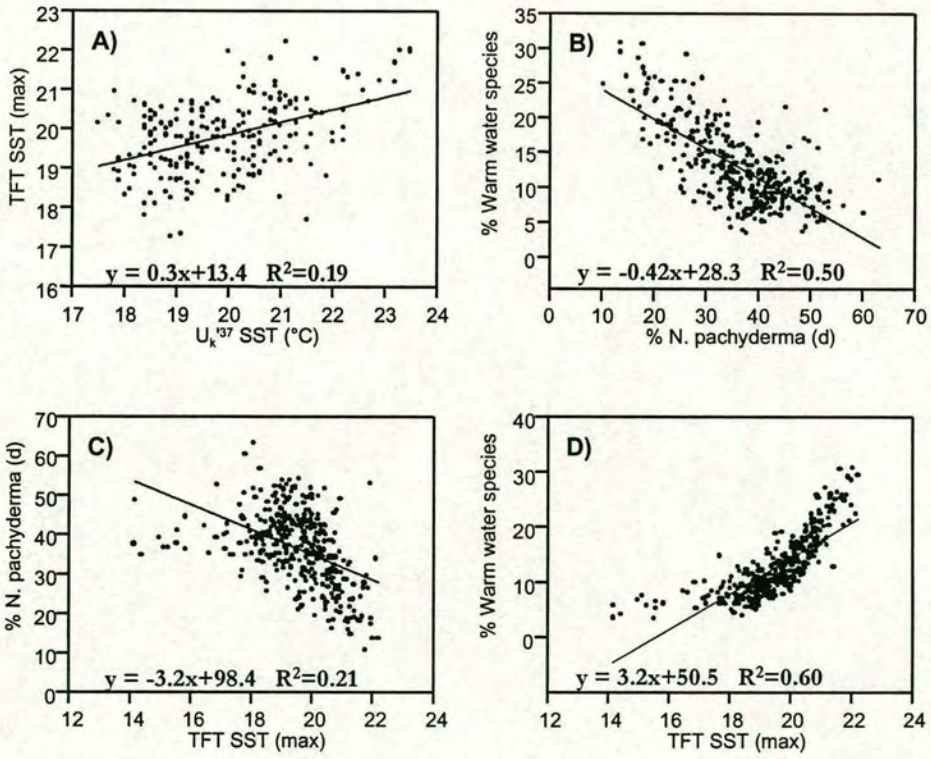

Figure 6.6: Scatter plots showing SSTs (TFT F271-24-5 and $U^{k'}_{37}$) in relation to the planktonic foraminiferal components of the TFT SST record in the Cape Basin spliced record.

non-analogue samples. The majority of the non-analogue samples are located in the early section of the core. Figure 6.6 shows relation between TFT input and output.

6.3.2 Alkenone SST record from core GeoB 3603-2 for the past 360 kyr.

As the $U^{k'}_{37}$ index is only determined by the temperature of the ambient watermass in which the flora were living (Müller *et al.*, 1998) and not influenced by other factors such as nutrient availability, the alkenone SST record should be and is more similar to the oxygen isotope curve than the faunal based SSTs (Figure 6.4). $U^{k'}_{37}$ SSTs are arguably a more accurate reflection of global climate forcing effects in the Cape Basin. The palaeo-SSTs for core GeoB 3603-2 based on the alkenone technique are presented in Figure 6.7 and show distinct glacial-interglacial variations that match those of the benthic $\delta^{18}O$ records. The mean annual temperature ranges from 23.5°C to 18°C. Peak sea surface temperatures of ~23.5°C occurred during MIS 5.5. Interglacials MIS 7.5 and 9.3 were also markedly warmer than other interglacial interstadials such as 7.1. SSTs during these warm intervals are higher than modern observations (Levitus and Boyer, 1994). Alkenone SSTs for this core indicate a glacial MIS 6 that was warmer than either MIS 2 or 8. This has been observed in other $U^{k'}_{37}$ SST records in the South Atlantic (Schneider *et al.*, 1999) and Arabian Sea (Rostek *et al.*, 1997). Average glacial SST estimates are cooler than present day mean annual SSTs in the area and are similar to temperatures recorded when upwelling is strong or when intrusions of subantarctic waters influence the SBS (Shannon *et al.*, 1989; Taunton-Clark, 1990; Levitus and Boyer, 1994).

6.4 Discussion

6.4.1 Comparison of alkenone and transfer function SST records

Past SSTs in the southern Cape Basin have been inferred from changes in the composition of planktonic foraminiferal assemblages and the $U^{k'}_{37}$ method. The calculation of faunal based SSTs using the different reference datasets and related transfer functions, apart from equation F81-25-5, revealed only small differences in

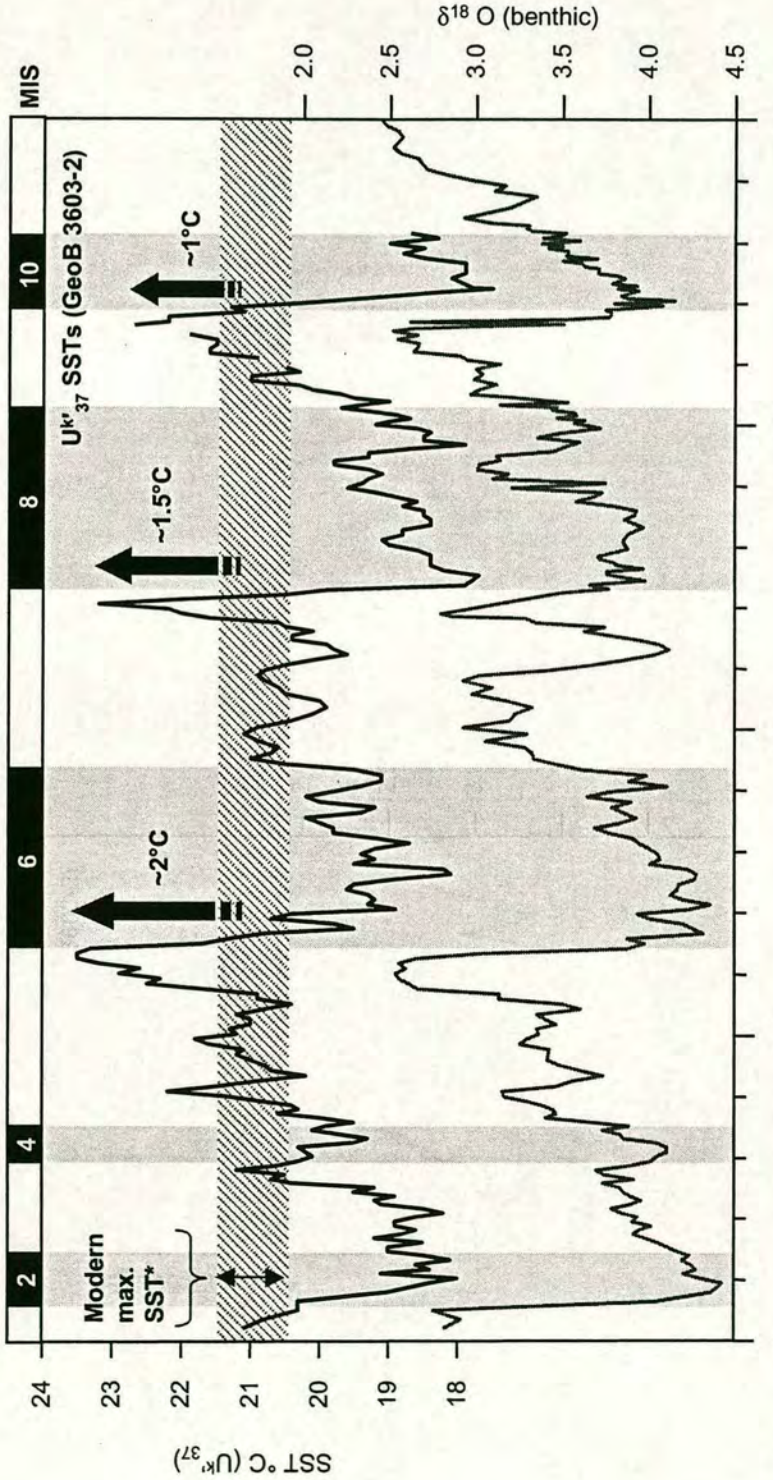

Figure 6.7: $U^{k'}_{37}$ palaeo-sea surface temperatures for core GeoB 3603-2 and benthic $\delta^{18}O$ record. Modern mean summer SST (~21°C) is indicated by dashed line (Levitus and Boyer, 1994). Black arrows highlight SSTs exceeding maximum modern surface temperatures in MIS 9.3, 7,5, and 5.5. Alkenone SST' data are presented in Appendix 4.

terms of the shape of the palaeo-temperature curve and the obtained absolute values (Sections in 6.2 and 6.3.1). The warmer temperatures calculated using F81-25-5 can be attributed to the location of a major proportion of the reference data core tops in the subpolar South Atlantic and consequently elevated palaeo-temperature values. All of the SST estimates (faunal and alkenone) provide temperature maxima in the interglacial climatic optimums 9.3, 7.5, 5.5 (and, for the TFT method, MIS 1), exceeding the modern average temperature values at the core location (~19°C mean annual, ~ 21°C maximum warm season). The coldest temperatures are observed in stages 2 and 6, where values below the present SST were observed.

There are apparent discrepancies between the observed absolute palaeo-temperatures from the alkenone and the TFT methods during the peak interglacial sub-stages (Figure 6.8). During MIS 9.3, 7.5, and 5.5 the maximum SSTs recorded by the coccoliths are higher by ~1. 5°C than those estimated by the foraminiferal method. Glacial mean annual temperatures recorded by the alkenone technique are comparable to the TFT summer season glacial SSTs, which are in close agreement with present day cold season SST observations (Levitus and Boyer, 1994). Alkenone based SST curves have been described as an 'annual' SST estimate in the NBS and equatorial Atlantic (Schneider *et al.*, 1995). Yet the annual SST record generated by the planktonic foraminiferal assemblages (Figure 6.9) shows cooler temperature estimates than the $U^{k'}_{37}$ SSTs throughout the past 360 kyr. The difference in interglacial SSTs recorded by the two techniques may be explained in two ways; either anomalously high $U^{k'}_{37}$ SSTs; or anomalously low TFT SSTs. These two possibilities are outlined below. In fact, the truth is probably a combination of both scenarios.

Scenario A: $U^{k'}_{37}$ anomaly

$U^{k'}_{37}$ SSTs are an indicator of the ambient water temperature at the time of the peak flux of coccolith production (Chapman *et al.*, 1996). In offshore surface waters off south west Africa coccolithophorids bloom in waters above a well developed thermocline (Mitchell-Innes and Winter, 1987; Giraudeau, 1993) and not in the centre of upwelling cells. A time-series sediment trap experiment (Wefer and Fischer, 1993) revealed two prominent maxima of alkenone export to the sediment during austral

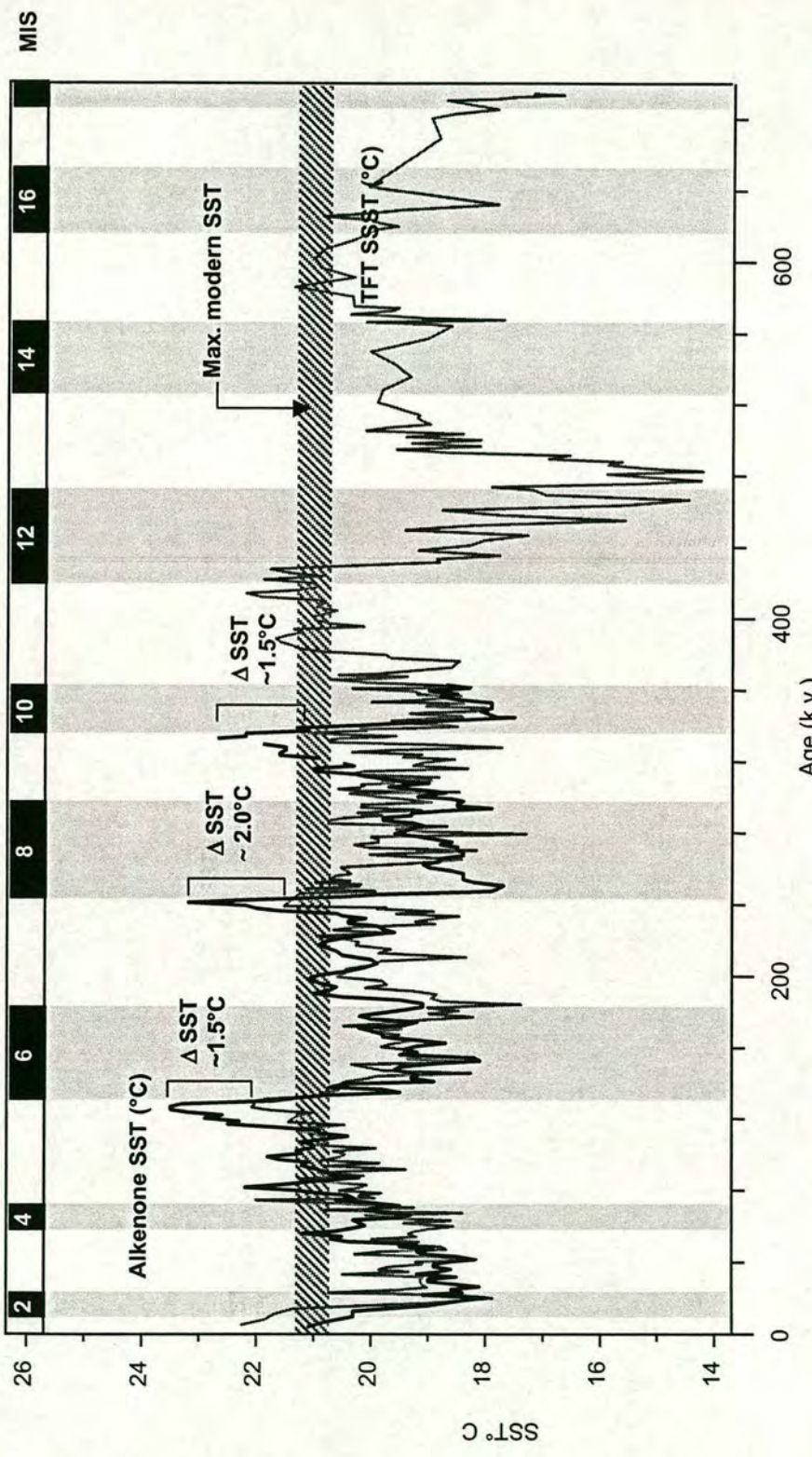

Figure 6.8 Comparison between proxy SST records in the Cape Basin. The alkenone record, showing mean annual temperatures for the past 0.36 Myr, is shown with the summer sea surface temperature (SSST) curve generated by the transfer function F271-24-5. Δ SST indicates the discrepancy between the alkenone SST and the TFT SSSTs during peak interglacial intervals.

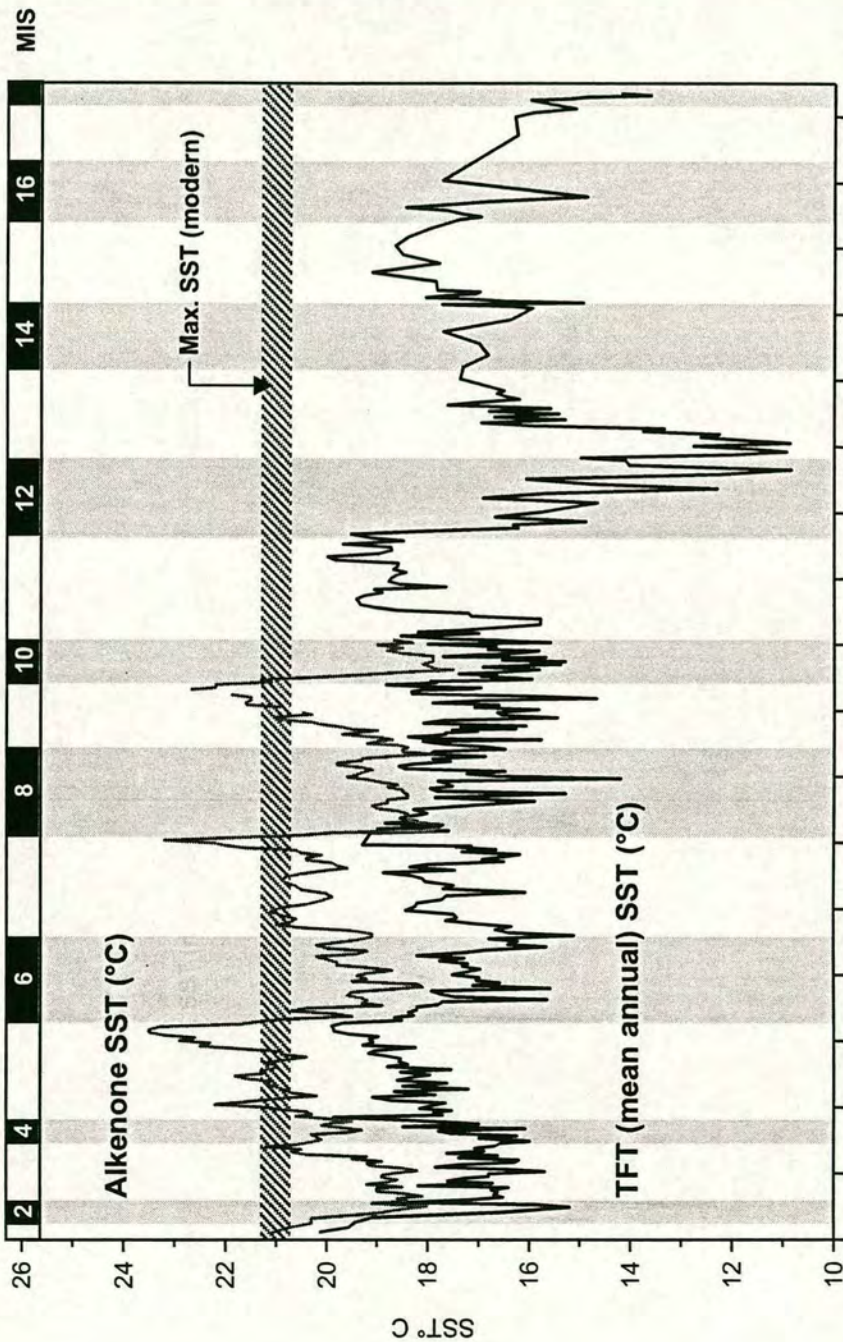

Figure 6.9 Comparison between proxy mean annual SST records in the Cape Basin. The alkenone record (grey), which spans the past 0.36 Myr (core GeoB 3603-2), is shown with an annual SST record generated by the transfer function F271-24-5 for the spliced record.

spring and autumn. As the upwelling of cold water occurs in the summer in the SBS, summer temperatures are lower than spring and autumn SSTs. Therefore, the alkenone blooms take place in the 'calorific' warm seasons rather than the meteorological summer. This may account for the $U^{k'}_{37}$ index showing warmer SSTs than the planktonic foraminifera. Furthermore, in times of high flux there could be greater water column remineralisation of certain alkenones. Such remineralisation would bias the record toward warmer temperatures (Prahl *et al.*, 1993). These factors may explain the observed discrepancy in the SSTs toward warmer $U^{k'}_{37}$ palaeo-temperature estimates (Figure 6.8).

Scenario B: TFT anomaly

Analysis of the faunal counts during the intervals of temperature offset between the alkenone and TFT SSTs, namely the MIS interglacial peaks 9.3, 7.5, and 5.5, reveal that they are characterised by a mixed assemblage of tropical – subtropical species (Figure 5.11). The analysis of the planktonic foraminiferal assemblages in chapter five has demonstrated that during these peak interglacial stages upwelling was suppressed (but not absent) in the southern Cape Basin and that advection from the Indian Ocean was strong. The relatively low (~20%) abundance of *N. pachyderma* (d) recorded during MIS 9.3, 7.5 and 5.5, corresponding to shallower upwelling, may contribute to lower TFT SST estimates during these intervals. The Imbrie-Kipp approach does attempt to overcome this problem to a certain degree, by the application of species weightings in the calculation procedure and in the defining of water mass characteristics as factors in the transfer function.

Despite the differences in SST estimates, the amplitude of glacial – interglacial change shown by each SST proxy record is ~4.5°C (Figures 6.4 and 6.6). Furthermore, the general trends and timings on a glacial – interglacial scale are similar for the $U^{k'}_{37}$ and the faunal palaeo-SSTs (Figure 6.9).

A multi-proxy reconstruction is justified because the biases in each method should cancel each other out. There are still very few sediment cores where it is possible to directly compare more than one SST proxy (Bard, 2001). The Cape Basin

records support these other data sets, being in general agreement about the amplitude of changes observed around the World ocean. Other mid-latitude sites in the Atlantic and Indian Oceans have also revealed discrepancies between alkenone and transfer function SSTs. Pichon *et al.* (1998) found alkenone temperatures to be ~2°C warmer than those from a diatom transfer function, similar to the inconsistency between the records presented here for the southern Cape Basin. Weaver *et al.* (1999) and Sikes and Keigwin (1996), working in the North Atlantic, reported similar deglacial warming from $U^{k'}_{37}$ and TFT SSTs despite the alkenone temperatures being ~4°C warmer. Both groups of workers suggested that the $U^{k'}_{37}$ data are representative of summer growth conditions rather than mean annual temperatures. More work is needed to assess the behaviour of foraminifera and alkenones under unusual conditions such as the those found at the juncture between the Indian and Atlantic Oceans. Nevertheless, in combination, these two sets of SST data should elucidate part of the complex palaeo-history of the southern Cape Basin.

6.4.2 Glacial temperatures and circulation offshore the Cape of Good Hope

Glacial surface water circulation offshore the Cape of Good Hope has varied considerably during the late Quaternary. SST data from this study reveal two dissimilar glacial periods that are distinct from other glacials in the time span. In contrast to SST records from mid-latitude South Atlantic and Southern Ocean, both SST techniques employed in the Cape Basin spliced record reveal only moderate cooling in MIS 6. Furthermore, this study documents that the coolest SSTs in MIS 6 occurred mid-glacial, in contrast to preceding and subsequent glacial periods, e.g. MIS 2/4, where coldest SSTs were achieved near the end of the period when ice volume was greatest (Figure 6.10). Sediment cores from further north in the South East Atlantic (Schneider *et al.*, 1995; Kirst *et al.*, 1999) show MIS 6 SST curves that are similar to the oxygen isotope record, a stage 6 which is as cold as MIS 2/4 and 8, and maximum cooling at the end of the glacial. However, a relatively warm MIS 6 is a global feature of tropical SST curves (Rostek *et al.*, 1993; 1997; Emeis *et al.*, 1995; Kirst *et al.*, 1999; Wolff *et al.*, 1999). The mechanism for this relative warmth is most likely of tropical origin, and it is therefore unusual to see this kind of SST pattern in the mid latitude spliced record in the southern Cape Basin. The origin of this tropical signal in this record lies in the position of the

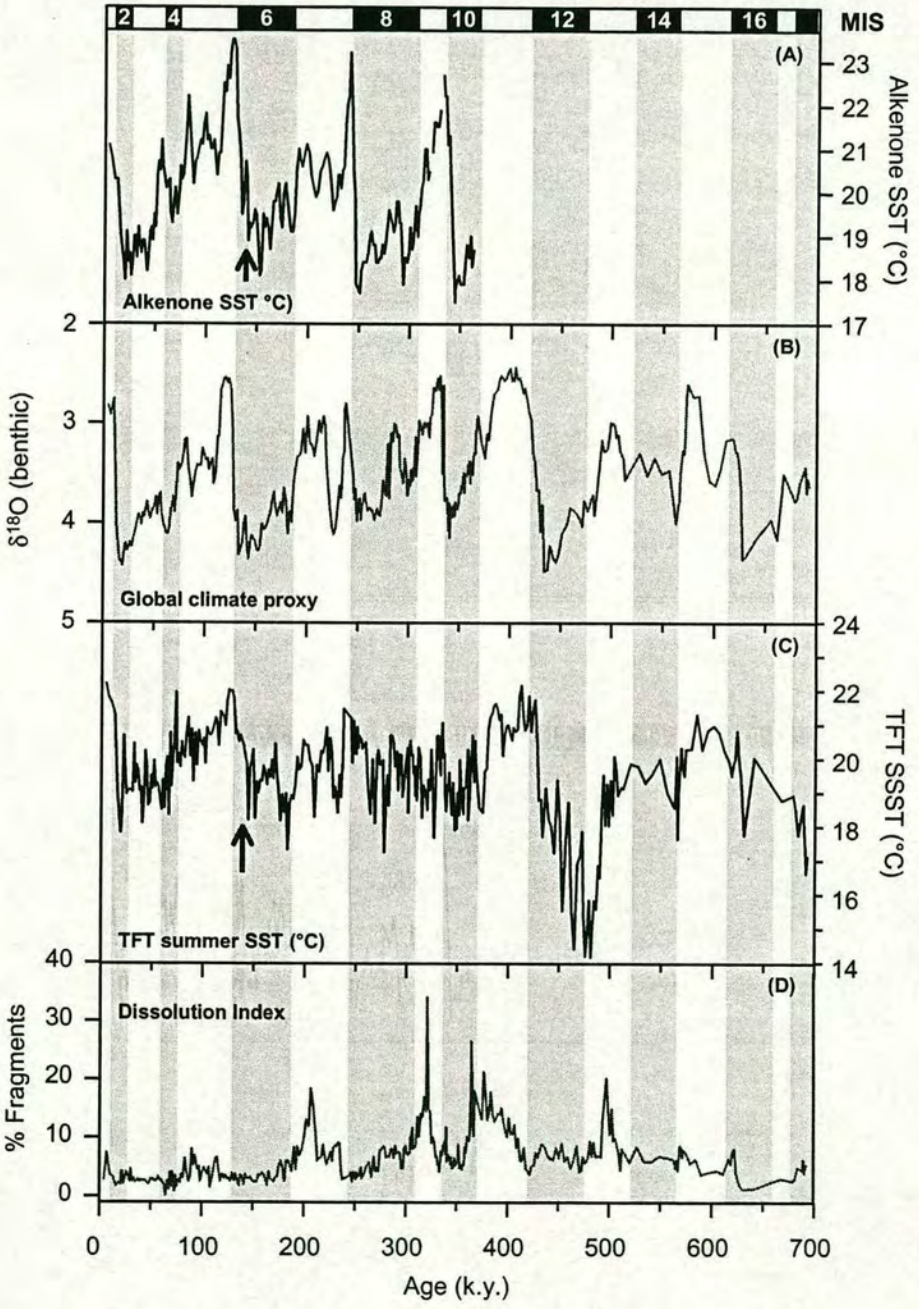

Figure 6.10 Comparison of the spliced Cape Basin record of **A)** alkenone mean SST (°C), **B)** % fragments, **C)** transfer function summer SST (°C), and **D)** benthic $\delta^{18}O$. Early warming at Termination II indicated by black arrows.

cores at the juncture between the Indian and Atlantic Oceans and is a direct response to insolation driven surface water warming in the tropical Indian ocean that is translated via advection from the Agulhas Current.

The SST record of MIS 12 is even more distinct than MIS 6 (Figure 6.11). According to the faunal based SSTs, the strongest glacial conditions in surface waters off the Cape of Good Hope in the South Atlantic occurred during MIS 12. The summer SSTs of ~14°C are colder than present day winter SSTs in the area of the sediment core. Clearly, these very low SSTs are associated with the increased abundance of *N. pachyderma* (s) and the lowest % warm species values down core (Figure 6.11). These SSTs may be derived from a steady shoaling of isotherms and either expansion of the SBS upwelling zone or a shift in its location due to sea-level change offshore the Cape of Good Hope (Lutjeharms and van Ballegooyen, 1984). An alternative explanation is a movement of the STF north of its present position, which would bring cool, nutrient rich, subantarctic waters to 35°S. If the observations about MIS 12 are not regionally forced, i.e. derived from a change in SBS upwelling, and occurred on a global scale, then this is most likely the cause of the extremely cold SSTs recorded by the transfer function. The largest amplitude change in oxygen isotope records of the past 6 Myr is observed at about 0.43 Ma, during the 12/11 termination (Mix *et al.*, 1995; Pisias *et al.*, 1995; Shackleton *et al.*, 1995). Additionally, the mid-Pleistocene transition, a switch from the dominance of the 41 kyr climate cycle to the 100 kyr cycle, has been reported as a time of intensified circulation (Jansen *et al.*, 1986). Palaeoceanographic data from ODP Hole 704 in the southern Ocean (46° 52.8'S, 7° 25.3'E) identifies MIS 12 as the most extreme glacial of the Pleistocene (Hodell, 1993). Hodell (1993) found that MIS 12 registered the highest $\delta^{18}O$ values of *N. pachyderma* (s), the lowest $CaCo_3$ content, the highest values of opaline silica and the highest rate of fragmentation during the past 700 kyr. Furthermore, Raymo *et al.* (1990) found that MIS 12 was the time of maximum suppression of NADW. Therefore, it is most likely that the percentage *N. pachyderma* (s) and associated low SSTs observed in the spliced Cape Basin record (Figure 6.11) are derived from subantarctic advection.

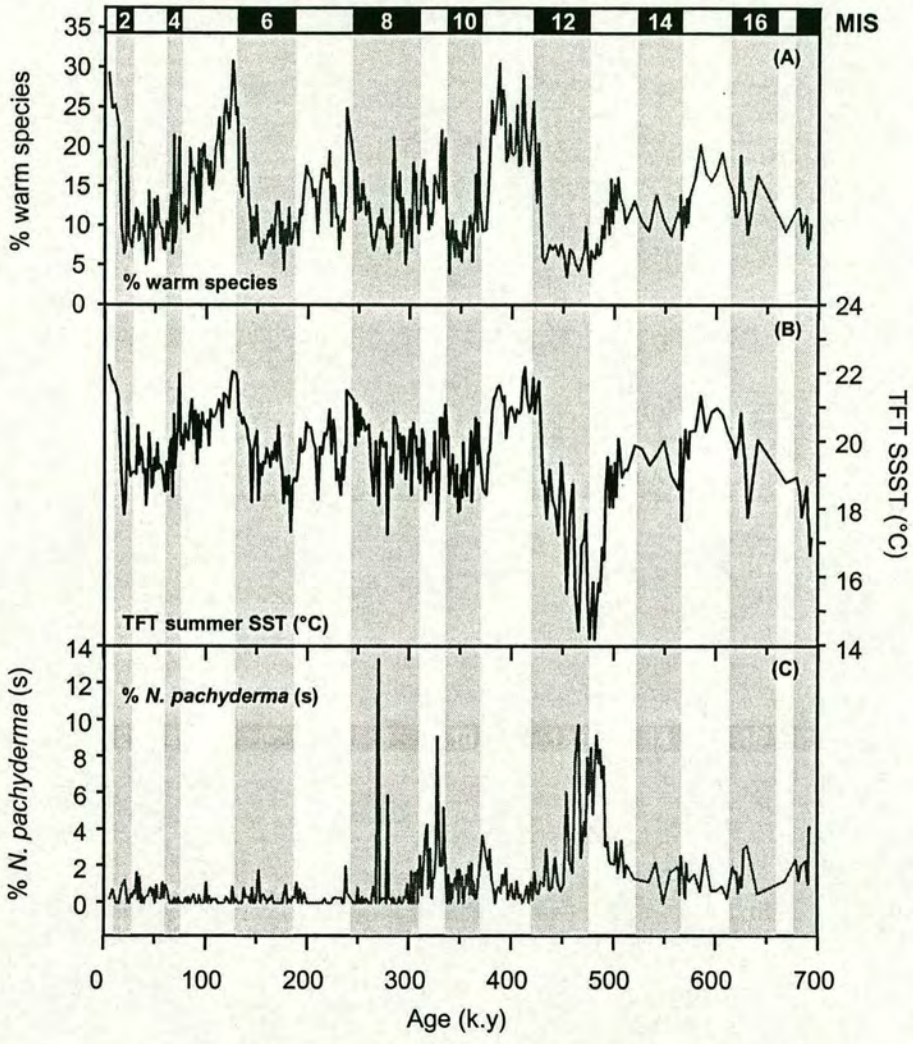

Figure 6.11 Comparison of **A)** % warm species (defined on Figure 5.6), **B)** transfer function summer SST (°C), and **C)** % *N. pachyderma* (s) for the spliced Cape Basin record.

6.4.3 A unique interglacial? MIS 9

Transfer function SSTs during the lightest oxygen isotope events of stage 9 are much cooler than those of preceding or subsequent interglacial periods. However, this record of relatively moderate MIS 9 surface water warming is not echoed in the alkenone SST curve (Figure 6.10). Other data from the spliced cores may help to explain the difference in the SST records for MIS 9. The percentage fragmentation curve (Figure 6.10D) shows a dissolution peak during the stage 9 interglacial. Enhanced dissolution may be caused by a change in the source of deep water or by enhanced productivity in the surface layers of the water column. The abundance record of *N. pachyderma* (s), shown on Figure 6.11C, also shows a peak during MIS 9, and this coincides with the lowered SSTs shown by the TFT. This abundance peak has been observed in other sediment cores in the region in locations to the north and south of the spliced record (Flores *et al.*, 1999; Chang *et al.*, 1999; Giraudeau *et al.*, 2000; Chen *et al.*, submitted; Rau, *pers. comm.*). Clearly the TFT SSTs are influenced by the presence of this cold water species.

The origin of this unusual 'spike' is difficult to determine. As the alkenone proxy does not record relatively cool MIS 9 SSTs, the coccolithophorid bloom and the increased abundance of *N. pachyderma* (s) must occur in different seasons. The *N. pachyderma* (s) can come from two sources (described in section 6. 4. 2): either a change in upwelling, or advection from south of the STF. *N. pachyderma* (s) has a strong association with present day seasonal upwelling in the SBS (Giraudeau, 1993) and also within watermasses south of the STF (Niebler and Gersonde, 1998). Examination of palaeo-climate records from the southern Atlantic and Indian Oceans suggests that the *N. pachyderma* (s) source in MIS 9 is unlikely to be advection of subantarctic waters. During this interval the APF and the STF were much further south than their present position (Howard and Prell, 1992; Hodell, 1993; Hodell *et al.* , 2000). Independent data from Antarctica, the Vostok Deuterium (δD), record supports the claim that MIS 9 was one of the warmest interglacials of the past 0.5 Myr (Petit *et al.*, 1999). However, a possible advection mechanism, described in Section 4.2.5, whereby a disturbance in the STF can lead to the entrainment of subantarctic waters in the wake of Agulhas eddies may account for the *N. pachyderma* (s) spike. A seasonal strengthening of upwelling in

the SBS is also difficult to explain, as this would require a change in the wind field. However, the enhanced dissolution would seem to support this source. In absence of further supporting data the source of the *N. pachyderma* (s) spike observed throughout cores in the Benguela region must remain unresolved.

6.4.4 Early surface water warming and a tropical signal in the Cape Basin during transitions

A clear and significant trend of sea-surface warming prior to global deglaciation is recorded in both sets of SST reconstructions. Such a leading pattern of SSTs in relation to $\delta^{18}O$ is not restricted to the southern Indian and Atlantic Oceans. It is observed in the Southern Ocean (Hays *et al.*, 1976; CLIMAP, 1984; Imbrie *et al.*, 1989, 1992, 1993; Howard and Prell, 1992; Layberie *et al.*, 1996; Brathauer and Abelmann, 1999), the equatorial Atlantic (Imbrie *et al.* , 1989; Schneider *et al.*, 1995) and the equatorial Pacific Ocean (Pisias and Mix, 1997). The Cape Basin is found at a key location linking these areas. Early warning is not seen in the North Atlantic (Schneider *et al.*, 1999). Research concerning late Quaternary deglacial transitions and the role of the southern hemisphere is currently receiving much attention (e.g. Henderson and Slowey, 2000; Shackleton, 2000; Mudelsee, 2001; Servant, 2001). The work above identifies, warming trends in many areas of the world ocean in advance of the 100 kyr eccentricity cycle, calling into question what drives the ice ages. Milankovitch had proposed that northern hemisphere summer insolation drove the climate cycles. However, warming trends at Termination II have been identified as early as ~135 k.y., significantly before the insolation peak at 127 k.y. (Henderson and Slowey, 2000). Waelbroeck *et al.* (1995) found that changes in Antarctic air temperature clearly lead changes in ice volume in both obliquity and precession bands and proposed that local variations in the radiative balance were not the main contributing factor as these induce immediate changes in surface temperatures. So, although there appears to be a glacial cycle periodicity of 100 kyr, the mechanism could be for example variability in the tropical ocean-atmosphere system, or changes in atmospheric CO_2 levels controlled by southern hemisphere $\sum CO_2$ concentrations (Shackleton, 2000; Mudelsee, 2001), and will be explored more fully in Chapter Seven.

Whilst the SST records presented here for the southern Cape Basin show very distinct early surface water warming trends prior to glacial terminations (Figure 6.10), the timing of the onset of early warming in the southern Cape Basin varies. Warming begins between ~3 and ~10 k.y. before the onset of global change, as shown by the benthic $\delta^{18}O$ curve. The various SST records differ slightly in their recording of early warming events. The transfer function SST curve suggests early surface water warming at the 12/11, 10/9, 8/7, and very early warming at the 6/5 transitions. In contrast, Termination II is the only clear early warming episode distinguished in the $U^{K'}_{37}$ SST record. Warming at Termination II in both palaeo-temperature records appears to have commenced ~10 k.y. before eustatic sea-level change. The combination of warmer than present SSTs and assemblages containing high abundance of typical Indian Ocean planktonic foraminiferal species (Figure 6.11) points towards a tropical origin for the early surface water warming in the southern Cape Basin at glacial terminations. Schneider *et al.* (1999) examined alkenone SST records from thirteen sediment cores from the south east Atlantic and Indian Ocean. They suggested that the strong signal of very early surface water warming (~10 k.y.) observed at Termination II was linked to the warmer glacial SSTs of MIS 6 and coldest SSTs occurring mid-glacial.

Peak SSTs in both proxy records are reached at the glacial terminations (Figure 6.10). A further notable feature of the Cape Basin records is the downcore abundance pattern of the percentage tropical-subtropical or 'warm' species (*Gs. sacculifer, Gr. menardii, P. obliquiloculata, Gg. digitata, S. dehiscens, G. hexagonus, Gr. hirsuta, Gr. truncatulinoides, Gs. ruber, Gg. rubenscens, Gs. conglobatus, Gr crassaformis, N. dutertrei, Ge. siphonifera,* and *Orbulina universa*) illustrated in Figure 6.11A. The largest proportion of 'warm' species is associated intimately with glacial terminations and closely follows the warm excursions of the TFT SST record (Figure 6.11). This association may be, in part, due to the transport of planktonic foraminiferal fauna directly from the Indian Ocean into the southern Cape Basin via Agulhas rings and eddies. Analysis of the planktonic foraminiferal assemblages in chapter five revealed that peak values of this warm species grouping are associated with a specific water mass type (Ocean Environmental Intervals/OEIs) typical for Agulhas waters. Figure 6.12 illustrates the close association of the palaeo-SST records, the percentage warm species, and the observed OEIs. SST

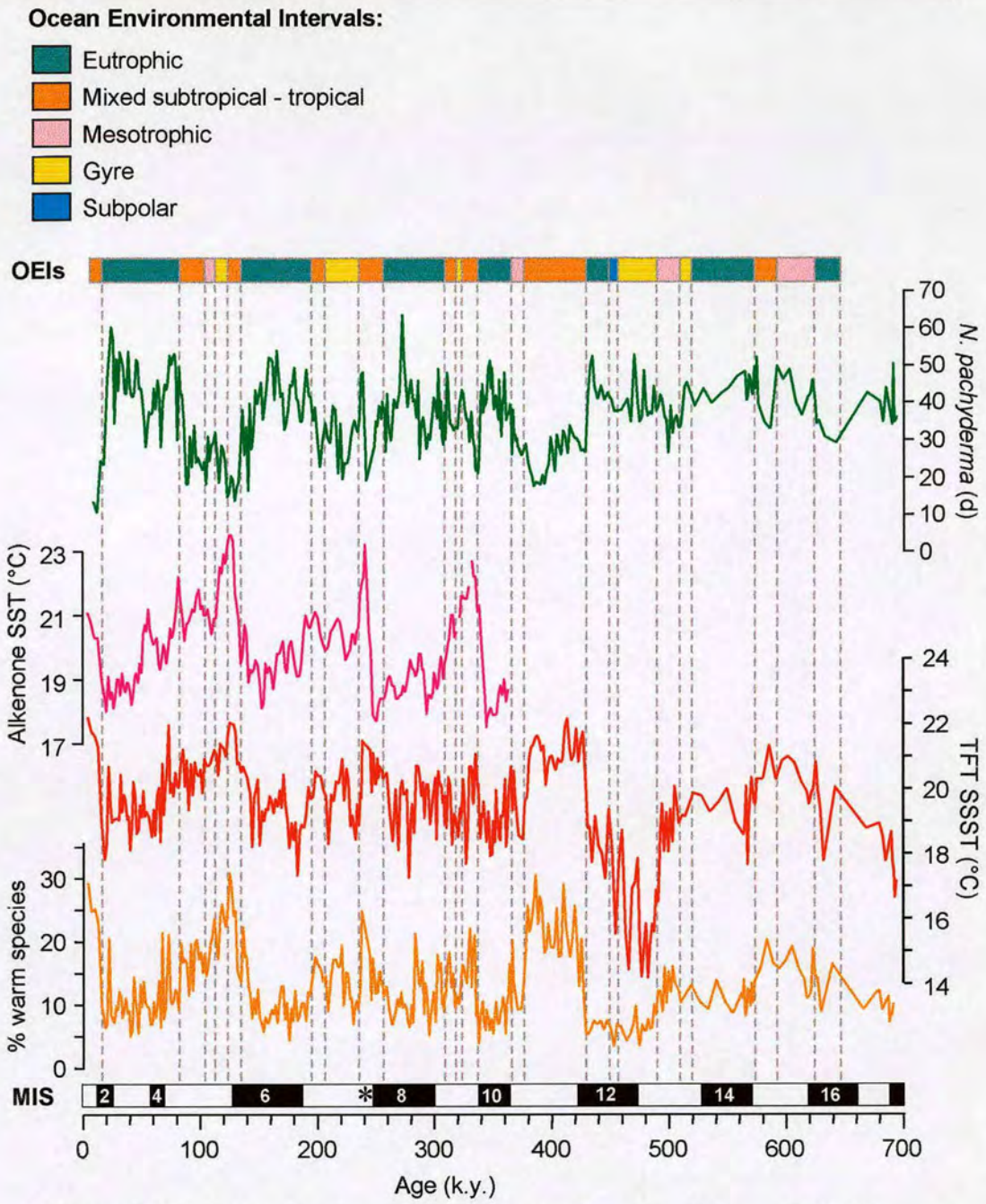

Figure 6.12 Relative abundance of % warm species, *N. pachyderma* (d), TFT summer SST (°C) and alkenone SST (°C) in relation to the Ocean Environmental Intervals (OEIs) and Marine Isotope Stages (MIS) identified in the Cape Basin spliced record. Splice point is indicated by asterisk.

fluctuations during interglacials indicate a general instability of surface water conditions in the south east Atlantic Ocean. This is supported by the identification of two distinct water mass types or OEIs during interglacial periods, the gyre assemblage OEI and the mixed subtropical-tropical (MST) OEI, respectively. The former prevails mid-interglacial (Figure 6.12) and the latter is a feature of transitional periods. The MST OEI is strongly indicative of greater advection from the Indian Ocean via the Agulhas Current during transitions and, to a lesser extent, interglacial warm stadials. This assertion is further supported by recent work of Giraudeau (Giraudeau, *pers. comm.*) on the accumulation rate of *Gr. menardii* in the late Quaternary. Giraudeau has only found concentrations of this species at terminations and that it is virtually absent at all other times, corroborating the MST OEI Indian Ocean link. Early warming therefore appears to be related to increased input of Indian Ocean water.

6.5 Conclusions

1. Multi-proxy SST analysis highlights regional variations in circulation and the sensitivity of each technique to other controlling factors. The relationship between the transfer function and alkenone SST records is weakly positive (Figure 6.6 A), due to the different sensitivities of each technique . Foraminiferal SSTs are more sensitive to frontal movements and seasonal water mass variability than alkenone temperature estimates.
2. The foraminiferal assemblages that determine the eventual transfer function SSTs are shown to correspond well with temperature change. There was a very strong inverse correlation (Figure 6.6 B) between the percentage warm water species and *N. pachyderma* (d). The relationships displayed between the individual foraminiferal 'cool' (*N. pachyderma* (d)) and 'warm' (proportion warm species) water indicators with TFT summer SSTs (Figure 6.6 C and D) support the case that the total foraminiferal assemblages are not merely the result of dilution effects of *N. pachyderma* (d).
3. Glacial surface water temperatures were 4-5°C cooler than present and upwelling in the southern Cape Basin was intensified. However, MIS 6 reveals only moderate cooling similar to records from tropical areas, in contrast to other mid-latitude palaeo-records in the South Atlantic. MIS 12 was the most extreme glacial period of

the past 700 kyr and experienced large scale advection of subantarctic waters from the Southern ocean.

4. SSTs in interglacials were generally at least as warm as modern values. MIS 5.5 was warmest interglacial according to both SST methods. MIS 11 was the longest interglacial. Planktonic foraminiferal records throughout the Cape Basin reveal that deep, seasonally restricted, upwelling probably occurred during MIS 9, a situation that is unlike those of preceding or subsequent interglacial intervals. $U^{k'}_{37}$ SSTs for stage 9 resemble records from other parts of the world ocean revealing very warm conditions during MIS 9 and southerly position of the APF and STF.
5. Early surface water warming in the Southern Cape Basin shows a tropical influence reflecting the cores location at the juncture between the Indian and Atlantic Oceans. This is strongest during Termination II when warming began ~10 k.y. before the changes in ice volume and is linked to increased advection from the Agulhas Current, driven by tropical forcing and the monsoon pump.

Chapter 7: Climate Connections

CHAPTER 7: UNDERSTANDING CLIMATE FORCING IN THE LATE QUATERNARY

As outlined in the introductory chapter, a major objective of this work is to understand not only what past environments existed, but also, the processes and mechanisms of climatic change during the Quaternary. This discussion-based chapter will examine several significant 'climatic connections', or themes, relevant to our interest in present and future climates, beginning with a detailed study of forcing mechanisms during one particular and crucially important interval, MIS 11. The chapter develops with a comparison of four interglacial periods in the late Quaternary to ascertain the validity of generalised assumptions about past warm periods. In addition, the Cape Basin palaeoceanographic records are placed in the context of hemispheric and insolation parameters, examining sub-Milankovitch variation in a glacial period. The record of Indian Ocean advection into the South Atlantic is considered in relation to global surface, and deep water circulation, as well as intra-hemispheric and inter-hemispheric connections and responses. The final section examines marine–terrestrial climate connections, in a study that combines palaeo-data from a wide variety of sources, to understand the links between cycles of upwelling intensity and continental aridity in southern Africa since the Last Interglacial.

7.1 UNDERSTANDING HEMISPHERIC CONNECTIONS AND CLIMATIC FORCING THROUGH A STUDY OF MIS 11.

7.1.1 Insight into natural climate variability

There has been much recent interest in understanding past climates that were as warm as, or warmer than, the present. Oxygen isotope stage 5.5 has been widely studied as a proxy for scenarios of human-induced climate warming. However, another interglacial may be a better analogue through which we can examine a future warm-world scenario (Berger and Loutre, 1991; McManus *et al.*, 1999a; 1999b). MIS 11, the interval between ~423 and 360 k.y., is distinguished by the longest period of sustained warmth during the late Quaternary (Poore *et al.*, 2000; Droxler and Farrell, 2000; Hodell

et al., 2000; Forsström, 2001). It was first identified by Kennett (1970) from a carbonate rich interval in Pacific Ocean sediment cores. A generalised picture of palaeoclimatic and oceanographic conditions during MIS 11 is presented in Table 7.1 (below).

Global MIS 11		FRONTAL ZONES	CLIMATE (CP. PRESENT)
SOUTHERN OCEAN	ATLANTIC SECTOR	South of PFZ: highest rate of opal production (Charles *et al.*, 1991) and $CaCO_3$ production (Hodell *et al.*, 2000)	ODP Hole 704B: warmer SSTs (Hodell, 1993); NADW flux: greater (Oppo *et al.*, 1990); SE Atlantic sector, similar SSTs, but longest warmth, weaker westerlies (Hodell *et al.*, 2000)
	INDIAN SECTOR	PFZ: located furthest south (Morley, 1989)	SSTs warm, high $CaCO_3$ (Howard and Prell, 1992)
ATLANTIC OCEAN		Polar Front further north at ~41°N Ruddiman and McIntyre (1976); Oceanic fronts further south in South Atlantic (Kunz-Pirrung *et al.*, 2000)	Labrador Sea: warmer SSTs (Aksu *et al.*, 1992); Cariaco Basin warmer, trades north (Poore and Dowsett, 2001); Bermuda Rise: sea-level +20m (Hearty *et al.*, 1999); UK: sea-level +13m (Bowen, 1999)
PACIFIC OCEAN		STF: similar to present (Weaver *et al.*, 1998; King and Howard, 2000)	SSTs similar (Shackleton *et al.*, 1990; King and Howard, 2000); weaker westerlies (King and Howard, 2000)
TERRESTRIAL		Colombia: tree line similar altitude to present (Hooghiemstra, 1989)	Vostok: δD warm (Petit *et al.*, 1999), Europe :warm, long (Reiller *et al.*, 2000) France: Holsteinian much longer than marine $\delta^{18}O$ (Tzedakis *et al.*, 1993)

Table 7.1 Summary of global conditions in MIS 11.

Various terrestrial and marine records from subpolar regions of the northern and southern hemispheres (Table 7.1) suggest that MIS 11 may have been one of the warmest interglacials of the past half million years (Ruddiman *et al.*, 1989; Howard and Prell, 1992; Burckle, 1993; Hodell, 1993; Howard, 1997; Droxler *et al.*, 1999, McManus *et al.*, 1999a; 1999b). In addition, several data sets from different parts of the world indicate that sea-level in MIS 11 was as at least ten, and possibly as much as twenty, metres higher than present (Brigham-Grette and Carter, 1992; Bowen, 1999; Hearty *et al.*, 1999a; 1999b) due to major, bipolar, ice-sheet disintegration such as that suggested

by Scherer *et al.* (1998). Yet, the evidence for warmer conditions is controversial and, at times, conflicting. Hodell *et al.* (2000), Shackleton *et al.* (1990), and King and Howard (2000) present SSTs that are similar to present. The high sea-level stands postulated for MIS 11 are disputed by Hodell *et al.* (2000) using isotopic data from the Southern Ocean. On the other hand, the case for raised sea-level in MIS 11 is supported by $\delta^{18}O_{ruber}$ records from the Cariaco Basin (Poore and Dowsett, 2001). One thing that is agreed upon by all workers is that the warming was sustained for longer than any other interglacial of the late Quaternary.

The reason why stage 11, in particular, is so important to our understanding of climate change lies in the insolation geometry. The orbital parameters of MIS 11 were similar to those presently prevailing (Berger and Loutre, 1991), with low orbital eccentricity, high obliquity, and low precessional amplitude (Figure 7.1). The transition from MIS 12 to MIS 11 (Termination 5) was the most extreme example of deglacial warming in the past 5 My (Figure 7.2), from a very cold glacial to a long, warm interglacial. This, however, cannot be explained with reference to Milankovitch forcing alone (Berger and Loutre, 1991). MIS 11 is an insolation paradox as strong global warming is coincident with overall depressed summer insolation, a consequence of a minimum in the 400 kyr eccentricity cycle (Kukla *et al.*, 1981; Imbrie *et al.*, 1992). This dichotomy, between the amplitudes of warming and insolation, has important implications for our understanding of the mechanisms of global climate change. Whether we are in a stage 11-type sustained interglacial or an Eemain-type interglacial is of significant interest given the current anthropogenic addition of greenhouse gases to an already warm climate.

7.1.2 How is MIS 11 different to interglacial stages 9, 7, 5, and 1?

A comparison of the Cape Basin oxygen isotope and planktonic foraminiferal warm species percentage abundance data for interglacial stages 11, 9, 7, and 5 (Figure 7.3) reveals that MIS 5 experienced earliest deglacial warming. In contrast, the preceding interglacials, 11, 9 and 7, show nearly in-phase increases of warm species and $\delta^{18}O$ (ice volume). As the relative percentage warm species is an indicator of the extent

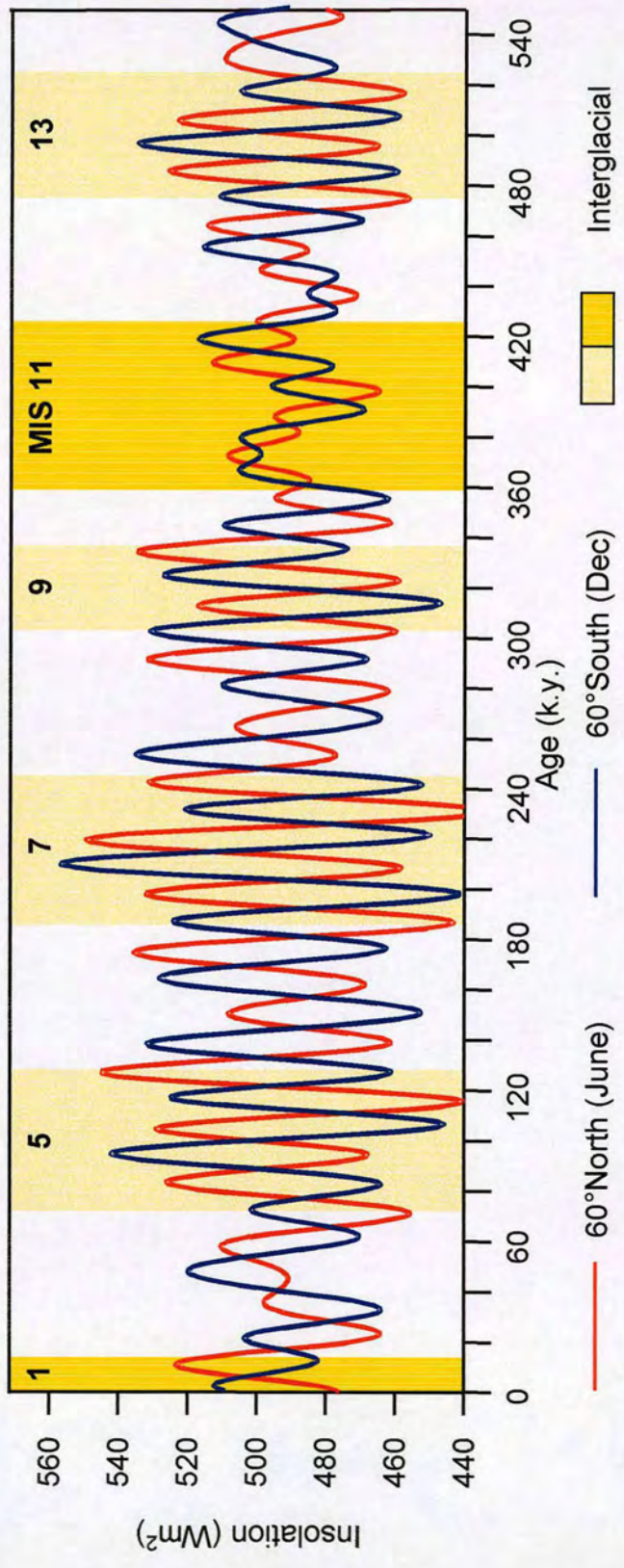

Figure 7.1 Summer insolation values for the past 550 k.y. Data from Berger and Loutre (1991).

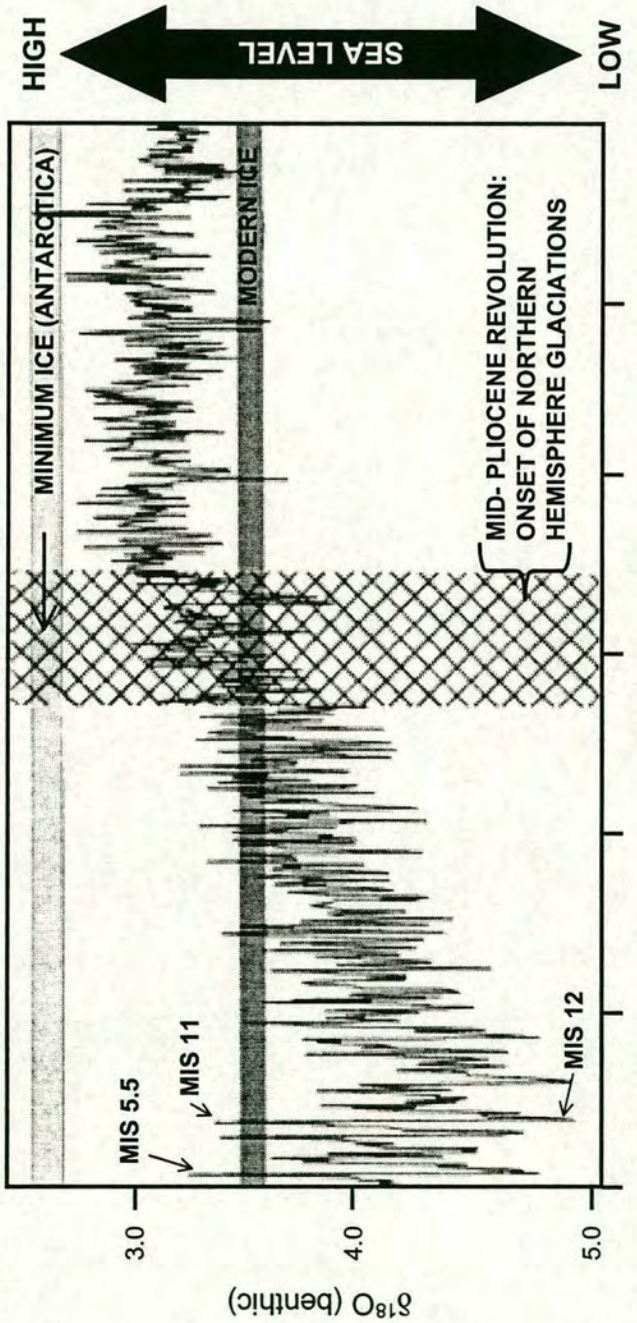

Figure 7.2 Benthic oxygen isotope record for ODP Site 846 for the past 6 My. Relative sea level change is indicated on the right hand side of the figure. The first large deglacial amplitude change occurs at the MIS 12/MIS 11 termination. (After Mix *et al.*, 1995; Pisias *et al.*, 1995; Shackleton *et al.*, 1995).

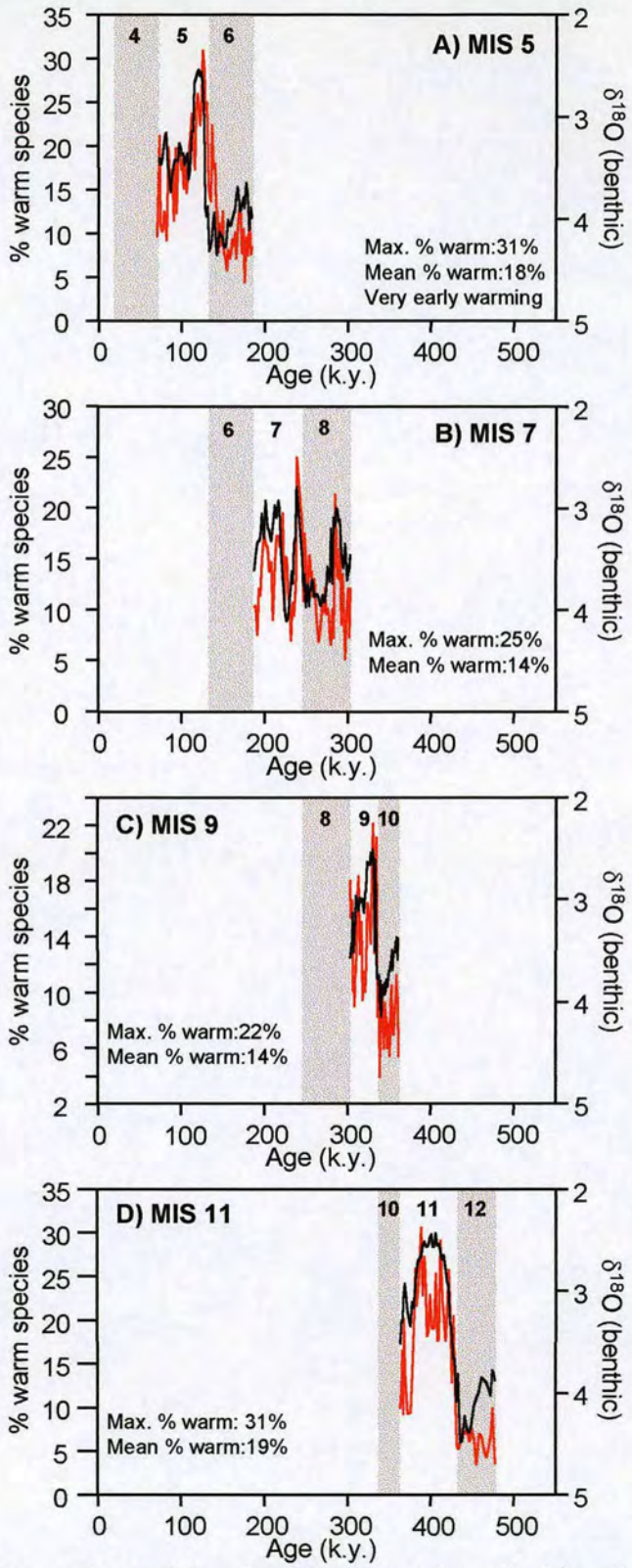

Figure 7.3 Comparison of four late Quaternary interglacial periods in the southern Cape Basin. Data presented are relative abundance of warm species and benthic $\delta^{18}O$. Glacial periods are shaded. MIS 5 is the only interglacial with very early warming.

of Indian Ocean advection via the Agulhas Current (Section 5.4.4) the driving mechanism for both advection and glacial-interglacial change may be related. Statistically the SST records (Figure 6.4) for the spliced core indicate that MIS 11 and 5 were alike. Peak warm season temperatures in MIS 11 and MIS 5 were similar and together were the 'warmest' intervals of the past 600 k.y (Figure 6.4). Mean annual SST for the entire interglacial was ~ 19°C in both MIS 5 and 11, matching the modern average temperature for surface waters offshore the Cape of Good Hope. During peak interglacials mean annual SSTs reached ~ 20.5°C. Mean summer SSTs for both interglacials were ~21°C, although peak warm season SSTs approached ~22.5°C in MIS 5 and 11 (Figure 6.4), thus demonstrating that overall SSTs in both MIS 5 and 11 were warmer than present. However, the insolation parameters for MIS 5 and MSI 11 show great differences in total insolation and amplitude (Figure 7.1) In MIS 5 the peak interglacial was relatively short-lived (Figure 6.4) and, unlike MIS 11, was followed by a cooler stadial within the interglacial.. The sustained nature of the stage 11 interglacial is also revealed in the planktonic foraminifera records. A detailed comparison is made between interglacials MIS 5 and 11 in Figure 7.4 which shows abundance data for subtropical and tropical species during each interglacial. Clear differences between MIS 5 and 11 are apparent. Firstly, the percentage of warm species in the faunal assemblage remains high (mean 19%) throughout the ~60 k.y. of stage 11 relative to MIS 5 due to a second, distinct, peak centred around ~ 390 k.y. As for other interglacials, the abundance of warm species in interglacial stages 9 and 7 are lower by ~5 to 8 percent than MIS 11 and 5 (Figure 7.3 B and C). Secondly, differences are observed in conditions prevailing during the preceding glacials. MIS 6 was comparatively warm; whilst MIS 12 was the most severe glacial of the late Quaternary (Figures 7.2 and 6.4). Indeed, Schneider *et al.,* (1999) suggested that these warm conditions offshore southwest Africa may have determined the early warming observed for MIS 5 and this is discussed in Section 6.4.4.

7.1.3 Surface circulation from MIS 12 to MIS 11 in the Cape Basin

The proxy records from the Cape Basin spliced record reveal large-scale variations for the entire glacial – interglacial cycle (Figure 7.5). During the MIS 13/12 transition there was strong subantarctic advection into the Benguela System as indicated

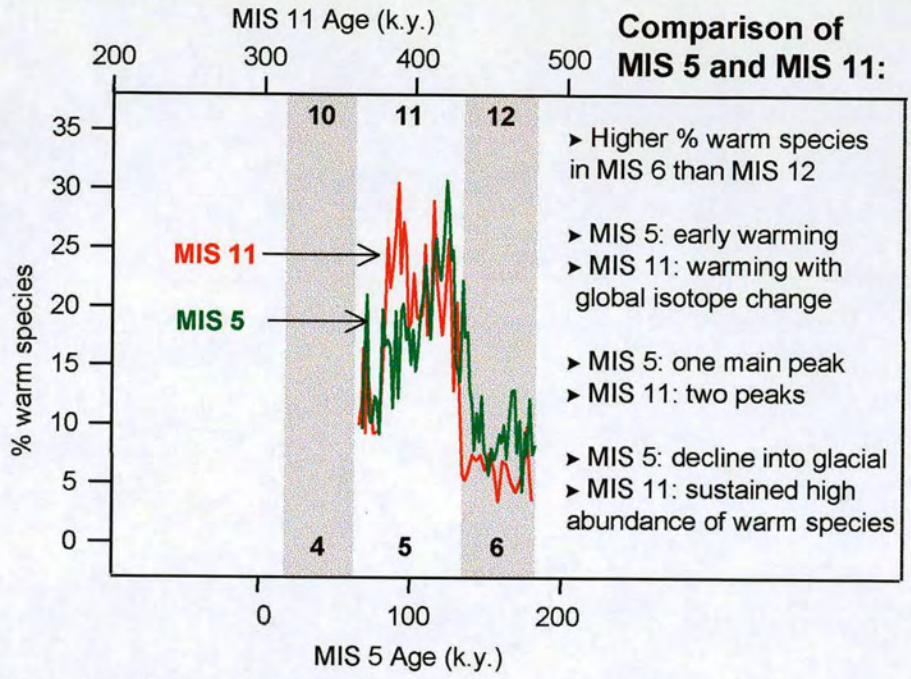

Figure 7.4 Contrasting records of percentage warm species in the Cape Basin spliced core during MIS 11 and 5. Data plotted with separate age scales. Glacial stages are shaded and labelled for each curve.

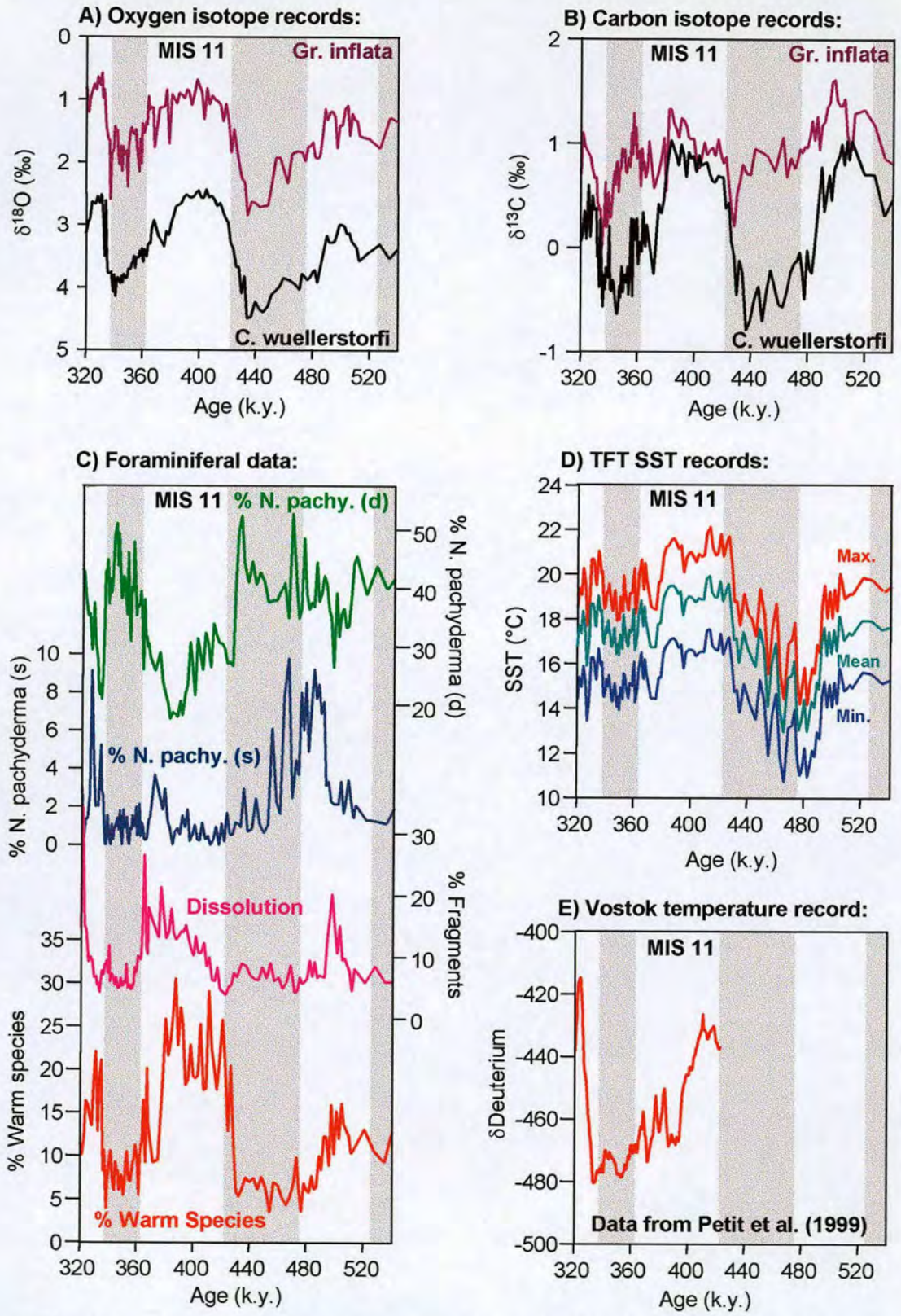

Figure 7.5 Cape Basin climate proxy records for the Mid-Pleistocene, plots A to D. Also shown in plot E is the Antarctic δD (‰) record (Petit *et al.*, 1999). Glacial periods are shaded grey.

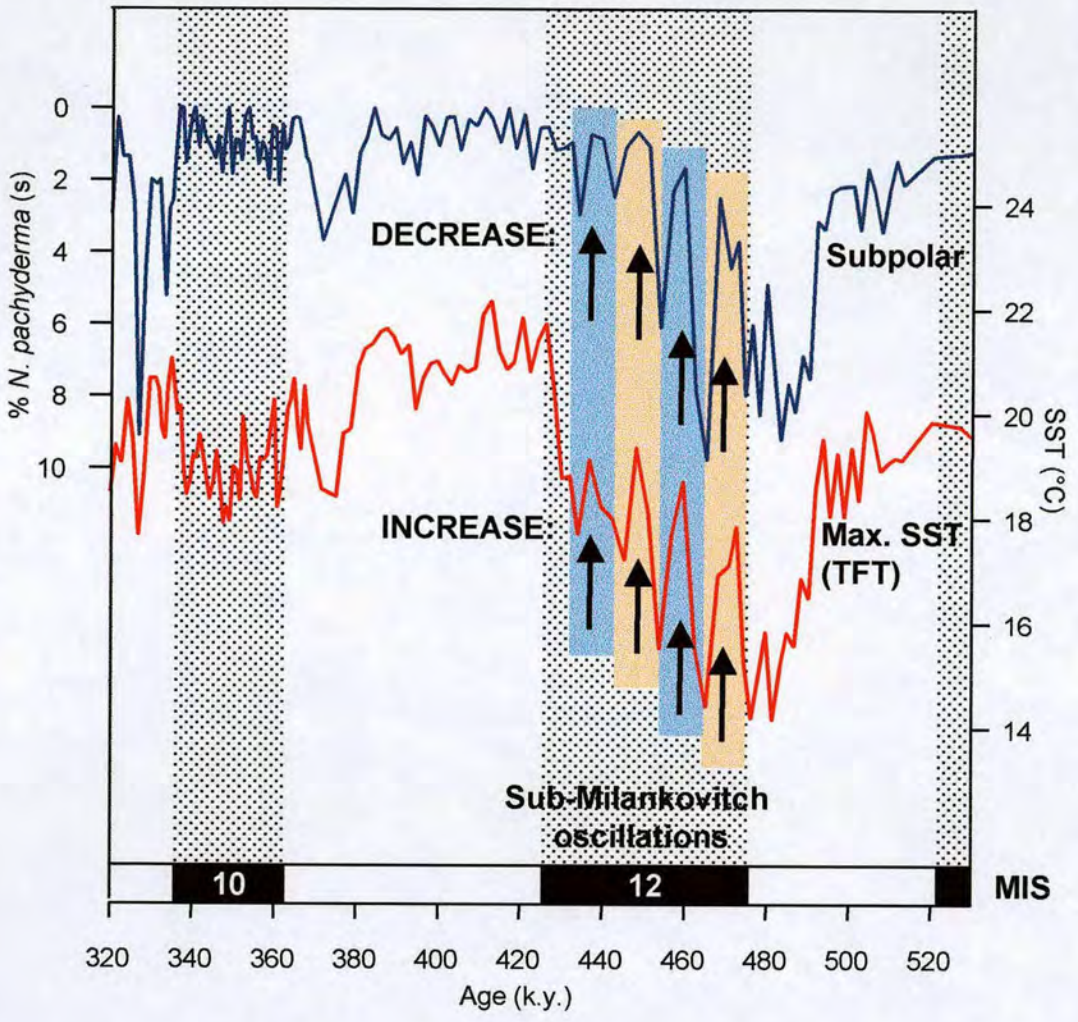

Figure 7.6 Sub-Milankovitch variations in MIS 12 offshore Southern Africa. SST oscillations and related surface water mass indicators. Increased SST (transfer function) is associated with decreases in subpolar advection/deep upwelling (*N. pachyderma* sinistral). Note the reversed scales for *N. pachyderma* (s).

by the *N. pachyderma* (s) curve (Figure 7.5C, discussed in Section 5.4.6). The dissolution profile (higher percentage fragments representing greater dissolution) shows a pattern of enhanced dissolution during transitions from interglacials to glacials, and greatest preservation occurs during glacial terminations (Figure 7.5C). Benthic and planktic $\delta^{18}O$ values for the past 700 k.y. show that heaviest values in MIS 12 and are lightest in MIS 11 (Figure 7.5A). The transition from MIS 12 to MIS 11 exhibits a distinct 2.0‰ fall in the benthic record of $\delta^{18}O$. This change is 0.5‰ greater than the estimated ice volume contribution for the glacial transitions (Poli *et al.*, 2000), implying a possible regional warming trend in the deep water masses during this interval as observed in the North Atlantic (Dwyer *et al.*, 1995). Throughout the period 550 – 320 *Gr. inflata* $\delta^{18}O$ values are ~2.0‰ lighter than *C. wuellerstorfi* (Figure 7.5A) suggesting a consistent and well-defined thermocline. However, planktonic foraminiferal abundance records for the same interval indicate that surface water conditions changed dramatically (Figure 7.5C). In the late Quaternary, the relative percentages of eutrophic species are generally highest during glacial periods, and are interpreted as intensified upwelling and filament production due to stronger winds associated with glacially-enhanced atmospheric circulation (Section 5.4.2). During MIS 11 there is a clear switch from eutrophic species to warm water species (Figure 7.5C). This is associated with the mixed tropical-subtropical OEI (Figure 5.10) and warm SSTs (Figure 7.5D).

7.1.4 Sub-Milankovitch SST variability in MIS 12

Superimposed on the glacial – interglacial cycle recorded offshore the Cape of Good Hope, sub-Milankovitch variations are observed. The TFT SST records in early MIS 12 reveal stepwise oscillations within an overall warming trend (Figure 7.5D). The periodicity of these oscillations is ~10 k.y. and the temperature range for each excursion is ~3°C. High frequency variability is also recorded by the planktonic foraminifera, and is most clearly seen in the *N. pachyderma* (s) record (Figure 7.5C). Diversity and cluster analysis (Chapter 5) revealed that this species is identified with a specific watermass type, the subpolar OEI (section 5.4.6) which is controlled by advection from south of the STF/SAF. The relationship between subantarctic advection and sub-Milankovitch SST excursions is illustrated in Figure 7.6. Synchronous sub-Milankovitch oscillations

are observed across the globe, suggesting global-scale forcing. MIS 12 SST fluctuations of the same magnitude and frequency as those reported here are recorded in the Pacific Ocean offshore New Zealand (King and Howard, 2000), as well as the Southern Ocean (Gersonde *et al.*, 2000). Mid-Pleistocene sub-Milankovitch events in the South Atlantic (Charles *et al.*, 1996) occur simultaneously with ice-rafting episodes in the North Atlantic (Oppo *et al.*, 1998; McManus *et al.*, 1999a), as do cycles in Antarctic margin sediments (Domack and Mayewski, 1999), the Equatorial Atlantic (Curry and Oppo, 1997), the Arabian Sea (Schulz *et al.*, 1998), and the Santa Barbara Basin (Hendy and Kennett, 1999). Therefore, the climatic processes controlling this subantarctic advection into the Cape Basin will involve a global-scale mechanism capable of causing rapid climatic change. The sub-Milankovitch variability observed in the Cape Basin and around the southern hemisphere in MIS 12 bear a strong resemblance to the MIS 2/4 P-S Events (i.e. *N. pachyderma* (s) increased abundance events) observed by Little *et al.*, (1997b) in the NBS. It was suggested these events were caused by changes in trade winds and upwelling intensity and were linked to the timing of North Atlantic Heinrich events. However, P-S Events are not observed in the SBS or cores further south, thus ruling out the possibility of subantarctic advection for the MSI 2/4 PS sub-Milankovitch events. It would appear that, although the MIS 2/4 P-S Events and MIS sub-Milankovitch oscillations occur during intense glacial periods, they are derived from different climatic processes Suggested mechanisms, or perhaps a combination of mechanisms, for the MIS 12 southern hemisphere events, include the following: primarily the effects of stronger winds and increased turbulence on the STF (Klinck and Smith, 1997), also from fluctuations in greenhouse gases (Broecker 1997b), and finally, precessional-controlled variations in equatorial heat budgets (Ghil, 1984; McIntyre and Molfino, 1996).

7.1.5 Deep watermasses in the Cape Basin

The carbon isotope component of ΣCO_2 is linked to deep water circulation patterns as its distribution in sea water is affected by photosynthesis and respiration. Deep water that is formed with a significant surface water component, e.g. modern NADW, is enriched in ^{13}C because photosynthesis has preferentially removed ^{12}C from

the ΣCO_2 of the surface water. Older deep watermasses have lower $\delta^{13}C$ values since much of the organic matter will have been remineralised in the water column. There has been glacial – interglacial variation in NADW production throughout the late Quaternary (Broecker *et al.*, 1985; Broecker and Denton *et al.*, 1989; Billups *et al.*, 1999). The Cape Basin $\delta^{13}C$ benthic curve reveals heaviest values in glacial MIS 12, which suggests that the deep water masses are nutrient-enriched, implying that NADW penetration is reduced and deep waters of a southern (Antarctic) origin are of increased importance in the Cape Basin (Duplessy *et al.*, 1988; Curry, 1996). If so, this may be the result of global-scale changes in the nature of deep water. Atlantic and Pacific deep water masses have been shown to have similar $\delta^{13}C$ values during MIS 12, supporting a severe reduction of NADW production at that time (Raymo *et al.*, 1990). Indeed NADW formation may have shut down, as proposed for the LGM (Boyle and Keigwin, 1987; Curry *et al.*, 1988; Duplessy *et al.*, 1988), given that estimated MIS 12 global ice volume was ~15% greater, and sea-level was ~20m lower than the LGM (Rohling *et al.*, 1998).

During MIS 11 the planktic and benthic $\delta^{13}C$ values converge (Figure 7.5B). The difference between benthic and planktic carbon isotope values is smallest during MIS 11, suggesting enhanced thermohaline circulation, or a change in surface productivity. Isotope data from additional planktonic species would be required to differentiate further between these signals (Kroon, 1988). However, mean benthic $\delta^{13}C$ values in MIS 11 are too high for deep watermasses with a significant southern component, i.e. $\delta^{13}C$ is >0.7‰ (Bickert and Wefer, 1996), supporting stronger NADW production and circulation. The case for maximum NADW productivity in MIS 11 is borne out by the benthic $\delta^{13}C$ gradient between the Pacific and the Atlantic Oceans. Greatest benthic $\delta^{13}C$ excursion between these basins occurs in MIS 11 (Raymo *et al.*, 1990) indicating very different nutrient properties for each ocean basin. Conversely, when NADW production is reduced, such as during MIS 12, the nutrient characteristics of the oceans converge.

7.1.6 Late Quaternary dissolution record

The dissolution pattern recorded in the Cape Basin spliced record (Figure 7.5C) is dissimilar to the characteristic Atlantic Ocean signal of greatest dissolution during glacial periods (Crowley, 1983; Balsam and McCoy, 1987). Similar carbonate dissolution trends to the spliced record have been documented in cores GeoB 1211 and GeoB 1214, located further north in the Benguela System (Bickert and Wefer, 1996). The dissolution pattern recorded in the Cape Basin resembles typical Pacific Ocean records (Berger, 1973; Farrell and Prell, 1989; Wu *et al.*, 1990; Le and Shackleton, 1992), particularly that of ODP Site 806B on the Ontong Java Plateau (Yasuda *et al.*, 1993). The Cape Basin dissolution records are also similar to datasets from the Indian Ocean (Bassinot *et al.*, 1994). The affinity of these dissolution records from equatorial areas and the southern hemisphere suggest that this variation is due to global changes in the carbon reservoir. The relationship between the summer insolation in the southern hemisphere and the dissolution profile for the Cape Basin (Figure 7.7) supports a possible southern origin for the dissolution patterns observed.

7.1.7 Hemispheric connections: observations in the Cape Basin throughout the late Quaternary

The Antarctic climatic record from Vostok presently extends to early MIS 11. The δ deuterium curve is a proxy for surface temperature changes and represents a southern hemisphere warming signal (Petit *et al.*, 1999). This curve can be used along with the Cape basin records, to investigate the nature of inter- and intra-hemispheric links in the Quaternary. Figure 7.8 shows the δD (‰) record with that of the percentage warm species from the spliced record. This correlation is based on the ^{18}O chronologies of Vostok and the spliced record. It is assumed that the ^{18}O of water vapour trapped in the Antarctic ice is a global ice volume signal that is synchronous with the $\delta^{18}O$ (*C. wuellerstorfi*) record in the Cape Basin. It is acknowledged that there may be a lag between atmospheric and marine $\delta^{18}O$ (Broecker and Henderson, 1998). Despite potential correlational problems, the signal of Indian Ocean advection into the South Atlantic (Section 5.4.4) bears a striking resemblance to the Antarctic record of warming for most of the late Quaternary, apart from MIS 11 when advection is sustained beyond the period of Vostok warming (Figure 7.8).

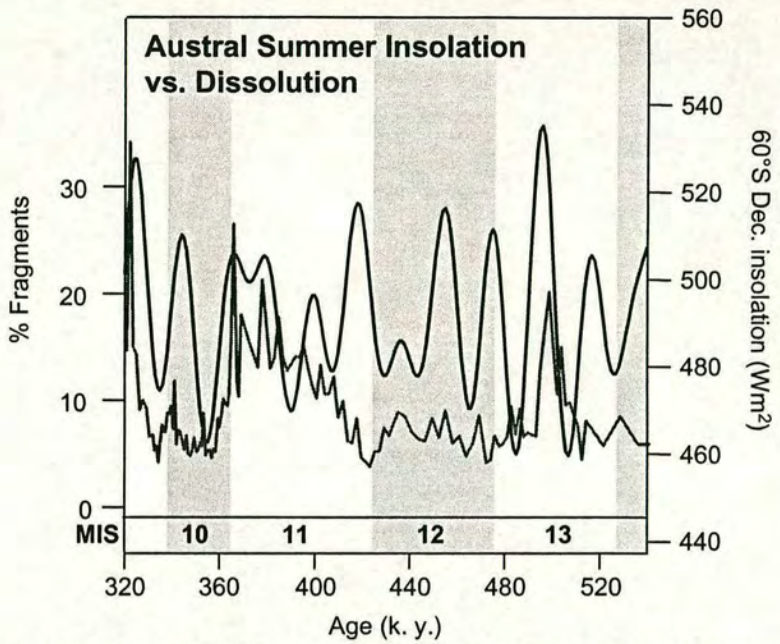

Figure 7.7 Spliced Cape Basin record of dissolution, calculated from percentage fragments (Le and Shackleton, 1992), plotted against southern hemisphere summer insolation (60°S). Dissolution peaks in the Cape Basin coincide with austral hemisphere insolation peaks suggesting a southern origin for the driving mechanism. Glacial periods are shaded grey.

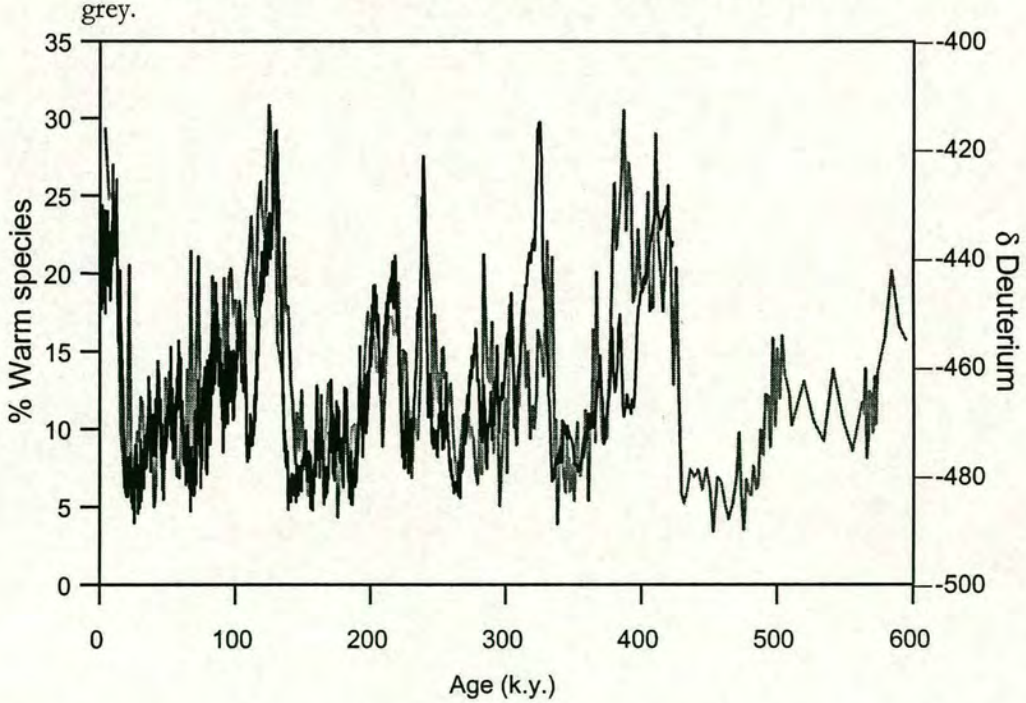

Figure 7.8 Comparison of Antarctic Vostok deuterium isotopic record ‰(δD) and percentage warm species from the Cape Basin spliced record.

Other records from the SBS show that palaeoceanographic changes around the Cape are strongly correlated to levels of northern hemisphere summer insolation (Figure 7.9A and B). That the abundance history of *N. pachyderma* (d), which is a signal of eutrophic watermasses in the SBS (Section 5.4.2), and the SST record, are linked to boreal summer insolation is not surprising. The amount of upwelling is determined, to a large extent, by the relative strength of the trade winds which is, in turn, controlled by the position of the ITCZ. Insolation in the summer in the northern hemisphere determines the position of the ITCZ, because of differential heating of continental landmasses and the ocean. These atmospheric processes are illustrated in Figure 5.12. The Indian Ocean advection signal also appears to be related to the northern hemisphere (Figure 7.10A). In addition to atmospheric mechanisms the abundance of subtropical and tropical species, recording relative flux from the Agulhas Current, may also be connected to the northern hemisphere through the thermohaline circulation. The oceanic area offshore the Cape of Good Hope is a 'hotspot' in terms of the global thermohaline circulation (Gordon, 1985; 1986; Gordon *et al.*, 1992). Section 7.1.5 has described how NADW production and the thermohaline circulation were enhanced in interglacials, specifically MIS 11, and this is primarily a northern hemisphere-driven signal.

In contrast to the records of eutrophic and advection-derived watermasses, the history of *Gr. inflata*, a signal of oligotrophic South Atlantic gyre waters (Section 5.4.3) in the Cape Basin, correlates with southern hemisphere summer insolation (Figure 7.10B). The relationship is complicated, but the overall pattern appears to be that increases in *Gr. inflata* are associated with peaks in austral summer insolation. If this means that relative input into the SBS from the South Atlantic Current is controlled by a regional, or hemispheric signal, then this is most likely related to the strength of the South Atlantic Anticyclone. Gyre influence is greatest when the South Atlantic gyre has expanded due to southern shift in the position of the STF (Figure 7.11C). Meridional movements of the STF are controlled by the Walker circulation (Tyson, 1986). Greater insolation during interglacials would lead to a positive pressure anomaly between the African subcontinent and the South Atlantic Anticyclone strengthening the anticyclone (Harrison, 1984; Mason and Jury, 1997).

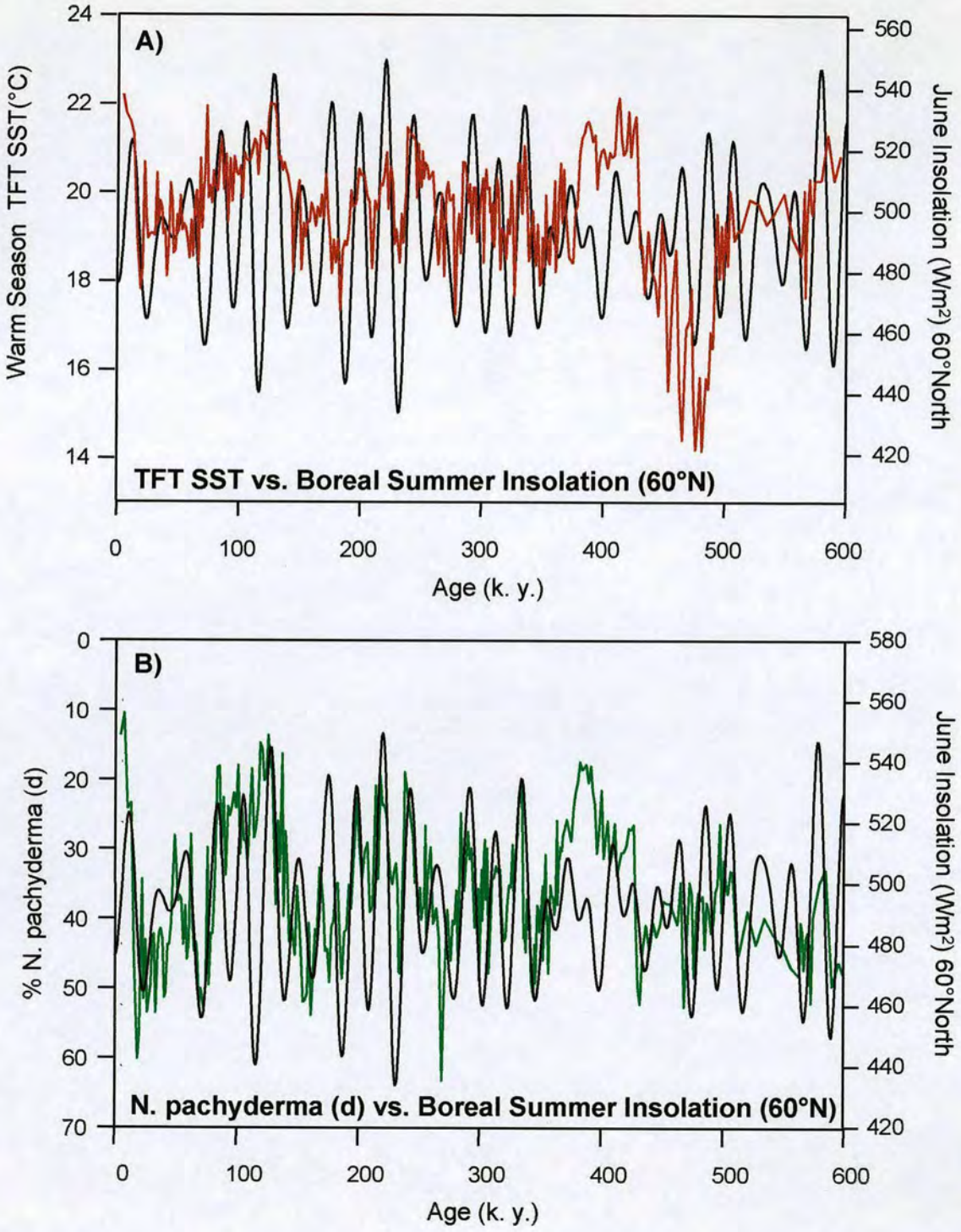

Figure 7.9 Cape Basin watermass indicators and summer insolation forcing A) Warm season SST, and B) Percentage *N. pachyderma* (d) - eutrophic/upwelling signal. Major changes in surface warming (A) and circulation (B) in waters offshore the Cape of Good Hope are associated with northern hemisphere summer insolation.

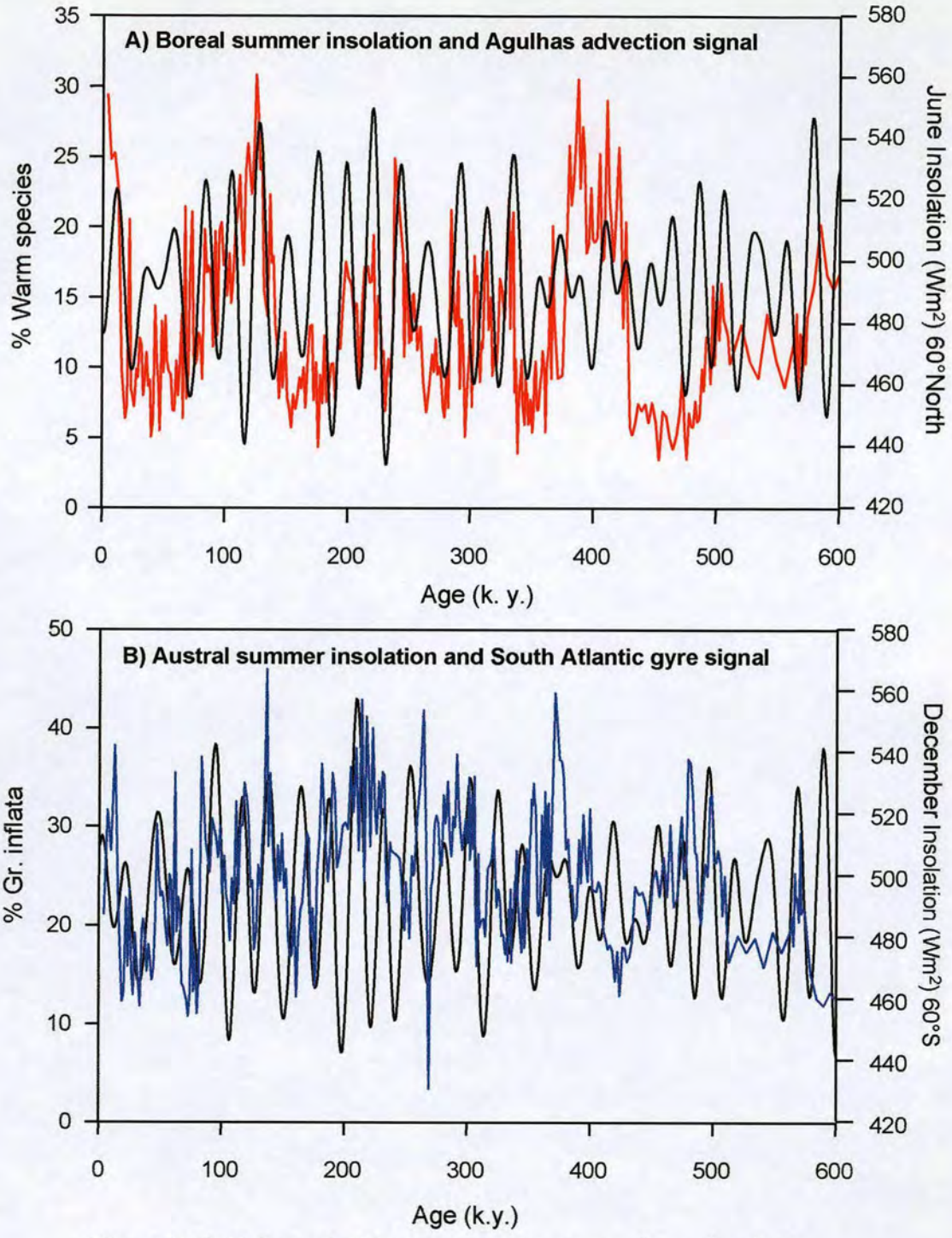

Figure 7.10 A) Record of the percentage warm species, a signal of advection from the Indian Ocean, in the waters offshore the Cape of Good Hope during the late Quaternary. Advection appears to switch from being mainly associated with boreal hemisphere insolation changes. B) Record of the percentage *Gr. inflata*, a signal of South Atlantic gyre waters. Gyre influence in the Cape Basin appears to be related to southern hemisphere insolation.

Changes in SBS upwelling, Agulhas Current advection records are synchronous with northern hemisphere summer insolation during most of the Quaternary (Figures 7.9B and 7.10A), suggesting rapid global climatic communication and response. Other terrestrial and oceanic archives have also recorded a synchronous hemispheric response (Lowell *et al.*, 1995; Bard *et al.*, 1997; Poli *et al.*, 2000). Two main theories have been put forward to explain the global transmission of the climate signals. The first concerns the ocean and communication via the thermohaline circulation (Imbrie *et al.*, 1992; 1993; Broecker; 1997b; Broecker and Henderson, 1998), and the second, employs the atmospheric transfer of moisture and heat energy (Sowers and Bender, 1995; Broecker, 1997a). Variations in NADW production are known to influence climatic change on Milankovitch time-scales (Broecker and Denton, 1989; Imbrie *et al.*, 1992; 1993). Thermohaline circulation and NADW convective overturn are associated with cross-equatorial heat transport from the South Atlantic. The south flowing NADW is compensated by a northward surface flow of return water (Gordon, 1986; Rintoul, 1991; Gordon *et al.*, 1992). Mix *et al.* (1986a) suggested that variations in deep water production may have influenced the northward transfer of heat and salt. Therefore, cessation of the thermohaline circulation may then lead to warming in the South Atlantic (Crowley, 1992; Charles *et al.*, 1996; Blunier *et al.*, 1998). This early warming is seen in the Cape Basin records (Section 6.4.4), most clearly for the MIS 6/5 termination. Comparison of Cape Basin proxies with the Vostok δD (temperature proxy) record (Figure 7.8) has shown that changes in the surface water circulation around southern Africa occurred simultaneously with variations in air temperature over Antarctica during the late Quaternary. This connection, where increased deep water formation is linked with warming periods in the southern hemisphere has been observed previously (Blunier *et al.*, 1998; Broecker and Henderson, 1998, Poli *et al.*, 2000) and are supported by this study.

7.1.8 MIS 11 palaeorecords: understanding the climate connections

The SST records from the Cape Basin for MIS 11, illustrated in Figure 7.5D, show an environment with summer SSTs warmer than present throughout much of the ~60 k.y. of the interglacial. The foraminiferal abundance records are marked by a sharp

GLACIAL

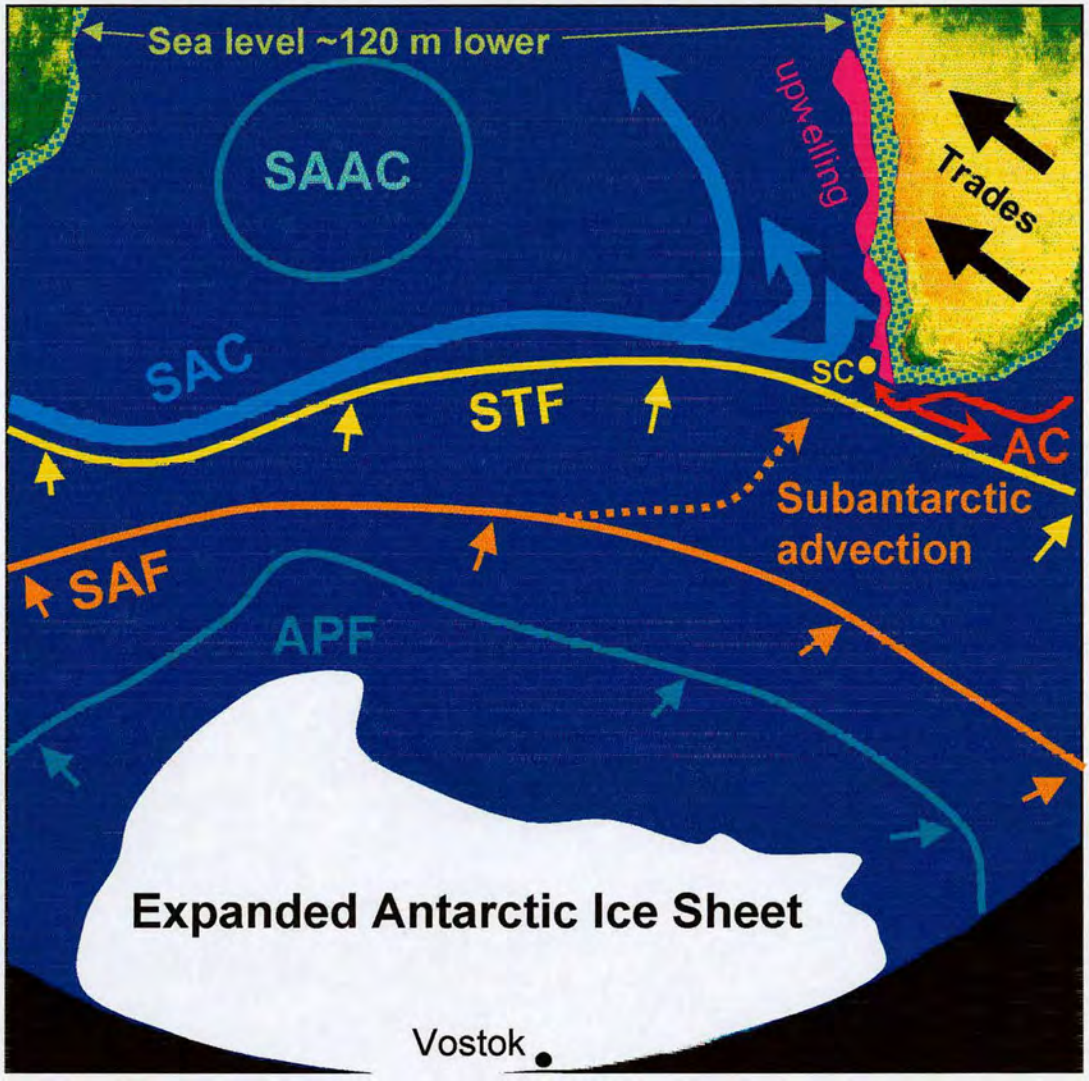

Figure 7.11A Schematic diagram of South Atlantic during glacial periods. Data from this study and Morley (1989), Oppo *et* al. (1990), Charles *et al.* (1991), Howard and Prell (1992), Imbrie *et* al. (1992), Hodell (1993), Little *et al.* (1997b), Flores *et al.* (1999), Petit *et al.* (1999), Hodell *et al.* (2000). SAAC - South Atlantic Anticyclone, SAC - South Atlantic Current, SC - Spliced Cape Basin core, AC - Agulhas Current, STF - Subtropical Front, SAF - Subantarctic Front, APF - Antarctic Polar Front.

EARLY INTERGLACIAL AND MIS 11

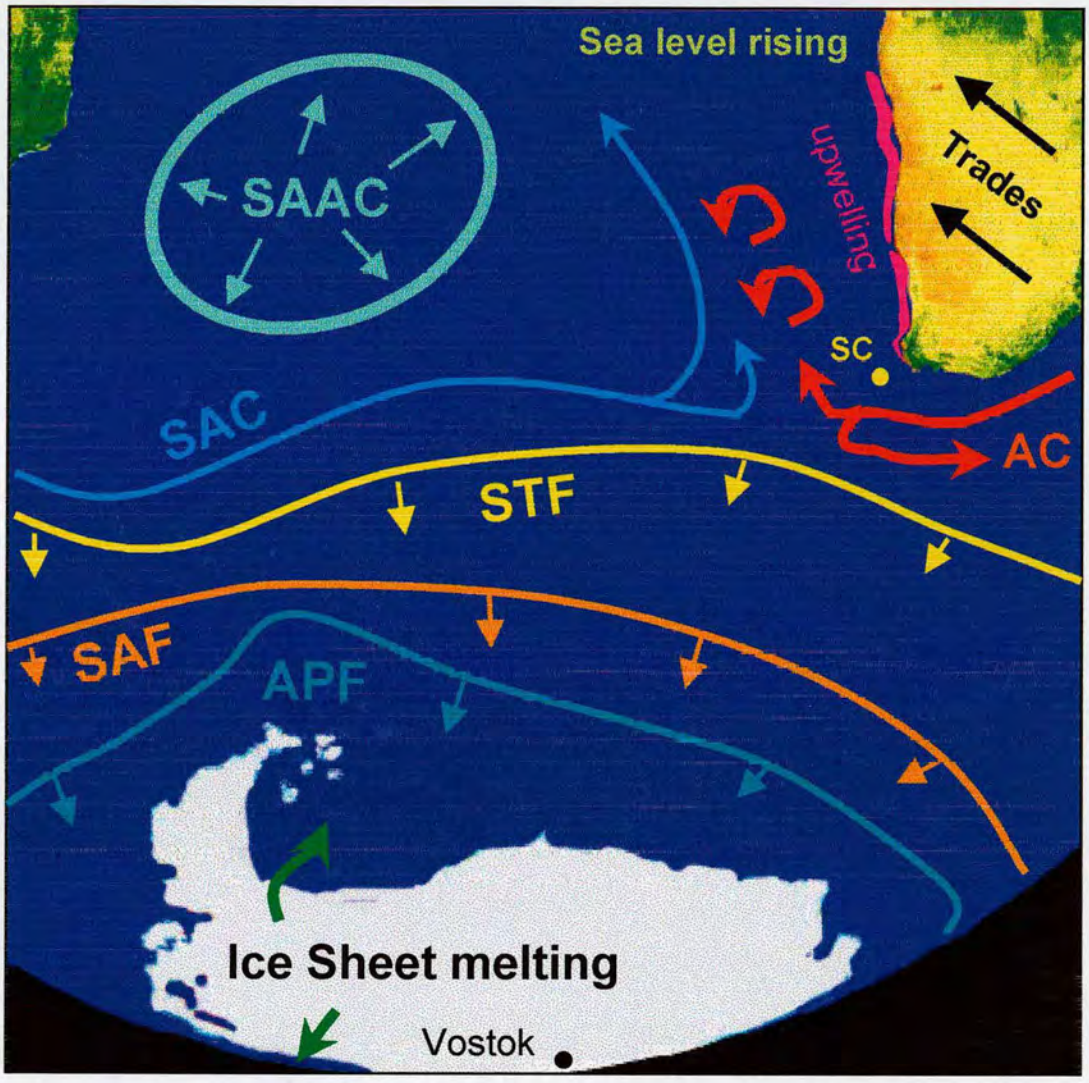

Figure 7.11B Schematic diagram of South Atlantic during early interglacial periods and conditions during MIS 11. Data from this study and Morley (1989), Oppo *et* al. (1990), Charles *et al.* (1991), Howard and Prell (1992), Imbrie *et* al. (1992), Hodell (1993), Little *et al.* (1997b), Flores *et al.* (1999), Petit *et al.* (1999), Hodell *et al.* (2000). SAAC - South Atlantic Anticyclone, SAC - South Atlantic Current, SC - Spliced Cape Basin core, AC - Agulhas Current, STF - Subtropical Front, SAF - Subantarctic Front, APF - Antarctic Polar Front.

MID - INTERGLACIAL

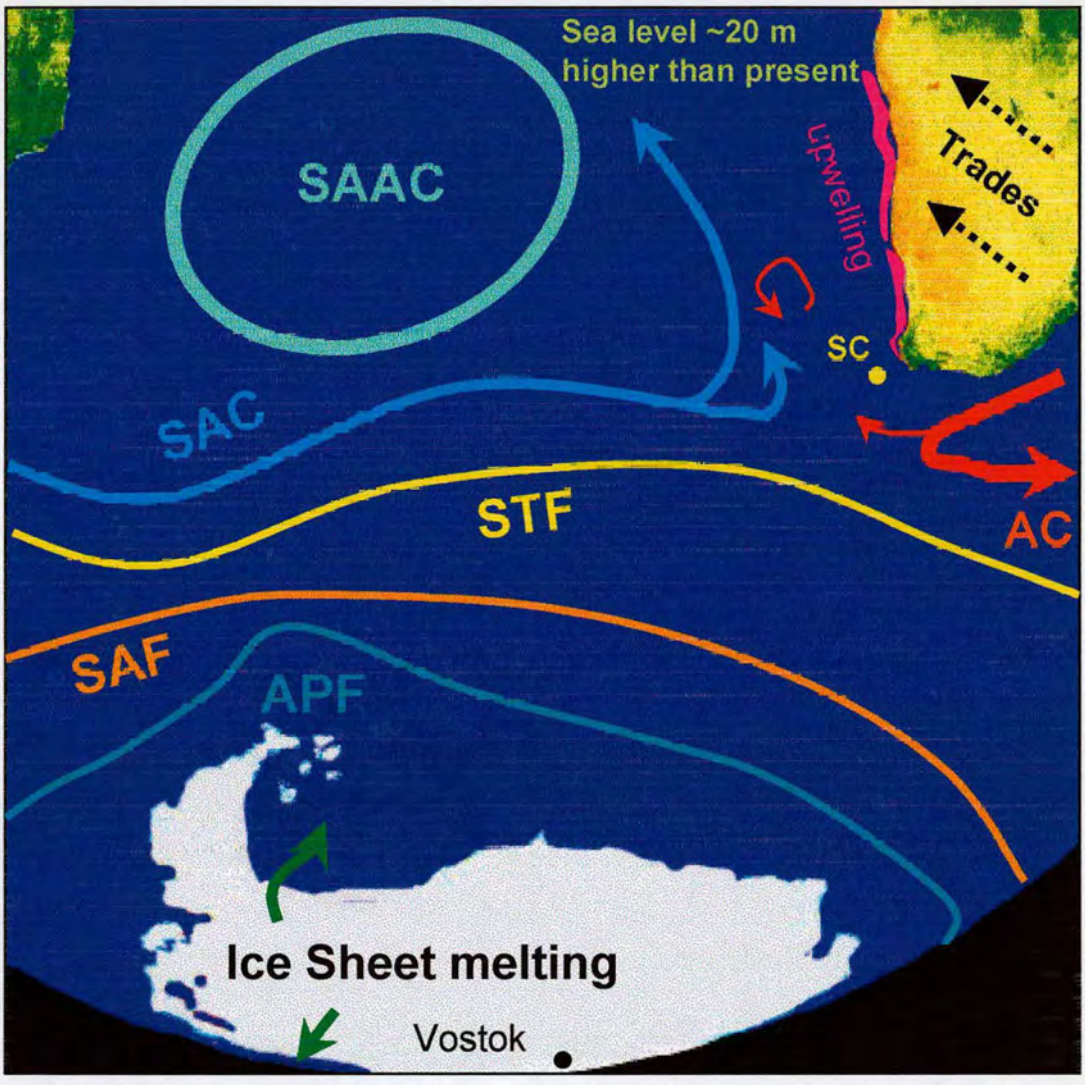

Figure 7.11C Schematic diagram of South Atlantic during interglacial periods. Data from this study and Morley (1989), Oppo *et* al. (1990), Charles *et al.* (1991), Howard and Prell (1992), Imbrie *et* al. (1992), Hodell (1993), Little *et al.* (1997b), Flores *et al.* (1999), Petit *et al.* (1999), Hodell *et al.* (2000). SAAC - South Atlantic Anticyclone, SAC - South Atlantic Current, SC - Spliced Cape Basin core, AC - Agulhas Current, STF - Subtropical Front, SAF - Subantarctic Front, APF - Antarctic Polar Front.

decrease in *N. pachyderma* (d) and an increase in the percentage of warm species. The entire MIS 11 interglacial interval is associated with the MST OEI (Figure 5.10), indicating this was a time when input from Indian Ocean was especially marked and continuous (Figure 7.11B). This is unique for late Quaternary interglacial offshore southern Africa. The usual mid-interglacial pattern of water mass circulation in the Cape Basin (Figure 7.11C) during the past 700 kyr has involved a shift from oligotrophic species associated with advection to South Atlantic gyre-associated oligotrophic planktonic foraminifera (Figure 5.10). A generalised scheme describing water mass (OEI), warm season SSTs (illustrated in Figure 6.4), and associated insolation forcing is outlined in Table 7.2 (below).

	CLIMATE INTERVAL	OEI / WATERMASS	WARM SEASON SST	INSOLATION
1	Glacial **(Figure 7.11A)**	Eutrophic/upwelling	~ 15 to 18°C	Northern (June)
2	Deglacial (termination)	MST/Agulhas advection	rapid warming	Northern (June)
3	Early interglacial **(Figure 7.11B)**	MST/Agulhas advection	~ 22.5°C (max)	Northern (June)
4	Mid-interglacial **(Figure 7.11C)**	Oligotrophic/gyre	~ 20 to 21°C	Southern (Dec.)
5	Interglacial cooling into glacial	MST/Agulhas advection	stepwise cooling	Northern (June)

Table 7.2 Generalised sequence of events in glacial–interglacial cycle in the Cape Basin.

As the Cape Basin is at a crucial juncture in the global circulation of heat and salt, unravelling the history of MIS 11 here may solve the seemingly contradictory story. Firstly, why MIS 11 did not follow the same pattern as subsequent interglacials? Why did the oligotrophic gyre-related watermasses not dominate in the Cape Basin during the mid-MIS 11 interval? Secondly, what was the impact of sustained, strong, advection of Indian Ocean surface waters on the thermohaline circulation? What were the

consequences? Finally, could sea-level have risen by 20m in a climate that may or may not have been warmer than the present (Table 7.1)?

The beginnings of the answers to all these questions probably lie in the insolation parameters which distinguish MIS 11 from other late Quaternary interglacial apart from the present. Hodell *et al.* (2000), examining material from the southern South Atlantic, suggested that the warmth of this interglacial, which was sustained for ~60 k.y., was due to low eccentricity and a diminished precessional amplitude. This proposal supposes that as the contrast between maximum and minimum insolation was reduced, fewer cold substages were induced, and transitional/early interglacial circulation were maintained. Other records from the around the Southern Ocean support a wide Indian-Atlantic Ocean connection during MIS 11. Throughout MIS 11, frontal zones in the southern hemisphere were ~3° south of their present positions (Morley 1989; Howard and Prell, 1992), ice rafted detritus was restricted to the margins of Antarctica (Howard and Prell, 1992), and the Agulhas Retroflection was in an extremely western position (Flores *et al.*, 1999). These conditions are depicted in Figure 7.11B. This situation, the 'open Cape valve' (Berger and Wefer, 1996) promotes the detachment of eddies, and filaments from the Agulhas Current (Lutjeharms, 1981; Shannon *et al.*, 1990a; Lutjeharms and van Ballegooyen, 1984; Gordon and Haxby, 1990; van Ballegooyen *et al.*, 1994), enabling pulses of warm, saline water to enter the Atlantic. Gordon (1996a, 1996b) highlighted the climatic effects that oscillations in the magnitude and intensity of the transport flux from the Indian Ocean might cause to the 'conveyor belt' circulation. The importance of this connectrion has been highlighted by numerous workers (Broecker *et al.* 1985; Gordon, 1985; 1986; Broecker, 1991; Gordon *et al.*, 1992, Macdonald and Wunsch, 1996; Lutjeharms, 1996; Garzoli *et al.* 1996). The transfer of surface waters from the Pacific and Indian Oceans to the Atlantic, which is recorded in the Cape Basin spliced record, is required to compensate for the export of NADW. That NADW production was intensified in MIS 11 is apparent. Whether driving force behind the increasing overturn in the thermohaline system comes from a 'pull' factor from the northern hemisphere i.e. the rapid sinking of surface waters in the North Atlantic, or as a result of a 'push' factor from the southern hemisphere i.e. CO_2 forcing causing warming and thus greater advection from the Indian Ocean leading to increased

cross-equatorial heat transfer, is very difficult to ascertain from this and other existing records. It is likely that a combination of the two factors are important in global climat connections and change on Quaternary timescales.

7.2 UNDERSTANDING CLIMATE FORCING THROUGH MARINE- CONTINENTAL CONNECTIONS

7.2.1 Background to African palaeoenvironmental investigations

Studies of terrestrial sediments and archaeological remains provide proxy evidence for palaeoclimatic change in the African subcontinent throughout the Quaternary. Early investigations focused on archaeological remains in cave deposits (Macrae, 1926; Dart and Del Grande, 1931; Clark, 1942). Recent developments in dating methods, such as optically stimulated luminescence, allow more detailed palaeoenvironmental interpretations to be obtained from southern African caves and the features within them; sediments; speleothems; and clastic deposits (Avery, 1982; Barham, 1993; Acheson, 1996). However, these deposits are often discontinuous in nature. Other, more temporally complete archives include pollen-bearing lake, river bank and flood plain sediments. However these sources are relatively scarce in arid regions, which cover a large proportion of sub-Saharan Africa. Cycles of aridity have been major features of Quaternary environmental change on the south west African continent (Tyson, 1986). These cycles are recorded in arid zone terrestrial deposits such as sand dunes (Stokes *et al.*, 1997). Modern SST changes around southern Africa have been shown to have a direct influence on precipitation patterns and aridity on the adjacent subcontinent (Walker, 1990; Jury, *et al.*, 1993). This section will address this by examining the SST records of oscillating upwelling intensification from the southern Cape Basin, together with terrestrially-derived records of aridity and dune reactivation in southwest Africa. The aim is to identify and describe the climatic history of ocean-continent linkages during the late Pleistocene.

7.2.2 Pleistocene records of aridity and SST variation in southern Africa

A number of studies have been conducted which indicate that SST anomalies drive changes in atmospheric circulation, leading to variations in the balance of continental and marine rainfall in southern Africa (see Jury, 1995 for review). The Kalahari and Namib deserts of southern Africa contain a record of continental aridity through an abundance of palaeo-lake basins, ephemeral stream channels, and aeolian dune forms. Present day atmospheric conditions preclude the formation of aeolian structures (Wiggs *et al.*, 1995). Stokes *et al.* (1997; 1998) used optically stimulated luminescence techniques to create an absolute age chronology for late Quaternary dune building and associated palaeoaridity in south western Africa. Shi *et al.* (2001), in a study that combined dinoflagellate data with terrestrially-derived pollen abundance records from a marine core in the Cape Basin, showed that as SSTs increased (weaker upwelling), there was an increase in vegetation characteristic of warm environments. In the same way, intensified upwelling and cooler Antarctic temperatures were associated with aridification. The palaeo-data generated from the spliced Cape Basin sediment core provide not only SST records but also an upwelling intensity proxy in the form of *N. pachyderma* (d) abundance variation. The detailed record, spanning the upper part of the sequence covering the past 150 k.y., of these different factors shows that during the LGM upwelling intensification and lowered SSTs coincide, producing atmospheric conditions which should lead to extensive continental aridity. Analysis of stable isotopes from Cango Cave stalagmites (Talma and Vogel, 1992) and artesian wells (Heaton *et al.*, 1986) show that temperatures in the southern Cape were 5-6°C cooler than present at the LGM. Records of identified and chronologically constrained arid periods, from Shi *et al.* (2000; 2001) and Stokes *et al.* (1997), are illustrated in Figure 7.12. Furthermore, other lines of terrestrial evidence, such as lacustrine and cave deposits, indicate that southern African climates during the LGM were dry (Partridge *et al.*, 1993a), confirming these interpretations.

However, other arid intervals are apparent in both glacial and interglacial periods. Dune building phase 1 (DB1) is interesting because it takes place during MIS 5, when SSTs are relatively warm and upwelling has not intensified (Figure 7.12). This arid phase is therefore anomalous, in that it does not fit the model described above linking

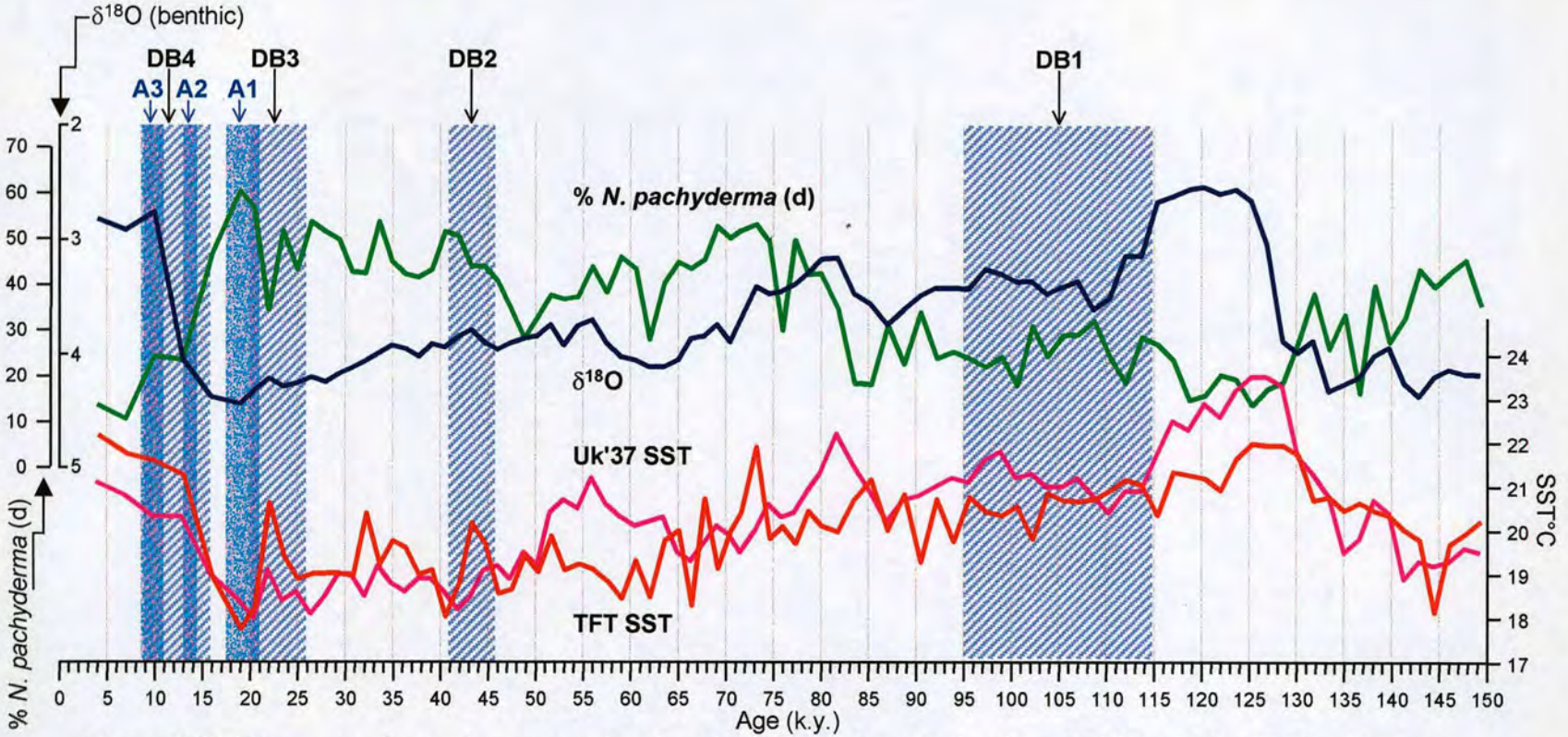

Figure 7.12 Climates on the south west margin of southern Africa since the last interglacial (~150 k.y. B. P.). Alkenone and transfer function (summer) SST curves are shown along with % *N. pachyderma* (d), a eutrophic water mass indicator species. The benthic $\delta^{18}O$ record is also included for comparison. Continental arid periods A1-3 (Shi *et al.*, 2000) and dune-building (arid) phases DB1-4 (Stokes *et al.*, 1997) are labelled. All LGM indicators suggest increased continental aridity during phases of intensified coastal upwelling, whilst other arid phases (DB1, 2 and 4; A3) are linked with warm SSTs. The cause of aridity during these intervals is due to stronger monsoonal circulation and a reduced moisture supply over SW Africa.

arid intervals to a strong SST gradient across the subcontinent. Other terrestrial data confirm the warm land temperatures at this time. Absolute dates from micromammalian remains in Border cave, which focussed on interpreting the environments for early hominids, support elevated temperatures (Grün *et al.*, 1990). The longest and most complete terrestrial palaeo-archive is the Pretoria Saltpan (PSP) which spans at least the past 200 k.y. (Partridge *et al.*, 1993b). The PSP records show aridity in MIS 6 and a rapid and pronounced shift towards greater humidity around 140 k.y., linked to the warming of MIS 5.5. However, during stages 5.4 and 5.2 there was a shift back to more arid conditions, which ties in with the DB1 episode identified by Stokes *et al.* (1997) and illustrated on Figure 7.12. Besides variations in upwelling, a further determinant of rainfall in southern Africa is the Walker circulation and tropical modulation of rainfall. In interglacials increased summer insolation, due to precession, strengthens the monsoon circulation (Kutzbach and Street-Perrott, 1985) and this changes the circulation within the troposphere as a whole over southern Africa and the adjacent oceans. SSTs rise and the inter-tropical convergence zone (ITCZ), under the influence of increased cross-equatorial transport, rests further north, leading to an increase in rainfall in the northern areas of the subcontinent. However, in the lee of the ITCZ, areas in the southern mid-latitudes suffer from a decreased moisture supply. At the same time as the northward shift in the ITCZ, a weaker westerly circulation would have occurred over the southern subcontinent (Cockroft *et al.*, 1987). An example of this is the winter rainfall area of the southern Cape. This area experienced dry conditions during the warmest intervals of MIS 5 (Deacon *et al.*, 1984) as the Westerlies were diverted far south of the subcontinent due to an expanded continental anticyclone (Walker, 1990). This mechanism explains the arid period DB1 identified by Stokes *et al.* (1997) and A3 (Shi *et al.*, 2000) in the early Holocene (Figure 7.12).

7.2.3 Summary of ocean-terrestrial linkages

Links between SST records from the Cape Basin and patterns of continental aridity highlight that during glacials aridity is intimately linked with the strength of upwelling. However, aridity phases in interglacials are caused by changes in insolation and tropical atmospheric circulation. Further evidence to support the possibility of boundary layer modification processes leading to ocean-atmosphere feedback exist.

Wet seasons in southern Africa are associated with higher average SSTs (Walker, 1990). A situation wherein these feedback processes were maintained within a globally favourable context could explain the prolonged warm nature of MIS 11 (Figure 5.12) and the rapid evolutionary development of *Homo sapiens* in favourable environments in southern Africa during this interval (C. Stringer *pers. comm.*, 2000).

7.3 Conclusions

1. Insolation is the primary mechanism driving long-term climatic change during the Quaternary. Secondary processes affecting climates and ocean circulation include changes in wind strength and subsequent shifts in frontal zones, intensity of the thermohaline circulation, and concentrations of greenhouse gases, principally CO_2. These mechanisms may dominate on shorter timescales and may modulate and/or amplify the effects of solar radiation.
2. NADW production is enhanced in interglacial periods of the late Quaternary. Maximum productivity was during MIS 11 and minimum production or perhaps temporary cessation occurred in MIS 12. In the SBS southern component deep watermasses replaced NADW during intervals of MIS 12 and some glacial periods of the Quaternary.
3. Sub-Milankovitch variations in surface water circulation the Cape Basin, and other areas of the southern hemisphere, are recorded during MIS 12. these are associated with changes in the position of frontal zones, allowing significant subantarctic advection into the Cape Basin.
4. Several distinct modes of surface water circulation are observed glacial – interglacial timescales. Greatest Indian Ocean advection occurs during transitional phases, the maximum being deglacial transitions and early interglacial periods. Advection continued throughout MIS 11, unlike other interglacials of the late Quaternary when oligotrophic South Atlantic gyre-related watermasses dominated during mid-interglacial intervals. Oligotrophic-gyre OEI watermasses are linked with southern hemisphere insolation forcing.

5. Quaternary variations in eutrophic/upwelling and advection via the Agulhas Current surface watermasses are largely driven by northern hemisphere summer insolation. This is not surprising given the location of the study area at a key juncture of surface return flow of the global thermohaline circulation.

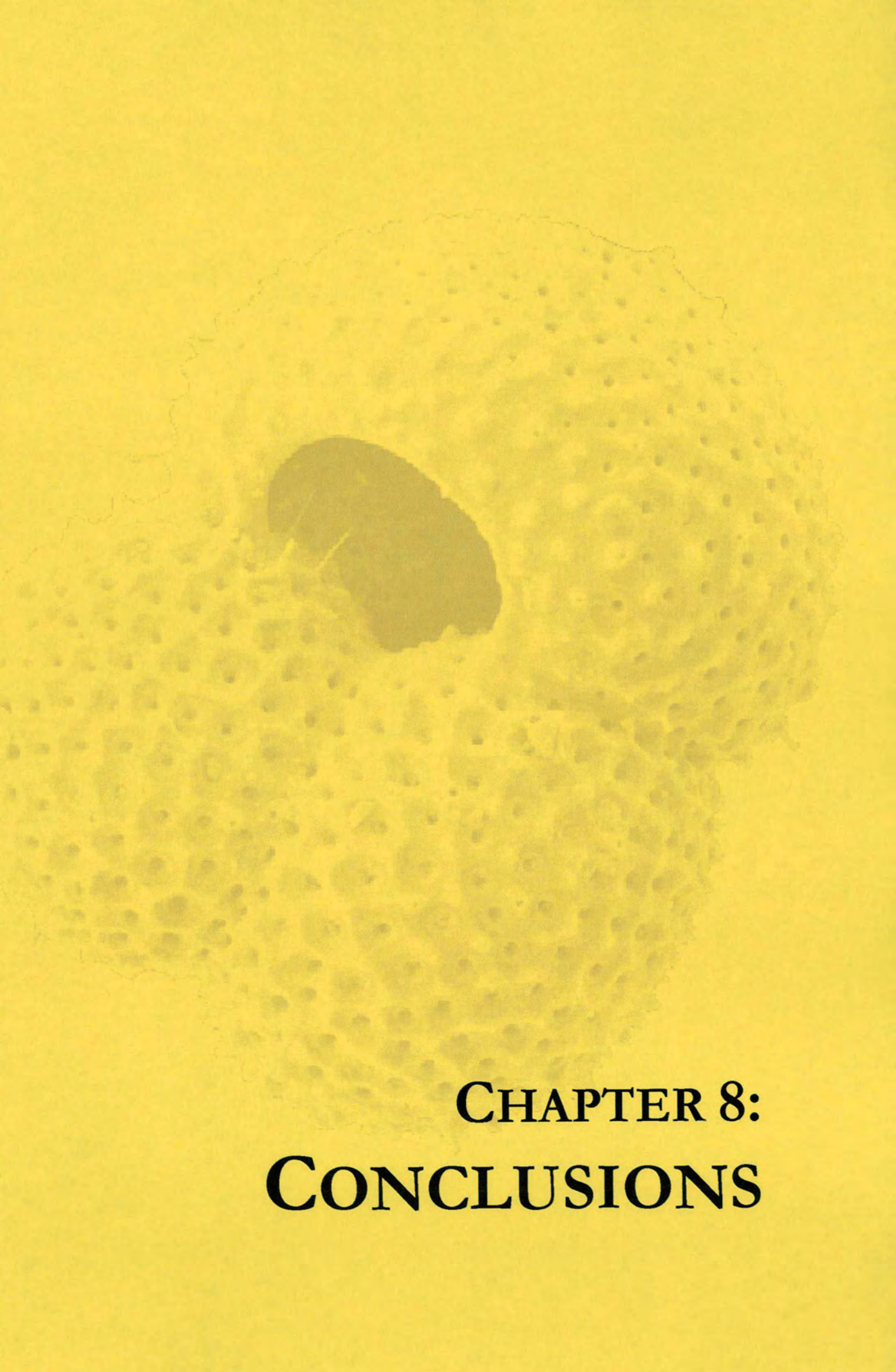

Chapter 8: Conclusions

CHAPTER 8: SUMMARY AND CONCLUSIONS

8.1 INTRODUCTION AND RESTATEMENT OF THESIS AIMS

The focus of this study has been to examine the changes in oceanographic circulation in the SBS during the late Quaternary and their implications for climatic change on a variety of scales. The first aim of this study was to use planktonic foraminiferal census data effectively in order to identify specific key water mass features and their temporal variation. The second was to employ several techniques to calculate and interpret past changes in SST to explore and explain the palaeoceanography in conjunction with the planktonic foraminifera data. These datasets were used to address several issues, as outlined in Section 1.4. Global questions were answered concerning the record and importance of advection from the Indian Ocean of the surface return flow of the thermohaline circulation. In addition, climatic feedbacks, dynamics connected with NADW production, insolation forcing in the northern and southern hemispheres, and their manifestations in the Cape Basin were identified and discussed. Furthermore, variable past warm climates and intervals were considered in relation to their relevance for climates of the present and immediate future. On a regional scale, the upwelling record of the SBS was compared to that of the NBS to understand better the scale and impact of temperature gradients along the southwest African margin. This theme was developed into an examination of the links between upwelling intensity and cycles of aridity since the last interglacial.

8.2 SUMMARY OF RESULTS

8.2.1 Planktonic foraminiferal assemblages

Past circulation and watermasses variation were identified and analysed using an quantitative approach to planktonic foraminiferal assemblages. The ecology and habitat preferences of individual taxa and groups of associated species were combined with statistical analysis of downcore foraminifera data to enable identification of specific water mass types. This was used to chronologically constrain periods of water mass dominance on the Cape Basin, named Ocean Environment Intervals (OEIs). Specific OEIs and sequences of OEIs were linked overall climatic patterns. Watermasses were

dominated by oligotrophic taxa linked to the Agulhas Current during peak interglacials and the climatic transitions from glacial to interglacial and vice versa. These periods are interpreted as intervals with high levels of surface water advection from the Indian Ocean. This interpretation was supported by data which showed these OEIs to be coincident with western retroflections of the Agulhas Current (Flores *et al.*, 1999). The most prolonged incidence of this OEI occurred during MIS 11. Glacial periods were marked by large increases in the abundance of eutrophic species such as *N. pachyderma* (d), and *Gg. bulloides*. Diversity and cluster analysis supported these biological and climatic associations and a eutrophic, glacial OEI was identified. The mechanisms identified were intensified SBS upwelling and increased production and advection of upwelling filaments offshore the main upwelling cells. The third major OEI consisted of another oligotrophic species grouping, but one which was more clearly associated with watermasses from the South Atlantic subtropical gyre than Agulhas Current eddies and filaments. This oligotrophic-gyre OEI was coincident with cool interglacial stadials and expansion of the South Atlantic anticyclone (SAAC).

8.2.2 SSTs

Reconstruction of past SSTs was made using two SST proxies, planktic foraminiferal-based transfer functions and the alkenone technique. This multiproxy approach enabled analysis of the timing and degree of surface warming, despite differences in the past SST estimates. The $U^{k'}_{37}$ SSTs record warmer temperatures than the TFTs and this offset is greatest during interglacial periods. Comparison of the SST records shows that the planktonic foraminifera were more sensitive than the alkenones to seasonal changes and frontal movements. Both techniques record glacial SSTs ~4°C cooler than present, a result of intensified upwelling and, in MIS 12, advection of subantarctic waters. Surface waters in past warm periods were at least as warm as today, and in MIS 5 and 11 SSTs were warmer than present maximum and mean annual temperatures. Warm SSTs in MIS 11 were sustained for ~60 k.y.

The southern hemisphere signal of early surface warming is observed in the Cape Basin. The mechanism associated with this warming is in response to a slow-

down in NADW production in the North Atlantic, which reduces cross-equatorial heat transfer. The deglacial transition into MIS 5 shows exceptionally early warming following a relatively warm MIS 6. Comparison with SSTs from the Indian Ocean and NBS reveal the Cape Basin is linked with tropical forcing. The very early warming is an Indian Ocean pattern only observed in the Atlantic in the Cape Basin.

8.2.3 Climate connections in the past and their implications

The ocean offshore southern Africa has a profound impact on continental climate (Tyson, 1986), although until now it has been difficult to tie detailed records of the two together during the Quaternary. Marine-terrestrial connections were examined in detail by comparing the record of upwelling intensity from the spliced core data and directly (dune reactivation (Stokes *et al.*, 1997; 1998)) and indirectly (marine pollen archives (Shi *et al.*, 2000)) documented cycles of continental aridity. Arid periods are coincident with enhanced upwelling and low SSTs during glacial periods. However, arid periods also are occasionally apparent in interglacial intervals, independent of the glacial mechanisms. These are linked to changes in tropical forcing and SST gradients in the SW Indian Ocean. Interglacials were generally associated with humid conditions on the subcontinent. A long interval of favourable conditions in MIS 11 may have contributed to the rise of *Homo sapiens* during this time.

At the global scale, a detailed comparison of the Cape Basin spliced core foraminiferal and SST time-series confirm that insolation is the primary mechanism driving long-term climatic change during the Quaternary. The relationship is complex; several modes of surface water circulation are observed at glacial – interglacial time-scales through the OEI analysis. Quaternary variations in eutrophic/upwelling and advection via the Agulhas Current surface watermasses are largely driven by northern hemisphere summer insolation. The location of the Cape Basin at a key juncture in surface return flow of the global thermohaline circulation ensures that this is so. Maximum Indian Ocean surface water advection occurs during deglacial transitions and early interglacial periods., but is normally replaced by oligotrophic South Atlantic gyre-related watermasses during mid-interglacial intervals. MIS 11 represents a major deviation from this pattern, whereby oligotrophic-gyre OEI watermasses do not

become established. Watermasses associated with the gyre are linked with southern hemisphere insolation forcing.

However, these large-scale processes are modulated by secondary mechanisms, such as changes in wind strength and subsequent shifts in frontal zones, variations in the intensity of thermohaline circulation, and concentrations of greenhouse gases, principally CO_2. For example, the variation in the production of NADW during glacials, in particular MIS 12, is seen in the SBS benthic $\delta^{13}C$ and $\delta^{18}O$ records, indicating an increased southern component to deep watermasses. Sub-millennial variations in surface water circulation the Cape Basin, and globally, are recorded during MIS 12. These are associated with changes in the position of oceanic frontal zones driven by atmospheric reorganizations independent of oceanic forcing, allowing significant subantarctic advection into the Cape Basin.

It is clear that changes in the distribution of insolation due to oscillations in the earth's solar orbit is the primary mechanism along with CO_2 in long term climatic variation. If MIS 11 is the best analogue for present and immediate future then it seems likely that interglacial conditions will continue for at least 10,000 years. However, given the similarity of climatic forcing between MIS 11 and now, if insolation changes very little over this time, then the importance of other climatic forcing mechanisms such as CO_2 (a substance which is a major and increasing by-product of modern society), will be magnified. Some Quaternary research studies imply that the sustained warm conditions of MIS 11 lead to instability and bi-polar collapse of major ice-sheets, which fits with modern observations of slightly increased sea-level and glacier retreat (Rignot, 1998).

8.3 FUTURE WORK

Several avenues for future work remain to be explored more fully and are identified as follows:

1. The results of this study would be complemented by examining a suite of cores located to the south of the present sites, e.g. Cape Agulhas and in the western Indian Ocean. IMAGES are returning to the area and this new set

of piston cores should be used to investigate the history of the flux of the current, variation in source waters for the current, and the impact of the monsoon system on the current strength. Identifying the mechanisms and factors which determine the strength of this current are the key to understanding the thermohaline circulation.

2. Problems with low analogue SST transfer functions need to addressed with more coretop samples from the area offshore the Benguela upwelling cells. This could form part of a wider programme of sampling the margins of upwelling cells globally.
3. Sediment trap studies in the SBS would allow a detailed analysis of the seasonality of the sediment and foraminiferal flux to the sea-floor and any bias that this may introduce into the palaeo-record.
4. In view of the outlined importance of MIS 11 to potential global warming scenarios, it is important that a detailed Holocene section be recovered and studied from the area, extending this analysis to the present day and allowing a direct link to sediment trap flux studies.
5. A more direct record of the strength of the SBS upwelling is needed, in order to look at any potential changes to the seasonality of upwelling at glacial/interglacial time-scales. This would be achieved by sampling nearer the core of the Cape upwelling cell.
6. The work by Darling (University of Edinburgh; e.g. Darling *et al.*, 2000) looking at the genetic variations of planktonic foraminifera is of particular value to palaeoceanography. It is of particular value in areas such as the Cape Basin, where the location is at the margin of several complexly interacting systems. Identification of morphotypes associated with specific watermasses would allow a more complete description of change.

REFERENCES

REFERENCES

Acheson, R., 1996. Sedimentological analysis of Late Pleistocene deposits from Mumbwa Cave. B.A. Thesis (unpublished), University of Oxford, 94 pp.

Aksu, A.E., Mudie, P.J., de Vernal, A. and Gillespie, H., 1992. Ocean-atmosphere responses to climate change in the Labrador Sea: Pleistocene plankton and pollen records. Palaeogeography, Palaeoclimatoclogy, Palaeoecology, 92: 121-138.

Auras-Schudnagies, A., Kroon, D., Ganssen, G., Hemleben, C. and van Hinte, J.E., 1989. Distributional pattern of planktonic foraminifers and pteropods in surface waters and core top sediments of the Red Sea, and adjacent areas controlled by the monsoonal regime and other ecological factors. Deep Sea Research, 36(10): 1515-1533.

Avery, D.M., 1982. Micromammals as palaeoenvironmental indicators and an interpretation of the late Quaternary in the southern Cape Province, South Africa. Annals of the South African Museum, 89: 183-374.

Balsam, W.L. and McCoy, F.W.J., 1987. Atlantic sediments: Glacial/interglacial comparisons. Paleoceanography, 2: 531-542.

Bard, E., 2001. Comparison of alkenone estimates with other temperature proxies. Geochemistry, Geophysics, Geosystems, 2: Paper number 2000GC000050.

Bard, E., Rostek, F. and Sonzogni, C., 1997. Interhemispheric synchroneiry of the last deglaciation inferred from alkenone paleothermometry. Nature, 385: 707-710.

Barham, L.S., 1993. Preliminary results from Mumbwa Caves, Central Zambia. Southern African Field Archaeology, 2: 108-110.

Bassinot, F.C., Beaufort, L., Vincent, E., Labeyrie, L.D., Rostek, F., Müller, P.J., Quidelleur, X. and Lancelot, Y., 1994. Coarse fraction fluctuations in pelagic carbonate sediments from the tropical Indian Ocean: A 1500 kyr record of carbonate dissolution. Paleoceanography, 9: 579-600.

Bé, A.W.H., 1967. Foraminifera families: Globigerinidae and Globorotaliidae: Zooplankton. Fiches d'identification du Zooplankton, Zooplankton Sheet 108: 1-9.

Bé, A.W.H., 1969. Planktonic foraminifera, Distribution of selected groups of marine invertebrates in waters south of 35°S latitude. Antarctic map Folio Series. Amer. Geogr. Soc., pp. 9-12, pls. 1-2.

Bé, A.W.H., 1977. An ecological, zoogeographic, and taxonomic review of recent planktonic foraminifera. In: A.T.S. Ramsay (Editor), Oceanic Micropaleontology. Acedemic Press, pp. 369-414.

Bé, A.W.H. and Hutson, W.H., 1977. Ecology of planktonic foraminifera and biogeographic patterns of life and fossil assemblages in the Indian Ocean. Micropaleontology, 23(4): 369-414.

Bé, A.W.H. and Tolderlund, D.S., 1971. Distribution and ecology of living planktonic foraminifera in surface waters of the Atlantic and Indian Oceans. In: B.M. Funnel and W.R. Riedel (Editors), The micropalaeontology of the oceans. Cambridge University Press, pp. 105-149.

Berger, A. and Loutre, M.F., 1991. Insolation values for the climate of the last 10 million years. Quaternary Science Reviews, 10: 297-317.

Berger, W.H., 1973. Deep Sea carbonates: Pleistocene dissolution cycles. Journal of Foraminiferal Research, 3: 187-195.

Berger, W.H. and Wefer, G., 1996. Expeditions into the past: palaeoceanographic studies in the South Atlantic. In: G. Wefer, W.H. Berger, G. Siedler and D.J. Webb (Editors), The South Atlantic: Present and Past Circulation. Springer-Verlag, Berlin Heidelberg, pp. 363-410.

Berger, W.S. and Wefer, G., 1990. Export production: seasonality and intermittency, and paleoceanogrphic implications. Palaeogeography, Palaeoclimatology, Palaeoecology., 89: 245-254.

Bertrand, P. and Shipboard Partcipants, 1997. Scientific Report of the NAUSICAA - IMAGES II Coring Cuise, Institut Français pour la Recherche et la Technologie Polaires, Bordeaux.

Bickert, T. and Wefer, G., 1996. Late Quaternary deep water circulation in the South Atlantic: reconstruction from carbonate dissolution and benthic stable isotopes. In: G. Wefer, W.H. Berger, G. Siedler and D.J. Webb (Editors), The South Atlantic: Present and Past Circulation. Springer-Verlag, Berlin Heidelberg, pp. 599-620.

Bijma, J., Erez, J. and Hemleben, C., 1990. Lunar and semi-lunar reproductive cycles in some spinose planktonic foraminifers. Journal of Foraminiferal Research, 20(2): 117-127.

Billups, K., Ravelo, A.C., Zachos, J.C. and Norris, R.D., 1999. Link between oceanic heat transport, thermohaline circulation, and the Intertropical Convergence Zone in the early Pleistocene. Geology, 27(4): 319-322.

Birks, H.J.B. and Birks, H.H., 1980. Quaternary Palaeoecology. Edward Arnold, London.

Bleil, U., Brück, L., Frederichs, T., Haese, R., Hensen, C., Hilgenfeldt, C., Hoek, R., Hübscher, C., von Lom-Keil, H., Janke, A., Kreutz, R., Keenan, J., Little, M., Martens, H., Rosiak, U., Schmidt, W., Schneider, R., Segl, M., Speiß, V., Uenzelmann-Neben, G. et al., 1996. Report and Preliminary Results of Meteor Cruise 34/1, Cape Town - Walvis Bay, 03.01.1996 - 26.01.1996. 77, University of Bremen, Bremen.

Boebel, O., Duncombe Rae, C., Garzoli, S., Lutjeharms, J., Richardson, P., Rossby, T., Schmid, C. and Zenk, W., 1998. Float experiment studies interocean exchanges at the tip of Africa. EOS, Transactions, American Geophysical Union, 79(1): 1, 7, 8.

Bolli, H.M., Ryan, W.B.F., Foresman, J.B., Hottman, W., Kagami, H., Longoria, J.F., McKnight, B.K., Melguen, M., Natland, J., Proto-Decima, F. and Siesser, W.G., 1978. Cape Basin Continental Rise - Sites 360 and 361. In: H.M. Bolli and W.B.F. Ryan (Editors), Initial Reports, DSDP 40. US Government Printing Office, Washington, pp. 29-182.

Boon, J.J., van der Meer, F.W., Schuyl, P.J.W., de Leeuw, J.W., Schenk, P.A. and Burlinghame, A.L., 1987. In: Initial Reports of the Deep Sea Drilling Project, Vols. 38, 39, 40, and 41, U. S. Govt. Printing Office, Washington D. C.

Bowen, D.Q., 1999. Stage 11 sea-level uncertainty: Revised British Isles estimate of ~13±3. EOS Transactions AGU, Fall Meeting Supplement, Abstract OS41C-05.

Boyle, E.A. and Keigwin, L., 1987. North Atlantic thermohaline circulation during the last 20,000 years: Link to high latitude surface temperature. Nature, 330: 35-40.

Bradshaw, J.S., 1959. Ecology of living planktonic foraminifera of the North and Equatorial Pacific Ocean. Cushman Foundation Foraminiferal Research, Contribution 10(2): 25-64.

Brady, H.B., 1884. Report on the foraminifera dredged by H. M. S. Challenger during the years 1873-1876, Challenger Expedition 1873-1876. Rept. Lon. Zool., 22: 1-814.

Brassell, S.C., Eglinton, G., Marlowe, I.T., Pflaumann, U. and Sarnthein, M., 1986. Molecular stratigraphy: a tool for climatic assessment. Nature, 320: 129-133.

Brathauer, U. and Abelmann, A., 1999. Late Quaternary variations in sea surface temperatures and their relationship to orbital forcing recorded in the Southern Ocean (Atlantic sector). Paleoceanography, 14(2): 135-148.

Brigham-Grette, J. and Carter, L.D., 1992. Pliocene marine transgressions of northern Alaska: Circumartic correlations and paleoclimatic interpretations. Arctic, 45(74-81).

Broecker, W.S., 1991. The Great Ocean Conveyor Belt. Oceanography, 4: 79-89.

Broecker, W.S., 1997a. Mountain glaciers: recorders of atmospheric water vapour content? Global Biogeochemical Cycles, 11: 589-597.

Broecker, W.S., 1997b. Thermohaline circulation, the Achilles heel of our climate system: Will man-made CO_2 upset the current balance? Science, 278: 1582-1588.

Broecker, W.S., Bond, G., Klas, M., Bonani, G. and Wolfli, W., 1990. A salt oscillator in the glacial Atlantic? 1. The concept. Paleoceanography, 5: 469-477.

Broecker, W.S. and Denton, G.H., 1989. The role of the ocean-atmosphere reorganisation in glacial cycles. Geochim Cosmologica Acta, 53: 2465-2501.

Broecker, W.S., Peteet, D.M. and Rind, D., 1985. Does the ocean atmosphere system have more than one stable mode of operation? Nature, 315: 21- 26.

Brummer, G.-J.A. and Kroon, D., 1988. Planktic foraminifers as tracers of ocean-climate history. Free University Press, Amsterdam.

Burckle, L.H., 1993. Late Quaternary interglacial stages warmer than present. Quaternary Science reviews, 12: 825-831.

Burton, K.W., Ling, H.F. and O'Nions, R.K., 1997. Closure of the Central American Isthmus and its effect on deep water formation in the North Atlantic. Nature, 386: 382-385.

Buzas, M.A. and Gibson, T.G., 1969. Species diversity: benthonic foraminifera in the Western North Atlantic. Science, 163: 72-75.

Byrne, D.A. and Gordon, A.L., 1995. Agulhas eddies: A synoptic view using Geosat ERM data. Journal of Physical Oceanography, 25: 902-917.

Chang, Y., -P., Chang, C.-C., Wang, L.-W., Chen, M.-T., and Wang, C.-H. 1999. Planktonic foraminiferal sea surface temperature variations in the southeast Atlantic Ocean: a high resolution record MD962085 of the past 400,000 years from the IMAGES II - NAUSICAA cruise. Terrestrial, Atmospheric and Ocean Sciences, 10(1): 185-200.

Chapman, M.R., Shackleton, N.J., Zhao, M. and Eglinton, G., 1996. Faunal and alkenone reconstructions of subtropical North Atlantic surface hydrography and paleotemperature over the last 28 kyr. Paleoceanography, 11(3): 343-357.

Chappell, J., 1987. Ocean volume change and the history of sea water. In: R.J.N. Devoy (Editor), Sea surface studies: a global view. Croom-Helm, London, pp. 56-72.

Charles, C.D., Frielich, P.N., Zibello, M.A., Mortlock, R.A. and Morley, J.J., 1991. Biogenic opal in Southern Ocean sediments over the last 450,000 years: Implications for surface water chemistry and circulation. Paleoceanography, 6(697-728).

Charles, C.D., Lynch-Stieglitz, J., Ninnemann, U.S. and Fairbanks, R.G., 1996. Climate connections between the hemisphere revealed by deep sea sediment core/ice core correlations. Earth and Planetary Science Letters, 142: 19-27.

Chen, M., -T., Chang, Y.-P., Chang, C., -C., Wang, L.-L., and Wang, C.-H., submitted. Late Quaternary sea surface temperature variations in the southeast Atlantic: a planktic foraminifer faunal record of the past 600,000 years (IMAGES II MD96 2085). Marine Geology (Special Volume).

Clark, J.D., 1942. Further excavations (1939) at Mumbwa Caves, Northern Rhodesia. Transactions of the Royal Sociaty of South Africa, 29: 133-201.

CLIMAP and Members, P., 1976. The surface of the Ice-Age earth. Science, 191: 1131-1137.

CLIMAP and Members, P., 1981. Seasonal reconstructions of the earth's surface at the last glacial maximum. Geological Society of America Map and Chart Series, MC 36.

CLIMAP and Members, P., 1984. The interglacial Ocean. Quaternary research, 21: 123-224.

Cockcroft, M.J., Wilkinson, M.J. and Tyson, P.D., 1987. The application of a present day climate model to the late Quaternary in Southern Africa. Climate Change, 10: 161-181.

Crowley, T.J., 1983. Calcium-carbonate preservation patterns in the central North Atlantic during the last 150,000 years. Marine Geology, 51: 1-14.

Crowley, T.J., 1992. North Atlantic Deep Water cools the South Atlantic. Paleoceanography, 7: 489-497.

Curry, W.B., 1996. Late Quaternary deep circulation in the Western Equatorial Atlantic. In: G. Wefer, W.H. Berger, G. Siedler and D.J. Webb (Editors), The South Atlantic: Present and Past Circulation. Springer-Verlag, Berlin Heidelberg, pp. 577-598.

Curry, W.B., Duplesy, J.C. and Labeyrie, L.D., 1988. Changes in the distribution of $\delta^{13}C$ of deep water ΣCO_2 between the last glaciation and the Holocene. Paleoceanography, 3: 317-342.

Curry, W.B. and Oppo, D.W., 1997. Synchronous, high-frequency oscillations in tropical sea surface temperatures and North Atlantic Deep Water production during the last glacial cycle. Paleoceanography, 12(1): 1-14.

Darling, K., Wade, C.M., Stewart, I.A., Kroon, D., Dingle, R. and Leigh Brown, A.J., 2000. Molecular evidence for genetic mixing of Arctic and Antarctic subpolar populations of planktonic foraminifers. Nature, 405: 43-47.

Dart, R.A. and Del Grande, N., 1931. The ancient iron smelting cavern at Mumbwa. Transactions of the Royal Society of South Africa, 19: 379-427.

De Leeuw, J.W., van der Meer, F.W., Rijpstra, W.I.C. and Schenk, P.A., 1980. On the occurrence and structural identification of long chain unsaturated ketones and hydrocarbons in sediments. In: A.G. Douglas and J.R. Maxwell (Editors), Advances on organic geochemistry, pp. 211-217.

De Ruijter, W., 1982. Asymptotic analysis of the Agulhas and Brasil Current Systems. Journal of Physical Oceanography, 12(4): 361-373.

De Ruijter, W.P.M. and Boudra, D.B., 1985. The wind-driven circulation in the South Atlantic - Indian Ocean - I. Numerical experiments in a one layer model. Deep Sea Research, 32(5): 557-574.

Deacon, J., Lancaster, N. and Scott, L., 1984. Evidence for late Quaternary climate change in southern Africa: summary of the proceedings of the SASQUA workshop held in Johannesburg, September 1983. In: J.C. Vogel (Editor), Late Cainozoic Palaeoclimates of the Southern Hemisphere. Balkema, Rotterdam, pp. 391-404.

Dengler, A.T., 1985. Relationship between physical and biological processes at an upwelling front off Peru, 15°S. Deep Sea Research, 32(11A): 1301-1315.

Diekmann, B., Petschick, R., Gingele, F.X., Fütterer, D.K., Abelmann, A., Brathauer, U., Gersonde, R. and Mackensen, A., 1996. Clay mineral fluctuations in Late Quaternary sediments of the south-eastern South Atlantic: implications for past changes of deep water advection. In: G. Wefer, W.H. Berger, G. Siedler and J. Webb (Editors), The South Atlantic: Present and Past Circulation. Springer-Verlag, Berlin Heidelberg, pp. 621-644.

Diester-Haas, L., 1985. Late Quaternary upwelling history off southwest Africa (DSDP Leg 75, HPC 532). In: K.J. Hsu and H.J. Weissert (Editors), South Atlantic Paleoceanography. Cambridge University Press, Cambridge, pp. 47-55.

Diester-Haas, L., 1988. Sea-level changes, carbonate dissolution and history of the Benguela Current in the Oligocene-Miocene off Southwest Africa (DSDP site 362, Leg 40). Marine Geology, 79: 213-242.

Diester-Haas, L., Heine, K., Rothe, P. and Schrader, H., 1988. Late Quaternary history of continental climate and the Benguela Current off south west Africa. Palaeogeography, Palaeoclimatology, Palaeoecology, 65: 81-91.

Diester-Haas, L., Meyers, P.A. and Rothe, P., 1992. The Benguela Current and associated upwelling on the southwest African Margin: a synthesis of the Neogene-Quaternary sedimentary record at DSDP sites 362 and 532. In: C.P. Summerhayes, W.L. Prell and K.C. Emeis (Editors), Upwelling systems : Evolution since the Miocene, pp. 331-342.

Dingle, R.V., 1995. Continental shelf upwelling and benthic Ostracoda in the Benguela System (southeastern Atlantic Ocean). Marine Geology, 122: 207-225.

Dingle, R.V., Bremner, J.M., Giradeau, J. and Buhmann, D., 1996. Modern and palaeo-oceanographic environments under Benguela upwelling cells off southern Namibia. Palaeogeography, Palaeoclimatology, Palaeoecology, 123: 85-105.

Dingle, R.V. and Nelson, G., 1993. Sea-bottom temperature, salinity, and dissolved oxygen on the continental margin off southwestern Africa. South African Journal of Marine Science, 13: 33-49.

Domack, E.W. and Mayewski, P.A., 1999. Bi-polar ocean linkages: Evidence from late Holocene Antarctic marine and Greenland ice-core records. The Holocene, 9: 247-251.

Donner, B. and Wefer, G., 1994. Flux and stable isotope composition of *Neogloboquadrina pachyderma* and other planktonic foraminifers in the Southern Ocean (Atlantic sector). Deep Sea Research, 41: 1733-1743.

D'Orbigny, A.D., 1826. Tableau méthodique de la classe des Céphalopodes. Ann. Sci. Nat. Paris, Ser. 1, 7: 1-277.

D'Orbigny, A.D., 1839. Foraminiferés. In: R. De la Sagra (Editor), Histoire physique, politique, et naturelle de l'ile de Cuba. Bertrand, pp. 1-224.

Dowsett, H.J. and Poore, R.Z., 1990. A new planktic foraminifer transfer function for estimating Pliocene-Holocene paleoceanographic conditions in the North Atlantic. Marine Micropaleontology, 16: 1-23.

Droxler, A., Burckle, L. and Poore, R., 1999. Documenting the past to model the future: MIS stage 11. JOI/USSAC Newsletter, 12(1): 6-7.

Droxler, A.W. and Farrell, J.W., 2000. Marine Isotope Stage 11 (MIS 11): new insights for a warm future. Global and Planetary Change, 24: 1-5.

Duplessy, J.C., Shackleton, N.J., Fairbanks, R.G., Labeyrie, L., Oppo, D. and Kallel, N., 1988. Deep water source variations during the last climatic cycle and their impact on the global deep water circulation. Paleoceanography, 3: 343-360.

Dwyer, G.S., Cronin, T.M., Baker, P.A., Raymo, M.E., Buzas, J.S. and Corrège, T., 1995. North Atlantic deepwater temperature change during Late Pliocene and Late Quaternary climate cycles. Science, 270: 1347-1350.

Ehrenberg, C.G., 1861. Elemente des tiefen Meeresgrundes in Mexikanische Golfstrome bei Florida; Über die tiefgrund-Verhältnisse des oceans am eingange der Davisstrasse und bei Island. In: K. Preuss (Editor), Science Academy, pp. 222-240 and 275-317.

Ekman, V.W., 1905. On the influence of the earth's rotation in ocean currents. Arch. Math. Astron. Phys., 2(11).

Emeis, K.-C., Anderson, D.M., Doose, H., Kroon, D. and Schultz-Bull, D., 1995. Sea-surface temperatures and the history of monsoon upwelling in the Northwest Arabian Sea during the last 500,000 years. Quaternary Research, 43: 355-361.

Emiliani, E., 1954. Depth habits of some species of pelagic foraminifera as indicated by oxygen isotope ratios. American Journal of Science, 252: 149-158.

Emiliani, E., 1955. Pleistocene temperatures. Journal of Geology, 63: 538-575.

Epstein, S.R., Buchsbaum, H.A., Lowenstam, B. and Urey, H.C., 1953. Revised carbonate-water isotopic temperature scale. Geological Society of America Bulletin, 64: 1315-1325.

Epstein, S.R. and Urey, H.C., 1951. Carbonate water isotopic temperature scale. Geological Society of America Bulletin, 62: 417-425.

Fairbanks, R.G., Sverdlove, M., Free, R., Wiebe, P.H. and Bé, A.W.H., 1982. Vertical distribution and isotopic fractionation of living planktonic foraminifera from the Panama Basin. Nature, 298: 841-844.

Fairbanks, R.G. and Wiebe, P.H., 1980. Foraminifera and chlorophyll maximum: vertical distribution, seasonal succession, and palaeoceanographic significance. Science, 209: 15424-15426.

Farrell, J.W. and Prell, W.L., 1989. Climatic change and $CaCO_3$ preservation: an 800,000 year bathymetric reconstruction from the central equatorial Pacific Ocean. Paleoceanography, 4: 447-466.

Fischer, G. and Wefer, G., 1996. Long-term observation of particle fluxes in the eastern Atlantic: Seasonality, changes of flux with depth and comparison with the sediment record. In: G. Wefer, W.H. Berger, G. Siedler and D.J. Webb (Editors), The South Atlantic: Present and Past Circulation. Springer-Verlag, Berlin Heidelberg, pp. 325-344.

Flores, J.-A., Gersonde, R. and Sierro, F.J., 1999. Pleistocene fluctuations in the Agulhas Current Retroflection based on the calcareous plankton record. Marine Micropaleontology, 37: 1-22.

Forsström, L., 2001. Duration of interglacials: a controversial question. Quaternary Science Reviews, 20: 1577-1586.

Gardner, J.V. and Hays, J.D., 1976. Responses of sea-surface temperature and circulation to global climatic change during the past 200,000 years in the Eastern Equatorial Atlantic Ocean. Geological Society of America, Memoir, 45: 221-246.

Garzoli, S.L. and Gordon, A.L., 1996. Origins and variability of the Benguela Current. Journal of Geophysical Research, 101(C1): 897-906.

Garzoli, S.L., Gordon, A.L., Kamenkovich, V., Pillsbury, D. and Duncombe-Rae, C., 1996. Variability and sources of the southeastern Atlantic circulation. Journal of Marine Research, 54: 1039-1071.

Gersonde, R., Abelmann, A., Bianchi, C., Cortese, G., Diekmann, B., Kuhn, G. and Kunz-Pirrung, M., 2000. Late and Middle Pleistocene terminations in the Southern Ocean - structure and climate variability revealed from microfossil records at submillennial resolution. EOS Transactions AGU, Fall Meeting Supplement, Abstract OS21B-04.

Ghil, M., 1984. Climate sensitivity, energy balance models, and oscillatory climate models. Journal of Geophysical Research, 89(D1): 1280-1284.

Giraudeau, J., 1993. Planktonic foraminiferal assemblages in surface sediments from the southwest African margin. Marine Geology, 110: 47-62.

Giraudeau, J., Bailey, G.W. and Pujol, C., 2000. A high-resolution time-series analysis of particle fluxes in the Northern Benguela coastal upwelling system: carbonate record of changes in biogenic production and particle transfer process. Deep Sea Research II, 47: 1999-2028.

Giraudeau, J., Pierre, K. and Herve, L., 2001. A late Quaternary, high resolution record of planktonic foraminiferal species distribution in the southern Benguela region: Site 1087. In: G. Wefer, W.H. Berger and C. Richter (Editors), Proceedings of Ocean Drilling Program, Scientific Results. Available from: <http://www.odp.tamu.edu/publications/175_SR/VOLUME/ CHAPTERS/ SR175_07.PDF>, pp. 1-26 (Online).

Giraudeau, J. and Rogers, J., 1994. Phytoplankton biomass and sea-surface temperature estimates from sea-bed distribution of nannofossils and planktonic foraminifera in the Benguela upwelling system. Micropaleontology, 40(3): 275-285.

Gordon, A.L., 1981. South Atlantic thermocline ventilation. Deep Sea Research Part I, 28: 1239-1264.

Gordon, A.L., 1985. Indian-Atlantic transfer of thermocline water at the Agulhas Retroflection. Science, 227: 1030-1032.

Gordon, A.L., 1986. Interocean exchange of thermocline water. Journal of Geophysical Research, 91(C4): 5037-5046.

Gordon, A.L., 1988. The South Atlantic: an overview of results from 1983-1988 research. Oceanography, November: 12-17.

Gordon, A.L., 1996a. Comment on the South Atlantic's role in the global circulation. In: G. Wefer, W.H. Berger, G. Siedler and D.J. Webb (Editors), The South Atlantic: Present and Past Circulation. Springer-Verlag, Berlin Heidelberg, pp. 121-124.

Gordon, A.L., 1996b. Communication between oceans. Nature, 382: 399-400.

Gordon, A.L. and Haxby, W.F., 1990. Agulhas eddies invade the South Atlantic: Evidence from Geosat altimeter and shipboard conductivity-temperature-depth survey. Journal of Geophysical Research- Oceans, 95: 3117-3125.

Gordon, A.L., Weiss, R.F., Smethie, W.M. and Warner, M.J., 1992. Thermocline and intermediate water communication between the South Atlantic and Indian Oceans. Journal of Geophysical Research, 97(C5): 7223-7240.

Grün, R., Beaumont, P.B. and Stringer, C.S., 1990. ESR dating evidence for early modern humans at Border Cave in South Africa. Nature, 344: 537-539.

Gründlingh, M.L., 1978. Drift of a satellite-tracked buoy in the southern Agulhas Current and Agulhas Return Current. Deep Sea Research, 25(12): 1209-1224.

Hale, W. and Pflaumann, U., 1999. Sea-surface temperature estimations using a Modern Analog Technique with foraminiferal assemblages from western Atlantic sediments. In: G. Fischer and G. Wefer (Editors), Use of proxies in paleoceanography: examples from the South Atlantic. Springer-Verlag, Berlin Heidleberg, pp. 69-90.

Harrison, S.P., Metcalfe, S.E., Street-Perrott, F.A., Pittcock, A.B., Roberts, C.N. and Salinger, M.J., 1984. A climatic model of the Last Glacial/Interglacial transition based on palaeotemperature and palaeohydrological evidence. In: J.C. Vogel (Editor), Late Cainozoic Palaeoclimates of the Southern Hemisphere. Balkema, Rotterdam, pp. 21-34.

Hays, J.D., Imbrie, J. and Shackleton, N., 1976. Variations in the earth's orbit: pacemaker of the ice ages. Science, 194: 1121-1132.

Hearty, P.J., Kindler, P., Cheng, H. and Edwards, R.L., 1999a. A +20m middle Pleistocene sea-level highstand (Bermuda and the Bahamas) due to partial collapse of Antarctic ice. Geology, 27(4): 375-378.

Hearty, P.J., Kindler, P., Cheng, H. and Edwards, R.L., 1999b. The Kaena highstand in Hawai'i: Further support for partial Antarctic ice collapse during marine isotope stage 11. EOS Transactions AGU(Fall Meeting Supplement): Abstract OS41C-06.

Heaton, T.H.E., Talma, A.S. and Vogel, J.C., 1986. Dissolved gas palaeotemperatures and ^{18}O variations derived from groundwater near Uitenhage, South Africa. Quaternary Research, 25: 79-88.

Hebbeln, D., Marchant, M., Freudenthal, T. and Wefer, G., 2000. Surface sediment distribution along the Chilean continental slope related to upwelling and productivity. Marine Geology, 164: 119-137.

Hemleben, C., Spindler, M. and Anderson, O.R., 1989. Modern Planktonic Foraminifera. Springer-Verlag, New York, 363 pp.

Henderson, G.M. and Slowey, N.C., 2000. Evidence from U-Th dating against Northern Hemisphere forcing of the penultimate deglaciation. Nature, 404: 61-66.

Hendy, I.L. and Kennett, J.P., 1999. Latest Quaternary North Pacific surface water responses imply atmosphere-driven climate instability. Geology, 27: 291-294.

Heusser, C.J., 1989. Polar perspective of late Quaternary climates in the Southern Hemisphere. Quaternary Research, 32: 60-71.

Hodell, D.A., 1993. Late Pleistocene palaeoceanography of the South Atlantic sector of the Southern Ocean: Ocean Drilling Program Hole 704A. Paleoceanography, 8: 47-67.

Hodell, D.A., Charles, C.D. and Ninnemann, U.S., 2000. Comparison of interglacial stages in the South Atlantic sector of the southern ocean for the past 450 kyr: implications for Marine Isotope Stage (MIS) 11. Global and Planetary Change, 24: 7-26.

Hooghiemstra, H., 1989. Quaternary and upper Pliocene glaciations and forest development in the tropical Andes: Evidence from a long high-resolution pollen record from the sedimentary basin of Bogota, Colombia. Palaeogeography, Palaeoclimatology, Palaeoecology, 72: 11-26.

Howard, W.R., 1997. A warm future in the past. Nature, 388: 418-419.

Howard, W.R. and Prell, W.L., 1984. A comparison of radiolarian and foraminiferal paleoecology in the southern Indian Ocean: new evidence for the interhemispheric timing of climate change. Quaternary Research, 21: 244-263.

Howard, W.R. and Prell, W.L., 1992. Late Quaternary surface circulation of the southern Indian Ocean and its relationship to orbital variations. Paleoceanography, 7(1): 79-117.

Hudson, J.D., 1977. Oxygen isotope studies on Cenozoic temperatures, oceans, and ice accumulation. Scottish Journal of Geology, 13(4): 313-325.

Hutson, W.H., 1977. Transfer functions under no-analog conditions: Experiments with Indian Ocean planktonic foraminifera. Quaternary Research, 8: 355-367.

Hutson, W.H., 1980. The Agulhas Current during the Late Pleistocene: analysis of the modern faunal analogs. Science, 207: 64-66.

Imbrie, J., Berger, A., Boyle, E.A., C., C.S., Duffy, A., Howard, W.R., Kukla, G., Kutzbach, J., Martinson, D.G., McIntyre, A., Mix, A.C., Molfino, B., Morley, J.J., Peterson, L.C., Pisias, N.G., Prell, W.L., Raymo, M.E., Shackleton, N.J. and Toggweiler, J.R., 1993. On the structure and origin of major glacial cycles 2: The 100,000 year cycle. Paleoceanography, 8: 699-735.

Imbrie, J., Boyle, E.A., C., C.S., Duffy, A., Howard, W.R., Kukla, G., Kutzbach, J., Martinson, D.G., McIntyre, A., Mix, A.C., Molfino, B., Morley, J.J., Peterson, L.C., Pisias, N.G., Prell, W.L.,

Raymo, M.E., Shackleton, N.J. and Toggweiler, J.R., 1992. On the structure and origin of major glacial cycles, 1: Linear response to Milankovitch forcing. Paleoceanography, 7: 701-738.

Imbrie, J., Hays, J.D., Martinson, D.G., McIntyre, A., Mix, A.C., Morley, J.J., Pisias, N.G., Prell, W.L. and Shackleton, N., 1984. The orbital theory of Pleistocene climate: support from a revised chronology of the marine $\delta^{18}O$ record. In: A.L. Berger, J. Imbrie, J.D. Hays, J. Kukla and J. Saltzman (Editors), Milankovitch and Climate. Part 1. Reidel, Hingham, Mass., pp. 269-305.

Imbrie, J. and Imbrie, K.P., 1979. Ice Ages: Solving the Mystery. Macmillan, London.

Imbrie, J. and Kipp, N.G., 1971. A new micropaleontological method for quantative paleoclimatology: Application to a late Pleistocene Caribbean core. In: K.K. Turkeyan (Editor), The Late Cenozoic glacial ages. Yale University Press, Newhaven and London, pp. 71- 181.

Imbrie, J., McIntyre, A. and Mix, A., 1989. Oceanic response to orbital forcing in the late Quaternary: Observational and experimental strategies. In: A. Berger (Editor), Climate and Geo-Sciences. Kluwer Academic Publishers, Norwell, Mass., pp. 121-164.

Imbrie, J., van Donk, J. and Kipp, N.G., 1973. Paleoclimatic investigation of a Late Pleistocene Caribbean deep-sea core: comparison of isotopic and faunal methods. Quaternary Research, 3: 10-38.

Jansen, J.H.F., Kuijpers, A. and Troelstra, S.R., 1986. A Mid-Bruhnes climate event: long term changes in global atmosphere and ocean circulation. Science, 233: 619-622.

Jury, M.R., 1985. Case studies of alongshore variations in wind-driven upwelling in the southern Benguela region. In: L.V. Shannon (Editor), Southern African Ocean Colour and Upwelling Experiment. Sea Fisheries Research Institute, Cape Town, pp. 29-46.

Jury, M.R., 1995. A review of research on ocean-atmosphere interactions and South African climate variability. South African Journal of Science, 91: 289-295.

Jury, M.R., Valentine, H.R. and Lutjeharms, J.R.E., 1993. Influence of the Agulhas Current on summer rainfall on the south east coast of South Africa. Journal of Applied Meteorology, 32: 1285-1305.

Kahn, M., 1979. Non-equilibrium oxygen and carbon isotopic fractionation in tests of living foraminifera. Oceanol. Acta, 2: 195-208.

Keigwin, L., 1978. Pliocene closing of the Ismuthus of Panama, based on stratigraphic evidence from nearby Pacific and Caribbean Sea cores. Geology, 6: 630-634.

Kemle-von Mücke, S. and Oberhänsli, H., 1999. The distribution of living planktic foraminifera in relation to southeast Atlantic oceanography. In: G. Fischer and G. Wefer (Editors), Use of proxies in paleoceanography: examples from the South Atlantic. Springer-Verlag, Berlin Heidelberg.

Kennett, J., 1970. Pleistocene paleoclimates and foraminiferal biostratigraphy in subantarctic deep-sea cores. Deep Sea Research, 17: 125-140.

Kennett, J.P. and Srinivasen, M.S., 1983. Neogene planktonic foraminifera: A phylogenetic atlas. Hutchinson Ross Publishing Co., 265 pp.

Kennett, J.P. and Venz, K., 1995. Late Quaternary climatically related planktonic foraminiferal assemblage changes: Hole 893A, Santa Barbara Basin, California. In: J.P. Kennett, J.G. Baldauf and M. Lyle (Editors), Proceedings of the Ocean Drilling Program. Scientific Results., pp. 281-293.

King, A.L. and Howard, W.R., 2000. Middle Pleistocene sea-surface temperature change in the southwest Pacific Ocean on orbital and suborbital timescales. Geology, 27(7): 659-662.

King, A.L. and Howard, W.R., 2001. Seasonality of foraminiferal flux in sediment traps at Chatham Rise, SW Pacific: Implications for paleotemperature estimations. Deep Sea Research I, 48: 1687-1708.

Kipp, N.G., 1976. New transfer function for estimating past sea-surface conditions from sea bed distribution of planktonic foraminiferal assemblages in the North Atlantic. Geological Society of America Memoir, 145: 3-41.

Kirst, G.J., Schneider, R.R., Müller, P.J., von Storch, E. and Wefer, G., 1999. Late Quaternary temperature variability in the Benguela Current System derived from alkenones. Quaternary Research, 52: 92-103.

Klinck, J.M. and Smith, D.A., 1993. Effect of wind changes during the last glacial maximum on the circulation in the Southern Ocean. Paleoceanography, 8: 427-433.

Klovan, J.E. and Imbrie, J., 1971. An algorithm and FORTRAN IV program for large scale Q-mode factor analysis. Mathematical Geology, 3: 61-67.

Kroon, D., 1988. The planktic $\delta^{13}C$ record, upwelling and climate. In: G.J. Brummer and D. Kroon (Editors), Planktonic foraminifers as tracers of ocean-climate history. Vrije Universiteit Te Amsterdam, Amsterdam, pp. 335-346.

Kroon, D., 1991. Distribution of extent planktonic foraminiferal assemblages in the Red Sea and northern Indian Ocean surface waters. Revista Española de Micropaleontología, 23(1): 37-74.

Kroon, D., Alexander, I. and Darling, K., 1993. Planktonic and benthic foraminiferal abundances and their ratios (P/B) as expressions of Middle-Late Quaternary changes in watermass distribution and flow intensity on the northeastern Australian Margin. In: J.A. McKenzie, P.J. Davies and A. Palmer-Julson (Editors), Proceedings of the Ocean Drilling Program, Scientific Results., pp. 181-188.

Kroon, D. and Ganssen, G., 1989. Northern Indian Ocean upwelling cells and the stable isotope composition of living planktonic foraminifera. Deep Sea Research, 36(8): 1219-1236.

Kukla, G., Berger, A.L., R. and Brown, J., 1981. Orbital signature of interglacials. Science, 290: 295-300.

Kunz-Pirrung, M., Bianchi, C. and Gersonde, R., 2000. Middle and late Pleistocene millennial-scale climate variations in sea-surface temperatures and sea-ice distribution in the Atlantic sector of the Southern Ocean. EOS Transactions AGU, Fall Meeting Supplement, Abstract OS21B-02, 81(48).

Kutzbach, J.E. and Street-Perrott, F.A., 1985. Milankovitch forcing of fluctuations in the level of tropical lakes from 18 to 0 kyr B. P. Nature, 317: 130-134.

Labeyrie, L., Labracherie, M., Gorfti, N., Pichon, J.J., Vautravers, M., Arnold, M., Duplessy, J.-C., Paterne, M., Michel, E., Duprat, J., Caralp, M. and Turon, J.-L., 1996. Hydrographic changes of the Southern Ocean (southeast Indian sector) over the last 230 kyr. Paleoceanography, 11(1): 57-76.

Le, J. and Shackleton, N.J., 1992. Carbonate dissolution fluctuations in the western equatorial Pacific during the late Quaternary. Paleoceanography, 7(1): 21-42.

Le, J. and Shackleton, N.J., 1994. Reconstructing paleoenvironments by transfer function: Model evaluation with simulated data. Marine Micropaleontology, 24: 187-199.

Levitus, S. and Boyer, T., 1994. World Ocean Atlas: Volume 4: Temperature, US Govt. Printing Office.

Little, M.G., 1997. Late Quaternary palaeoceanography of the Benguela upwelling system. Ph.D. (unpublished) Thesis, University of Edinburgh, 185 pp.

Little, M.G., Schneider, R.R., Kroon, D., Price, B., Bickert, T. and Wefer, G., 1997a. Rapid palaeoceanographic changes in the Benguela Upwelling System for the last 160,000 years as indicated by abundances of planktonic foraminifera. Palaeogeography, Palaeoclimatology, Palaeoecology., 130: 135-161.

Little, M.G., Schneider, R.R., Kroon, D., Price, B., Summerhayes, C.P. and Segl, M., 1997b. Trade wind forcing of upwelling, seasonality, and Heinrich events as a response to sub-Milankovitch climate variability. Paleoceanography, 12(4): 568-576.

Lowell, T.V., Heusser, C.J., G., A.B., Moreno, P.I., Hauser, A., Heusser, L.E., Schluechter, C., Marchant, D.R. and Denton, G.H., 1995. Interhemispheric correlation of Late Pleistocene glacial events. Science, 269(1541-1549).

Lutjeharms, J., R. E., 1981. Features of the southern Agulhas current circulation from satellite remote sensing. South African Journal of Science, 77: 231-236.

Lutjeharms, J.R.E., 1996. The exchange of waters between the South Indian and South Atlantic Oceans. In: G. Wefer, W.H. Berger, G. Siedler and D.J. Webb (Editors), The South Atlantic: Present and Past Circulation. Springer-Verlag, Berlin Heidelberg, pp. 125-162.

Lutjeharms, J.R.E. and Gordon, A.L., 1987. Shedding of an Agulhas ring observed at sea. Nature, 325: 138-140.

Lutjeharms, J.R.E. and Meeuwis, J.M., 1987. The extent and variability of South-east Atlantic upwelling, The Benguela and Comparable Ecosystems. South African Journal of Marine Science. Sea Fisheries Research Institute, Republic of South Africa Department of Environmental Affairs, Cape Town, pp. 51-62.

Lutjeharms, J.R.E., Shillington, F.A. and Duncombe Rae, C.M., 1991. Observations of extreme upwelling filaments in the South East Atlantic Ocean. Science, 253: 774-776.

Lutjeharms, J.R.E. and Stockton, P.L., 1987. Kinematics of the upwelling front off southern Africa, The Benguela and Comparable Ecosystems. South African Journal of Marine Science. Sea Fisheries Research Institute, Republic of South Africa Department of Environmental Affairs, Cape Town, pp. 35-49.

Lutjeharms, J.R.E. and Valentine, H.R., 1988. Evidence for persistent Agulhas rings southwest of Cape Town. South African Journal of Science, 84: 781-783.

Lutjeharms, J.R.E. and van Ballegooyen, R.C., 1984. Topographic control in the Agulhas Current system. Deep Sea Research, 31(11): 1321-1337.

Lutjeharms, J.R.E. and van Ballegooyen, R.C., 1988. The retroflection of the Agulhas Current. Journal of Physical Oceanography, 18(11): 1570-1583.

Lutjeharms, J.R.E., Walters, N.M. and Allanson, B.R., 1985. Oceanic frontal systems and biological enhancement. In: W.R. Siegfried, P.R. Condy and R.M. Laws (Editors), Antarctic nutrient cycles and food webs. Springer-Verlag, Berlin, pp. 11-21.

Macdonald, A.M. and Wunsch, C., 1996. An estimate of global ocean circulation and heat fluxes. Nature, 382: 436-439.

Macrae, F.B., 1926. The Stone Age in northern Rhodesia. N.A.D.A., 1: 67-68.

Marchant, M., Hebbeln, D. and Wefer, G., 1998. Seasonal flux patterns of planktic foraminifera in the Peru-Chile Current. Deep Sea Research I, 45: 1161-1185.

Martinson, D.G., Pisias, N.G., Hays, J.D., Imbrie, J., Moore, T.D. and Shackleton, N.J., 1987. Age dating and the orbital theory of the ice ages: development of a high-resolution 0 to 300,000- year chronostratigraphy. Quaternary Research, 27: 1-29.

Mason, S.J. and Jury, M.R., 1997. Climatic variability and change over South Africa: a reflection on underlying processes. Progress in Physical Geography, 21(1): 23-50.

McIntyre, A. and Molfino, B., 1996. Forcing of Atlantic equatorial and subpolar millennial cycles by precession. Science, 274: 1867-1870.

McIntyre, A., Ruddiman, W.F., Karlin, K. and Mix, A.C., 1989. Surface water response of the Equatorial Atlantic Ocean to orbital forcing. Paleoceanography, 4(1): 19-55.

McManus, J., Oppo, D. and Cullen, J., 1999a. Duration and stability of optimum climate conditions during marine isotope stage 11, a prominent late Pleistocene interglacial. EOS (Transactions, American Geophysical Union), 80: F10.

McManus, J.F., Oppo, D.W. and Cullen, J.L., 1999b. Marine isotope stage 11 (MIS 11) as analog for the current Holocene interglacial. EOS Transactions AGU, Fall Meeting Supplement, Abstract OS41C-01.

Milankovitch, M., 1930. Mathematische Klimalehre und Astronomische Theorie der Klimaschwankungen. Gebruder Borntraeger, 176 pp.

Mitchell-Innes, B.A. and Winter, A., 1987. Coccolithophores: A major phytoplankton component in mature upwelled waters off the Cape Peninsula, in March 1983. Marine Biology, 95: 25-30.

Mix, A.C., Le, J. and Shackleton, N.J., 1995. Benthic foraminiferal stable isotope stratigraphy of Site 846: 0-1.8 Ma. In: N.G. Pisias, L.A. Mayer, T.R. Janacek, T.R. Palmer-Julson and T.H. van Andel (Editors), Proceedings of the Ocean Drilling Program Scientific Results: Volume 138. Ocean Drilling Program, College Station, Texas, pp. 839-854.

Mix, A.C. and Morey, A.E., 1996. Climate feedback and Pleistocene variations in the Atlantic South Equatorial Current. In: G. Wefer, W.H. Berger, G. Siedler and D.J. Webb (Editors), The South Atlantic : Present and Past Circulation. Springer-Verlag, Berlin Heidelberg, pp. 503-525.

Mix, A.C., Morey, A.E., Pisias, N.G. and Hostetler, S.W., 1999. Foraminiferal faunal estimates of paleotemperature: Circumventing the no-analog problem yields cool ice age tropics. Paleoceanography, 14(3): 350-359.

Mix, A.C. and Ruddiman, W.F., 1985. Structure and timing of the last deglaciation: oxygen isotope evidence. Quaternary Science Reviews, 4: 59-108.

Mix, A.C., Ruddiman, W.F. and McIntyre, A., 1986a. Late Quaternary paleoceanography of the tropical Atlantic, 1: Spatial variability of annual mean sea surface temperatures, 0-20,000 B. P. Paleoceanography, 1(1): 43-66.

Mix, A.C., Ruddiman, W.F. and McIntyre, A., 1986b. Late Quaternary paleoceanography of the tropical Atlantic, 2: The seasonal cycle of sea surface temperatures, 0-20,000 B. P. Paleoceanography, 1(3): 339-353.

Mooers, C.N.K., Collins, C.A. and Smith, R.L., 1976. The dynamic structure of the frontal zone in the coastal upwelling region off Oregon. Journal of Physical Oceanography, 6: 3-21.

Morley, J., 1989. Variations in high latitude oceanographic fronts in the southern Indian Ocean: an estimation based on faunal changes. Paleoceanography, 4(5): 547-554.

Morley, J.J. and Hays, J.D., 1979. Comparison of glacial and interglacial oceanographic conditions in the South Atlantic from variations in calcium carbonate and radiolarian distributions. Quaternary Research, 12: 396-408.

Mudelsee, M., 2001. The phase relations among atmospheric CO_2 content, temperature, and global ice volume over the past 420 ka. Quaternary Science Reviews, 20: 583-589.

Mulitza, S. and Rühlemann, C., 2000. African monsoonal precipitation modulated by interhemispheric temperature gradients. Quaternary Research, 53(2): 270-274.

Müller, P.J., Cepek, M., Ruhland, G. and Schneider, R.R., 1997. Alkenone and coccolithophorid species changes in late Quaternary sediments from the Walvis Ridge: implications for the alkenone paleotemperature method. Palaeogeography, Palaeoclimatology, Palaeoecology, 135: 71-96.

Müller, P.J., Kirst, G., Ruhland, G., von Storch, I. and Rosell-Melé, A., 1998. Calibration of alkenone paleotemperature index $U^{k'}_{37}$ based on core tops from the eastern South Atlantic and the global ocean (60°N-60°S). Geochim. Cosmochim. Acta, 62: 1757-1772.

Murray, J., 1897. On the distribution of the pelagic foraminifera at the surface and on the floor of the ocean. Natural Science (Ecology), 11: 17-27.

Murray, J., 1995. Microfossil indicators of ocean water masses, circulation, and climate. In: D.W.J. Bosence and P.A. Allison (Editors), Marine palaeoenvironmental analysis from fossils. Geological Society Special Publication, pp. 245-264.

Nelson, G. and Hutchings, L., 1983. The Benguela Upwelling area. Progress in Oceanography, 1: 333-356.

Newell, R.E., Gould-Stewart, S. and Chung, J.C., 1981. A possible interpretation of paleoclimatic reconstruction for 18,000 B.P. for the region 60°N to 60°S, 60°W to 100°E. Palaeoecology of Africa: 13-19.

Niebler, H.S., 1995. Rekonstrukionen von Paläo-Umweltparametern anhand van stabilen Isotopen und Faunen-Vergesellschaftungen planktisher Foraminiferen im Südatlantik. Reports of Polar Research, 167. AWI, Bremerhaven, 198 pp.

Niebler, H.-S., Arz, H., Donner, B., Mulitza, S., Pätzold, J. and Wefer, G., submitted. 18-ka time slice reconstruction of the sea surface water temperature distribution in the South Atlantic Ocean-evidence from planktonic foraminifera. Paleoceanography.

Niebler, H.-S. and Gersonde, R., 1998. A planktic foraminiferal transfer function for the southern South Atlantic Ocean. Marine Micropaleontology, 34: 213-234.

Oberhänsli, H., 1991. Upwelling signals at the northeastern Walvis Ridge during the past 500,000 years. Paleoceanography, 6(1): 53-71.

Oberhänsli, H., Bérnier, C., Meinecke, G., Schmidt, H., Schneider, R. and Wefer, G., 1992. Planktonic foraminfers as tracers of ocean currents in the eastern South Atlantic. Paleoceanography, 7: 607-632.

Olson, D.B. and Evans, R.H., 1986. Rings of the Agulhas Current. Deep Sea Research, 33(1): 27-42.

Olson, D.B., Fine, R.A. and Gordon, A.L., 1992. Convective modifications of water masses in the Agulhas. Deep Sea Research, 39: S163-S181.

Oppo, D.W., McManus, J.F. and Cullen, J.L., 1998. Abrupt climate events 500,000 to 340,000 years ago: Evidence from Subpolar North Atlantic sediments. Science, 279: 1335-1338.

Ortiz, J.A., Mix, A.C. and Collier, R.W., 1995. Environmental control of living symbiotic and asymbiotic foraminifera of the California Current. Paleoceanography, 10(6): 987-1009.

Ottens, J.J., 1991. Planktic foraminifera as North Atlantic water mass indicators. Oceanologica Acta, 14(2): 123-140.

Ottens, J.J. and Nederbragt, A.J., 1992. Planktic foraminiferal diversity as indicator of ocean environments. Marine Micropaleontology, 19: 13-28.

Parker, W.K. and Jones, T.R., 1865. On some foraminifera from the North Atlantic and Arctic Oceans, including Davis Straits and Baffin Bay. Royal Society of London Philosophical Transactions, 155: 325-441.

Partridge, T.C., 1993. Warming phases in Southern Africa during the last 150,000 years: an overview. Palaeogeography, Palaeoclimatology and Palaeoecology, 101: 237-244.

Partridge, T.C., Avery, D.M., Botha, G.A., Brink, J.S., Deacon, J., Herbert, R.S., Maud, R.R., Scott, L., Talma, A.S. and Vogel, J.C., 1990. Late Pleistocene and Holocene climatic changes in southern Africa. South African Journal of Science, 86: 302-306.

Partridge, T.C., DeMendocal, P.B., Lorentz, S.A., Paiker, M.J. and Vogel, J.C., 1997. Orbital forcing of climate over South Africa: A 200,000-year rainfall record from the Pretoria Saltpan. Quaternary Science Reviews, 16: 1125-1132.

Partridge, T.C., Kerr, S.L., Metcalfe, S.E., Scott, L., Talma, A.S. and Vogel, J.C., 1993. The Pretoria Saltpan: a 200,000 year southern African lacustrine sequence. Palaeogeography, Palaeoclimatology and Palaeoecology, 101: 317-337.

Peterson, R.G. and Stramma, L., 1991. Upper-level circulation in the South Atlantic Ocean. Progress in Oceanography, 26: 1-73.

Pether, J., 1993. Relict Shells of Subantarctic mollusca from the Orange Shelf, Benguela region, off southwestern Africa. The Veliger, 36(3): 276-284.

Pether, J., 1994. Molluscan evidence for enhanced deglacial advection of Agulhas water in the Benguela Current, off southwestern Africa. Palaeogeography, Palaeoclimatology, Palaeoecology, 111: 99-117.

Petit, J.R., Jouzel, J., Raynaud, D., Barkov, N.I., Barnola, J.-M., Basile, I., Bender, M., Chappellaz, J., Davis, M., Delaygue, G., Delmotte, M., Kotlyakov, V.M., Legrand, M., Lipenkov, V.Y., Lorius, C., Pépin, L., Ritz, C., Saltzmann, E. and Stievenard, M., 1999. Climate and atmospheric history of the past 420,000 years from the Vostok ice core, Antarctica. Nature, 399: 429-436.

Pflaumann, U., Duprat, J., Pujol, C. and Labeyerie, L.D., 1996. SIMMAX: A modern analog technique to deduce Atlantic sea surface temperatures from planktonic foraminifera in deep-sea sediments. Paleoceanography, 11(1): 15-35.

Pichon, J.-J., Sikes, E.L., Hiramatsu, C. and Robertson, L., 1998. Comparison of $U^{k'}_{37}$ and diatom assemblage sea surface temperature estimates with atlas derived data in Holocene sediments from the southern west Indian Ocean. Journal of Marine Systems, 17: 541-554.

Pisias, N.G., Mayer, L.A. and Mix, A.C., 1995. Palaeoceanography of the Eastern Equatorial Pacific during the Neogene: Synthesis of Leg 138 Drilling Results. In: N.G. Pisias, L.A. Mayer, T.R. Janacek, T.R. Palmer-Julson and T.H. van Andel (Editors), Proceedings of the Ocean Drilling Program Scientific Results: Volume 138. Ocean Drilling Program, College Station, Texas, pp. 5-21.

Pisias, N.G. and Mix, A.C., 1997. Spatial and temporal variability of the eastern equatorial Pacific during the late Pleistocene: Evidence from Radiolaria microfossils. Paleoceanography, 12: 381-393.

Poli, M.S., Thunnall, R.C. and Dio, D., 2000. Millennial-scale changes in North Atlantic Deep Water circulation during marine isotope stages 11 and 12: Linkage to Antarctic climate. Geology, 28(9): 807-810.

Poore, R.Z. and Dowsett, H.J., 2001. Pleistocene reduction of polar ice caps: Evidence from Cariaco Basin sediments. Geology, 29(1): 71-74.

Poore, R.Z., Schroeder, J. and McMahon, A., 2000. Planktic foraminifer census data and $\delta^{18}O$ and $\delta^{13}C$ analyses of *Globigerinoides ruber* from marine isotope stage 11 (MIS 11) marine sediments in Ocean Drilling Program (ODP) Site 1002. U.S. Geological Survey Open File Report, 00-035:1-10.

Prahl, F.G., Collier, R.B., Dymond, J., Lyle, M. and Sparrow, M.A., 1993. A biomarker perspective on prymnesiophyte productivity in the northeast Pacific Ocean. Deep Sea Research, 40: 2061-2076.

Prahl, F.G., Muelhausen, L.A. and Zahnle, D.L., 1988. Further evaluation of long-chain alkenones as indicators of paleoceanographic conditions. Geochim. Cosmochim. Acta, 52: 2303-2310.

Prahl, F.G., Pisias, N., Sparrow, M.A. and Sabin, A., 1995. Assessment of sea surface temperature at 42°N in the California Current over the last 30,000 years. Paleoceanography, 10(4): 763-773.

Prahl, F.G. and Wakeman, S.G., 1987. Calibration of unsaturation patterns in long chain ketone compositions for paleotemperature assessment. Nature, 330: 367-369.

Prell, W.L., 1985. The stability of low latitude sea surface temperatures: an evaluation of the CLIMAP reconstructions with emphasis on the positive SST anomalies. US Dept. of Energy, Washington D.C., 1-60 pp.

Prell, W.L. and Curry, W.B., 1981. Faunal and isotopic indices of monsoonal upwelling. Oceanol Acta, 4: 333-351.

Prell, W.L., Hutson, W.H. and Williams, D.F., 1979. The Subtropical Convergence and late Quaternary circulation in the Southern Ocean. Marine Micropalaeontology, 4: 225-234.

Prell, W.L., Hutson, W.H., Williams, D.F., Bé, A.W.H., Geitzenauer, K. and Molfino, B., 1980. Surface circulation of the Indian Ocean during the Last Glacial Maximum, approximately 18,000yr B.P. Quaternary Research, 14: 309-336.

Prell, W.L., Imbrie, J., Martinson, D.G., Morley, J.J., Pisias, N.G., Shackleton, N.J. and Streeter, H.F., 1986. Graphic correlations of oxygen isotope stratigraphy application to the Late Quaternary. Paleoceanography, 1(2): 137-162.

Radke, M., Sittart, H.G. and Welte, D.H., 1978. Removal of soluble organic matter from rock samples with a flow through extraction cell. Anal. Chem., 50: 663-665.

Ramstein, G., Fluteau, F. and Joussaume, S., 1997. Effect of orogeny, plate motion, and land-sea distribution on Eurasian climate change over the past 30 million years. Nature, 386: 788-795.

Ravelo, A.C. and Fairbanks, R.G., 1992. Oxygen isotopic composition of multiple species of planktonic foraminifera; records of the modern photic zone temperature gradient. Paleoceanography, 7(6): 815-831.

Ravelo, A.C., Fairbanks, R.G. and Philander, S.G.M., 1990. Reconstructing tropical Atlantic hydrography using planktonic foraminifera and an ocean model. Paleoceanography, 5: 409-431.

Raymo, M.E., Ruddiman, W.F., Shackleton, N.J. and Oppo, D.W., 1990. Evolution of Atlantic-Pacific $\delta^{13}C$ gradients over the past 2.5 m.y. Earth Planetary Science Letters, 97: 353-368.

Reid, J.R., 1989. On the total geostrophic circulation of the South Atlantic ocean: flow patterns, tracers and transports. Progress in Oceanography, 23: 149-244.

Reid, J.R., 1996. On the circulation of the South Atlantic Ocean. In: G. Wefer, W.H. Berger, G. Siedler and D.J. Webb (Editors), The South Atlantic: Present and Past Circulation. Springer-Verlag, Berlin Heidelberg, pp. 13-44.

Reille, M., de Beaulieu, J.-L., Svobodova, H., V., A.-P. and Goeury, C., 2000. Pollen analytical biostratigraphy of the last five climatic cycles from a long contineltal sequence from the Velay region (Massif Central, France). Journal of Quaternary Science, 15: 665-685.

Rennell, J., 1778. A chart of the bank of Lagullas and the southern coast of Africa, London.

Reynolds, L.A. and Thunnell, R.C., 1985. Seasonal succession of planktonic foraminifera in the subpolar North Pacific. Journal of Foraminiferal Research, 15: 282-301.

Rignot, E.J., 1998. Fast recession of a West Antarctic glacier. Science, 281: 549-551.

Rind, D. and Peteet, D., 1985. Terrestrial conditions at the last glacial maximum and CLIMAP sea surface estimates: Are they consistent? Quaternary Research, 24: 1-22.

Rintoul, S.R., 1991. South Atlantic interbasin exchange. Journal of Geophysical Research, 96(C2): 2675-2692.

Rohling, E.J., Fenton, M., Jorissen, F.J., Bertrand, P., Ganssen, G. and Caulet, J.P., 1998. Magnitudes of sea-level lowstands of the past 500,000 years. Nature, 394: 162-165.

Rosell-Melé, A., Carter, J.F., Parry, A.T. and Eglinton, G., 1995a. Determination of the $U^{k'}_{37}$ index in geological samples. Anal. Chem., 67: 1283-1289.

Rosell-Melé, A., Eglintion, G., Pflaumann, U. and Sarnthein, M., 1995b. Atlantic core top calibration of the $U^{k'}_{37}$ index as a sea surface paleotemperature indicator. Geochim. Cosmochim. Acta, 59: 3099-3107.

Rostek, F., Bard, E., Beaufort, L., Sonzogni, C. and Ganssen, G., 1997. Sea surface temperature and productivity records for the past 240 kyr in the Arabian Sea. Deep Sea Research II, 44(6-7): 1461-1480.

Rostek, F., Ruhland, G., Bassino, F.C., Müller, P.J., Labeyrie, L.D., Lancelot, Y. and Bard, E., 1993. Reconstructing sea surface temperature and salinity using $\delta^{18}O$ and alkenone records. Nature, 364: 319-321.

Ruddiman, W.F. and McIntyre, A., 1976. Northeast Atlantic paleoclimatic changes over the past 600,000 years. , 145: 111-146.

Ruddiman, W.F., Raymo, M.E., Martinson, G.G., Clement, B.M. and Brackman, J., 1989. Pleistocene evolution: Northern hemisphere ice sheets and North Atlantic Ocean. Paleoceanography, 4: 353-412.

Salinger, M.J., 1984. New Zealand climate: the last 5 million years. In: J.C. Vogel (Editor), Late Cainozoic Palaeoclimates of the Southern Hemisphere. Balkema, Rotterdam.

Sarnthein, M., Winn, K., Duplessy, J.-C. and Fontugne, M.R., 1988. Global variations of surface ocean productivity in low and mid latitudes: influence on CO_2 reservoirs of the deep ocean and atmosphere during the last 21,000 years. Paleoceanography, 3(3): 361-399.

Sautter, L.R. and Thunnell, R.C., 1991. Seasonal variability in the $\delta^{18}O$ and $\delta^{13}C$ of planktonic foraminifera from an upwelling environment: Sediment trap results from the San Pedro Basin, Southern California Bight. Paleoceanography, 6(3): 301-334.

Scherer, R.P., Aldahan, A., Tulaczyk, S., Possnert, G., Engelhardt, H. and Kamb, B., 1998. Pleistocene collapse of the West Antarctic ice sheet. Science, 281: 82-85.

Schmidt, H., 1992. Der Benguela Strom im Bereich des Walfisch Rückens im Spätquartär., Universität Bremen, Bremen.

Schmitz, W.J., 1995. On the interbasin-scale thermohaline circulation. Review of Geophysics, 33: 151-173.

Schneider, R.R., Müller, P.J. and Acheson, R., 1999. Atlantic alkenone sea surface temperature records: low versus mid-latitudes and differences between hemispheres. In: F. Abrantes and A. Mix (Editors), 6th International Conference on Paleoceanography. Plenum Press, Lisbon, August 1998.

Schneider, R.R., Müller, P.J. and Ruhland, G., 1995. Late Quaternary surface circulation in the east equatorial South Atlantic: Evidence from alkenone sea surface temperatures. Paleoceanography, 10(2): 197-219.

Schneider, R.R., Müller, P.J., Ruhland, G., Meinecke, G., Schmidt, H. and Wefer, G., 1996. Late Quaternary surface temperatures and productivity in the East-Equatorial South Atlantic: response to changes in trade/monsoon wind forcing and surface water advection. In: G. Wefer, W.H. Berger, G. Siedler and D.J. Webb (Editors), The South Atlantic: Present and Past Circulation. Springer-Verlag, Berlin Heidelberg, pp. 527-551.

Schneider, R.R., Müller, P.J. and Wefer, G., 1994. Late Quaternary paleoproductivity changes off the Congo deduced from stable isotopes of planktonic foraminifera. Palaeogeography, Palaeoclimatology, Palaeoecology, 110: 255-274.

Schott, W., 1935. Die Foraminiferen aus dem aequatorialen Teil des Atlantischen Ozeans. Deutsch Atl. Exped. Meteor 1925-1927, 3: 34-134.

Schultz, H., von Rad, U. and Erlenkeuser, H., 1998. Correlation between Arabian Sea and Greenland climate oscillations of the past 110,000 years. Nature, 393: 54-57.

Scott, L., 1989. Climatic conditions in southern Africa since the Last Glacial Maximum, inferred from pollen analysis. Palaeogeography, Palaeoclimatology, Palaeoecology, 70: 345-353.

Servant, J., 2001. The 100 kyr cycle of deglaciation during the last 450 kyr: a new interpretation of oceanic and ice core data. Global and Planetary Change, 29: 121-133.

Shackleton, N.J., 1987. Oxygen isotopes, ice volume, and sea level. Quaternary Science Reviews, 6: 183-190.

Shackleton, N.J., 2000. The 100,000 year Ice-Age cycle identified and found to lag temperature, carbon dioxide, and orbital eccentricity. Science, 289: 1897-1902.

Shackleton, N.J., Berger, A. and Peltier, W.R., 1990. An alternative astronomical calibration of the lower Pleistocene time scale based on ODP Site 677. Transactions of the Royal Society of Edinburgh: Earth Sciences, 81: 251-261.

Shackleton, N.J., Hall, M.A. and Pate, D., 1995. Stable Pliocene isotope stratigraphy of Site 846. In: N.G. Pisias, L.A. Mayer, T.R. Janacek, T.R. Palmer-Julson and T.H. van Andel (Editors), Proceedings of the Ocean Drilling Program: Scientific Results Volume 138. Ocean Drilling Program, College Station, Texas, pp. 337-355.

Shackleton, N.J. and Kennett, J.P., 1975. Late Cenozoic oxygen and carbon isotope changes at DSDP Site 284: implications for glacial history of the Northern Hemisphere and Antarctica. In: J.P. Kennett, C.C. von der Borch and S.S. Party (Editors), Initial Reports of the DSDP, Leg 29, Lyttleton, NZ to Wellington, NZ, March - April 1973, pp. 743-755.

Shackleton, N.J. and Opdyke, N.D., 1973. Oxygen-isotope and paleomagnetic stratigraphy of equatorial Pacific core V28-238: oxygen isotope temperatures and ice volumes on a 10^5 year and 10^6 year scale. Quaternary Research, 3: 39-55.

Shannon, C.E., 1949. The mathematical theory of environments. In: C.E. Shannon and W. Weaver (Editors), The mathematical theory of communication. University of Illinois Press, Urbana, pp. 1 - 93.

Shannon, L.V., 1985. The Benguela Ecosystem: Part I. Evolution of the Benguela physical features and processes. Oceanographic Marine Biological Annual Review, 23: 105-182.

Shannon, L.V., Agenbag, J.J., Walker, N.D. and Lutjeharms, J.R.E., 1990a. A major perturbation in the Agulhas Retroflection area in 1986. Deep Sea Research, 37(3): 493-512.

Shannon, L.V., Lutjeharms, J.R.E. and Agenbag, J.J., 1989. Episodic input of Subantarctic water into the Benguela region. South African Journal of Science, 85: 317-322.

Shannon, L.V., Lutjeharms, J.R.E. and Nelson, G., 1990b. Causative mechanisms for intra-annual and interannual variability in the marine environment around Southern Africa. South African Journal of Science, 86: 356-373.

Shannon, L.V., Mostert, S.A., Walters, N.M. and Anderson, F.P., 1983. Chlorophyll concentrations in the southern Benguela Current region as determined by satellite. (*Nimbus-7* coastal zone scanner). Journal of Plankton Research, 5(4): 565-583.

Shannon, L.V. and Nelson, G., 1996. The Benguela: large scale features and processes and system variability. In: G. Wefer, W.H. Berger, G. Siedler and D.J. Webb (Editors), The South Atlantic: Present and Past Circulation. Springer-Verlag, Berlin Heidelberg, pp. 163-210.

Shannon, L.V. and Pillar, S.C., 1986. The Benguela Ecosystem Part III. Plankton. Oceanographic Marine Biological Annual Review, 24: 65-170.

Shannon, L.V., Walters, N.M. and Mostert, S.A., 1985. Satellite observations of surface temperature and near-surface chlorophyll in the southern Benguela region. In: L.V. Shannon (Editor), Southern African Ocean Colour and Upwelling Experiment. Sea Fisheries Research Institute, Cape Town, pp. 183-210.

Shi, N., Dupont, L.M., Beug, H.-J. and Schneider, R., 2000. Correlation between vegetation in southwestern Africa and oceanic upwelling in the past 21,000 years. Quaternary Research, 54: 72-80.

Shi, N., Schneider, R., Beug, H.-J. and Dupont, L.M., 2001. Southeast trade wind variations during the last 135 kyr: evidence from pollen spectra in eastern South Atlantic sediments. Earth and Planetary Science Letters, 187: 311-321.

Sikes, E.L., Farrington, J.W. and Keigwin, L.D., 1991. Use of alkenone unsaturation ratio $U^{k'}_{37}$ to determine past sea surface temperatures: core top SST calibrations and methodology considerations. Earth Planetary Science Letters, 104: 36-47.

Sikes, E.L. and Keigwin, L.D., 1994. Equatorial Atlantic sea surface temperature for the last 30 kyr : A comparison of $U^{k'}_{37}$, $\delta^{18}O$, and foraminiferal assemblage temperature estimates. Paleoceanography, 9(1): 31-45.

Sikes, E.L. and Keigwin, L.D., 1996. A re-examination of northeast Atlantic sea surface temperature and salinity over the past 16 kyr. Paleoceanography, 11: 327-342.

Sowers, T. and Bender, M., 1995. Climate records covering the Last Deglaciation. Science, 269: 210-214.

Spero, H.J., Bijma, J., Lea, D.W. and Bemis, B.E., 1997. Effect of seawater carbonate concentration on foraminiferal carbon and oxygen isotopes. Nature, 390: 497-500.

Stokes, S., Haynes, G., Thomas, D.S.G., Horrocks, J.L., Higginson, M. and Malifa, M., 1998. Punctuated aridity in southern Africa during the last glacial cycle: The chronology of linear dune construction in the northeastern Kalahari. Palaeogeography, Palaeoclimatology, Palaeoecology, 137: 305-322.

Stokes, S., Thomas, D.S.G. and Washington, R., 1997. Multiple episodes of aridity in southern Africa since the last interglacial period. Nature, 388: 154-158.

Stramma, L. and Peterson, R.G., 1989. Geostrophic transport in the Benguela Current Region. Journal of Physical Oceanography, 19: 1440-1448.

Stutzer, S. and Krauss, W., 1998. Mean circulation and transports in the South Atlantic Ocean: combining model and drifter data. Journal of Geophysical Research, 103(C13): 30,985-31,002.

Summerhayes, C.P., Kroon, D., Rosell-Melé, A., Jordan, R.W., Schrader, H.-J., Hearn, R., Villaneuva, J., Grimalt, J.O. and Eglinton, G., 1995. Variability in the Benguela Current upwelling system over the past 70,000 years. Progress in Oceanography, 35: 207-251.

Sverdrup, H.U., Johnson, M.W. and Flemming, R.H., 1942. The Oceans. Prentice Hall, Englewood Cliffs, N. J., 1087 pp.

Talma, A.S. and Vogel, J.C., 1992. Late Quaternary palaeotemperatures derived from a speleothem from Cango Caves, Cape Province, South Africa. Quaternary Research, 37: 203-213.

Tankard, A.J. and Rogers, J., 1978. Late Cenozoic palaeoenvironments on the west coast of southern Africa. Journal of Biogeography, 5: 319-337.

Taunton-Clark, J., 1985. The formation, growth, and decay of upwelling tongues in response to mesoscale wind field during summer. In: L.V. Shannon (Editor), Southern African Ocean Colour and Upwelling Experiment. Sea Fisheries Research Institute, Cape Town, pp. 47-61.

Taunton-Clark, J., 1990. Environmental events within the south-east Atlantic (1906-1985) identified by analysis of sea surface temperature and wind data. South African Journal of Science, 86(7-10): 470-472.

Thiede, J., 1975. Distribution of foraminifera in surface waters of a coastal upwelling area. Nature, 253: 712-714.

Tolderlund, D.S. and Bé, A.W.H., 1971. Seasonal distribution of planktonic foraminifera in the western North Atlantic. Micropaleontology, 17: 297-329.

Tyson, P.D., 1986. Climate Change and Variability in Southern Africa. Oxford University Press, 220 pp.

Tzedakis, P.C., Andrieu, V., de Beaulieu, J.-L., Crowhurst, S., Folloeri, M., Hooghiemstra, H., Magri, D., Reille, M., Sadori, L., Shackleton, N.J. and Wijmstra, T.A., 1997. Comparison of terrestrial and marine records of changing climate of the last 500,000 years. Earth and Planetary Science Lettters, 150: 171-176.

Ufkes, E., Jansen, J.H.F. and Brummer, G.J.A., 1998. Living planktonic foraminifera in the eastern South Atlantic during spring: indicators of water masses, upwelling, and the Congo (Zaire) River plume. Marine Micropaleontology, 33: 27-53.

Ufkes, E., Jansen, J.H.F. and Schneider, R.R., 2000. Anomalous occurrences of *Neogloboquadrina pachyderma* (left) in a 420 k.y. upwelling record from Walvis Ridge (SE Atlantic). Marine Micropaleontology, 40(1-2): 23-42.

Ufkes, E. and Zachariasse, W.-J., 1993. Origin of coiling differences in living neogloboquadrinids in the Walvis Bay region, off Namibia, southwest Africa. Micropaleontology, 39(3): 283-287.

Urey, H.C., 1947. The thermodynamic properties of isotopic substances. Journal of the Chemical Society, 1974: 562-581.

Van Ballegooyen, R.C., L., G.M. and Lutjeharms, J.R.E., 1994. Eddy fluxes of heat and salt from the southwest Indian Ocean into the southeast Atlantic Ocean: a case study. Journal of Geophysical Research, 99: 14053 - 14070.

Van Foreest, D., Shillington, F.A. and Legeckis, R., 1984. Large scale, stationary, frontal features in the Benguela Current system. Continental Shelf Research, 3(4): 465-474.

van Leeuwen, R.J.W., 1989. Sea-floor distribution and Late Quaternary faunal patterns of planktonic and benthic foraminifers in the Angola Basin. Utrecht Micropaleontological Bulletins, 38: 288 pp.

Van Zinderen Bakker, E.M., 1976. The evolution of late Quaternary palaeoclimates of southern Africa. Palaeoceology of Africa, 9: 160-202.

Waelbroeck, C., Jouzel, J., Labeyrie, L., Lorius, C., Labracherie, M., Stiévenard, M. and Barkov, N.I., 1995. A comparison of the Vostok ice deuterium record and series from Southern Ocean core MD 88-770 over the last two glacial-interglacial cycles. Climate Dynamics, 12: 113-123.

Walker, N.D., 1990. Links between South African summer rainfall and temperature variability of the Agulhas and Benguela Current Systems. Journal of Geophysical Research, 95(C3): 3297 - 3319.

Watkins, J.M. and Mix, A.C., 1998. Testing the effects of tropical temperature, productivity, and mixed-layer depth on foraminiferal transfer functions. Paleoceanography, 13(1): 96-105.

Weaver, P.P.E., Carter, L. and Neil, H.L., 1998. Response of surface water masses and circulation to late Quaternary climate change east of New Zealand. Paleoceanography, 13(1): 70-83.

Weaver, P.P.E., Chapman, M.R., Eglinton, G., Zhao, M., Rutledge, D. and Read, G., 1999. Combined coccolith, foraminiferal, and biomarker reconstruction of paleoceanographic conditions over the last 120 kyr in the northern North Atlantic (59°N, 23°W). Paleoceanography, 14: 336-349.

Wefer, G., Berger, W.H., Bickert, T., Donner, B., Fischer, G., Kemle-von Mücke, S., Meinecke, G., Müller, P.J., Mulitza, S., Niebler, H.-S., Pätzold, J., Schimdt, H., Schneider, R.R. and Segl, M., 1996. Late Quaternary surface circulation in the South Atlantic: the stable isotope record and implications for heat transport and productivity. In: G. Wefer, W.H. Berger, G. Siedler and D.J. Webb (Editors), The South Atlantic: Present and Past Circulation. W, Berlin Heidelberg, pp. 461-502.

Wefer, G., Berger, W.H., Bijma, J. and Fischer, G., 1999. Clues to ocean history: a brief overview of proxies. In: G. Fischer and G. Wefer (Editors), Use of proxies in paleoceanography: examples from the South Atlantic. Springer-Verlag, Berlin Heidelberg, pp. 1-68.

Wefer, G. and Fischer, G., 1993. Seasonal patterns of vertical particle flux in equatorial and coastal upwelling areas of the eastern Atlantic. Deep Sea Research Part I, 40: 1613-1645.

Wiggs, G.F.S., Thomas, D.S.G., Bullard, J.F. and Livingstone, G., 1995. Dune mobility and vegetation cover in the southwest Kalahari desert. Earth Surface Processes and Landforms, 20: 515-530.

Wilkinson, L., 1989. The system of statistics. SYSTAT Inc, Evantson, Illinois, 822 pp.

Williams, D.F. and Johnson, W.C., 1975. Diversity of Recent planktonic foraminifera in the Southern Indian Ocean and late Pleistocene paleotemperatures. Quaternary Research, 5: 237-250.

Williams, M., Dunkerley, D., de Deckker, P., Kershaw, P. and Chappell, J., 1998. Quaternary Environments. Arnold, Sydney, 329 pp.

Williams, M.A.J., Dunkerley, D.L., Deckker, P.D., Kershaw, A.P. and Stokes, T., 1993. Quaternary Environments. Edward Arnold, London, 434 pp.

Wolff, T., Mulitza, S., Rühlemann, C. and Wefer, G., 1999. Response of the tropical Atlantic thermocline to late Quaternary trade wind changes. Paleoceanography, 14(3): 374-383.

Wu, G., Herguera, J.C. and Berger, W.H., 1990. Differential dissolution: Modification of late Pleistocene oxygen isotope records in the western Equatorial Pacific. Paleoceanography, 5: 581-594.

Yasuda, M., Berger, W.H., Wu, G., Burke, S. and Schmidt, H., 1993. Foraminiferal preservation record for the last million years: Site 805, Ontong Java Plateau. Proceeding of ODP, Scientific Results, 130: 491-508.

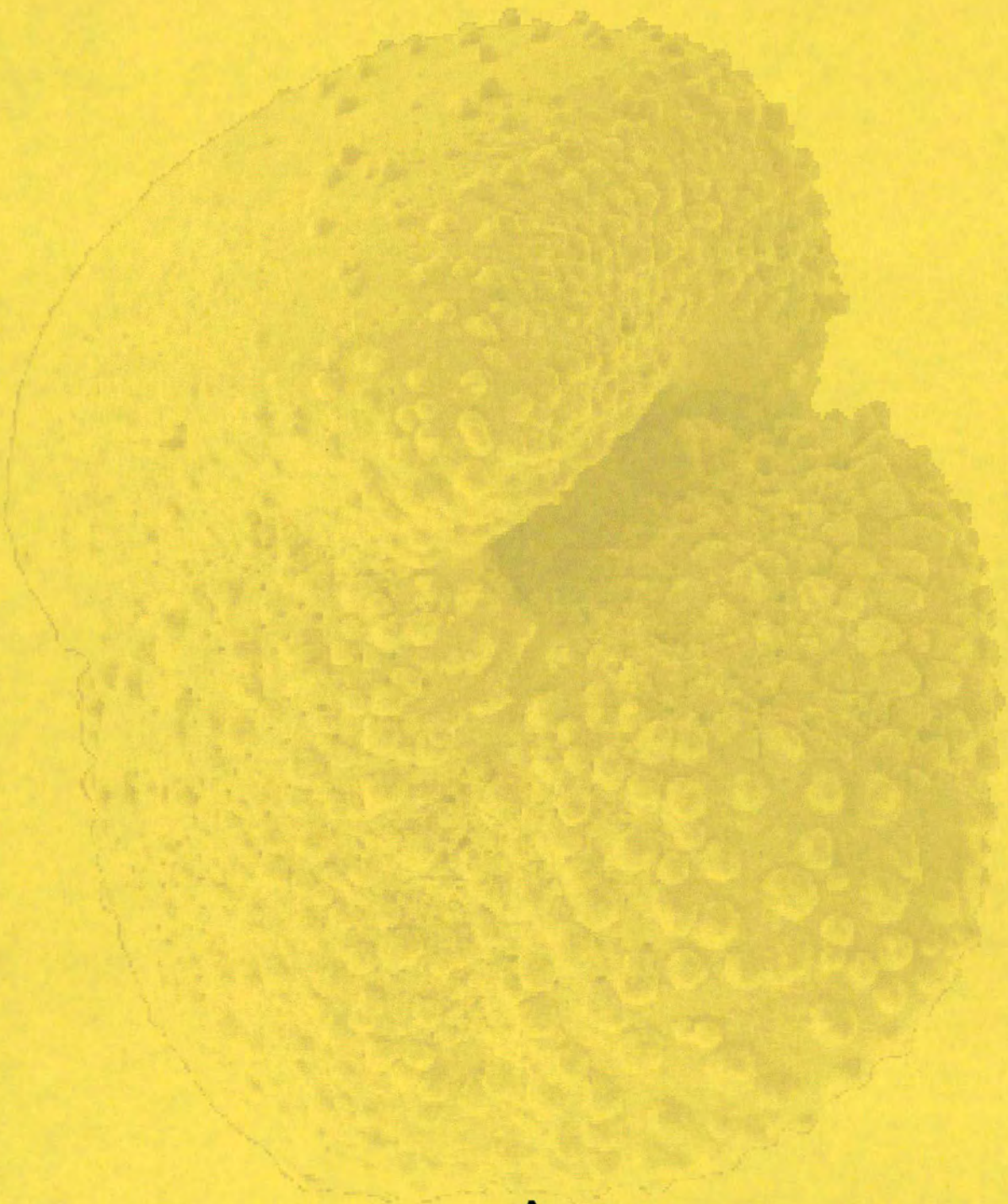

Appendix

APPENDIX 1.1

Planktonic foraminifera classification, follows Bé (1967; 1977), Hemleben *et al.* (1989), and Kennett and Srinivasan (1983).

Candeina nitida d'Orbigny, 1839
Globigerina bulloides d'Orbigny, 1826
Globigerina calida (Parker), 1962
Globigerina digitata (Brady), 1879
Globigerina falconensis Blow, 1959
Globigerina rubenscens (Hofker), 1956
Globigerinella siphonifera (d'Orbigny), 1839 [*Globigerinella aequilateralis* (Brady), 1839]
Globigerinita glutinata (Egger), 1895
Globigerinita uvula (Ehrenberg), 1861 [= *Globigerinita bradyi* (Weisner), 1931]
Globigerinoides conglobatus (Brady), 1879
Globigerinoides ruber (d'Orbigny), 1839
Globigerinoides sacculifer (Brady), 1877 [=*Globigerinoides trilobus* (Reuss) form]
Globigerinoides tenellus (Parker), 1958
Globorotalia cavernula (Bé), 1967
Globorotalia crassaformis ssp. (Galloway and Wissler), 1927
Globorotalia hirsuta (d'Orbigny), 1839
Globorotalia inflata (d'Orbigny), 1839
Globorotalia menardii (Parker, Jones, and Brady), 1865
Globorotalia scitula (Brady), 1882
Globorotalia theyeri (Fleisher), 1974
Globorotalia truncatuliniodes (d'Orbigny), 1839
Globorotalia tumida (Brady), 1882
Globorotaloides hexagonus (Natland), 1938
Neogloboquadrina dutertrei (d'Orbigny), 1839 [=*Globigerina eggeri* (Rhumbler)]
Neogloboquadrina pachyderma (Ehrenberg), 1861
Orbulina universa (d'Orbigny), 1839
Pulleniatina obliquiloculata (Parker and Jones), 1865
Sphaeroidinella dehiscens (Parker and Jones), 1865
Turborotalita quinqueloba (Natland), 1938

APPENDIX 2.1

Isotope data for spliced records from cores GeoB 3603-2 and MD96 2081. GeoB 3603-2 from 8 cm to 703 cm (grey), MD962081 from 983 cm to 2113 cm.

Depth (cmbsf)	Time (k.y.)	$\delta^{18}O$ cibicides	$\delta^{13}C$ cibicides
8	4.00	2.82	0.55
13	7.00	2.92	0.36
18	10.00	2.76	0.61
23	13.00	4.04	0.05
28	16.00	4.37	0.00
33	19.00	4.43	0.10
38	20.50	4.31	0.17
43	22.00	4.21	-0.10
48	23.50	4.28	-0.12
53	25.00	4.25	-0.02
58	26.50	4.20	0.01
63	28.00	4.24	0.04
68	29.39	4.17	-0.28
73	30.78	4.12	-0.12
78	32.17	4.06	-0.09
83	33.56	3.99	-0.04
88	34.94	3.92	0.04
93	36.33	3.95	0.09
98	37.72	4.02	0.07
103	39.11	3.91	0.24
108	40.50	3.94	0.14
113	41.89	3.85	0.18
118	43.28	3.79	0.31
123	44.67	3.90	0.40
128	46.06	3.96	0.27
133	47.44	3.90	0.58
138	48.83	3.86	0.22
143	50.22	3.84	0.31
148	51.61	3.74	0.15
153	53.00	3.92	-0.09
158	54.50	3.75	0.06
163	56.00	3.70	-0.07
168	57.50	3.90	-0.05
173	59.00	4.02	-0.23
178	60.50	4.05	0.05
183	62.00	4.11	-0.07
188	63.50	4.11	-0.32
193	65.00	4.05	0.02
198	66.36	3.86	0.28
203	67.73	3.84	0.24
208	69.09	3.74	0.11
213	70.45	3.89	0.14
223	73.18	3.41	0.17
228	74.55	3.47	0.31
233	75.91	3.45	0.37
238	77.27	3.39	0.43
243	78.64	3.29	0.63
248	80.00	3.17	0.67
253	81.75	3.16	0.58
258	83.50	3.47	0.30
263	85.25	3.56	0.46
268	87.00	3.74	0.54
273	88.71	3.61	0.63
278	90.43	3.49	0.45
283	92.14	3.42	0.46
293	95.57	3.43	0.33
298	97.29	3.26	0.53
303	99.00	3.30	0.46
308	100.60	3.37	0.16
313	102.20	3.36	0.43
318	103.80	3.47	0.27
323	105.40	3.41	0.21
328	107.00	3.36	0.11
333	108.67	3.61	0.39
338	110.33	3.51	0.61
343	112.00	3.14	0.40
348	113.67	3.14	0.59
353	115.33	2.67	0.51
358	117.00	2.62	0.60
363	118.67	2.56	0.64
368	120.33	2.54	0.69
373	122.00	2.60	0.59
378	123.63	2.56	0.52
383	125.25	2.66	0.51
388	126.88	3.04	0.26
393	128.50	3.88	0.01
398	130.13	3.98	0.01
403	131.75	3.86	0.00
408	133.38	4.32	-0.17
413	135.00	4.26	0.08
418	136.57	4.20	-0.03
423	138.14	4.01	0.26
428	139.71	3.94	0.15
433	141.29	4.24	0.03
438	142.86	4.36	-0.25
443	144.43	4.20	-0.28
448	146.00	4.13	-0.20
453	147.67	4.17	-0.36
458	149.33	4.18	-0.21
463	151.00	4.27	-0.30
468	152.67	4.28	-0.22
473	154.33	4.23	-0.38
478	156.00	4.01	-0.12
483	157.67	4.07	-0.26
488	159.33	4.06	-0.08
493	161.00	4.01	-0.30
498	162.67	3.95	-0.52
503	164.33	3.91	0.03
508	166.00	3.78	0.11
513	167.67	3.69	0.18
518	169.33	3.84	-0.17
523	171.00	3.93	-0.15
528	172.71	3.86	-0.43
533	174.43	3.79	-0.20
538	176.14	3.90	0.07
543	177.86	3.65	0.45
548	179.57	3.78	0.16
553	181.29	4.11	-0.30
558	183.00	3.89	-0.13
563	184.83	3.99	-0.11
568	186.67	3.62	-0.03
573	188.50	3.47	0.08
578	190.33	3.34	0.00
583	192.17	3.33	0.31
588	194.00	3.29	0.24
593	196.20	3.06	0.37
598	198.40	3.30	0.22
603	200.60	2.93	0.35
608	202.80	3.20	0.22
613	205.00	3.23	0.24
618	207.20	3.33	0.54
623	209.40	3.18	0.45
628	211.60	2.98	0.48
633	213.80	3.10	0.48
638	216.00	2.93	0.59
643	217.71	3.02	0.48
648	219.43	3.42	-0.11
653	221.14	3.67	-0.11
658	222.86	3.86	-0.28
663	224.57	4.04	0.06
668	226.29	4.12	0.09
673	228.00	4.07	-0.08
678	229.43	3.95	0.08
683	230.86	3.78	-0.19
688	232.29	3.63	-0.13
693	233.71	3.75	-0.06
698	235.14	3.35	0.39
703	236.57	3.29	0.22
983	**237.17**	**2.86**	**0.56**
988	**238.00**	**2.80**	**0.01**
993	**245.00**	**3.50**	**-0.13**
998	**246.33**	**3.77**	**-0.07**
1003	**247.67**	**3.66**	**0.04**
1008	**249.00**	**3.98**	**-0.07**
1013	**250.00**	**3.86**	**-0.02**
1018	**251.00**	**3.76**	**-0.21**
1023	**252.00**	**3.76**	**-0.03**
1028	**253.00**	**3.97**	**0.05**
1033	**254.00**	**3.82**	**-0.17**
1038	**255.00**	**3.80**	**-0.08**
1043	**256.00**	**3.72**	**-0.48**
1048	**257.00**	**3.71**	**-0.36**
1053	**259.40**	**3.88**	**-0.29**
1058	**261.80**	**3.85**	**-0.64**
1063	**264.20**	**3.88**	**-0.08**
1068	**266.60**	**3.97**	**-0.45**
1073	**269.00**	**3.86**	**-0.45**
1078	**270.50**	**3.92**	**-0.59**
1083	**272.00**	**3.93**	**-0.39**
1088	**273.50**	**3.80**	**-0.46**
1093	**275.00**	**3.58**	**-0.34**
1098	**276.50**	**3.68**	**-0.23**
1103	**278.00**	**3.73**	**0.03**
1108	**279.50**	**3.21**	**0.44**
1113	**281.00**	**3.75**	**-0.07**
1118	**282.50**	**3.10**	**0.07**
1123	**284.00**	**3.19**	**-0.15**
1128	**285.50**	**3.01**	**0.38**
1133	**287.00**	**3.02**	**0.20**
1138	**288.50**	**3.14**	**0.32**
1143	**290.00**	**3.12**	**0.21**
1148	**291.50**	**3.45**	**-0.06**
1153	**293.00**	**3.52**	**-0.14**
1158	**294.50**	**3.60**	**0.22**
1163	**296.00**	**3.36**	**-0.04**
1168	**297.50**	**3.49**	**0.37**
1173	**299.00**	**3.72**	**0.11**
1178	**299.85**	**3.64**	**0.10**
1183	**300.69**	**3.57**	**-0.15**
1188	**301.54**	**3.63**	**0.26**
1193	**302.38**	**3.47**	**0.59**
1198	**303.23**	**3.58**	**0.13**
1203	**304.08**	**3.57**	**0.48**
1208	**304.92**	**3.44**	**0.36**
1213	**305.77**	**3.47**	**0.39**
1218	**306.62**	**3.14**	**0.12**
1223	**307.46**	**3.53**	**0.25**
1228	**308.31**	**3.37**	**0.13**
1233	**309.15**	**3.21**	**0.25**
1238	**310.00**	**2.97**	**0.21**
1243	**311.67**	**3.02**	**0.08**
1248	**313.33**	**3.12**	**0.21**
1253	**315.00**	**2.99**	**0.03**
1258	**316.67**	**3.04**	**-0.03**
1263	**318.33**	**3.00**	**-0.08**
1268	**320.00**	**3.14**	**0.05**
1273	**321.38**	**2.95**	**0.12**
1278	**322.75**	**2.91**	**0.35**
1283	**324.13**	**2.64**	**0.08**
1288	**325.50**	**2.66**	**0.60**
1293	**326.88**	**2.67**	**0.10**
1298	**328.25**	**2.55**	**0.50**
1303	**329.63**	**2.66**	**0.36**
1308	**331.00**	**2.52**	**0.38**
1313	**331.77**	**2.64**	**-0.09**
1318	**332.54**	**2.96**	**-0.03**
1323	**333.31**	**3.51**	**-0.38**
1328	**334.08**	**2.62**	**0.27**
1333	**334.85**	**3.53**	**-0.16**
1338	**335.62**	**3.77**	**-0.57**
1343	**336.38**	**3.78**	**-0.27**
1348	**337.15**	**3.78**	**-0.40**
1353	**337.92**	**3.75**	**-0.19**
1358	**338.69**	**3.92**	**-0.22**
1363	**339.46**	**4.08**	**-0.29**
1368	**340.23**	**3.80**	**0.21**
1373	**341.00**	**4.15**	**-0.40**
1378	**341.82**	**3.88**	**-0.42**
1383	**342.64**	**3.84**	**-0.31**
1388	**343.45**	**3.89**	**-0.38**
1393	**344.27**	**3.94**	**-0.48**
1398	**345.09**	**3.82**	**-0.60**
1403	**345.91**	**3.93**	**-0.64**
1408	**346.73**	**3.79**	**-0.55**
1413	**347.55**	**3.83**	**-0.37**
1418	**348.36**	**3.86**	**-0.48**
1423	**349.18**	**3.82**	**-0.18**
1428	**350.00**	**3.71**	**-0.43**
1433	**350.82**	**3.71**	**-0.26**
1438	**351.64**	**3.71**	**-0.32**
1443	**352.29**	**3.63**	**-0.34**
1448	**353.27**	**3.61**	**-0.18**
1453	**354.09**	**3.50**	**-0.45**
1458	**354.91**	**3.70**	**-0.16**
1463	**355.73**	**3.52**	**0.28**
1468	**356.55**	**3.53**	**-0.47**
1473	**357.36**	**3.53**	**0.27**

Depth (cmbsf)	Time (k.y.)	$\delta^{18}O$ cibicides	$\delta^{13}C$ cibicides
1478	358.18	3.42	0.07
1483	359.00	3.50	0.23
1488	359.82	3.38	0.28
1493	360.64	3.60	-0.16
1498	361.45	3.39	-0.05
1503	362.27	3.49	0.06
1508	363.09	3.52	-0.04
1513	363.91	3.32	0.34
1518	364.73	3.29	0.18
1523	365.55	3.31	0.01
1528	366.36	3.09	0.22
1538	368.00	2.93	0.08
1543	371.50	3.20	-0.25
1548	375.00	3.35	0.42
1553	376.76	3.11	0.33
1558	378.53	3.17	0.46
1563	380.29	2.97	0.70
1568	382.06	2.83	0.89
1573	383.82	2.71	1.03
1583	387.35	2.66	0.88
1588	389.12	2.56	0.79
1593	390.88	2.52	0.99
1598	392.65	2.55	0.89
1603	394.41	2.57	0.68
1608	396.18	2.55	0.92
1613	397.94	2.48	0.86
1618	399.71	2.45	0.88
1623	401.47	2.57	0.73
1628	403.24	2.57	0.89
1633	405.00	2.44	0.79
1638	406.93	2.56	0.81
1643	408.87	2.54	0.82
1648	410.80	2.60	0.71
1653	412.73	2.70	0.64
1658	414.67	2.65	0.63
1663	416.60	2.77	0.69
1668	418.53	2.89	0.68
1673	420.47	2.96	0.68
1678	422.40	3.30	0.38
1683	424.33	3.38	0.44
1688	426.27	3.67	0.07
1693	428.20	3.67	-0.08
1698	430.13	4.09	-0.45
1703	432.07	3.82	-0.12
1708	434.00	4.49	-0.23
1713	436.85	4.47	-0.79
1718	439.69	4.23	-0.70
1723	442.54	4.35	-0.49
1728	445.39	4.39	-0.37
1733	448.23	4.31	-0.70
1738	451.08	4.12	-0.40
1743	453.92	4.06	-0.21
1748	456.77	3.99	-0.36
1753	459.62	3.85	-0.54
1758	462.46	3.87	-0.57
1763	465.31	3.90	-0.43
1768	468.15	3.95	-0.23
1773	471.00	4.03	-0.14
1778	472.75	3.78	-0.12
1783	474.50	3.82	-0.04
1788	476.25	3.88	-0.19
1793	478.00	3.84	-0.49
1798	479.75	3.76	-0.02
1803	481.50	3.72	-0.21
1808	483.25	3.92	-0.24
1813	485.00	3.73	-0.01
1828	490.25	3.17	0.78
1833	492.00	3.28	0.35
1838	493.75	3.28	0.53
1843	495.50	3.26	0.70
1848	497.25	3.14	0.46
1853	499.00	2.99	0.76
1858	500.75	3.00	0.83
1863	502.50	3.02	0.89
1868	504.25	3.14	1.00
1873	506.00	3.12	0.80
1878	507.75	3.27	1.03
1883	509.50	3.31	0.85
1888	511.25	3.36	1.03
1893	513.00	3.57	0.96
1898	520.14	3.43	0.71
1903	527.29	3.30	0.70
1908	534.43	3.53	0.31
1913	541.57	3.35	0.51
1918	548.71	3.51	0.84
1923	555.86	3.47	0.29

Depth (cmbsf)	Time (k.y.)	$\delta^{18}O$ cibicides	$\delta^{13}C$ cibicides
1928	563.00	4.00	0.22
1933	564.10	3.94	0.14
1938	565.20	3.83	0.20
1943	566.30	3.78	-0.13
1948	567.40	3.48	0.06
1958	569.60	3.27	0.32
1963	570.70	3.31	0.07
1968	571.80	3.14	0.54
1973	572.90	2.72	0.42
1978	574.00	2.61	0.32
1983	579.38	2.73	0.55
1988	584.75	2.72	0.52
1993	590.13	3.31	0.05
1998	595.50	3.58	-0.02
2003	600.88	3.62	0.42
2008	606.25	3.45	0.28
2013	611.63	3.17	0.13
2018	617.00	3.15	0.41
2023	618.83	3.16	0.02
2028	620.67	3.28	0.32
2033	622.50	3.29	0.08
2038	624.33	3.41	-0.35
2043	626.17	3.66	-0.16
2048	628.00	4.36	-0.21
2053	631.00	4.34	-0.05
2058	641.00	4.16	-0.29
2063	656.00	3.97	-0.37
2068	662.00	4.16	-0.13
2073	668.00	3.51	-0.31
2078	679.00	3.78	-0.03
2083	681.50	3.75	-0.09
2088	684.00	3.59	-0.45
2093	689.00	3.44	-0.50
2098	690.00	3.52	-0.41
2103	691.00	3.70	-0.30
2108	692.00	3.56	-0.28
2113	693.00	3.64	-0.13

APPENDIX 2.2

Benthic isotope data from core GeoB 3603-2.

Depth (cmbsf)	Time (k.y.)	$\delta^{18}O$ cibicides	$\delta^{13}C$ cibicides
8	4.00	2.82	0.55
13	7.00	2.92	0.36
18	10.00	2.76	0.61
23	13.00	4.04	0.05
28	16.00	4.37	0.00
33	19.00	4.43	0.10
38	20.50	4.31	0.17
43	22.00	4.21	-0.10
48	23.50	4.28	-0.12
53	25.00	4.25	-0.02
58	26.50	4.20	0.01
63	28.00	4.24	0.04
68	29.39	4.17	-0.28
73	30.78	4.12	-0.12
78	32.17	4.06	-0.09
83	33.56	3.99	-0.04
88	34.94	3.92	0.04
93	36.33	3.95	0.09
98	37.72	4.02	0.07
103	39.11	3.91	0.24
108	40.50	3.94	0.14
113	41.89	3.85	0.18
118	43.28	3.79	0.31
123	44.67	3.90	0.40
128	46.06	3.96	0.27
133	47.44	3.90	0.58
138	48.83	3.86	0.22
143	50.22	3.84	0.31
148	51.61	3.74	0.15
153	53.00	3.92	-0.09
158	54.50	3.75	0.06
163	56.00	3.70	-0.07
168	57.50	3.90	-0.05
173	59.00	4.02	-0.23
178	60.50	4.05	0.05
183	62.00	4.11	-0.07
188	63.50	4.11	-0.32
193	65.00	4.05	0.02
198	66.36	3.86	0.28
203	67.73	3.84	0.24
208	69.09	3.74	0.11
213	70.45	3.89	0.14
223	73.18	3.41	0.17
228	74.55	3.47	0.31
233	75.91	3.45	0.37
238	77.27	3.39	0.43
243	78.64	3.29	0.63
248	80.00	3.17	0.67
253	81.75	3.16	0.58
258	83.50	3.47	0.30
263	85.25	3.56	0.46
268	87.00	3.74	0.54
273	88.71	3.61	0.63
278	90.43	3.49	0.45
283	92.14	3.42	0.46
293	95.57	3.43	0.33
298	97.29	3.26	0.53
303	99.00	3.30	0.46
308	100.60	3.37	0.16
313	102.20	3.36	0.43
318	103.80	3.47	0.27
323	105.40	3.41	0.21
328	107.00	3.36	0.11
333	108.67	3.61	0.39
338	110.33	3.51	0.61
343	112.00	3.14	0.40
348	113.67	3.14	0.59
353	115.33	2.67	0.51
358	117.00	2.62	0.60
363	118.67	2.56	0.64
368	120.33	2.54	0.69
373	122.00	2.60	0.59
378	123.63	2.56	0.52
383	125.25	2.66	0.51
388	126.88	3.04	0.26
393	128.50	3.88	0.01
398	130.13	3.98	0.01
403	131.75	3.88	0.00
408	133.38	4.32	-0.17
413	135.00	4.26	0.08
418	136.57	4.20	-0.03
423	138.14	4.01	0.26
428	139.71	3.94	0.15
433	141.29	4.24	0.03
438	142.86	4.36	-0.25
443	144.43	4.20	-0.28
448	146.00	4.13	-0.20
453	147.67	4.17	-0.36
458	149.33	4.18	-0.21
463	151.00	4.27	-0.30
468	152.67	4.28	-0.22
473	154.33	4.23	-0.38
478	156.00	4.01	-0.12
483	157.67	4.07	-0.26
488	159.33	4.06	-0.08
493	161.00	4.01	-0.30
498	162.67	3.95	-0.52
503	164.33	3.91	0.03
508	166.00	3.78	0.11
513	167.67	3.69	0.18
518	169.33	3.84	-0.17
523	171.00	3.93	-0.15
528	172.71	3.86	-0.43
533	174.43	3.79	-0.20
538	176.14	3.90	0.07
543	177.86	3.65	0.45
548	179.57	3.78	0.16
553	181.29	4.11	-0.30
558	183.00	3.89	-0.13
563	184.83	3.99	-0.11
568	186.67	3.62	-0.03
573	188.50	3.47	0.08
578	190.33	3.34	0.00
583	192.17	3.33	0.31
588	194.00	3.29	0.24
593	196.20	3.06	0.37
598	198.40	3.30	0.22
603	200.60	2.93	0.35
608	202.80	3.20	0.22
613	205.00	3.23	0.24
618	207.20	3.33	0.54
623	209.40	3.18	0.45
628	211.60	2.98	0.48
633	213.80	3.10	0.48
638	216.00	2.93	0.59
643	217.71	3.02	0.48
648	219.43	3.42	-0.11
653	221.14	3.67	-0.11
658	222.86	3.86	-0.28
663	224.57	4.04	0.06
668	226.29	4.12	0.09
673	228.00	4.07	-0.08
678	229.43	3.95	0.08
683	230.86	3.78	-0.19
688	232.29	3.63	-0.13
693	233.71	3.75	-0.06
698	235.14	3.35	0.39
703	236.57	3.29	0.22
708	238.00	2.90	0.48
713	239.57	2.81	0.52
718	241.14	2.90	0.44
723	242.71	3.61	0.03
728	244.29	3.80	0.07
733	245.86	3.95	-0.13
738	247.43	4.21	-0.33
743	249.00	4.27	-0.01
748	250.67	4.06	0.08
753	252.33	4.01	-0.09
758	254.00	3.99	-0.32
763	255.67	4.02	-0.36
768	257.33	3.98	-0.20
773	259.00	4.08	-0.47
778	260.67	4.04	-0.58
783	262.33	4.21	-0.54
788	264.00	4.16	-0.56
793	265.67	4.19	-0.64
798	267.33	4.08	-0.39
803	269.00	4.14	-0.47
808	270.50	4.10	-0.49
813	272.00	4.00	-0.38
818	273.50	3.91	-0.20
823	275.00	3.97	-0.18
828	276.50	3.83	0.22
833	278.00	3.77	0.28
838	279.50	3.65	0.06
843	281.00	3.56	0.16
848	282.50	3.34	0.14
853	284.00	3.32	0.25
858	285.50	3.33	0.32
863	287.00	3.34	0.32
868	288.33	3.30	0.03
873	289.67	3.35	-0.02
878	291.00	3.70	-0.15
883	292.33	3.80	-0.19
888	293.67	3.86	-0.22
893	295.00	3.92	-0.28
898	296.33	3.71	0.00
903	297.67	3.93	0.07
908	299.00	3.84	0.18
913	300.10	3.79	0.27
918	301.20	3.79	0.25
923	302.30	3.72	0.58
928	303.40	3.62	0.42
933	304.50	3.53	0.35
938	305.60	3.49	-0.08
943	306.70	3.72	0.04
948	307.80	3.58	0.16
953	308.90	3.53	0.18
958	310.00	3.60	-0.03
963	311.50	3.17	0.35
968	313.00	3.17	0.33
973	314.50	3.18	-0.03
983	317.50	3.15	-0.21
988	319.00	3.32	-0.13
993	320.50	2.99	0.38
998	322.00	2.82	0.32
1003	323.50	2.67	0.65
1008	325.00	2.80	0.30
1013	326.50	2.95	0.57
1018	328.00	2.62	0.64
1028	331.00	2.50	0.43
1043	335.71	2.97	-0.03
1048	337.29	4.12	-0.24
1053	338.86	3.97	-0.43
1058	340.43	4.09	-0.28
1063	342.00	4.34	-0.34
1068	343.63	4.40	-0.18
1072	344.93	4.35	-0.25
1073	345.25	4.42	-0.28
1083	348.50	4.32	-0.26
1088	350.13	4.16	-0.34
1093	351.75	4.03	-0.27
1098	353.38	3.96	-0.17
1103	355.00	3.94	-0.19
1108	356.63	3.92	-0.38
1113	358.25	4.23	-0.28
1118	359.88	4.12	-0.58
1123	361.50	4.18	-0.44
1128	363.13	4.24	-0.67
1133	364.75	4.26	-0.83

APPENDIX 2.3

Benthic isotope data from core MD96 2081.

Depth (cmbsf)	Time (k.y.)	$\delta^{18}O$	$\delta^{13}C$
8	3.40	0.66	2.66
13	4.05	0.50	3.07
18	4.70	0.84	2.28
23	5.35	0.64	2.47
28	6.00	0.28	2.72
33	6.65	0.65	2.10
38	7.30	0.34	3.13
43	7.95	0.58	2.68
48	8.60	0.55	2.65
53	9.25	0.55	2.71
58	9.90	0.06	3.40
63	10.55	0.41	2.60
73	11.85	0.23	3.03
78	12.50	0.29	3.20
83	13.15	-0.06	3.71
88	13.80	0.15	3.66
93	14.45	0.46	3.54
98	15.10	0.25	3.46
103	15.75	0.13	3.65
108	16.40	-0.05	4.18
118	17.70	0.19	4.04
123	18.35	-0.01	4.16
128	19.00	-0.05	4.24
133	19.69	-0.16	4.29
138	20.38	0.11	4.20
143	21.08	0.09	4.23
148	21.77	0.10	4.28
153	22.46	0.18	4.26
158	23.15	0.21	4.01
163	23.85	0.15	4.15
168	24.54	0.11	3.94
173	25.23	0.17	4.00
178	25.92	0.14	3.97
183	26.62	0.20	3.87
188	27.31	0.18	3.84
193	28.00	0.16	3.62
198	29.25	0.08	3.23
203	30.50	0.18	3.78
208	31.75	0.33	3.85
213	33.00	0.36	3.70
218	34.25	0.13	3.76
223	35.50	0.21	3.56
228	36.75	0.24	3.49
233	38.00	0.27	3.76
238	39.25	0.17	3.58
243	40.50	0.44	3.56
248	41.75	0.33	3.60
253	43.00	0.32	3.44
258	44.25	0.31	3.45
263	45.50	0.16	3.64
268	46.75	0.42	3.74
273	48.00	0.25	3.68
278	49.25	0.21	3.47
283	50.50	0.28	3.52
288	51.75	0.08	3.35
293	53.00	0.38	3.58
298	54.71	0.06	3.29
303	56.43	0.25	3.61
308	58.14	0.18	3.52
313	59.86	-0.07	3.67
318	61.57	-0.11	3.62
323	63.29	-0.05	3.78
328	65.00	0.04	3.79
333	65.94	0.05	4.00
338	66.89	-0.12	3.68
343	67.83	-0.09	3.81
348	68.78	0.02	3.60
353	69.72	-0.03	3.95
358	70.67	-0.03	3.83
363	71.61	0.01	3.73
373	73.50	-0.10	3.62
378	74.44	-0.10	3.43
383	75.39	0.33	3.49
388	76.33	0.54	3.72
393	77.28	0.30	3.33
398	78.22	0.59	3.27
403	79.17	0.46	3.24
408	80.11	0.46	3.22
413	81.06	0.66	3.35
418	82.00	0.57	3.29
423	82.94	0.53	3.23
428	83.89	0.64	2.98
433	84.83	0.52	3.03
443	86.72	0.68	3.00
448	87.67	0.65	3.00
458	89.56	0.45	2.90
463	90.50	0.12	2.90
468	91.44	0.26	3.15
473	92.39	0.13	2.91
478	93.33	0.11	3.10
483	94.28	0.41	3.33
488	95.22	0.37	2.83
493	96.17	0.22	3.42
498	97.11	0.67	3.14
503	98.06	0.61	2.86
508	99.00	0.50	2.96
513	100.00	0.55	2.84
518	101.00	0.61	2.87
523	102.00	0.49	3.07
528	103.00	0.62	2.93
533	104.00	0.55	3.06
538	105.00	0.48	3.04
543	106.00	0.09	3.09
548	107.00	0.26	3.18
558	110.00	0.24	3.28
563	111.50	0.40	2.99
568	113.00	0.42	3.27
573	114.50	0.57	2.56
578	116.00	0.51	2.62
583	117.50	0.09	3.03
588	119.00	0.21	3.17
593	120.50	0.31	2.37
598	122.00	0.52	2.64
603	123.18	0.44	2.19
608	124.36	0.01	3.20
613	125.55	0.46	2.51
618	126.73	0.25	2.38
623	127.91	0.31	2.51
628	129.09	-0.01	3.03
633	130.27	0.18	3.27
638	131.45	0.02	3.56
643	132.64	-0.11	3.11
648	133.82	0.19	2.31
653	135.00	-0.02	3.84
658	138.67	0.23	3.23
663	142.33	0.15	3.94
668	146.00	-0.13	3.87
673	146.63	-0.24	3.93
678	147.25	-0.32	3.76
683	147.88	-0.16	3.91
688	148.50	0.06	3.96
693	149.13	-0.22	3.95
698	149.75	-0.21	3.96
703	150.38	-0.24	3.95
708	151.00	-0.25	3.85
713	154.33	-0.46	3.82
718	157.67	-0.28	4.07
723	161.00	-0.05	4.00
728	164.33	-0.15	3.93
733	167.67	-0.10	3.90
738	171.00	0.00	3.56
743	172.20	-0.09	3.71
748	173.40	-0.20	3.55
753	174.60	-0.04	3.61
758	175.80	0.09	3.83
763	177.00	0.07	3.79
768	178.20	-0.02	3.70
773	179.40	-0.21	3.65
778	180.60	-0.03	3.68
783	181.80	0.00	3.79
788	183.00	-0.06	3.81
793	184.57	-0.21	3.74
798	186.14	-0.01	3.86
803	187.71	-0.09	3.82
808	189.29	-0.06	3.43
813	190.86	-0.38	3.59
818	192.43	0.08	3.76
823	194.00	-0.08	3.74
828	195.57	0.32	3.44
833	197.14	0.02	3.41
838	198.71	0.14	3.37
843	200.29	-0.14	3.47
848	201.86	-0.17	3.37
853	203.43	0.45	2.98
858	205.00	0.23	3.12
863	206.57	0.34	2.97
868	208.14	0.59	3.28
873	209.71	-0.23	2.69
878	211.29	0.26	2.91
883	212.86	0.18	3.11
888	214.43	0.46	2.94
893	216.00	0.76	2.78
898	217.71	0.29	2.66
903	219.43	0.51	2.86
908	221.14	-0.21	3.32
913	222.86	-0.14	3.34
918	224.57	-0.04	3.48
923	226.29	-0.06	3.38
928	228.00	-0.19	3.64
933	228.83	-0.45	3.70
938	229.67	-0.09	3.61
943	230.50	-0.05	3.53
948	231.33	0.14	3.26
953	232.17	-0.07	3.31
958	233.00	0.50	3.21
963	233.83	0.17	3.36
968	234.67	0.03	3.37
973	235.50	0.22	3.31
978	236.33	0.09	3.48
983	237.17	-0.04	3.40
988	238.00	0.56	2.86
993	245.00	0.01	2.80
998	246.33	-0.13	3.50
1003	247.67	-0.07	3.77
1008	249.00	0.04	3.66
1013	250.00	-0.07	3.98
1018	251.00	-0.02	3.86
1023	252.00	-0.21	3.76
1028	253.00	-0.03	3.76
1033	254.00	0.05	3.97
1038	255.00	-0.17	3.82
1043	256.00	-0.08	3.80
1048	257.00	-0.48	3.72
1053	259.40	-0.36	3.71
1058	261.80	-0.29	3.88
1063	264.20	-0.64	3.85
1068	266.60	-0.08	3.88
1073	269.00	-0.45	3.97
1078	270.50	-0.45	3.86
1083	272.00	-0.59	3.92
1088	273.50	-0.39	3.93
1093	275.00	-0.46	3.80
1098	276.50	-0.34	3.58
1103	278.00	-0.23	3.68
1108	279.50	0.03	3.73
1113	281.00	0.44	3.21
1118	282.50	-0.07	3.75
1123	284.00	0.07	3.10
1128	285.50	-0.15	3.19
1133	287.00	0.38	3.01
1138	288.50	0.20	3.02
1143	290.00	0.32	3.14
1148	291.50	0.21	3.12
1153	293.00	-0.06	3.45
1158	294.50	-0.14	3.52
1163	296.00	0.22	3.60
1168	297.50	-0.04	3.36
1173	299.00	0.37	3.49
1178	299.85	0.11	3.72
1183	300.69	0.10	3.64
1188	301.54	-0.15	3.57
1193	302.38	0.26	3.63
1198	303.23	0.59	3.47
1203	304.08	0.13	3.58
1208	304.92	0.48	3.57
1213	305.77	0.36	3.44
1218	306.62	0.39	3.47

Depth (cmbsf)	Time (k.y.)	$\delta^{18}O$	$\delta^{13}C$
1223	307.46	0.12	3.14
1228	308.31	0.25	3.53
1233	309.15	0.13	3.37
1238	310.00	0.25	3.21
1243	311.67	0.21	2.97
1248	313.33	0.08	3.02
1253	315.00	0.21	3.12
1258	316.67	0.03	2.99
1263	318.33	-0.03	3.04
1268	320.00	-0.08	3.00
1273	321.38	0.05	3.14
1278	322.75	0.12	2.95
1283	324.13	0.35	2.91
1288	325.50	0.08	2.64
1293	326.88	0.60	2.66
1298	328.25	0.10	2.67
1303	329.63	0.50	2.55
1308	331.00	0.36	2.66
1313	331.77	0.38	2.52
1318	332.54	-0.09	2.64
1323	333.31	-0.03	2.96
1328	334.08	-0.38	3.51
1333	334.85	0.27	2.62
1338	335.62	-0.16	3.53
1343	336.38	-0.57	3.77
1348	337.15	-0.27	3.78
1353	337.92	-0.40	3.78
1358	338.69	-0.19	3.75
1363	339.46	-0.22	3.92
1368	340.23	-0.29	4.08
1373	341.00	0.21	3.80
1378	341.82	-0.40	4.15
1383	342.64	-0.42	3.88
1388	343.45	-0.31	3.84
1393	344.27	-0.38	3.89
1398	345.09	-0.48	3.94
1403	345.91	-0.60	3.82
1408	346.73	-0.64	3.93
1413	347.55	-0.55	3.79
1418	348.36	-0.37	3.83
1423	349.18	-0.48	3.86
1428	350.00	-0.18	3.82
1433	350.82	-0.43	3.71
1438	351.64	-0.26	3.71
1443	352.29	-0.32	3.71
1448	353.27	-0.34	3.63
1453	354.09	-0.18	3.61
1458	354.91	-0.45	3.50
1463	355.73	-0.16	3.70
1468	356.55	0.28	3.52
1473	357.36	-0.47	3.53
1478	358.18	0.27	3.53
1483	359.00	0.07	3.42
1488	359.82	0.23	3.50
1493	360.64	0.28	3.38
1498	361.45	-0.16	3.60
1503	362.27	-0.05	3.39
1508	363.09	0.06	3.49
1513	363.91	-0.04	3.52
1518	364.73	0.34	3.32
1523	365.55	0.18	3.29
1528	366.36	0.01	3.31
1538	368.00	0.22	3.09
1543	371.50	0.08	2.93
1548	375.00	-0.25	3.20
1553	376.76	0.42	3.35
1558	378.53	0.33	3.11
1563	380.29	0.46	3.17
1568	382.06	0.70	2.97
1573	383.82	0.89	2.83
1583	387.35	1.03	2.71
1588	389.12	0.88	2.66
1593	390.88	0.79	2.56
1598	392.65	0.99	2.52
1603	394.41	0.89	2.55
1608	396.18	0.68	2.57
1613	397.94	0.92	2.55
1618	399.71	0.86	2.48
1623	401.47	0.88	2.45
1628	403.24	0.73	2.57
1633	405.00	0.89	2.57
1638	406.93	0.79	2.44
1643	408.87	0.81	2.56
1648	410.80	0.82	2.54
1653	412.73	0.71	2.60
1658	414.67	0.64	2.70
1663	416.60	0.63	2.65
1668	418.53	0.69	2.77
1673	420.47	0.68	2.89
1678	422.40	0.68	2.96
1683	424.33	0.38	3.30
1688	426.27	0.44	3.38
1693	428.20	0.07	3.67
1698	430.13	-0.08	3.67
1703	432.07	-0.45	4.09
1708	434.00	-0.12	3.82
1713	436.85	-0.23	4.49
1718	439.69	-0.79	4.47
1723	442.54	-0.70	4.23
1728	445.39	-0.49	4.35
1733	448.23	-0.37	4.39
1738	451.08	-0.70	4.31
1743	453.92	-0.40	4.12
1748	456.77	-0.21	4.06
1753	459.62	-0.36	3.99
1758	462.46	-0.54	3.85
1763	465.31	-0.57	3.87
1768	468.15	-0.43	3.90
1773	471.00	-0.23	3.95
1778	472.75	-0.14	4.03
1783	474.50	-0.12	3.78
1788	476.25	-0.04	3.82
1793	478.00	-0.19	3.88
1798	479.75	-0.49	3.84
1803	481.50	-0.02	3.76
1808	483.25	-0.21	3.72
1813	485.00	-0.24	3.92
1828	490.25	-0.01	3.73
1833	492.00	0.78	3.17
1838	493.75	0.35	3.28
1843	495.50	0.53	3.28
1848	497.25	0.70	3.26
1853	499.00	0.46	3.14
1858	500.75	0.76	2.99
1863	502.50	0.83	3.00
1868	504.25	0.89	3.02
1873	506.00	1.00	3.14
1878	507.75	0.80	3.12
1883	509.50	1.03	3.27
1888	511.25	0.85	3.31
1893	513.00	1.03	3.36
1898	520.14	0.96	3.57
1903	527.29	0.71	3.43
1908	534.43	0.70	3.30
1913	541.57	0.31	3.53
1918	548.71	0.51	3.35
1923	555.86	0.84	3.51
1928	563.00	0.22	4.00
1933	564.10	0.14	3.94
1938	565.20	0.20	3.83
1943	566.30	-0.13	3.78
1948	567.40	0.06	3.48
1958	569.60	0.32	3.27
1963	570.70	0.07	3.31
1968	571.80	0.54	3.14
1973	572.90	0.42	2.72
1978	574.00	0.32	2.61
1983	579.38	0.55	2.73
1988	584.75	0.52	2.72
1993	590.13	0.05	3.31
1998	595.50	-0.02	3.58
2003	600.88	0.42	3.62
2008	606.25	0.28	3.45
2013	611.63	0.13	3.17
2018	617.00	0.41	3.15
2023	618.83	0.02	3.16
2028	620.67	0.32	3.28
2033	622.50	0.08	3.29
2038	624.33	-0.35	3.41
2043	626.17	-0.16	3.66
2048	628.00	-0.21	4.36
2053	631.00	-0.05	4.34
2058	641.00	-0.29	4.16
2063	656.00	-0.37	3.97
2068	662.00	-0.13	4.16
2073	668.00	-0.31	3.51
2078	679.00	-0.03	3.78
2083	681.50	-0.09	3.75
2088	684.00	-0.45	3.59
2093	689.00	-0.50	3.44
2098	690.00	-0.41	3.52
2103	691.00	-0.30	3.70
2108	692.00	-0.28	3.56
2113	693.00	-0.13	3.64

APPENDIX 2.4

Planktonic (*Gr. inflata*) isotope data from core MD96 2081.

Depth (cmbsf)	Time (k.y.)	$\delta^{18}O$	$\delta^{13}C$
3	2.75	1.14	0.56
8	3.40	1.06	1.04
13	4.05	0.44	0.70
18	4.70	2.16	0.92
23	5.35	0.91	0.57
28	6.00	1.07	0.63
33	6.65	1.47	0.84
38	7.30	1.69	0.90
43	7.95	0.62	0.86
48	8.60	0.95	0.71
53	9.25	1.41	0.68
58	9.90	1.59	0.46
63	10.55	1.01	0.38
68	11.20	0.91	0.58
73	11.85	1.14	0.40
78	12.50	1.06	0.16
83	13.15	1.40	0.36
88	13.80	1.68	0.52
93	14.45	1.62	0.35
98	15.10	1.83	0.28
103	15.75	1.69	0.48
108	16.40	1.83	0.39
113	17.05	1.86	0.51
118	17.70	1.97	0.60
123	18.35	2.03	0.46
128	19.00	1.80	0.50
133	19.69	1.97	0.49
138	20.38	1.46	0.73
143	21.08	1.65	0.47
148	21.77	1.81	0.59
153	22.46	1.58	0.09
158	23.15	2.00	0.73
163	23.85	2.00	0.61
168	24.54	1.65	0.61
173	25.23	1.82	0.86
178	25.92	1.69	0.58
183	26.62	2.06	0.69
188	27.31	1.26	0.40
193	28.00	1.54	0.61
198	29.25	1.78	0.72
203	30.50	2.13	0.88
208	31.75	1.47	0.48
213	33.00	1.50	0.41
218	34.25	1.73	0.49
223	35.50	1.88	0.95
228	36.75	1.43	0.40
233	38.00	1.49	0.64
238	39.25	1.49	0.80
243	40.50	1.52	0.72
248	41.75	1.28	0.59
253	43.00	1.68	0.90
258	44.25	1.75	0.82
263	45.50	1.28	0.16
268	46.75	1.39	0.87
273	48.00	1.60	0.64
278	49.25	1.50	0.58
283	50.50	1.48	0.65
288	51.75	1.47	0.38
293	53.00	1.26	0.35
298	54.71	1.45	0.33
303	56.43	1.44	0.33
308	58.14	1.54	0.49
313	59.86	1.83	0.34
318	61.57	1.78	0.75
323	63.29	1.60	0.58
328	65.00	1.38	0.78
333	65.94	1.88	0.68
338	66.89	1.77	0.85
343	67.83	1.63	0.47
348	68.78	1.32	0.42
353	69.72	1.44	0.43
358	70.67	1.69	0.65
363	71.61	1.65	0.84
368	72.56	1.41	0.69
373	73.50	1.14	0.60
378	74.44	1.55	0.77
383	75.39	1.48	0.75
388	76.33	1.52	0.77
393	77.28	1.34	0.74
398	78.22	1.23	0.84
403	79.17	1.08	0.53
408	80.11	1.45	0.92
413	81.06	1.32	1.11
418	82.00	0.87	0.77
423	82.94	1.13	0.92
428	83.89	0.98	0.63
433	84.83	0.92	0.78
438	85.78	1.24	0.84
443	86.72	1.04	0.61
448	87.67	1.06	0.58
458	89.56	1.18	0.54
463	90.50	1.21	0.68
468	91.44	0.98	0.57
473	92.39	1.47	0.93
478	93.33	1.35	1.03
483	94.28	1.33	0.77
488	95.22	1.43	0.59
493	96.17	1.00	0.74
498	97.11	1.15	0.64
503	98.06	1.25	1.06
508	99.00	1.08	0.52
513	100.00	1.02	0.82
518	101.00	1.01	0.80
523	102.00	1.00	0.58
533	104.00	1.17	0.68
538	105.00	0.96	0.47
543	106.00	1.01	0.51
548	107.00	1.02	0.62
553	108.50	1.30	0.66
558	110.00	1.02	0.62
563	111.50	0.91	0.68
568	113.00	1.05	0.56
573	114.50	0.63	0.64
578	116.00	0.91	0.66
583	117.50	0.55	0.54
588	119.00	0.45	0.54
593	120.50	0.56	0.47
598	122.00	0.48	0.36
603	123.18	0.61	0.57
608	124.36	0.88	0.50
613	125.55	0.59	0.45
618	126.73	0.77	0.37
623	127.91	0.82	0.24
628	129.09	0.97	0.15
633	130.27	1.29	0.28
638	131.45	1.29	0.22
643	132.64	1.83	0.18
648	133.82	1.65	0.36
653	135.00	2.09	0.32
658	138.67	1.61	0.35
663	142.33	1.54	0.21
668	146.00	1.64	0.39
673	146.63	2.11	0.45
678	147.25	1.70	0.26
683	147.88	1.43	0.41
688	148.50	1.71	0.32
693	149.13	1.86	0.22
698	149.75	1.75	0.32
703	150.38	1.81	0.30
708	151.00	2.00	0.42
713	154.33	2.24	0.38
718	157.67	1.84	0.24
723	161.00	1.63	0.31
728	164.33	1.72	0.28
733	167.67	1.87	0.33
738	171.00	1.87	0.55
743	172.20	1.68	0.39
748	173.40	2.06	0.44
778	180.60	1.50	0.05
783	181.80	1.53	0.23
788	183.00	1.48	0.11
793	184.57	1.40	0.13
798	186.14	1.46	0.51
803	187.71	1.82	0.59
808	189.29	1.71	0.53
813	190.86	1.47	0.53
818	192.43	1.55	0.55
823	194.00	1.36	0.46
828	195.57	1.40	0.75
833	197.14	1.31	0.81
838	198.71	0.93	0.53
843	200.29	1.09	0.45
848	201.86	0.75	0.75
853	203.43	0.76	0.55
858	205.00	1.39	1.01
863	206.57	1.39	0.58
868	208.14	1.22	0.75
873	209.71	1.11	0.65
878	211.29	0.95	0.66
883	212.86	1.01	0.84
888	214.43	0.76	0.90
893	216.00	1.04	0.77
898	217.71	1.02	0.88
903	219.43	0.82	0.78
908	221.14	1.07	0.42
913	222.86	1.05	0.06
918	224.57	1.10	0.20
923	226.29	1.23	0.19
928	228.00	1.51	0.51
933	228.83	1.43	0.41
938	229.67	1.41	0.42
943	230.50	1.52	0.53
948	231.33	1.43	0.59
953	232.17	1.11	0.36
958	233.00	1.43	0.59
963	233.83	1.51	0.86
968	234.67	1.31	0.83
973	235.50	1.16	0.65
978	236.33	1.28	0.83
983	237.17	1.16	0.59
988	238.00	0.77	0.24
993	245.00	0.83	0.25
998	246.33	1.41	0.32
1003	247.67	1.28	0.16
1008	249.00	1.65	0.29
1013	250.00	1.81	0.48
1018	251.00	1.58	0.41
1023	252.00	1.98	0.63
1028	253.00	1.17	0.51
1033	254.00	1.36	0.31
1038	255.00	1.56	0.24
1043	256.00	1.71	0.40
1048	257.00	1.29	0.25
1053	259.40	1.84	0.21
1058	261.80	2.34	0.64
1063	264.20	1.81	0.14
1068	266.60	1.88	0.41
1073	269.00	1.81	0.30
1078	270.50	1.76	0.51
1083	272.00	2.02	0.75
1088	273.50	2.29	0.67
1093	275.00	2.08	0.86
1098	276.50	2.42	0.93
1103	278.00	1.66	0.76
1108	279.50	1.46	0.77
1113	281.00	1.93	0.71
1118	282.50	1.31	0.79
1123	284.00	1.81	1.06
1128	285.50	1.41	1.01
1133	287.00	1.23	0.96
1138	288.50	1.80	1.03
1143	290.00	1.51	0.98
1148	291.50	1.39	0.86
1153	293.00	1.47	0.78
1158	294.50	1.59	1.06
1163	296.00	1.44	0.84
1168	297.50	1.31	0.68
1173	299.00	1.65	1.12
1183	300.69	1.45	0.72
1188	301.54	1.96	1.12
1193	302.38	2.42	1.06
1198	303.23	1.50	0.83
1203	304.08	1.30	0.93
1208	304.92	1.16	1.16
1213	305.77	1.93	0.94
1218	306.62	1.10	0.66
1223	307.46	1.20	0.90

Depth (cmbsf)	Time (k.y.)	$\delta^{18}O$	$\delta^{13}C$
1228	308.31	1.63	0.85
1233	309.15	1.65	1.12
1238	310.00	1.18	0.79
1243	311.67	1.08	0.60
1248	313.33	1.28	0.69
1258	316.67	0.98	0.72
1263	318.33	0.94	0.67
1268	320.00	0.81	0.70
1273	321.38	1.21	1.10
1278	322.75	0.97	0.97
1288	325.50	0.76	0.89
1293	326.88	0.85	0.86
1298	328.25	0.64	0.74
1303	329.63	0.78	0.66
1308	331.00	0.58	0.67
1313	331.77	0.98	0.43
1318	332.54	0.84	0.41
1323	333.31	1.16	0.35
1328	334.08	1.44	0.37
1333	334.85	1.55	-0.02
1338	335.62	1.64	0.23
1343	336.38	1.65	0.20
1348	337.15	2.60	0.63
1353	337.92	1.86	0.19
1358	338.69	1.84	0.24
1363	339.46	1.78	0.53
1368	340.23	1.43	0.32
1373	341.00	1.52	0.28
1378	341.82	1.49	0.42
1383	342.64	1.89	0.59
1388	343.45	2.05	0.73
1393	344.27	1.74	0.60
1398	345.09	2.15	0.82
1403	345.91	1.75	0.82
1408	346.73	1.89	0.53
1413	347.55	1.88	0.76
1418	348.36	1.82	0.75
1423	349.18	2.40	0.95
1428	350.00	1.76	0.87
1433	350.82	1.57	0.94
1438	351.64	1.45	0.76
1442	352.29	1.46	0.71
1448	353.27	1.55	0.82
1453	354.09	1.56	0.86
1458	354.91	1.48	0.77
1463	355.73	1.75	1.10
1468	356.55	1.92	0.89
1473	357.36	2.16	1.29
1478	358.18	1.63	0.98
1483	359.00	2.03	1.15
1488	359.82	1.38	0.85
1493	360.64	1.55	0.90
1498	361.45	1.49	0.93
1503	362.27	1.35	0.58
1508	363.09	1.41	0.95
1513	363.91	0.95	0.74
1518	364.73	1.17	0.82
1523	365.55	1.12	0.67
1528	366.36	1.15	0.73
1533	367.18	1.13	0.78
1538	368.00	1.77	1.02
1543	371.50	1.14	0.57
1548	375.00	1.12	0.73
1553	376.76	0.84	0.87
1558	378.53	1.71	1.05
1563	380.29	0.92	0.54
1568	382.06	1.01	1.32
1573	383.82	1.07	1.32
1578	385.59	0.90	1.19
1583	387.35	0.93	1.13
1588	389.12	0.98	1.05
1593	390.88	0.84	1.24
1598	392.65	0.88	1.22
1603	394.41	1.09	1.16
1608	396.18	0.90	1.05
1613	397.94	0.68	1.04
1618	399.71	0.78	1.04
1623	401.47	0.88	0.82
1628	403.24	1.31	0.76
1633	405.00	0.82	0.86
1638	406.93	1.08	1.01
1643	408.87	0.94	0.89
1648	410.80	1.01	0.94
1653	412.73	1.03	0.96
1658	414.67	1.09	0.88
1663	416.60	1.35	1.04
1668	418.53	1.07	0.90
1673	420.47	1.36	0.81
1678	422.40	1.85	0.87
1683	424.33	1.47	0.59
1688	426.27	1.81	0.37
1693	428.20	2.06	0.21
1698	430.13	2.27	0.52
1703	432.07	2.33	0.63
1708	434.00	2.85	0.80
1713	436.85	2.64	0.71
1718	439.69	2.66	0.70
1723	442.54	2.72	0.95
1733	448.23	2.69	0.91
1738	451.08	2.34	0.88
1743	453.92	1.93	0.81
1748	456.77	1.92	0.73
1758	462.46	2.33	1.06
1763	465.31	1.87	0.68
1768	468.15	1.83	0.86
1773	471.00	1.83	0.76
1778	472.75	1.84	0.84
1783	474.50	1.98	0.95
1788	476.25	1.76	0.91
1793	478.00	1.74	0.97
1798	479.75	1.67	0.96
1803	481.50	1.92	1.07
1808	483.25	1.94	1.22
1813	485.00	1.88	1.03
1818	486.75	1.56	1.26
1823	488.50	1.15	0.94
1828	490.25	1.32	1.18
1833	492.00	1.20	1.21
1838	493.75	1.19	1.35
1843	495.50	1.28	1.39
1848	497.25	1.77	1.59
1853	499.00	1.40	1.61
1858	500.75	1.41	1.40
1863	502.50	1.14	1.36
1868	504.25	1.09	1.36
1873	506.00	1.57	1.43
1878	507.75	1.22	1.09
1883	509.50	1.32	0.99
1888	511.25	1.34	0.94
1893	513.00	1.58	1.29
1898	520.14	1.63	1.32
1903	527.29	1.77	1.17
1908	534.43	1.28	0.86
1913	541.57	1.38	0.79
1918	548.71	1.55	1.05
1923	555.86	1.67	0.90
1928	563.00	2.17	0.91
1933	564.10	2.04	0.76
1938	565.20	1.28	0.75
1943	566.30	1.21	0.34
1948	567.40	1.78	0.90
1953	568.50	1.25	0.51
1958	569.60	1.21	0.76
1963	570.70	1.29	0.60
1968	571.80	1.17	0.70
1973	572.90	1.56	1.22
1978	574.00	1.03	0.82
1983	579.38	1.16	0.90
1988	584.75	0.99	0.72
1998	595.50	1.44	0.56
2003	600.88	1.90	0.93
2008	606.25	1.87	1.07
2013	611.63	1.03	0.37
2018	617.00	1.10	0.56
2023	618.83	1.26	0.79
2028	620.67	1.89	1.02
2033	622.50	1.41	0.91
2038	624.33	1.18	0.96
2043	626.17	1.09	0.09
2048	628.00	2.21	0.41
2053	631.00	1.90	0.52
2058	641.00	2.44	0.34
2063	656.00	1.84	0.03
2068	662.00	1.72	0.19
2073	668.00	2.21	0.44
2078	679.00	1.67	0.07
2083	681.50	1.69	0.23
2088	684.00	1.70	-0.01
2093	689.00	1.88	0.37
2098	690.00	1.38	0.02
2103	691.00	1.33	0.16
2108	692.00	1.74	0.37
2113	693.00	1.02	0.36

APPENDIX 3.1

Spliced Cape Basin core planktonic foraminiferal assemblage counts.

Cm below seafloor	Time (kyr)	Plk. total (not incl benthics)	N. pac (R)	Gr. inflata	Gg. bulloides	Ga. glutinata	Gs. ruber	Gr. truncatulinoides	N. dutertrei	N. pac (L)	O. universa	Gr. scitula	Gs. sacculifer	Gr. crassaformis	Ga. siphonifera	Gg. falconensis	Gg. quinqueloba	Gr. hirsuta	G. hexagona	Gr. menardii	Gg.rubescens	Gs. conglobatus	G. calida	Gs. tenellus	G. digitata	P. obliquiloculata	rubr(pk)	G. theyeri	Gr cavernula	Ga. uvula	Sphaer. dehiscens	Candeina nitid	Unknown	Benthics	Fragments
8	4.00	510	70	107	116	43	44	23	20	1	6	6	18	13	15	14	1	4	1	4	0	0	0	0	0	3	0	0	0	0	0	0	1	8	107
13	7.00	408	43	129	101	8	31	14	15	3	2	14	13	0	9	0	0	8	4	3	2	0	1	6	0	0	0	0	2	0	0	0	0	5	151
18	10.00	309	75	85	48	12	18	6	16	0	6	5	6	7	11	2	0	2	4	0	0	1	0	2	0	0	0	0	1	1	1	0	0	5	90
23	13.00	393	92	150	56	0	15	9	14	0	13	4	11	3	13	0	0	5	0	3	2	1	0	2	0	0	0	0	0	0	0	0	0	6	82
28	16.00	417	193	92	73	12	10	6	2	4	6	2	2	2	6	0	0	6	0	0	0	1	0	0	0	0	0	0	0	0	0	0	0	0	57
33	19.00	410	247	50	66	14	7	10	0	5	4	2	0	0	2	0	0	3	0	0	0	0	0	0	0	0	0	0	0	0	0	0	0	2	79
38	20.50	373	211	49	60	18	1	4	6	2	3	3	3	4	3	1	2	0	3	0	0	0	0	0	0	0	0	0	0	0	0	0	0	3	59
43	22.00	317	109	72	68	1	15	11	5	0	9	2	10	0	7	0	0	7	0	0	0	1	0	0	0	0	0	0	0	0	0	0	0	3	80
48	23.50	451	233	71	65	34	5	3	2	0	7	1	5	8	4	2	4	2	0	0	2	0	0	0	0	0	0	0	1	2	0	0	0	7	74
53	25.00	394	170	93	69	11	10	6	2	2	0	3	1	0	9	0	12	2	0	1	0	0	2	1	0	0	0	0	0	0	0	0	0	5	76
58	26.50	321	172	49	49	15	7	4	2	1	0	2	2	1	2	3	6	2	3	0	0	0	1	0	0	0	0	0	0	0	0	0	0	3	107
63	28.00	436	224	56	77	18	11	4	0	3	4	3	3	9	5	5	7	1	6	0	0	0	0	0	0	0	0	0	0	0	0	0	0	9	116
68	29.39	391	194	75	56	24	8	11	0	2	5	1	0	2	6	3	0	3	1	0	0	0	0	0	0	0	0	0	0	0	0	0	0	5	77
73	30.78	481	205	81	89	30	9	10	3	8	10	3	9	5	1	1	6	0	11	0	0	0	0	0	0	0	0	0	0	0	0	0	0	7	178
78	32.17	468	198	67	89	40	19	7	6	1	8	2	1	3	6	7	8	0	0	3	0	0	0	0	0	1	0	0	1	1	0	0	0	4	92
83	33.56	427	229	50	65	38	11	9	0	6	3	2	4	2	2	1	1	1	1	0	1	0	0	0	0	0	0	0	1	0	0	0	0	1	103
88	34.94	451	203	88	82	29	20	3	3	0	5	2	1	3	2	4	0	3	3	0	0	0	0	0	0	0	0	0	0	0	0	0	0	2	87
93	36.33	471	199	97	105	9	20	8	2	2	8	5	2	4	6	1	1	0	0	1	0	0	0	0	0	0	1	0	0	0	0	0	0	5	96
98	37.72	313	130	59	65	29	7	7	0	0	4	0	0	5	3	1	2	1	0	0	0	0	0	0	0	0	0	0	0	0	0	0	0	0	73
103	39.11	341	147	52	89	17	2	7	0	1	6	3	5	4	4	1	0	0	0	1	2	0	0	0	0	0	0	0	0	0	0	0	0	2	68
108	40.50	521	268	94	112	15	5	7	4	2	1	3	3	2	3	1	0	0	1	0	0	0	0	0	0	0	0	0	0	0	0	0	0	6	114
113	41.89	253	128	42	50	13	5	2	1	1	0	2	1	4	2	0	1	0	0	0	1	0	0	0	0	0	0	0	0	0	0	0	0	3	55
118	43.28	411	180	59	68	19	15	8	4	3	5	2	3	7	14	3	15	1	0	1	0	0	1	0	0	0	1	0	0	2	0	0	0	5	87
123	44.67	488	214	76	110	28	24	7	3	4	5	3	0	1	7	2	0	1	0	0	2	0	0	0	0	0	1	0	0	0	0	0	0	2	106
128	46.06	460	187	96	100	23	6	8	5	2	7	1	1	9	2	6	3	2	0	0	0	0	1	0	0	0	0	0	1	0	0	0	0	3	87
133	47.44	404	140	122	77	37	6	7	0	3	2	3	2	1	3	0	0	1	0	0	0	0	0	0	0	0	0	0	0	0	0	0	0	1	68
138	48.83	302	85	76	76	14	11	11	0	0	8	5	0	3	4	4	2	3	0	0	0	0	0	0	0	0	0	0	0	0	0	0	0	2	52
143	50.22	406	133	93	105	28	13	11	0	4	6	4	0	0	6	0	0	3	0	0	0	0	0	0	0	0	0	0	0	0	0	0	0	3	96
148	51.61	359	135	84	64	17	8	16	6	1	7	5	3	0	2	1	3	1	3	2	1	0	0	0	0	0	0	0	0	0	0	0	0	8	82
153	53.00	370	136	84	77	24	10	18	1	1	4	6	0	3	2	1	1	1	0	0	0	0	1	0	0	0	0	0	0	0	0	0	0	1	83
158	54.50	389	145	78	85	31	7	14	1	1	1	3	1	0	5	7	1	7	1	0	1	0	0	0	0	0	0	0	0	0	0	0	0	5	79
163	56.00	358	157	64	70	26	10	9	2	4	4	3	2	3	1	0	0	3	0	0	0	0	0	0	0	0	0	0	0	0	0	0	0	4	79
168	57.50	374	143	94	91	15	5	7	4	1	1	3	3	2	3	1	0	0	1	0	0	0	0	0	0	0	0	0	0	0	0	0	0	8	100
173	59.00	409	188	100	62	23	6	8	1	4	4	3	3	0	1	0	0	4	1	0	0	0	1	0	0	0	0	0	0	0	0	0	0	2	89
178	60.50	297	129	49	61	19	9	7	0	2	3	3	0	4	6	2	1	1	0	0	1	0	0	0	0	0	0	0	0	0	0	0	0	5	65
183	62.00	415	116	147	89	25	3	15	3	1	3	3	1	1	5	1	0	2	0	0	0	0	0	0	0	0	0	0	0	0	0	0	0	5	70
188	63.50	405	163	78	92	25	7	6	4	0	8	4	1	3	10	1	0	2	0	1	0	0	0	0	0	0	0	0	0	0	0	0	0	1	59
193	65.00	464	208	106	70	9	11	12	16	0	10	7	8	0	1	0	0	1	2	0	0	2	0	0	0	1	0	0	0	0	0	0	0	11	4
198	66.36	380	165	80	85	22	4	4	4	0	4	1	0	6	2	1	1	0	0	0	0	0	0	0	0	0	0	0	1	0	0	0	0	6	79
203	67.73	397	180	56	66	8	11	22	24	1	5	1	8	1	2	0	0	3	2	3	2	2	0	0	0	0	0	0	0	0	0	0	0	2	36
208	69.09	414	218	57	82	17	8	7	5	0	2	2	3	3	1	6	0	0	3	0	0	0	0	0	0	0	0	0	0	0	0	0	0	4	131
213	70.45	479	240	62	108	18	12	4	10	0	8	5	7	1	2	0	0	2	0	0	0	0	0	0	0	0	0	0	0	0	0	0	0	6	63
218	71.56	329	170	41	33	15	9	14	1	1	6	5	6	3	5	10	3	3	2	2	0	0	0	0	0	0	0	0	0	0	0	0	0	3	109
223	73.18	375	199	40	29	21	29	8	8	0	3	7	16	4	2	0	0	6	2	0	0	1	0	0	0	0	0	0	0	0	0	0	0	3	26
228	74.55	456	225	60	79	21	11	8	4	0	3	13	4	7	4	6	0	3	4	0	0	2	0	0	0	0	0	0	2	0	0	0	0	6	126
233	75.91	355	106	98	76	35	8	7	5	0	1	4	3	5	5	0	0	2	0	0	0	0	0	0	0	0	0	0	0	0	0	0	0	5	46
238	77.27	409	203	54	76	19	9	14	1	0	2	8	5	3	4	2	4	3	1	1	0	0	0	0	0	0	0	0	0	0	0	0	0	3	91
243	78.64	330	139	57	58	26	8	9	7	1	1	5	5	1	8	0	3	2	0	0	0	0	0	0	0	0	0	0	0	0	0	0	0	6	59
248	80.00	520	220	57	138	32	17	12	6	0	4	5	1	8	12	6	0	1	0	1	0	0	0	0	0	0	0	0	0	0	0	0	0	6	152
253	81.75	307	107	47	69	49	5	4	3	1	0	5	6	2	1	0	1	2	3	0	0	2	0	0	0	0	0	0	0	0	0	0	0	5	76
258	83.50	359	66	133	66	16	27	21	2	0	4	4	5	2	7	3	0	2	1	0	0	0	0	0	0	0	0	0	0	0	0	0	0	11	185
263	85.25	359	65	117	66	28	20	0	5	1	9	2	4	1	6	10	0	4	1	0	2	6	8	2	0	2	0	0	0	0	0	0	0	5	120
268	87.00	407	126	117	63	19	18	32	1	2	2	5	3	3	3	4	1	4	0	0	0	0	0	0	0	4	0	0	0	0	0	0	0	5	81
273	88.71	618	140	167	143	51	18	30	6	0	6	12	16	4	5	0	0	10	2	2	0	2	0	1	0	1	0	0	2	0	0	0	0	6	146
278	90.43	316	107	80	72	14	11	14	1	0	3	6	0	3	3	1	0	0	0	0	1	0	0	0	0	0	0	0	0	0	0	0	0	7	204
283	92.14	234	56	72	34	24	10	11	2	1	9	1	4	4	0	0	0	1	3	1	0	0	0	0	0	1	0	0	0	0	0	0	0	1	99
288	93.89	352	89	105	91	15	8	10	1	0	8	5	2	0	8	1	0	5	0	0	1	0	3	0	0	0	0	0	0	0	0	0	0	5	194
293	95.57	386	92	111	76	23	11	17	7	0	16	3	7	0	10	0	4	3	3	0	1	1	0	1	0	0	0	0	0	0	0	0	0	4	144
298	97.29	350	77	94	82	20	11	16	15	0	10	1	4	7	5	5	0	2	0	0	0	0	0	0	0	1	0	0	0	0	0	0	0	1	143
303	99.00	273	66	82	56	15	10	3	4	3	9	3	9	1	0	0	0	10	1	0	0	0	0	1	0	0	0	0	0	0	0	0	0	4	55
308	100.60	367	66	85	118	20	21	27	0	0	4	4	2	2	6	6	0	3	1	2	0	0	0	0	0	0	0	0	0	0	0	0	0	7	113
313	102.20	259	80	70	61	7	12	10	3	1	6	1	2	0	1	0	0	4	0	0	1	0	0	0	0	0	0	0	0	0	0	0	0	3	101
318	103.80	321	78	74	75	29	15	12	4	0	3	3	5	5	9	4	0	2	2	0	0	1	0	0	0	0	0	0	0	0	0	0	0	9	116
323	105.40	427	123	94	114	29	10	12	10	1	10	3	8	2	3	0	0	3	1	1	1	0	0	1	0	1	0	0	0	0	0	0	0	4	127
328	107.00	571	166	105	121	63	22	28	5	1	6	11	5	9	6	9	0	8	1	3	0	0	2	0	0	0	0	0	0	0	0	0	0	12	227
333	108.67	421	135	104	70	19	17	25	11	1	2	3	7	6	1	2	1	6	1	4	0	3	3	0	0	0	0	0	0	0	0	0	0	5	49
338	110.33	506	123	112	121	36	14	32	8	0	9	4	8	9	12	4	0	9	2	2	1	0	0	0	0	0	0	0	0	0	0	0	0	5	123
343	112.00	292	54	95	45	10	8	23	2	0	0	3	19	2	1	9	4	3	0	5	0	6	3	0	0	0	0	0	0	0	0	0	0	3	118
348	113.67	432	123	100	86	27	29	32	1	0	2	4	12	0	5	6	0	4	0	0	0	1	0	0	0	0	0	0	0	0	0	0	0	4	214
353	115.33	296	80	89	57	11	15	11	2	0	3	3	7	6	0	1	1	7	0	0	0	0	3	0	0	0	0	0	0	0	0	0	0	5	155
358	117.00	343	81	103	47	24	20	21	5	0	6	4	8	6	4	2	0	10	1	0	0	0	0	0	0	1	0	0	0	0	0	0	0	2	119
363	118.67	305	45	105	60	13	20	19	11	1	6	0	12	5	3	0	0	3	0	0	0	0	2	0	0	0	0	0	0	0	0	0	0	1	62
368	120.33	405	64	133	73	31	40	21	5	1	6	1	13	2	3	5	0	4	0	0	1	0	0	0	0	1	1	0	0	0	0	0	0	2	122
373	122.00	350	71	108	60	16	29	19	6	0	4	3	10	2	2	10	2	5	1	0	0	0	2	0	0	0	0	0	0	0	0	0	0	4	83
378	123.63	390	75	93	86	23	25	16	10	0	6	7	16	8	11	4	0	7	0	0	0	0	0	2	0	1	0	0	0	0	0	0	0	7	112
383	125.25	461	63	113	81	47	46	16	26	4	11	6	29	2	3	2	0	5	1	0	0	2	3	0	0	1	0	0	0	0	0	0	0	4	106
388	126.88	372	64	65	78	44	43	10	15	0	4	7	16	6	2	7	0	0	8	1	0	0	0	1	1	0	0	0	0	0	0	0	0	6	89
393	128.50	458	86	89	99	48	44	12	13	1	7	8	16	0	7	5	0	0	5	3	1	2	12	0	0	0	0	0	0	0	0	0	0	7	95

Cm below seafloor	Time (kyr)	Plk. total (not incl benthics)	N. pac (R)	Gr. inflata	Gg. bulloides	Ga. glutinata	Gs. ruber	Gr. truncatulinoides	N. dutertrei	N. pac (L)	O. universa	Gr. scitula	Gs. sacculifer	Gr. crassaformis	Ge. siphonifera	Gg. falconensis	Gg. quinqueloba	Gr. hirsuta	G. hexagona	Gr. menardii	Gg.rubescens	Gs. conglobatus	G. calida	Gs. tenellus	G. digitata	P. obliquiloculata	rubr(pk)	G. theyeri	Gr cavernula	Ga. uvula	Sphaer. dehiscens	Candeina nitid	Unknown	Benthics	Fragments
398	130.13	322	89	84	37	25	18	15	6	0	3	2	7	11	11	1	1	0	5	3	0	1	1	0	0	0	0	0	2	0	0	0	0	4	100
403	131.75	381	145	91	66	16	18	10	10	0	5	3	3	1	8	0	0	1	3	0	0	0	1	0	0	0	0	0	0	0	0	0	0	10	79
408	133.38	489	127	141	96	46	23	13	5	0	4	2	6	7	9	3	1	0	3	0	0	1	0	2	0	0	0	0	0	0	0	0	0	3	148
413	135.00	272	91	86	36	12	15	6	5	0	6	7	2	1	0	1	1	0	0	2	0	0	1	0	0	0	0	0	0	0	0	0	0	0	58
418	136.57	368	60	169	36	16	10	17	8	3	23	1	3	10	8	0	0	0	1	1	0	1	0	0	0	0	0	0	0	0	0	0	1	5	53
423	138.14	304	121	85	35	5	9	6	9	1	15	3	4	0	4	1	0	5	0	1	0	0	0	0	0	0	0	0	0	0	0	0	0	9	87
428	139.71	291	80	103	50	4	17	12	0	1	6	0	4	1	11	1	0	0	1	0	0	0	0	0	0	0	0	0	0	0	0	0	0	3	73
433	141.29	313	102	92	59	13	12	12	2	1	7	1	5	0	2	2	2	1	0	0	0	0	0	0	0	0	0	0	0	0	0	0	0	6	49
438	142.86	452	196	113	51	36	13	20	6	0	3	1	2	4	3	2	0	1	1	0	0	0	0	0	0	0	0	0	0	0	0	0	0	3	135
443	144.43	477	189	106	96	21	3	10	1	4	6	8	11	4	0	5	11	0	2	0	0	0	0	0	0	0	0	0	0	0	0	0	0	8	115
448	146.00	381	162	107	52	16	7	3	7	0	9	2	6	6	3	0	0	0	1	0	0	0	0	0	0	0	0	0	0	0	0	0	0	7	92
453	147.67	258	117	63	41	12	9	3	1	0	3	3	3	0	2	0	0	1	0	0	0	0	0	0	0	0	0	0	0	0	0	0	0	6	68
458	149.33	441	156	129	54	34	17	0	1	3	4	6	9	17	4	4	0	0	2	0	0	1	0	0	0	0	0	0	0	0	0	0	0	1	99
463	151.00	333	133	79	46	15	10	5	1	6	4	4	1	4	1	7	17	0	0	0	0	0	0	0	0	0	0	0	0	0	0	0	0	2	63
468	152.67	362	162	93	54	20	11	1	1	0	8	2	0	0	4	4	1	0	1	0	0	0	0	0	0	0	0	0	0	0	0	0	0	3	75
473	154.33	440	229	84	82	10	6	1	0	2	5	6	8	0	4	1	0	0	1	0	0	0	1	0	0	0	0	0	0	0	0	0	0	0	87
478	156.00	436	226	73	74	14	14	4	1	2	2	6	2	5	7	5	1	0	0	0	0	0	1	0	0	0	0	0	0	0	0	0	0	2	126
483	157.67	471	239	80	77	29	14	7	3	1	2	4	2	2	1	0	6	0	0	0	0	2	2	0	0	0	0	0	0	0	0	0	0	4	135
488	159.33	396	161	91	85	23	7	6	6	0	2	1	6	1	2	3	0	0	1	0	0	0	0	0	0	0	0	0	0	0	0	0	1	0	6	126
493	161.00	465	251	59	77	21	17	11	0	1	1	3	5	6	3	0	10	0	0	0	0	0	0	0	0	0	0	0	0	0	0	0	0	0	7	135
498	162.67	448	218	83	93	8	11	8	2	1	6	3	3	2	4	3	0	0	0	0	0	2	0	0	0	0	0	1	0	0	0	0	0	3	102
503	164.33	481	200	104	101	21	22	12	1	2	2	3	3	1	5	0	2	0	2	0	0	0	0	0	0	0	0	0	0	0	0	0	0	3	71
508	166.00	425	181	95	82	29	16	7	1	0	1	8	0	0	4	0	0	0	0	0	1	0	0	0	0	0	0	0	0	0	0	0	0	2	143
513	167.67	452	148	118	89	39	10	20	3	0	2	5	4	1	5	2	2	1	0	0	1	1	1	0	0	0	0	0	0	0	0	0	0	5	105
518	169.33	420	146	123	71	21	6	18	0	0	4	3	3	15	6	2	0	0	2	0	0	0	0	0	0	0	0	0	0	0	0	0	0	3	91
523	171.00	400	153	115	63	15	13	7	3	0	4	1	8	4	4	1	0	4	3	1	0	1	0	0	0	0	0	0	0	0	0	0	0	5	79
528	172.71	420	188	79	87	31	11	10	2	0	3	2	0	0	5	1	0	0	0	1	0	0	0	0	0	0	0	0	0	0	0	0	0	3	106
533	174.43	396	176	86	62	23	7	14	6	0	3	4	0	3	3	1	3	0	3	0	1	1	0	0	0	0	0	0	0	0	0	0	0	3	106
538	176.14	349	172	48	81	18	4	2	0	2	0	10	1	5	3	2	0	0	0	0	0	0	0	1	0	0	0	0	0	0	0	0	0	4	144
543	177.86	414	171	105	69	21	7	9	5	4	3	2	2	7	3	0	3	1	0	1	0	1	0	0	0	0	0	0	0	0	0	0	0	8	199
548	179.57	311	125	90	63	5	8	7	0	0	3	5	0	0	5	0	0	0	0	0	0	0	0	0	0	0	0	0	0	0	0	0	0	9	123
553	181.29	498	175	181	62	9	10	20	4	1	15	6	3	4	2	1	0	0	2	0	0	1	2	0	0	0	0	0	0	0	0	0	0	6	103
558	183.00	321	112	104	74	2	1	10	1	0	6	3	3	0	3	2	0	0	0	0	0	0	0	0	0	0	0	0	0	0	0	0	0	6	154
563	184.83	288	125	80	39	13	7	12	1	1	2	2	1	0	0	1	3	1	0	0	0	0	0	0	0	0	0	0	0	0	0	0	0	7	139
568	186.67	324	158	79	45	8	11	16	3	1	1	0	1	0	1	0	0	0	0	0	0	0	0	0	0	0	0	0	0	0	0	0	0	6	132
573	188.50	448	188	126	53	24	18	12	0	5	1	3	1	6	1	2	1	3	1	0	3	0	0	0	0	0	0	0	0	0	0	0	0	7	154
578	190.33	336	140	119	39	9	19	2	0	0	1	0	0	0	2	4	0	1	0	0	0	0	0	0	0	0	0	0	0	0	0	0	0	5	225
583	192.17	392	138	131	42	29	10	5	3	3	3	1	5	7	6	1	0	2	4	2	0	0	0	0	0	0	0	0	0	0	0	0	0	6	144
588	194.00	310	120	80	59	11	6	10	6	0	5	5	5	0	3	0	0	0	0	0	0	0	0	0	0	0	0	0	0	0	0	0	0	4	211
593	196.20	344	106	94	58	25	14	23	2	2	4	7	2	4	0	1	0	1	0	1	0	0	0	0	0	0	0	0	0	0	0	0	0	8	190
598	198.40	343	78	103	74	15	9	23	5	0	4	6	6	4	7	5	1	0	0	1	1	0	1	0	0	0	0	0	0	0	0	0	0	6	218
603	200.60	366	108	111	61	19	16	23	9	0	3	2	2	3	1	1	0	0	0	2	1	0	4	0	0	0	0	0	0	0	0	0	0	8	292
608	202.80	307	106	91	48	13	12	15	4	0	8	0	3	0	5	0	0	2	0	0	0	0	0	0	0	0	0	0	0	0	0	0	0	8	321
613	205.00	286	87	103	38	14	10	11	4	0	6	1	2	3	1	0	3	1	1	0	0	0	0	1	0	0	0	0	0	0	0	0	0	2	273
618	207.20	309	90	97	56	11	6	17	5	0	5	8	1	0	11	2	0	0	0	0	0	0	0	0	0	0	0	0	0	0	0	0	0	4	456
623	209.40	258	101	98	26	5	3	11	0	0	1	5	2	3	2	0	0	1	0	0	0	0	0	0	0	0	0	0	0	0	0	0	0	13	321
628	211.60	338	129	93	49	6	17	21	5	0	1	9	3	1	1	3	0	0	0	0	0	0	0	0	0	0	0	0	0	0	0	0	0	11	298
633	213.80	315	66	135	49	7	12	15	3	0	1	3	4	15	0	1	0	2	1	0	0	1	0	0	0	0	0	0	0	0	0	0	0	2	153
638	216.00	384	132	94	53	23	26	29	2	1	3	15	4	1	0	0	0	0	1	0	0	0	0	0	0	0	0	0	0	0	0	0	0	6	202
643	217.71	299	58	123	45	19	19	18	0	0	3	3	2	2	0	2	1	2	1	0	0	1	0	0	0	0	0	0	0	0	0	0	0	5	159
648	219.43	379	90	135	65	19	24	16	4	0	2	6	1	6	5	2	0	0	2	1	0	0	1	0	0	0	0	0	0	0	0	0	0	10	265
653	221.14	346	89	105	48	18	27	17	5	0	7	5	2	7	6	4	2	0	0	0	0	2	2	0	0	0	0	0	0	0	0	0	0	3	185
658	222.86	305	77	122	62	7	10	8	3	0	4	5	3	0	2	2	0	0	0	0	0	0	0	0	0	0	0	0	0	0	0	0	0	8	132
663	224.57	398	120	127	67	17	17	12	7	1	4	1	8	4	2	2	1	2	1	0	0	0	2	0	0	3	0	0	0	0	0	0	0	7	202
668	226.29	322	108	94	57	11	14	18	1	1	5	1	3	1	4	1	0	1	0	1	0	0	0	0	0	0	1	0	0	0	0	0	0	5	194
673	228.00	330	116	114	49	6	13	10	0	1	3	2	3	5	0	0	6	1	1	0	0	0	0	0	0	0	0	0	0	0	0	0	0	3	157
678	229.43	368	122	115	75	8	10	21	0	1	0	3	3	2	5	3	0	0	0	0	0	0	0	0	0	0	0	0	0	0	0	0	0	8	243
683	230.86	349	112	124	60	25	6	10	2	1	0	2	1	3	1	0	0	0	0	0	0	1	1	0	0	0	0	0	0	0	0	0	0	7	242
688	232.29	342	123	120	58	3	5	12	3	1	5	2	3	2	2	2	0	1	0	0	0	1	0	0	0	0	0	0	0	0	0	0	0	6	233
693	233.71	330	157	89	32	12	11	12	3	0	0	5	2	4	1	0	0	1	0	0	0	1	0	0	0	0	0	0	0	0	0	0	0	6	240
698	235.14	323	155	72	55	7	9	14	3	0	0	4	1	0	2	0	0	0	0	0	0	1	0	0	0	0	0	0	0	0	0	0	0	1	236
703	236.57	383	131	100	73	19	13	15	3	3	5	7	5	1	3	0	2	0	1	0	0	0	2	0	0	0	0	0	0	0	0	0	0	17	159
983	237.17	352	105	100	61	22	16	16	8	7	1	5	1	0	3	1	2	1	0	2	0	0	0	0	0	0	0	1	0	0	0	0	0	10	121
988	238.00	358	68	99	57	25	52	10	8	2	5	3	9	0	2	5	7	1	2	0	0	0	0	0	0	0	0	0	2	0	1	0	0	0	7	80
993	245.00	373	106	100	58	30	37	10	4	0	4	7	4	2	6	5	0	0	0	0	0	0	0	0	0	0	0	0	0	0	0	0	0	2	103
998	246.33	550	192	136	106	32	22	16	8	0	4	6	3	3	2	0	18	0	0	1	0	0	1	0	0	0	0	0	0	0	0	0	0	11	176
1003	247.67	547	183	117	82	46	32	27	6	0	6	3	12	4	6	10	11	0	0	2	0	0	0	0	0	0	0	0	0	0	0	0	0	4	109
1008	249.00	478	187	93	86	29	28	17	9	4	8	2	2	1	2	4	4	0	0	1	1	0	0	0	0	0	0	0	0	0	0	0	0	5	156
1013	250.00	513	197	125	73	32	22	17	4	0	6	9	2	2	7	12	5	0	0	0	0	0	0	0	0	0	0	0	0	0	0	0	0	4	124
1018	251.00	391	139	85	59	28	25	6	3	0	1	7	4	1	10	12	7	0	0	0	3	0	0	0	0	0	0	1	0	0	0	0	0	4	92
1023	252.00	363	146	80	48	27	23	11	3	0	2	7	1	0	2	5	7	0	0	1	0	0	0	0	0	0	0	0	0	0	0	0	0	7	116
1028	253.00	575	221	107	81	55	30	19	6	2	7	10	5	10	9	0	10	0	0	0	0	1	0	1	0	0	0	2	0	1	0	0	0	6	156
1033	254.00	486	187	118	68	25	34	19	0	0	4	6	3	6	5	5	2	0	0	2	1	0	0	1	0	0	0	0	0	0	0	0	0	2	134
1038	255.00	514	137	139	73	56	20	13	4	1	8	10	3	6	6	16	14	0	1	4	1	0	0	0	2	0	0	0	0	0	0	0	0	8	172
1043	256.00	411	174	103	51	13	16	12	6	0	6	4	5	6	4	3	6	0	0	1	0	0	0	1	0	0	0	0	0	0	0	0	0	6	158
1048	257.00	410	142	103	80	23	20	7	4	1	4	8	4	1	4	0	6	0	0	0	1	1	0	0	0	0	1	0	0	0	0	0	0	6	98
1053	259.40	558	166	175	85	35	46	7	6	0	4	12	2	2	2	5	8	0	0	2	0	0	0	0	1	0	0	0	0	0	0	0	0	8	171
1058	261.80	468	191	161	54	12	22	4	2	0	4	1	0	7	2	4	3	0	0	1	0	0	0	0	0	0	0	0	0	0	0	0	0	4	192
1063	264.20	457	176	191	39	13	16	2	2	4	6	1	0	3	0	0	2	1	0	0	1	0	0	0	0	0	0	0	0	0	0	0	0	9	209
1068	266.60	317	136	90	36	14	10	3	2	0	3	1	6	0	0	11	2	2	0	1	0	0	0	0	0	0	0	0	0	0	0	0	0	8	84
1073	269.00	330	209	11	6	19	18	2	2	44	8	1	0	2	1	0	4	1	0	2	0	0	0	0	0	0	0	0	0	0	0	0	0	9	178
1078	270.50	383	198	91	34	17	29	2	0	0	4	4	2	0	0	2	0	0	0	0	0	0	0	0	0	0	0	0	0	0	0	0	0	18	131
1083	272.00	366	165	91	43	15	27	0	2	1	8	0	1	2	2	2	5	0	0	2	0	0	0	0	0	0	0	0	0	0	0	0	0	9	145
1088	273.50	475	184	144	75	18	22	5	3	1	5	2	3	1	1	1	3	2	1	2	0	0	0	1	0	0	0	0	1	0	0	0	0	10	164

Cm below seafloor	Time (kyr)	Plk. total (not incl benthics)	N. pac (R)	Gr. inflata	Gg. bulloides	Ga. glutinata	Gs. ruber	Gr. truncatulinoides	N. dutertrei	N. pac (L)	O. universa	Gr. scitula	Gs. sacculifer	Gr. crassaformis	Ge. siphonifera	Gg. falconensis	Gg. quinqueloba	Gr. hirsuta	G. hexagona	Gr. menardii	Gg.rubescens	Gs. conglobatus	G. calida	Gs. tenellus	G. digitata	P. obliquiloculata	rubr(pk)	G. theyeri	Gr cavernula	Ga. uvula	Sphaer. dehiscens	Candeina nitid	Unknown	Benthics	Fragments
1093	275.00	328	141	102	29	11	15	4	3	1	5	3	1	0	2	4	4	0	1	1	1	0	0	0	0	0	0	0	0	0	0	0	10	203
1098	276.50	343	158	104	31	15	18	4	1	0	5	1	3	0	0	2	0	0	0	0	0	1	0	0	0	0	0	0	0	0	0	0	7	217
1103	278.00	390	157	104	61	16	21	2	1	23	1	0	2	0	1	0	1	0	0	0	0	0	0	0	0	0	0	0	0	0	0	0	9	266
1108	279.50	450	184	117	79	32	15	6	1	1	2	3	0	3	2	1	4	0	0	0	0	0	0	0	0	0	0	0	0	0	0	0	6	307
1113	281.00	392	141	130	64	15	23	7	1	1	2	1	1	3	0	1	0	0	0	0	0	0	0	0	0	2	0	0	0	0	0	0	9	208
1118	282.50	492	226	149	54	17	7	12	4	0	6	8	1	1	4	2	1	0	0	0	0	0	0	0	0	0	0	0	0	0	0	0	11	269
1123	284.00	330	82	114	54	9	25	19	8	1	10	0	3	3	2	0	0	0	0	0	0	0	0	0	0	0	0	0	0	0	0	0	7	177
1128	285.50	392	134	113	52	19	27	18	4	0	2	5	2	6	2	3	1	0	0	4	0	0	0	0	0	0	0	0	0	0	0	0	1	251
1133	287.00	441	159	119	58	24	26	16	2	0	5	15	2	0	4	0	7	0	0	2	2	0	0	0	0	0	0	0	0	0	0	0	4	283
1138	288.50	471	149	146	69	26	27	21	3	0	4	8	1	3	3	1	0	11	1	0	0	0	0	1	0	0	0	0	0	0	0	0	9	246
1143	290.00	291	80	87	46	16	19	6	4	1	7	8	1	9	1	1	3	0	1	0	0	0	1	0	0	0	0	0	0	0	0	0	3	200
1148	291.50	343	108	128	59	16	8	12	2	0	3	2	1	0	2	0	1	1	0	0	0	0	0	0	0	0	0	0	0	0	0	0	7	200
1153	293.00	328	98	105	57	18	7	13	6	0	7	1	4	2	5	4	1	0	0	0	0	0	0	0	0	0	0	0	0	0	0	0	7	200
1158	294.50	306	108	90	41	25	14	7	0	1	2	5	1	4	4	2	1	0	0	1	0	0	0	0	0	0	0	0	0	0	0	0	2	178
1163	296.00	358	148	99	60	26	8	2	3	1	1	1	0	1	2	0	5	0	0	1	0	0	0	0	0	0	0	0	0	0	0	0	5	137
1168	297.50	388	155	114	44	32	13	4	1	4	5	1	1	3	3	3	2	2	0	0	0	0	1	0	0	0	0	0	0	0	0	0	4	145
1173	299.00	325	116	100	45	14	19	6	0	0	5	4	1	0	2	2	10	0	0	1	0	0	0	0	0	0	0	0	0	0	0	0	6	217
1178	299.85	317	155	90	16	11	11	5	2	0	14	2	2	1	1	3	2	0	0	2	0	0	0	0	0	0	0	0	0	0	0	0	9	218
1183	300.69	303	124	86	34	13	14	4	4	1	3	5	6	2	1	5	1	0	0	0	0	0	0	0	0	0	0	0	0	0	0	0	6	190
1188	301.54	349	115	122	58	22	9	7	1	6	5	0	2	1	0	0	1	0	0	0	0	0	0	0	0	0	0	0	0	0	0	0	9	203
1193	302.38	409	165	109	53	19	25	12	6	0	2	7	3	0	0	4	3	0	0	1	0	0	0	0	0	0	0	0	0	0	0	0	11	231
1198	303.23	340	105	101	44	14	26	12	3	0	13	8	2	0	3	2	5	0	2	0	0	0	0	0	0	0	0	0	0	0	0	0	12	202
1203	304.08	530	152	176	98	20	15	13	5	0	32	1	9	3	3	0	2	0	1	0	0	0	0	0	0	0	0	0	0	0	0	0	9	311
1208	304.92	429	160	119	55	17	29	12	3	7	3	2	4	9	5	0	0	0	2	1	0	0	0	0	0	1	0	0	0	0	0	0	3	354
1213	305.77	545	163	191	68	16	29	18	13	9	10	6	7	7	4	0	1	0	2	0	0	0	0	0	0	0	1	0	0	0	0	0	9	386
1218	306.62	447	164	102	73	52	12	10	9	7	1	4	4	0	1	0	0	1	6	0	0	0	0	0	0	1	0	0	0	0	0	0	7	418
1223	307.46	386	185	75	62	21	19	6	4	0	2	1	0	7	1	0	0	1	1	0	0	0	0	0	0	0	0	0	0	0	0	0	115	249
1228	308.31	391	175	62	91	17	16	6	0	7	3	4	3	3	1	0	0	0	2	1	0	0	0	0	0	0	0	0	0	0	0	0	8	266
1233	309.15	356	139	97	63	11	17	10	7	3	3	1	1	0	1	0	0	0	1	2	0	0	0	0	0	0	0	0	0	0	0	0	5	236
1238	310.00	546	188	108	97	61	19	15	1	14	4	16	3	16	0	0	0	0	2	0	1	1	0	0	0	0	0	0	0	0	0	0	7	385
1243	311.67	436	149	89	89	19	19	23	8	2	2	8	9	10	1	7	0	0	1	0	0	0	0	0	0	0	0	0	0	0	0	0	3	475
1248	313.33	416	135	86	71	21	16	15	5	7	3	7	10	17	1	10	0	0	6	1	1	1	0	3	0	0	0	0	0	0	0	0	2	341
1253	315.00	339	113	64	68	28	8	9	1	12	1	8	1	11	3	3	0	0	5	1	1	1	0	0	1	0	0	0	0	0	0	0	7	385
1258	316.67	420	138	108	63	22	18	9	11	18	3	8	3	5	8	0	0	1	3	1	1	0	0	0	0	0	0	0	0	0	0	0	9	451
1263	318.33	372	147	97	64	8	14	7	2	3	0	15	1	4	3	3	0	1	2	1	0	0	0	0	0	0	0	0	0	0	0	0	5	507
1268	320.00	437	189	117	49	7	14	8	4	13	3	5	3	11	5	7	0	0	2	0	0	0	0	0	0	0	0	0	0	0	0	0	6	507
1273	321.38	359	153	106	51	6	13	8	3	1	1	6	6	5	0	0	0	0	0	0	0	0	0	0	0	0	0	0	0	0	0	0	12	980
1278	322.75	517	198	136	70	20	17	9	3	7	2	8	1	16	4	12	3	1	6	1	2	0	0	0	0	0	1	0	0	0	0	0	4	619
1283	324.13	514	181	112	58	55	20	14	4	7	1	11	8	21	2	6	0	1	7	2	0	3	0	0	1	0	0	0	0	0	0	0	14	590
1288	325.50	495	176	117	49	44	16	15	5	13	0	11	10	14	3	3	4	2	8	1	3	1	0	0	0	0	0	0	0	0	0	0	3	359
1293	326.88	538	158	121	69	35	31	14	2	49	1	7	8	12	4	11	9	0	5	1	0	0	0	0	0	1	0	0	0	0	0	0	8	431
1298	328.25	492	184	93	68	38	22	15	5	22	3	12	5	11	1	3	4	0	1	2	1	0	0	1	0	0	1	0	0	0	0	0	11	364
1303	329.63	451	137	86	70	56	29	17	5	9	3	6	7	8	3	2	0	0	5	3	2	0	0	2	0	0	1	0	0	0	0	0	1	237
1308	331.00	422	117	73	78	42	18	26	2	9	10	3	12	12	4	2	1	1	3	3	1	0	0	2	1	0	2	0	0	0	0	0	8	228
1313	331.77	400	91	68	83	55	21	19	10	8	1	3	10	2	3	9	6	5	1	0	3	0	0	0	1	0	1	0	0	0	0	0	2	170
1318	332.54	518	112	97	123	85	34	0	7	19	2	3	11	1	6	9	3	0	4	1	0	0	0	0	0	1	0	0	0	0	0	0	3	237
1323	333.31	496	116	81	82	81	33	17	11	26	2	3	7	6	8	6	7	3	5	0	0	0	0	0	1	0	1	0	0	0	0	0	13	166
1328	334.08	388	81	84	84	49	28	15	8	11	1	0	11	5	4	0	0	0	3	0	0	0	0	4	0	0	0	0	0	0	0	0	5	183
1333	334.85	423	107	80	62	69	29	15	4	11	3	3	15	7	7	0	0	0	4	2	2	0	0	0	1	0	2	0	0	0	0	0	6	262
1338	335.62	494	169	117	63	61	27	12	4	6	5	4	7	4	6	1	1	1	4	1	0	0	0	1	0	0	0	0	0	0	0	0	6	282
1343	336.38	439	188	71	68	70	15	6	1	0	2	4	1	5	3	2	0	2	1	0	0	0	0	0	0	0	0	0	0	0	0	0	5	247
1348	337.15	425	178	92	64	41	16	7	4	0	8	0	1	5	4	1	2	0	0	0	0	0	0	2	0	0	0	0	0	0	0	0	5	298
1353	337.92	390	175	79	52	40	9	9	1	6	7	0	1	2	1	5	1	0	2	0	0	0	0	0	0	0	0	0	0	0	0	0	5	272
1358	338.69	336	125	82	64	40	2	2	2	3	2	2	2	0	2	6	1	0	1	0	0	0	0	0	0	0	0	0	0	0	0	0	8	252
1363	339.46	363	151	83	61	29	3	9	3	1	2	8	2	3	2	2	3	0	1	0	0	0	0	0	0	0	0	0	0	0	0	0	3	211
1368	340.23	348	136	96	72	11	6	9	1	0	1	1	6	1	2	1	1	3	0	0	1	0	0	0	0	0	0	0	0	0	0	0	11	329
1373	341.00	373	148	84	70	24	9	5	1	4	0	6	1	5	4	2	0	1	2	1	6	0	0	0	0	0	0	0	0	0	0	0	1	175
1378	341.82	351	153	76	42	19	7	7	2	1	3	1	2	0	2	14	8	3	2	1	0	7	0	0	0	1	0	0	0	0	0	0	2	203
1383	342.64	517	253	104	68	33	11	6	2	4	2	3	6	4	2	5	7	0	4	0	2	0	0	1	0	0	0	0	0	0	0	0	11	289
1393	344.27	423	216	73	53	33	9	4	2	5	5	2	0	4	0	8	8	0	0	0	1	0	0	0	0	0	0	0	0	0	0	0	3	183
1398	345.09	423	185	96	65	22	11	9	1	6	8	3	0	3	4	5	2	1	1	0	1	0	0	0	0	0	0	0	0	0	0	0	5	226
1403	345.91	511	252	133	48	26	11	12	0	4	6	1	5	0	4	4	1	4	0	0	0	0	0	0	0	0	0	0	0	0	0	0	4	203
1408	346.73	441	191	78	76	45	8	10	6	8	4	0	2	3	0	4	3	2	0	1	0	0	0	0	0	0	0	0	0	0	0	0	10	171
1413	347.55	404	154	79	101	30	4	5	1	3	7	1	1	3	0	6	6	1	2	0	0	0	0	0	0	0	0	0	0	0	0	0	2	170
1418	348.36	328	127	91	67	16	3	6	0	0	2	3	3	6	0	3	1	0	0	0	0	0	0	0	0	0	0	0	0	0	0	0	3	171
1423	349.18	324	136	76	49	16	4	8	2	6	2	2	0	1	3	7	7	1	2	1	1	0	0	0	0	0	0	0	0	0	0	0	8	136
1428	350.00	447	183	97	72	53	5	7	3	4	7	1	4	0	0	4	1	1	3	0	2	0	0	0	0	0	0	0	0	0	0	0	5	192
1433	350.82	335	125	97	55	30	8	0	1	3	5	2	2	1	1	2	3	0	0	0	0	0	0	0	0	0	0	0	0	0	0	0	4	160
1438	351.64	340	120	99	60	25	7	1	5	5	5	3	1	4	0	0	4	1	0	0	0	0	0	0	0	0	0	0	0	0	0	0	5	155
1443	352.29	339	156	111	3	34	4	14	1	1	1	1	3	1	1	2	0	1	1	2	0	0	0	0	1	1	0	0	0	0	0	0	9	238
1448	353.27	383	136	123	43	38	5	12	9	0	8	1	0	3	1	2	0	0	0	0	1	0	0	0	1	0	0	0	0	0	0	0	6	151
1453	354.09	451	139	155	86	27	9	10	5	4	3	4	1	1	4	1	0	0	2	0	0	0	0	0	0	0	0	0	0	0	0	0	8	192
1458	354.91	371	149	120	54	18	5	7	3	3	4	0	2	0	1	1	0	0	4	0	0	0	0	0	0	0	0	0	0	0	0	0	8	161
1463	355.73	388	153	125	49	25	5	6	4	6	7	1	2	0	0	2	0	1	1	0	1	0	0	0	0	0	0	0	0	0	0	0	7	142
1468	356.55	315	151	83	33	10	6	6	3	3	2	0	1	0	5	9	0	1	0	0	1	0	0	0	0	1	0	0	0	0	0	0	5	138
1473	357.36	515	214	110	77	49	7	4	8	6	14	2	0	0	3	9	1	4	2	2	2	1	0	0	0	0	0	0	0	0	0	0	8	216
1478	358.18	500	176	105	76	60	12	13	8	10	3	2	2	0	5	9	10	1	1	1	0	0	2	3	1	1	0	0	0	0	0	0	12	333
1483	359.00	420	155	90	77	31	15	5	5	2	6	5	2	11	1	7	6	1	0	1	0	0	0	0	0	0	0	0	0	0	0	0	9	249
1488	359.82	354	130	89	53	28	12	7	5	2	3	4	1	0	1	10	1	1	0	6	0	0	0	0	0	0	1	0	0	0	0	0	8	247
1493	360.64	466	174	145	52	27	4	9	8	10	15	2	0	1	0	7	4	0	1	4	0	2	0	1	0	0	0	0	0	0	0	0	8	378
1498	361.45	446	176	122	72	35	6	4	2	2	3	2	1	4	1	8	5	1	1	1	0	0	0	0	0	0	0	0	0	0	0	0	10	351
1503	362.27	344	125	89	62	27	7	8	8	4	4	0	1	4	1	1	2	0	0	1	0	0	0	0	0	0	0	0	0	0	0	0	5	262
1508	363.09	301	78	101	58	21	8	6	2	3	3	1	8	0	4	4	2	0	1	1	0	0	0	0	0	0	0	0	0	0	0	0	4	254
1513	363.91	318	121	92	41	21	11	7	3	1	4	1	3	2	2	3	0	0	4	1	0	0	0	1	0	0	0	0	0	0	0	0	11	411

Cm below seafloor	Time (kyr)	Plk. total (not incl benthics)	N. pac (R)	Gr. inflata	Gg. bulloides	Ga. glutinata	Gs. ruber	Gr. truncatulinoides	N. dutertrei	N. pac (L)	O. universa	Gr. scitula	Gs. sacculifer	Gr. crassaformis	Ge. siphonifera	Gg. falconensis	Gg. quinqueloba	Gr. hirsuta	G. hexagona	Gr. menardii	Gg.rubescens	Gs. conglobatus	G. calida	Gs. tenellus	G. digitata	P. obliquiloculata	rubr(pk)	G. theyeri	Gr cavernula	Ga. uvula	Sphaer. dehiscens	Candeina nitid	Unknown	Benthics	Fragments
1518	364.73	378	118	87	54	40	19	13	10	1	4	3	3	8	0	11	0	3	1	1	0	0	2	0	0	0	0	0	0	0	0	0	13	800
1523	365.55	333	105	106	44	33	8	16	5	1	1	3	2	3	1	1	0	1	3	0	0	0	0	0	0	0	0	0	0	0	0	0	19	508
1528	366.36	414	123	134	71	31	12	11	6	3	1	3	2	5	0	9	1	0	1	0	0	0	1	0	0	0	0	0	0	0	0	0	19	387
1533	367.18	448	136	83	84	39	21	25	12	6	9	2	7	7	1	7	0	5	1	0	2	0	1	0	0	0	0	0	0	0	0	0	9	374
1538	368.00	404	114	107	65	43	15	14	9	6	4	8	1	4	1	2	1	2	3	2	1	0	2	0	0	0	0	0	0	0	0	0	19	581
1543	371.50	326	84	142	31	24	5	7	4	12	3	2	4	2	0	1	0	1	1	3	0	0	0	0	0	0	0	0	0	0	0	0	19	401
1548	375.00	446	129	164	51	37	5	7	11	11	5	4	2	7	1	8	0	3	1	0	0	0	0	0	0	0	0	0	0	0	0	0	12	469
1553	376.76	325	78	119	43	23	9	14	3	6	3	5	5	3	1	6	0	1	5	1	0	0	0	0	0	0	0	0	0	0	0	0	12	554
1558	378.53	411	90	143	43	33	24	20	3	12	3	6	2	7	8	3	3	7	2	2	0	0	0	0	0	0	0	0	0	0	0	0	17	562
1563	380.29	314	64	87	40	23	15	30	7	4	7	9	4	9	1	4	0	1	5	2	0	0	1	0	0	0	0	1	0	0	0	0	8	326
1568	382.06	497	87	143	80	56	44	27	4	4	4	14	11	9	1	3	0	1	5	1	0	0	0	0	0	0	3	0	0	0	0	0	17	556
1573	383.82	316	59	74	43	50	41	15	1	0	5	10	1	4	1	4	1	1	4	0	0	0	1	0	0	1	0	0	0	0	0	0	5	450
1578	385.59	403	74	97	64	45	32	32	14	3	2	10	6	6	6	1	0	0	5	0	0	3	2	0	0	0	1	0	0	0	0	0	4	452
1583	387.35	459	82	94	89	36	44	39	16	4	4	13	6	14	3	1	0	1	7	5	1	0	0	0	0	0	0	0	0	0	0	0	7	469
1588	389.12	365	75	77	64	50	34	15	9	2	4	12	4	7	2	2	0	0	5	1	0	1	0	0	0	1	0	0	0	0	0	0	14	391
1593	390.88	387	70	111	51	34	26	33	10	6	4	8	10	12	5	1	0	1	3	0	1	0	1	0	0	0	0	0	0	0	0	0	9	437
1598	392.65	425	92	103	66	38	29	29	18	4	11	8	7	2	3	3	3	0	3	0	4	0	0	0	0	0	1	1	0	0	0	0	13	476
1603	394.41	375	88	117	57	27	18	23	4	7	4	7	6	8	2	2	2	0	0	2	1	0	0	0	0	0	0	0	0	0	0	0	13	454
1608	396.18	453	139	122	61	28	22	32	11	1	3	8	4	3	2	9	0	2	2	2	2	0	0	0	0	0	0	0	0	0	0	0	11	471
1613	397.94	377	102	92	57	24	28	30	13	2	0	7	5	0	0	6	1	0	3	1	5	1	0	0	0	0	0	0	0	0	0	0	9	342
1618	399.71	381	82	121	64	25	32	11	3	4	5	9	9	1	5	1	0	0	4	1	2	0	2	0	0	0	0	0	0	0	0	0	12	311
1623	401.47	370	116	88	55	27	26	26	7	1	4	7	1	0	4	5	1	0	0	1	1	0	0	0	0	0	0	0	0	0	0	0	2	395
1628	403.24	416	119	98	76	28	27	34	5	1	1	8	1	1	5	4	1	0	1	0	3	1	1	0	1	0	0	0	0	0	0	0	7	353
1633	405.00	428	111	100	67	25	30	39	5	5	2	7	7	7	1	3	1	1	0	2	12	1	0	0	1	0	1	0	0	0	0	0	6	363
1638	406.93	319	103	78	48	26	17	19	8	1	4	5	1	1	3	2	0	0	0	2	0	0	0	0	1	0	0	0	0	0	0	0	8	312
1643	408.87	405	124	96	71	33	26	20	12	2	1	6	6	2	1	0	1	0	1	0	2	0	0	0	0	1	0	0	0	0	0	0	9	273
1648	410.80	524	138	102	74	48	59	32	15	0	6	7	8	7	6	2	0	3	1	0	10	2	0	0	3	0	1	0	0	0	0	0	13	417
1653	412.73	322	109	60	46	26	15	15	9	1	15	5	10	1	3	0	0	0	0	3	0	1	0	0	0	0	3	0	0	0	0	0	6	160
1658	414.67	421	135	74	62	47	29	17	17	4	5	10	5	6	3	2	0	0	2	0	0	1	1	0	0	0	1	0	0	0	0	0	9	202
1663	416.60	439	134	79	93	42	26	18	5	0	7	10	5	10	2	4	0	2	0	0	1	0	0	0	1	0	0	0	0	0	0	0	9	293
1668	418.53	443	135	77	75	49	30	20	9	5	10	8	5	4	3	2	0	1	2	0	6	2	0	0	0	0	0	0	0	0	0	0	2	168
1673	420.47	553	163	79	95	56	55	21	30	1	7	10	11	8	5	6	1	0	4	0	1	0	0	0	0	0	0	0	0	0	0	0	4	191
1678	422.40	473	128	82	98	44	34	25	14	8	2	10	5	6	6	5	0	0	1	2	0	3	0	0	0	0	0	0	0	0	0	0	4	143
1683	424.33	546	149	70	157	86	34	0	11	3	3	10	8	2	2	0	0	2	3	2	2	1	0	0	0	0	1	0	0	0	0	0	3	229
1688	426.27	388	103	69	80	49	31	7	10	2	2	6	5	3	8	0	0	0	3	2	2	2	0	0	4	0	0	0	0	0	0	0	4	163
1693	428.20	345	140	61	48	39	15	4	3	4	4	4	6	4	2	5	0	0	2	0	1	0	1	0	2	0	0	0	0	0	0	0	2	205
1698	430.13	449	223	73	84	32	9	5	5	1	4	1	2	0	2	0	0	1	2	0	0	0	0	0	0	0	0	0	0	0	0	0	5	241
1703	432.07	424	222	71	73	24	10	1	5	4	4	5	1	0	1	3	0	0	0	0	0	0	0	0	0	0	0	0	0	0	0	0	7	264
1708	434.00	405	180	74	92	16	5	2	5	12	4	1	2	0	1	5	1	0	0	2	1	2	0	0	0	0	0	0	0	0	0	0	10	288
1713	436.85	418	171	100	82	23	10	4	4	3	4	2	1	3	1	4	2	1	0	3	0	0	0	0	0	0	0	0	0	0	0	0	9	284
1718	439.69	463	206	107	94	8	8	6	5	4	6	1	1	0	2	6	5	2	0	2	0	0	0	0	0	0	0	0	0	0	0	0	8	259
1723	442.54	406	165	95	92	9	13	3	1	10	4	1	1	1	3	4	0	0	0	0	0	2	0	0	2	0	0	0	0	0	0	0	5	207
1728	445.39	378	161	84	79	22	2	10	1	4	10	0	0	0	0	3	2	0	0	0	0	0	0	0	0	0	0	0	0	0	0	0	4	186
1733	448.23	466	191	91	101	30	12	3	4	3	8	1	3	0	5	5	9	0	0	0	0	0	0	0	0	0	0	0	0	0	0	0	4	309
1738	451.08	373	140	92	84	20	5	2	5	4	4	0	0	3	1	10	0	0	0	0	0	0	0	0	3	0	0	0	0	0	0	0	5	194
1743	453.92	410	155	105	89	15	5	3	6	25	0	0	0	0	0	5	2	0	0	0	0	0	0	0	0	0	0	0	0	0	0	0	3	294
1748	456.77	349	132	80	80	12	9	1	3	8	3	2	1	4	1	1	10	0	0	1	0	0	0	0	1	0	0	0	0	0	0	0	8	168
1753	459.62	427	168	115	51	42	5	2	7	7	3	5	4	1	4	1	10	2	0	0	0	0	0	0	0	0	0	0	0	0	0	0	2	228
1758	462.46	411	168	94	63	22	5	1	1	32	6	0	2	4	2	3	8	0	0	0	0	0	0	0	0	0	0	0	0	0	0	0	4	159
1763	465.31	451	157	136	69	10	8	4	3	44	0	2	0	3	0	5	9	1	0	0	0	0	0	0	0	0	0	0	0	0	0	0	5	216
1768	468.15	366	193	80	50	10	7	3	3	9	1	0	0	4	0	0	5	0	0	1	0	0	0	0	0	0	0	0	0	0	0	0	3	253
1773	471.00	360	144	82	64	15	5	7	3	16	2	2	3	1	2	2	10	0	0	2	0	0	0	0	0	0	0	0	0	0	0	0	1	120
1778	472.75	408	142	114	76	9	10	2	9	15	5	6	2	8	1	4	2	1	0	2	0	0	0	0	0	0	0	0	0	0	0	0	5	145
1783	474.50	439	160	136	57	14	3	2	5	35	8	0	4	3	0	2	10	0	0	0	0	0	0	0	0	0	0	0	0	0	0	0	6	235
1788	476.25	400	194	99	63	2	1	3	4	24	3	0	1	0	0	0	4	0	0	2	0	0	0	0	0	0	0	0	0	0	0	0	3	183
1793	478.00	399	156	103	62	8	5	8	3	34	8	0	0	3	0	3	6	0	0	0	0	0	0	0	0	0	0	0	0	0	0	0	8	192
1798	479.75	369	134	136	52	2	7	6	5	18	2	0	0	1	0	1	4	0	0	1	0	0	0	0	0	0	0	0	0	0	0	0	4	196
1803	481.50	419	157	153	49	3	0	7	7	30	3	0	2	4	1	0	3	0	0	0	0	0	0	0	0	0	0	0	0	0	0	0	11	316
1808	483.25	381	140	127	36	8	3	7	4	35	4	0	2	8	1	2	4	0	0	0	0	0	0	0	0	0	0	0	0	0	0	0	11	207
1813	485.00	392	174	108	42	14	1	11	4	30	3	0	3	0	1	0	0	0	0	1	0	0	0	0	0	0	0	0	0	0	0	0	7	288
1818	486.75	345	130	94	52	10	2	7	4	29	0	1	3	3	0	5	2	1	0	2	0	0	0	0	0	0	0	0	0	0	0	0	5	181
1823	488.50	423	165	91	66	20	13	11	5	29	3	3	2	6	0	1	6	0	0	0	0	1	0	0	1	0	0	0	0	0	0	0	8	238
1828	490.25	480	202	97	74	21	5	15	7	36	2	3	2	3	4	4	3	1	0	1	0	0	0	0	0	0	0	0	0	0	0	0	15	263
1833	492.00	418	170	102	40	35	2	19	8	13	7	3	2	4	3	4	0	3	0	3	0	0	0	0	0	0	0	0	0	0	0	0	15	225
1838	493.75	389	141	102	35	44	9	12	8	13	3	0	8	1	3	6	1	2	0	0	0	1	0	0	0	0	0	0	0	0	0	0	18	402
1843	495.50	305	107	76	59	18	4	10	3	7	1	2	1	2	2	2	6	1	0	1	1	0	1	0	0	1	0	0	0	0	0	0	18	404
1848	497.25	322	85	106	43	23	5	27	7	7	3	2	4	1	3	1	3	0	0	0	0	1	1	0	0	0	0	0	0	0	0	0	9	520
1853	499.00	373	146	124	40	12	7	21	4	8	2	0	0	1	3	2	2	0	0	0	0	0	0	0	0	0	0	0	0	1	0	0	22	455
1858	500.75	376	119	100	65	18	17	17	7	8	4	2	3	5	2	4	3	0	1	0	0	0	0	0	1	0	0	0	0	0	0	0	13	318
1863	502.50	418	148	110	53	26	11	20	6	14	0	9	2	3	4	1	7	1	1	0	0	2	0	0	0	0	0	0	0	0	0	0	30	503
1868	504.25	362	132	100	41	17	17	12	13	6	5	3	0	2	6	2	2	0	0	2	0	0	1	0	1	0	0	0	0	0	0	0	15	274
1873	506.00	437	145	114	66	33	16	12	8	10	1	3	5	8	6	2	4	0	0	2	0	0	0	0	0	1	0	0	0	1	0	0	8	342
1878	507.75	410	137	86	72	23	18	10	10	14	3	12	1	3	5	3	7	0	0	2	0	1	0	0	0	0	3	0	0	0	0	0	11	286
1883	509.50	392	150	98	53	20	14	15	6	9	2	6	3	5	1	4	3	1	0	1	0	0	0	0	0	0	1	0	0	0	0	0	13	238
1888	511.25	419	185	82	74	20	13	13	11	6	0	4	2	1	2	3	2	0	0	0	0	0	0	0	1	0	0	0	0	0	0	0	7	152
1893	513.00	381	173	62	60	28	10	15	3	8	2	4	2	1	4	1	4	2	0	2	0	0	0	0	0	0	0	0	0	0	0	0	6	247
1898	520.14	375	146	71	64	33	7	16	13	5	2	3	4	1	5	0	4	0	0	0	0	0	0	0	0	1	0	0	0	0	0	0	7	173
1903	527.29	400	175	69	62	33	16	5	7	5	0	3	4	5	3	7	4	0	2	0	0	0	0	0	0	0	0	0	0	0	0	0	3	273
1908	534.43	444	177	83	75	45	14	13	4	5	1	9	2	6	1	4	4	0	0	0	0	0	1	0	0	0	0	0	0	0	0	0	4	209
1913	541.57	318	134	50	49	23	10	8	5	7	3	3	6	6	3	3	5	2	0	0	0	1	0	0	0	0	0	0	0	0	0	0	5	151
1918	548.71	388	170	75	70	24	6	9	5	0	5	3	10	4	2	1	4	0	0	0	0	0	0	0	0	0	0	0	0	0	0	0	3	211
1923	555.86	476	223	82	68	42	11	6	8	8	4	6	1	7	3	1	5	0	0	1	0	0	0	0	0	0	0	0	0	0	0	0	10	251
1928	563.00	410	198	80	47	23	7	13	8	8	1	2	0	8	8	0	4	3	0	0	0	0	0	0	0	0	0	0	0	0	0	0	7	206
1933	564.10	392	159	82	63	27	5	11	2	7	5	3	6	5	5	4	4	1	1	0	0	0	0	0	2	0	0	0	0	0	0	0	5	183

Cm below seafloor	Time (kyr)	Plk. total (not incl benthics)	N. pac (R)	Gr. inflata	Gg. bulloides	Ga. glutinata	Gs. ruber	Gr. truncatulinoides	N. dutertrei	N. pac (L)	O. universa	Gr. scitula	Gs. sacculifer	Gr. crassaformis	Ge. siphonifera	Gg. falconensis	Gg. quinqueloba	Gr. hirsuta	G. hexagona	Gr. menardii	Gg.rubescens	Gs. conglobatus	G. calida	Gs. tenellus	G. digitata	P. obliquiloculata	rubr(pk)	G. theyeri	Gr cavernula	Ga. uvula	Sphaer. dehiscens	Candeina nitid	Unknown	Benthics	Fragments
1938	565.20	418	175	75	68	23	9	11	12	2	2	5	6	4	4	6	6	2	0	0	0	7	0	0	1	0	0	0	0	0	0	0	0	6	160
1943	566.30	308	146	78	25	19	2	10	7	8	4	0	0	0	0	4	3	1	0	1	0	0	0	0	0	0	0	0	0	0	0	0	0	5	153
1948	567.40	447	207	100	50	29	12	12	11	8	1	0	1	1	3	8	3	1	0	0	0	0	0	0	0	0	0	0	0	0	0	0	0	7	156
1953	568.50	346	148	79	38	23	12	8	11	5	0	1	1	5	5	3	6	0	0	1	0	0	0	0	0	0	0	0	0	0	0	0	0	7	183
1958	569.60	369	155	75	37	41	16	9	9	2	4	1	1	1	1	5	8	1	0	2	0	1	0	0	0	0	0	0	0	0	0	0	0	6	258
1963	570.70	348	172	102	28	8	13	5	4	1	3	0	5	3	0	3	0	0	0	1	0	0	0	0	0	0	0	0	0	0	0	0	0	8	235
1968	571.80	411	179	87	48	18	18	8	7	9	5	3	2	2	10	8	4	1	2	0	0	0	0	0	0	0	0	0	0	0	0	0	0	15	217
1973	572.90	370	193	80	31	14	12	3	11	5	4	0	3	2	2	2	7	1	0	0	0	0	0	0	0	0	0	0	0	0	0	0	0	0	234
1978	574.00	420	167	91	53	32	20	9	8	5	2	4	7	4	4	0	10	1	0	0	0	0	0	0	1	1	0	0	0	1	0	0	0	3	262
1983	579.38	378	132	57	69	39	24	12	9	6	5	4	4	2	3	3	8	1	0	0	0	0	0	0	0	0	0	0	0	0	0	0	0	7	170
1988	584.75	470	155	59	73	62	31	17	13	3	9	5	6	8	9	9	9	0	0	1	0	1	0	0	0	0	0	0	0	0	0	0	0	7	236
1993	590.13	380	189	45	38	20	14	6	14	10	10	1	7	1	3	5	8	2	3	2	0	0	0	0	1	0	0	1	0	0	0	0	0	7	111
1998	595.50	416	192	55	51	38	17	7	22	3	3	1	5	5	4	2	6	1	1	0	0	0	0	0	0	0	0	2	0	1	0	0	0	3	133
2003	600.88	426	208	53	48	37	22	4	13	3	13	1	2	2	2	0	4	3	4	2	0	0	0	0	5	0	0	0	0	0	0	0	0	8	146
2008	606.25	438	176	72	69	27	25	11	17	4	5	3	2	7	8	1	2	0	8	1	0	0	0	0	0	0	0	0	0	0	0	0	0	3	155
2013	611.63	366	134	82	65	17	6	11	21	1	7	3	5	1	1	5	1	3	1	2	0	0	0	0	0	0	0	0	0	0	0	0	0	9	111
2018	617.00	407	169	92	52	23	21	12	8	8	9	4	1	1	3	1	1	0	0	2	0	0	0	0	0	0	0	0	0	0	0	0	0	5	207
2023	618.83	416	176	95	53	32	12	7	6	7	5	1	1	3	7	2	4	1	1	2	0	0	0	0	1	0	0	0	0	0	0	0	0	11	183
2028	620.67	406	187	53	68	42	14	9	9	7	3	0	2	3	2	4	0	0	2	1	0	0	0	0	0	0	0	0	0	0	0	0	0	3	250
2033	622.50	355	147	75	58	27	11	10	8	2	4	2	2	4	1	1	1	0	1	1	0	0	0	0	0	0	0	0	0	0	0	0	0	10	231
2038	624.33	418	143	75	71	39	30	11	14	6	5	3	4	8	3	2	0	0	3	1	0	0	0	0	0	0	0	0	0	0	0	0	0	3	133
2043	626.17	456	160	77	86	50	16	9	3	4	3	5	3	16	6	5	4	2	4	0	0	2	0	0	0	1	0	0	0	0	0	0	0	8	99
2048	628.00	399	134	56	77	53	21	6	6	12	5	2	3	10	0	5	2	0	5	1	0	0	0	0	0	0	0	1	0	0	0	0	0	3	59
2053	631.00	419	129	87	92	49	5	4	3	13	7	4	1	10	6	0	8	1	0	0	0	0	0	0	0	0	0	0	0	0	0	0	0	2	40
2058	641.00	391	114	78	90	33	16	15	3	2	7	3	1	8	2	4	3	2	8	2	0	0	0	0	0	0	0	0	0	0	0	0	0	0	40
2073	668.00	413	176	87	81	19	5	11	2	5	5	1	3	5	4	4	2	1	0	2	0	0	0	0	0	0	0	0	0	0	0	0	0	1	98
2078	679.00	376	151	80	64	19	6	13	9	9	5	6	1	4	4	2	0	1	0	2	0	0	0	0	0	0	0	0	0	0	0	0	0	2	79
2083	681.50	403	140	91	82	30	4	9	5	5	3	1	2	19	4	2	3	3	0	0	0	0	0	0	0	0	0	0	0	0	0	0	0	1	92
2088	684.00	350	154	68	70	11	5	7	5	7	4	0	0	8	2	5	2	0	0	0	0	1	1	0	0	0	0	0	0	0	0	0	0	0	138
2093	689.00	391	133	86	87	25	9	16	2	9	3	5	3	9	1	2	0	0	0	1	0	0	0	0	0	0	0	0	0	0	0	0	0	4	141
2098	690.00	423	213	96	62	8	8	12	4	6	4	3	2	0	0	1	4	0	0	0	0	0	0	0	0	0	0	0	0	0	0	0	0	7	211
2103	691.00	381	132	126	67	15	2	12	6	4	3	1	1	5	1	0	4	1	1	0	0	0	0	0	0	0	0	0	0	0	0	0	0	2	119
2108	692.00	382	134	116	67	10	3	15	4	16	3	1	0	1	4	0	4	0	0	1	0	0	3	0	0	0	0	0	0	0	0	0	0	4	152
2113	693.00	372	135	122	47	12	9	18	1	15	2	1	0	4	0	1	1	3	0	1	0	0	0	0	0	0	0	0	0	0	0	0	0	3	163

APPENDIX 3.2

Foraminiferal assemblage counts for core GeoB 3603-2.

Cm below seafloor	Time (kyr)	Plk. total (not incl benthics)	N. pac (R)	Gr. inflata	Gg. bulloides	Ga. glutinata	Gs. ruber	Gr. truncatulinoides	N. dutertrei	N. pac (L)	O. universa	Gr. scitula	Gs. sacculifer	Gr. crassaformis	Ge. siphonifera	Gg. falconensis	Gg. quinqueloba	Gr. hirsuta	G. hexagona	Gr. menardii	Gg.rubescens	Gs. conglobatus	G. calida	Gs. tenellus	G. digitata	P. obliquiloculata	rubr(pk)	G. theyeri	Gr cavernula	Ga. uvula	Sphaer. dehiscens	Candeina nitid	Unknown	Benthics	Fragments
8	4.00	510	70	107	116	43	44	23	20	1	6	6	18	13	15	14	1	4	1	4	0	0	0	0	3	0	0	0	0	0	0	1	8	107
13	7.00	408	43	129	101	8	31	14	15	3	2	14	13	0	9	0	0	8	4	3	2	0	1	6	0	0	0	2	0	0	0	0	5	151
18	10.00	309	75	85	48	12	18	6	16	0	6	5	6	7	11	2	0	2	4	0	0	1	0	2	0	0	0	1	1	1	0	0	5	90
23	13.00	393	92	150	56	0	15	9	14	0	13	4	11	3	13	0	0	5	0	3	2	1	0	2	0	0	0	0	1	0	0	0	6	82
28	16.00	417	193	92	73	12	10	6	2	4	6	2	2	2	6	0	0	6	0	0	0	1	0	0	0	0	0	0	0	0	0	0	0	57
33	19.00	410	247	50	66	14	7	10	0	5	4	2	0	0	2	0	0	3	0	0	0	0	0	0	0	0	0	0	0	0	0	0	2	79
38	20.50	373	211	49	60	18	1	4	6	2	3	3	3	4	3	1	2	0	3	0	0	0	0	0	0	0	0	0	0	0	0	0	3	59
43	22.00	317	109	72	68	1	15	11	5	0	9	2	10	0	7	0	0	7	0	0	0	1	0	0	0	0	0	0	0	0	0	0	3	80
48	23.50	451	233	71	65	34	5	3	2	0	7	1	5	8	4	2	4	2	0	0	2	0	0	0	0	0	0	1	2	0	0	0	7	74
53	25.00	394	170	93	69	11	10	6	2	2	0	3	1	0	9	0	12	2	0	1	0	0	2	1	0	0	0	0	0	0	0	0	5	76
58	26.50	321	172	49	49	15	7	4	2	1	0	2	2	1	2	3	6	2	3	0	0	0	1	0	0	0	0	0	0	0	0	0	3	107
63	28.00	436	224	56	77	18	11	4	0	3	4	3	3	9	5	5	7	1	6	0	0	0	0	0	0	0	0	0	0	0	0	0	9	116
68	29.39	391	194	75	56	24	8	11	0	2	5	1	0	2	6	3	0	3	1	0	0	0	0	0	0	0	0	0	0	0	0	0	5	77
73	30.78	481	205	81	89	30	9	10	3	8	10	3	9	5	1	1	6	0	11	0	0	0	0	0	0	0	0	0	0	0	0	0	7	178
78	32.17	468	198	67	89	40	19	7	6	1	8	2	1	3	6	7	8	0	0	3	0	0	0	0	0	1	0	0	1	1	0	0	4	92
83	33.56	427	229	50	65	38	11	9	0	6	3	2	4	2	2	1	1	1	0	1	0	0	0	0	0	0	0	0	1	0	0	0	1	103
88	34.94	451	203	88	82	29	20	3	3	0	5	2	1	3	2	4	0	3	3	0	0	0	0	0	0	0	0	0	0	0	0	0	2	87
93	36.33	471	199	97	105	9	20	8	2	2	8	5	2	4	6	1	1	0	0	1	0	0	0	0	0	1	0	0	0	0	0	0	5	96
98	37.72	313	130	59	65	29	7	7	0	0	4	0	0	5	3	1	2	1	0	0	0	0	0	0	0	0	0	0	0	0	0	0	0	73
103	39.11	341	147	52	89	17	2	7	0	1	6	3	5	4	4	1	0	0	0	1	2	0	0	0	0	0	0	0	0	0	0	0	2	68
108	40.50	521	268	94	112	15	5	7	4	2	1	3	3	2	3	1	0	0	1	0	0	0	0	0	0	0	0	0	0	0	0	0	6	114
113	41.89	253	128	42	50	13	5	2	1	1	0	2	1	4	2	0	1	0	0	1	0	0	0	0	0	0	0	0	0	0	0	0	3	55
118	43.28	411	180	59	68	19	15	8	4	3	5	2	3	7	14	3	15	1	0	1	0	0	1	0	0	1	0	0	2	0	0	0	5	87
123	44.67	488	214	76	110	28	24	7	3	4	5	3	0	1	7	2	0	1	0	0	2	0	0	0	0	1	0	0	0	0	0	0	2	106
128	46.06	460	187	96	100	23	6	8	5	2	7	1	1	9	2	6	3	2	0	0	0	0	1	0	0	0	0	1	0	0	0	0	3	87
133	47.44	404	140	122	77	37	6	7	0	3	2	3	2	1	3	0	0	1	0	0	0	0	0	0	0	0	0	0	0	0	0	0	1	68
138	48.83	302	85	76	76	14	11	11	0	0	8	5	0	3	4	4	2	3	0	0	0	0	0	0	0	0	0	0	0	0	0	0	2	52
143	50.22	406	133	93	105	28	13	11	0	4	6	4	0	0	6	0	0	3	0	0	0	0	0	0	0	0	0	0	0	0	0	0	3	96
148	51.61	359	135	84	64	17	8	16	6	1	7	5	3	0	2	1	3	1	3	2	1	0	0	0	0	0	0	0	0	0	0	0	8	82
153	53.00	370	136	84	77	24	10	18	1	1	4	6	0	3	2	1	1	1	0	0	0	1	0	0	0	0	0	0	0	0	0	0	1	83
158	54.50	389	145	78	85	31	7	14	1	1	1	3	1	0	5	7	1	7	1	0	1	0	0	0	0	0	0	0	0	0	0	0	5	79
163	56.00	358	157	64	70	26	10	9	2	4	4	3	2	3	1	0	0	3	0	0	0	0	0	0	0	0	0	0	0	0	0	0	4	79
168	57.50	374	143	94	91	15	5	7	4	1	1	3	3	2	3	1	0	0	1	0	0	0	0	0	0	0	0	0	0	0	0	0	8	100
173	59.00	409	188	100	62	23	6	8	1	4	4	3	3	0	1	0	0	4	1	0	0	0	1	0	0	0	0	0	0	0	0	0	2	89
178	60.50	297	129	49	61	19	9	7	0	2	3	3	0	4	6	2	1	1	0	0	1	0	0	0	0	0	0	0	0	0	0	0	5	65
183	62.00	415	116	147	89	25	3	15	3	1	3	3	1	1	5	1	0	2	0	0	0	0	0	0	0	0	0	0	0	0	0	0	5	70
188	63.50	405	163	78	92	25	7	6	4	0	8	4	1	3	10	1	0	2	0	1	0	0	0	0	0	0	0	0	0	0	0	0	1	59
193	65.00	464	208	106	70	9	11	12	16	0	10	7	8	0	1	0	0	1	2	0	0	2	0	0	0	1	0	0	0	0	0	0	11	4
198	66.36	380	165	80	85	22	4	4	0	4	1	0	6	2	1	1	0	0	0	0	0	0	0	0	0	0	0	1	0	0	0	0	6	79
203	67.73	397	180	56	66	8	11	22	24	1	5	1	8	1	2	0	0	3	2	3	2	2	0	0	0	0	0	0	0	0	0	0	2	36
208	69.09	414	218	57	82	17	8	7	5	0	2	2	3	3	1	6	0	0	3	0	0	0	0	0	0	0	0	0	0	0	0	0	4	131
213	70.45	479	240	62	108	18	12	4	10	0	8	5	7	1	2	0	0	2	0	0	0	0	0	0	0	0	0	0	0	0	0	0	6	63
218	71.56	329	170	41	33	15	9	14	1	1	6	5	6	3	5	10	3	3	2	2	0	0	0	0	0	0	0	0	0	0	0	0	3	109
223	73.18	375	199	40	29	21	29	8	8	0	3	7	16	4	2	0	0	6	2	0	0	1	0	0	0	0	0	0	0	0	0	0	3	26
228	74.55	456	225	60	79	21	11	8	4	0	3	13	4	7	4	6	0	3	4	0	0	2	0	0	0	0	0	0	2	0	0	0	6	126
233	75.91	355	106	98	76	35	8	7	5	0	1	4	3	5	5	0	0	2	0	0	0	0	0	0	0	0	0	0	0	0	0	0	5	46
238	77.27	409	203	54	76	19	9	14	1	0	2	8	5	3	4	2	4	3	1	1	0	0	0	0	0	0	0	0	0	0	0	0	3	91
243	78.64	330	139	57	58	26	8	9	7	1	1	5	5	1	8	0	3	2	0	0	0	0	0	0	0	0	0	0	0	0	0	0	6	59
248	80.00	520	220	57	138	32	17	12	6	0	4	5	1	8	12	6	0	1	0	1	0	0	0	0	0	0	0	0	0	0	0	0	6	152
253	81.75	307	107	47	69	49	5	4	3	1	0	5	6	2	1	0	1	2	3	0	0	2	0	0	0	0	0	0	0	0	0	0	5	76
258	83.50	359	66	133	66	16	27	21	2	0	4	4	5	2	7	3	0	2	1	0	0	0	0	0	0	0	0	0	0	0	0	0	11	185
263	85.25	359	65	117	66	28	20	0	5	1	9	2	4	1	6	10	0	4	1	0	2	6	8	2	0	2	0	0	0	0	0	0	5	120
268	87.00	407	126	117	63	19	18	32	1	2	2	5	3	3	3	4	1	4	0	0	0	0	0	0	0	4	0	0	0	0	0	0	5	81
273	88.71	618	140	167	143	51	18	30	6	0	6	12	16	4	5	0	0	10	2	2	0	2	0	1	0	1	0	0	2	0	0	0	6	146
278	90.43	316	107	80	72	14	11	14	1	0	3	6	0	3	3	1	0	0	0	0	1	0	0	0	0	0	0	0	0	0	0	0	7	204
283	92.14	234	56	72	34	24	10	11	2	1	9	1	4	4	0	0	0	1	3	1	0	0	0	0	0	1	0	0	0	0	0	0	1	99
288	93.89	352	89	105	91	15	8	10	1	0	8	5	2	0	8	1	0	5	0	0	1	0	3	0	0	0	0	0	0	0	0	0	5	194
293	95.57	386	92	111	76	23	11	17	7	0	16	3	7	0	10	0	4	3	3	0	1	1	0	1	0	0	0	0	0	0	0	0	4	144
298	97.29	350	77	94	82	20	11	16	15	0	10	1	4	7	5	5	0	2	0	0	0	0	0	0	0	1	0	0	0	0	0	0	1	143
303	99.00	273	66	82	56	15	10	3	4	3	9	3	9	1	0	0	0	10	1	0	0	0	0	1	0	0	0	0	0	0	0	0	4	55
308	100.60	367	66	85	118	20	21	27	0	0	4	4	2	2	6	6	0	3	1	2	0	0	0	0	0	0	0	0	0	0	0	0	7	113
313	102.20	259	80	70	61	7	12	10	3	1	6	1	2	0	1	0	0	4	0	0	1	0	0	0	0	0	0	0	0	0	0	0	3	101
318	103.80	321	78	74	75	29	15	12	4	0	3	3	5	5	9	4	0	2	2	0	0	1	0	0	0	0	0	0	0	0	0	0	9	116
323	105.40	427	123	94	114	29	10	12	10	1	10	3	8	2	3	0	0	3	1	1	1	0	0	1	0	1	0	0	0	0	0	0	4	127
328	107.00	571	166	105	121	63	22	28	5	1	6	11	5	9	6	9	0	8	1	3	0	0	2	0	0	0	0	0	0	0	0	0	12	227
333	108.67	421	135	104	70	19	17	25	11	1	2	3	7	6	1	2	1	6	1	4	0	3	3	0	0	0	0	0	0	0	0	0	5	49
338	110.33	506	123	112	121	36	14	32	8	0	9	4	8	9	12	4	0	9	2	2	1	0	0	0	0	0	0	0	0	0	0	0	5	123
343	112.00	292	54	95	45	10	8	23	2	0	0	3	19	2	1	9	4	3	0	5	0	6	3	0	0	0	0	0	0	0	0	0	3	118
348	113.67	432	123	100	86	27	29	32	1	0	2	4	12	0	5	6	0	4	0	0	0	1	0	0	0	0	0	0	0	0	0	0	4	214
353	115.33	296	80	89	57	11	15	11	2	0	3	3	7	6	0	1	1	7	0	0	0	0	3	0	0	0	0	0	0	0	0	0	5	155
358	117.00	343	81	103	47	24	20	21	5	0	6	4	8	6	4	2	0	10	1	0	0	0	0	0	0	0	0	0	0	0	0	0	2	119
363	118.67	305	45	105	60	13	20	19	11	1	6	0	12	5	3	0	0	3	0	0	0	0	2	0	0	0	0	0	0	0	0	0	1	62
368	120.33	405	64	133	73	31	40	21	5	1	6	1	13	2	3	5	0	4	0	0	0	1	0	0	0	0	0	1	1	0	0	0	2	122
373	122.00	350	71	108	60	16	29	19	6	0	4	3	10	2	2	10	2	5	1	0	0	0	2	0	0	0	0	0	0	0	0	0	4	83
378	123.63	390	75	93	86	23	25	16	10	0	6	7	16	8	11	4	0	7	0	0	0	0	0	2	0	1	0	0	0	0	0	0	7	112
383	125.25	461	63	113	81	47	46	16	26	4	11	6	29	2	3	2	0	5	1	0	0	2	3	0	0	1	0	0	0	0	0	0	4	106
388	126.88	372	64	65	78	44	43	10	15	0	4	7	16	6	2	7	0	0	8	1	0	0	0	1	1	0	0	0	0	0	0	0	6	89
393	128.50	458	86	89	99	48	44	12	13	1	7	8	16	0	7	5	0	0	5	3	1	2	12	0	0	0	0	0	0	0	0	0	7	95

Cm below seafloor	Time (kyr)	Plk. total (not incl benthics)	N. pac (R)	Gr. inflata	Gg. bulloides	Ga. glutinata	Gs. ruber	Gr. truncatulinoides	N. dutertrei	N. pac (L)	O. universa	Gr. scitula	Gs. sacculifer	Gr. crassaformis	Ge. siphonifera	Gg. falconensis	Gg. quinqueloba	Gr. hirsuta	G. hexagona	Gr. menardii	Gg.rubescens	Gs. conglobatus	G. calida	Gs. tenellus	G. digitata	P. obliquiloculata	rubr(pk)	G. theyeri	Gr cavernula	Ga. uvula	Sphaer. dehiscens	Candeina nitid	Unknown	Benthics	Fragments
398	130.13	322	89	84	37	25	18	15	6	0	3	2	7	11	11	1	1	0	5	3	0	1	1	0	0	0	0	0	2	0	0	0	0	4	100
403	131.75	381	145	91	66	16	18	10	10	0	5	3	3	1	8	0	0	1	3	0	0	0	1	0	0	0	0	0	0	0	0	0	0	10	79
408	133.38	489	127	141	96	46	23	13	5	0	4	2	6	7	9	3	1	0	3	0	0	1	0	2	0	0	0	0	0	0	0	0	0	3	148
413	135.00	272	91	86	36	12	15	6	5	0	6	7	2	1	0	1	1	0	0	2	0	0	1	0	0	0	0	0	0	0	0	0	0	0	58
418	136.57	368	60	169	36	16	10	17	8	3	23	1	3	10	8	0	0	0	1	1	0	1	0	0	0	0	0	0	0	0	0	0	1	5	53
423	138.14	304	121	85	35	5	9	6	9	1	15	3	4	0	4	1	0	5	0	1	0	0	0	0	0	0	0	0	0	0	0	0	0	9	87
428	139.71	291	80	103	50	4	17	12	0	1	6	0	4	1	11	1	0	0	0	1	0	0	0	0	0	0	0	0	0	0	0	0	0	3	73
433	141.29	313	102	92	59	13	12	12	2	1	7	1	5	0	2	2	2	1	0	0	0	0	0	0	0	0	0	0	0	0	0	0	0	6	49
438	142.86	452	196	113	51	36	13	20	6	0	3	1	2	4	3	2	0	1	1	0	0	0	0	0	0	0	0	0	0	0	0	0	0	3	135
443	144.43	477	189	106	96	21	3	10	1	4	6	8	11	4	0	5	11	0	2	0	0	0	0	0	0	0	0	0	0	0	0	0	0	8	115
448	146.00	381	162	107	52	16	7	3	7	0	9	2	6	6	3	0	0	0	1	0	0	0	0	0	0	0	0	0	0	0	0	0	0	7	92
453	147.67	258	117	63	41	12	9	3	1	0	3	3	3	0	2	0	0	1	0	0	0	0	0	0	0	0	0	0	0	0	0	0	0	6	68
458	149.33	441	156	129	54	34	17	0	1	3	4	6	9	17	4	4	0	0	2	0	0	1	0	0	0	0	0	0	0	0	0	0	0	1	99
463	151.00	333	133	79	46	15	10	5	1	6	4	4	1	4	1	7	17	0	0	0	0	0	0	0	0	0	0	0	0	0	0	0	0	2	63
468	152.67	362	162	93	54	20	11	1	1	0	8	2	0	0	4	4	1	0	1	0	0	0	0	0	0	0	0	0	0	0	0	0	0	3	75
473	154.33	440	229	84	82	10	6	1	0	2	5	6	8	0	0	4	1	0	0	0	1	0	0	0	1	0	0	0	0	0	0	0	0	0	87
478	156.00	436	226	73	74	14	14	4	1	2	2	6	2	5	7	5	1	0	0	0	0	0	0	0	0	0	0	0	0	0	0	0	0	2	126
483	157.67	471	239	80	77	29	14	7	3	1	2	4	2	2	1	0	6	0	0	0	0	2	2	0	0	0	0	0	0	0	0	0	0	4	135
488	159.33	396	161	91	85	23	7	6	6	0	2	1	6	1	2	3	0	0	1	0	0	0	0	0	0	0	0	0	0	0	0	0	1	0	6	126
493	161.00	465	251	59	77	21	17	11	0	1	1	3	5	6	3	0	10	0	0	0	0	0	0	0	0	0	0	0	0	0	0	0	0	7	135
498	162.67	448	218	83	93	8	11	8	2	1	6	3	3	2	4	3	0	0	0	0	0	2	0	0	0	0	0	1	0	0	0	0	0	3	102
503	164.33	481	200	104	101	21	22	12	1	2	2	3	3	1	5	0	2	0	2	0	0	0	0	0	0	0	0	0	0	0	0	0	0	3	71
508	166.00	425	181	95	82	29	16	7	1	0	1	8	0	0	4	0	0	0	0	0	1	0	0	0	0	0	0	0	0	0	0	0	0	2	143
513	167.67	452	148	118	89	39	10	20	3	0	2	5	4	1	5	2	2	1	0	0	1	1	1	0	0	0	0	0	0	0	0	0	0	5	105
518	169.33	420	146	123	71	21	6	18	0	0	4	3	3	15	6	2	0	0	0	2	0	0	0	0	0	0	0	0	0	0	0	0	0	3	91
523	171.00	400	153	115	63	15	13	7	3	0	4	1	8	4	4	1	0	4	3	1	0	1	0	0	0	0	0	0	0	0	0	0	0	5	79
528	172.71	420	188	79	87	31	11	10	2	0	3	2	0	0	5	1	0	0	0	1	0	0	0	0	0	0	0	0	0	0	0	0	0	3	106
533	174.43	396	176	86	62	23	7	14	6	0	3	4	0	3	3	1	3	0	3	0	1	1	0	0	0	0	0	0	0	0	0	0	0	3	106
538	176.14	349	172	48	81	18	4	2	0	2	0	10	1	5	3	2	0	0	0	0	0	0	0	1	0	0	0	0	0	0	0	0	0	4	144
543	177.86	414	171	105	69	21	7	9	5	4	3	2	2	7	3	0	3	1	0	1	0	1	0	0	0	0	0	0	0	0	0	0	0	8	199
548	179.57	311	125	90	63	5	8	7	0	0	3	5	0	0	5	0	0	0	0	0	0	0	0	0	0	0	0	0	0	0	0	0	0	9	123
553	181.29	498	175	181	62	9	10	20	4	1	15	6	3	4	2	1	0	0	2	0	0	1	2	0	0	0	0	0	0	0	0	0	0	6	103
558	183.00	321	112	104	74	2	1	10	1	0	6	3	3	0	3	2	0	0	0	0	0	0	0	0	0	0	0	0	0	0	0	0	0	6	154
563	184.83	288	125	80	39	13	7	12	1	1	2	2	1	0	0	1	3	1	0	0	0	0	0	0	0	0	0	0	0	0	0	0	0	7	139
568	186.67	324	158	79	45	8	11	16	3	1	1	0	1	0	1	0	0	0	0	0	0	0	0	0	0	0	0	0	0	0	0	0	0	6	132
573	188.50	448	188	126	53	24	18	12	0	5	1	3	1	6	1	2	1	3	1	0	3	0	0	0	0	0	0	0	0	0	0	0	0	7	154
578	190.33	336	140	119	39	9	19	2	0	0	1	0	0	0	2	4	0	1	0	0	0	0	0	0	0	0	0	0	0	0	0	0	0	5	225
583	192.17	392	138	131	42	29	10	5	3	3	3	1	5	7	6	1	0	2	4	2	0	0	0	0	0	0	0	0	0	0	0	0	0	6	144
588	194.00	310	120	80	59	11	6	10	6	0	5	5	5	0	3	0	0	0	0	0	0	0	0	0	0	0	0	0	0	0	0	0	0	4	211
593	196.20	344	106	94	58	25	14	23	2	2	4	7	2	4	0	1	0	1	0	1	0	0	0	0	0	0	0	0	0	0	0	0	0	8	190
598	198.40	343	78	103	74	15	9	23	5	0	4	6	6	4	7	5	1	0	0	1	1	0	1	0	0	0	0	0	0	0	0	0	0	6	218
603	200.60	366	108	111	61	19	16	23	9	0	3	2	2	3	1	1	0	0	0	2	1	0	4	0	0	0	0	0	0	0	0	0	0	8	292
608	202.80	307	106	91	48	13	12	15	4	0	8	0	3	0	5	0	0	2	0	0	0	0	0	0	0	0	0	0	0	0	0	0	0	8	321
613	205.00	286	87	103	38	14	10	11	4	0	6	1	2	3	1	0	3	1	1	0	0	0	0	1	0	0	0	0	0	0	0	0	0	2	273
618	207.20	309	90	97	56	11	6	17	5	0	5	8	1	0	11	2	0	0	0	0	0	0	0	0	0	0	0	0	0	0	0	0	0	4	456
623	209.40	258	101	98	26	5	3	11	0	0	1	5	2	3	2	0	0	1	0	0	0	0	0	0	0	0	0	0	0	0	0	0	0	13	321
628	211.60	338	129	93	49	6	17	21	5	0	1	9	3	1	1	3	0	0	0	0	0	0	0	0	0	0	0	0	0	0	0	0	0	11	298
633	213.80	315	66	135	49	7	12	15	3	0	1	3	4	15	0	1	0	2	1	0	0	1	0	0	0	0	0	0	0	0	0	0	0	2	153
638	216.00	384	132	94	53	23	26	29	2	1	3	15	4	1	0	0	0	0	1	0	0	0	0	0	0	0	0	0	0	0	0	0	0	6	202
643	217.71	299	58	123	45	19	19	18	0	0	3	3	2	2	0	2	1	2	1	0	0	1	0	0	0	0	0	0	0	0	0	0	0	5	159
648	219.43	379	90	135	65	19	24	16	4	0	2	6	1	6	5	2	0	0	2	1	0	0	1	0	0	0	0	0	0	0	0	0	0	10	265
653	221.14	346	89	105	48	18	27	17	5	0	7	5	2	7	6	4	2	0	0	0	0	2	2	0	0	0	0	0	0	0	0	0	0	3	185
658	222.86	305	77	122	62	7	10	8	3	0	4	5	3	0	2	2	0	0	0	0	0	0	0	0	0	0	0	0	0	0	0	0	0	8	132
663	224.57	398	120	127	67	17	17	12	7	1	4	1	8	4	2	2	1	2	1	0	0	0	2	0	0	0	3	0	0	0	0	0	0	7	202
668	226.29	322	108	94	57	11	14	18	1	1	5	1	3	1	4	1	0	1	0	1	0	0	0	0	0	0	0	1	0	0	0	0	0	5	194
673	228.00	330	116	114	49	6	13	10	0	1	3	2	3	5	0	0	6	1	1	0	0	0	0	0	0	0	0	0	0	0	0	0	0	3	157
678	229.43	368	122	115	75	8	10	21	0	1	0	3	3	2	5	3	0	0	0	0	0	0	0	0	0	0	0	0	0	0	0	0	0	8	243
683	230.86	349	112	124	60	25	6	10	2	1	0	2	1	3	1	0	0	0	0	0	0	1	1	0	0	0	0	0	0	0	0	0	0	7	242
688	232.29	342	123	120	58	3	5	12	3	1	5	2	3	2	2	2	0	1	0	0	0	0	0	0	0	0	0	0	0	0	0	0	0	6	233
693	233.71	330	157	89	32	12	11	12	3	0	0	5	2	4	1	0	0	1	0	0	1	0	0	0	0	0	0	0	0	0	0	0	0	6	240
698	235.14	323	155	72	55	7	9	14	3	0	0	4	1	0	2	0	0	0	0	0	1	0	0	0	0	0	0	0	0	0	0	0	0	1	236
703	236.57	383	131	100	73	19	13	15	3	3	5	7	5	1	3	0	2	0	1	0	0	0	2	0	0	0	0	0	0	0	0	0	0	17	159
708	238.00	363	108	103	84	9	21	17	4	1	2	4	5	2	3	0	0	0	0	0	0	0	0	0	0	0	0	0	0	0	0	0	0	3	149
713	239.57	469	100	139	80	36	33	22	10	2	8	4	12	10	1	0	0	4	0	2	0	4	1	0	0	0	1	0	0	0	0	0	0	7	95
718	241.14	396	84	91	87	35	32	13	14	0	1	5	18	5	6	0	0	0	2	0	1	0	0	1	0	0	1	0	0	0	0	0	0	6	127
723	242.71	417	121	115	71	28	27	14	7	0	5	3	9	4	3	1	2	0	5	0	0	0	1	0	0	1	0	0	0	0	0	0	0	5	134
728	244.29	381	126	123	78	4	13	10	1	1	4	2	11	2	2	0	1	0	1	0	0	2	0	0	0	0	0	0	0	0	0	0	0	5	98
733	245.86	310	129	88	45	8	9	15	8	1	1	2	0	2	0	0	0	0	0	0	0	0	1	0	0	0	1	0	0	0	0	0	0	3	137
738	247.43	456	201	97	81	11	11	14	6	1	6	2	6	5	5	7	0	1	2	0	0	0	0	0	0	0	0	0	0	0	0	0	0	3	142
743	249.00	513	162	109	115	36	13	19	7	0	6	4	1	6	1	7	10	1	13	0	0	3	0	0	0	0	0	0	0	0	0	0	0	8	130
748	250.67	298	117	72	64	1	7	12	3	0	4	1	6	0	7	2	0	0	0	2	0	0	0	0	0	0	0	0	0	0	0	0	0	2	88
753	252.33	345	112	83	57	28	8	16	1	0	1	3	3	17	1	2	4	2	3	0	1	0	3	0	0	0	0	0	0	0	0	0	0	4	138
758	254.00	343	129	74	73	9	11	17	2	1	4	3	4	0	4	5	0	5	1	1	0		0	0	0	0	0	0	0	0	0	0	0	2	210
763	255.67	429	153	122	63	18	18	15	2	0	8	5	2	6	5	1	6	0	2	0	0	0	3	0	0	0	0	0	0	0	0	0	0	2	187
768	257.33	412	172	120	62	10	18	9	4	2	1	3	2	3	3	2	0	0	0	1	0	0	0	0	0	0	0	0	0	0	0	0	0	1	215
773	259.00	228	82	88	25	10	3	5	1	0	1	2	2	4	2	0	2	1	0	0	0	0	0	0	0	0	0	0	0	0	0	0	0	2	117
778	260.67	406	171	132	43	10	6	3	0	0	6	4	2	11	17	1	0	0	0	0	0	0	0	0	0	0	0	0	0	0	0	0	0	4	224
783	262.33	335	104	149	27	19	10	4	2	0	2	3	0	11	1	2	0	0	0	0	1	0	0	0	0	0	0	0	0	0	0	0	0	7	140
788	264.00	424	207	121	46	6	12	4	2	0	6	2	0	6	5	5	0	1	0	0	0	0	1	0	0	0	0	0	0	0	0	0	0	15	208
793	265.67	346	155	107	36	14	9	1	2	1	0	3	3	0	2	1	11	0	0	1	0	0	0	0	0	0	0	0	0	0	0	0	0	4	99
798	267.33	385	221	71	56	4	11	1	0	1	6	4	0	1	5	3	0	0	0	1	0	0	0	0	0	0	0	0	0	0	0	0	0	8	220
803	269.00	371	171	86	56	17	11	1	1	3	5	4	1	1	1	5	3	3	0	0	0	1	1	0	0	0	0	0	0	0	0	0	0	9	164
808	270.50	322	157	73	48	16	7	6	0	2	2	1	2	0	0	6	0	2	0	0	0	0	0	0	0	0	0	0	0	0	0	0	0	11	203
813	272.00	450	193	113	53	43	6	9	3	0	10	3	1	9	1	1	0	0	1	3	1	0	0	0	0	0	0	0	0	0	0	0	0	5	184

Cm below seafloor	Time (kyr)	Plk. total (not incl benthics)	N. pac (R)	Gr. inflata	Gg. bulloides	Ga. glutinata	Gs. ruber	Gr. truncatulinoides	N. dutertrei	N. pac (L)	O. universa	Gr. scitula	Gs. sacculifer	Gr. crassaformis	Ge. siphonifera	Gg. falconensis	Gg. quinqueloba	Gr. hirsuta	G. hexagona	Gr. menardii	Gg.rubescens	Gs. conglobatus	G. calida	Gs. tenellus	G. digitata	P. obliquiloculata	rubr(pk)	G. theyeri	Gr cavernula	Ga. uvula	Sphaer. dehiscens	Candeina nitid	Unknown	Benthics	Fragments
818	273.50	369	184	109	38	7	13	6	0	1	6	1	0	0	2	1	0	0	1	0	0	0	0	0	0	0	0	0	0	0	0	0	13	245
823	275.00	356	150	94	62	15	10	3	1	0	1	2	3	5	2	1	4	2	0	0	0	0	1	0	0	0	0	0	0	0	0	0	11	235
828	276.50	313	141	92	47	9	6	8	1	1	2	2	1	1	2	0	0	0	0	0	0	0	0	0	0	0	0	0	0	0	0	0	5	326
833	278.00	425	165	135	62	28	10	7	1	0	2	2	1	7	1	2	0	1	0	0	0	1	0	0	0	0	0	0	0	0	0	0	6	384
838	279.50	349	129	85	78	18	4	15	2	1	3	5	1	0	6	2	0	0	0	0	0	0	0	0	0	0	0	0	0	0	0	0	11	303
843	281.00	285	132	84	35	6	9	5	1	1	3	2	0	2	2	0	0	2	1	0	0	0	0	0	0	0	0	0	0	0	0	0	7	205
848	282.50	487	200	127	65	27	17	16	3	5	7	4	1	5	2	2	0	4	0	1	0	1	0	0	0	0	0	0	0	0	0	0	7	354
853	284.00	290	109	83	29	15	10	18	3	0	6	7	1	3	1	0	0	0	1	1	2	0	1	0	0	0	0	0	0	0	0	0	3	164
858	285.50	338	127	98	42	23	13	20	2	1	1	5	1	4	0	0	0	0	0	0	1	0	0	0	0	0	0	0	0	0	0	0	3	249
863	287.00	354	114	123	42	12	12	15	4	1	5	6	4	5	5	0	1	1	3	0	0	0	0	0	0	0	1	0	0	0	0	0	9	242
868	288.33	299	101	85	34	18	12	12	5	1	5	4	3	3	10	1	0	0	0	1	1	1	0	0	0	0	2	0	0	0	0	0	2	210
873	289.67	277	79	104	28	14	12	19	1	1	5	1	3	6	0	0	2	2	0	0	0	0	0	0	0	0	0	0	0	0	0	0	5	260
878	291.00	327	123	91	49	20	13	9	4	0	7	2	0	7	0	0	0	0	0	2	0	0	0	0	0	0	0	0	0	0	0	0	9	350
883	292.33	459	116	206	51	27	12	5	4	0	8	2	2	17	2	0	4	1	0	1	0	0	1	0	0	0	0	0	0	0	0	0	10	280
888	293.67	405	182	132	40	17	10	8	2	1	3	0	1	0	4	3	0	1	0	1	0	0	0	0	0	0	0	0	0	0	0	0	12	255
893	295.00	396	156	114	56	17	11	15	3	1	10	0	3	2	4	2	0	1	1	0	0	0	0	0	0	0	0	0	0	0	0	0	14	251
898	296.33	295	129	87	45	9	4	4	1	0	1	3	4	2	2	3	0	0	0	1	0	0	0	0	0	0	0	0	0	0	0	0	10	183
903	297.67	397	141	168	42	3	8	13	2	1	9	0	2	0	2	0	1	2	0	0	0	1	1	0	0	1	0	0	0	0	0	0	19	163
908	299.00	353	141	119	46	8	9	12	4	1	7	2	3	0	1	0	0	0	0	0	0	0	0	0	0	0	0	0	0	0	0	0	12	237
913	300.10	397	158	132	42	9	3	9	4	9	19	1	0	7	0	2	0	1	1	0	0	0	0	0	0	0	0	0	0	0	0	0	10	297
918	301.20	367	140	125	40	20	9	14	2	1	7	1	4	0	2	0	0	1	0	0	1	0	0	0	0	0	0	0	0	0	0	0	13	344
923	302.30	435	166	169	46	14	10	6	6	0	9	2	2	2	0	0	3	0	0	0	0	0	0	0	0	0	0	0	0	0	0	0	10	370
928	303.40	325	124	128	27	4	13	11	1	3	6	2	1	2	2	0	0	0	0	1	0	0	0	0	0	0	0	0	0	0	0	0	5	230
933	304.50	352	100	128	48	19	18	8	6	2	6	4	0	1	7	0	0	0	0	0	1	2	1	1	0	0	0	0	0	0	0	0	5	264
938	305.60	328	111	127	39	11	15	5	3	0	3	5	0	3	3	1	0	0	0	1	0	1	0	0	0	0	0	0	0	0	0	0	18	390
943	306.70	360	164	110	38	8	16	5	2	0	0	2	0	6	0	1	5	2	0	0	0	0	1	0	0	0	0	0	0	0	0	0	6	204
948	307.80	326	142	94	46	3	11	12	1	5	6	3	0	1	1	1	0	0	0	0	0	0	0	0	0	0	0	0	0	0	0	0	7	236
953	308.90	346	154	61	65	18	5	15	4	1	7	3	1	0	2	2	1	0	3	2	0	0	0	1	0	1	0	0	0	0	0	0	6	271
958	310.00	329	137	97	41	9	5	14	1	1	3	1	5	2	5	4	0	3	0	0	1	0	0	0	0	0	0	0	0	0	0	0	5	266
963	311.50	370	103	163	35	18	10	15	7	0	6	1	3	4	0	1	0	2	0	0	0	1	1	0	0	0	0	0	0	0	0	0	14	281
968	313.00	318	138	85	36	13	14	16	4	1	4	2	2	0	2	0	0	1	0	0	0	0	0	0	0	0	0	0	0	0	0	0	5	232
973	314.50	395	76	140	81	27	10	17	3	8	8	8	2	5	2	0	0	2	0	2	0	2	0	1	0	0	1	0	0	0	0	0	7	445
978	316.05	327	97	102	48	25	15	10	4	4	3	7	4	1	4	1	0	2	0	0	0	0	0	0	0	0	0	0	0	0	0	0	10	370
983	317.50	487	119	154	77	42	21	10	5	12	13	5	3	15	1	1	2	0	4	2	1	0	0	0	0	0	0	0	0	0	0	0	22	835
988	319.00	317	121	102	50	11	5	13	4	0	2	1	0	1	5	0	0	0	0	2	0	0	0	0	0	0	0	0	0	0	0	0	13	476
993	320.50	302	73	132	31	15	9	6	5	4	2	2	7	3	3	2	1	4	1	0	1	0	0	0	0	0	1	0	0	0	0	0	10	437
998	322.00	307	130	107	37	8	9	3	2	0	1	5	3	0	0	0	0	2	0	0	0	0	0	0	0	0	0	0	0	0	0	0	6	306
1003	323.50	376	101	148	55	8	15	14	5	1	6	5	2	4	3	2	2	0	2	1	2	0	0	0	0	0	0	0	0	0	0	0	12	355
1008	325.00	297	109	102	37	6	8	11	2	3	5	5	3	3	2	0	0	1	0	0	0	0	0	0	0	0	0	0	0	0	0	0	9	283
1013	326.50	335	117	70	57	17	22	15	1	8	1	7	3	5	0	1	3	1	4	2	1	0	0	0	0	0	0	0	0	0	0	0	2	194
1018	328.00	335	123	82	61	11	11	20	1	5	5	2	3	1	5	4	0	0	1	0	0	0	0	0	0	0	0	0	0	0	0	0	3	204
1023	329.90	396	108	109	78	30	11	22	4	1	4	4	6	5	1	2	2	1	0	2	2	0	2	1	0	0	1	0	0	0	0	0	8	255
1028	331.00	316	112	83	64	11	14	13	3	0	4	2	0	2	3	4	0	0	1	0	0	0	0	0	0	0	0	0	0	0	0	0	7	194
1033	332.91	405	72	91	121	34	22	17	15	6	4	2	4	2	1	7	0	0	5	0	1	0	0	0	0	1	0	0	0	0	0	0	4	193
1038	334.07	352	109	81	71	26	21	9	9	1	2	9	3	0	7	0	0	0	2	1	0	0	0	0	1	0	0	0	0	0	0	0	2	167
1043	335.71	438	116	92	91	52	28	9	8	3	1	6	9	3	2	3	1	3	3	0	3	2	1	0	0	1	1	0	0	0	0	0	4	184
1048	337.29	320	105	89	50	30	19	6	1	0	3	1	3	2	6	3	0	1	0	1	0	0	0	0	0	0	0	0	0	0	0	0	8	248
1053	338.86	278	78	63	56	32	13	5	9	2	4	5	3	1	2	0	0	0	1	1	0	0	0	0	0	3	0	0	0	0	0	0	3	169
1058	340.43	369	142	94	69	26	12	9	0	0	4	0	1	2	5	1	0	3	0	1	0	0	0	0	0	0	0	0	0	0	0	0	10	223
1063	342.00	429	176	85	85	29	22	5	2	1	7	2	1	0	3	2	0	0	1	1	2	0	3	1	0	0	1	0	0	0	0	0	8	221
1068	343.63	384	197	88	63	13	4	9	0	0	5	1	0	0	4	0	0	0	0	0	0	0	0	0	0	0	0	0	0	0	0	0	8	189
1073	344.93	353	154	70	77	12	12	6	0	2	10	1	0	0	2	4	0	2	0	1	0	0	0	0	0	0	0	0	0	0	0	0	4	155
1078	345.25	355	134	86	75	20	7	7	1	0	9	1	2	1	7	1	0	2	1	0	0	0	1	0	0	0	0	0	0	0	0	0	4	165
1083	348.50	428	136	127	69	28	14	12	3	1	17	2	2	2	4	2	0	0	4	2	0	1	2	0	0	0	0	0	0	0	0	0	13	204
1088	350.13	333	118	76	70	21	18	6	2	2	7	1	0	0	4	4	0	2	0	1	0	0	0	0	0	1	0	0	0	0	0	0	2	193
1093	351.75	420	156	98	86	26	9	9	3	0	9	6	6	3	1	0	0	2	1	1	1	1	1	1	0	0	0	0	0	0	0	0	5	234
1098	353.38	369	121	116	83	19	4	9	1	0	5	1	2	1	2	2	0	3	0	0	0	0	0	0	0	0	0	0	0	0	0	0	8	255
1103	355.00	396	138	117	66	20	19	2	1	1	5	5	1	1	1	3	4	2	3	1	2	0	0	1	0	3	0	0	0	0	0	0	6	251
1108	356.63	368	149	88	75	20	13	6	0	0	2	4	3	2	3	1	0	0	0	1	0	0	0	1	0	0	0	0	0	0	0	0	7	221
1113	358.25	315	164	57	47	9	10	7	2	0	2	1	0	1	3	4	5	1	1	0	0	0	0	0	0	1	0	0	0	0	0	0	9	186
1118	359.88	335	123	82	61	11	11	20	1	5	5	2	3	1	5	4	0	0	1	0	0	0	0	0	0	0	0	0	0	0	0	0	3	204
1123	361.50	433	235	72	53	29	8	3	3	3	7	2	3	0	3	1	1	2	3	1	0	2	0	0	0	2	0	0	0	0	0	0	9	222
1128	363.13	362	195	78	57	11	6	2	0	0	5	2	0	0	1	4	0	0	0	1	0	0	0	0	0	0	0	0	0	0	0	0	5	167
1133	364.75	409	147	100	72	33	16	3	10	1	6	1	2	6	0	4	4	1	0	1	0	0	2	0	0	0	0	0	0	0	0	0	8	209

APPENDIX 3.3

Foraminiferal assemblage counts for core MD96-2081.

Cm below seafloor	Time (kyr)	Plk. total (not incl benthics)	N. pac (R)	Gr. inflata	Gg. bulloides	Ga. glutinata	Gs. ruber	Gr. truncatulinoides	N. dutertrei	N. pac (L)	O. universa	Gr. scitula	Gs. sacculifer	Gr. crassaformis	Ge. siphonifera	Gg. falconensis	Gg. quinqueloba	Gr. hirsuta	G. hexagona	Gr. menardii	Gg.rubescens	Gs. conglobatus	G. calida	Gs. tenellus	G. digitata	P. obliquiloculata	rubr(pk)	G. theyeri	Gr cavernula	Ga. uvula	Sphaer. dehiscens	Candeina nitid	Unknown	Benthics	Fragments
963		462	160	145	75	34	16	14	8	0	0	2	4	1	0	0	1	0	0	1	0	0	0	1	0	0	0	0	0	0	0	0	11	233
968		477	148	183	51	30	20	9	8	2	2	2	4	0	5	8	2	3	0	0	0	0	0	0	0	0	0	0	0	0	0	0	20	210
973		513	180	137	92	34	19	10	7	9	1	8	1	2	1	4	5	1	0	2	0	0	0	0	0	0	0	0	0	0	0	0	10	253
978		318	102	103	42	14	22	9	3	0	1	6	2	0	3	5	4	0	0	1	0	0	0	1	0	0	0	0	0	0	0	0	8	148
983	237.17	352	105	100	61	22	16	16	8	7	1	5	1	0	3	1	2	1	0	2	0	0	0	0	0	0	1	0	0	0	0	0	10	121
988	238.00	358	68	99	57	25	52	10	8	2	5	3	9	0	2	5	7	1	2	0	0	0	0	0	0	0	2	0	1	0	0	0	7	80
993	245.00	373	106	100	58	30	37	10	4	0	4	7	4	2	6	5	0	0	0	0	0	0	0	0	0	0	0	0	0	0	0	0	2	103
998	246.33	550	192	136	106	32	22	16	8	0	4	6	3	3	2	0	18	0	0	1	0	0	0	1	0	0	0	0	0	0	0	0	11	176
1003	247.67	547	183	117	82	46	32	27	6	0	6	3	12	4	6	10	11	0	0	2	0	0	0	0	0	0	0	0	0	0	0	0	4	109
1008	249.00	478	187	93	86	29	28	17	9	4	8	2	2	1	2	4	4	0	0	1	1	0	0	0	0	0	0	0	0	0	0	0	5	156
1013	250.00	513	197	125	73	32	22	17	4	0	6	9	2	2	7	12	5	0	0	0	0	0	0	0	0	0	0	0	0	0	0	0	4	124
1018	251.00	391	139	85	59	28	25	6	3	0	1	7	4	1	10	12	7	0	0	0	3	0	0	0	0	0	1	0	0	0	0	0	4	92
1023	252.00	363	146	80	48	27	23	11	3	0	2	7	1	0	2	5	7	0	0	1	0	0	0	0	0	0	0	0	0	0	0	0	7	116
1028	253.00	575	221	107	81	55	30	19	6	2	7	10	5	10	9	0	10	0	0	0	0	1	0	1	0	0	0	0	1	0	0	0	6	156
1033	254.00	486	187	118	68	25	34	19	0	0	4	6	3	6	5	5	2	0	0	2	1	0	0	1	0	0	0	0	0	0	0	0	2	134
1038	255.00	514	137	139	73	56	20	13	4	1	8	10	3	6	6	16	14	0	1	4	1	0	0	0	2	0	0	0	0	0	0	0	8	172
1043	256.00	411	174	103	51	13	16	12	6	0	6	4	5	6	4	3	6	0	0	1	0	0	0	1	0	0	0	0	0	0	0	0	6	158
1048	257.00	410	142	103	80	23	20	7	4	1	4	8	4	1	4	0	6	0	0	0	1	1	0	0	0	0	1	0	0	0	0	0	6	98
1053	259.40	558	166	175	85	35	46	7	6	0	4	12	2	2	2	5	8	0	0	2	0	0	0	0	0	0	0	0	0	0	0	0	8	171
1058	261.80	468	191	161	54	12	22	4	2	0	4	1	0	7	2	4	3	0	0	1	0	0	0	0	0	0	0	0	0	0	0	0	4	192
1063	264.20	457	176	191	39	13	16	2	2	4	6	1	0	3	0	0	2	1	0	0	1	0	0	0	0	0	0	0	0	0	0	0	9	209
1068	266.60	317	136	90	36	14	10	3	2	0	3	1	6	0	0	11	2	2	0	1	0	0	0	0	0	0	0	0	0	0	0	0	8	84
1073	269.00	330	209	11	6	19	18	2	2	44	8	1	0	2	1	0	4	1	0	2	0	0	0	0	0	0	0	0	0	0	0	0	9	178
1078	270.50	383	198	91	34	17	29	2	0	0	4	4	2	0	0	2	0	0	0	0	0	0	0	0	0	0	0	0	0	0	0	0	18	131
1083	272.00	366	165	91	43	15	27	0	2	1	8	0	1	2	2	2	5	0	0	2	0	0	0	0	0	0	0	0	0	0	0	0	9	145
1088	273.50	475	184	144	75	18	22	5	3	1	5	2	3	1	1	1	3	2	1	2	0	0	0	1	0	0	0	0	1	0	0	0	10	164
1093	275.00	328	141	102	29	11	15	4	3	1	5	3	1	0	2	4	4	0	1	1	1	0	0	0	0	0	0	0	0	0	0	0	10	203
1098	276.50	343	158	104	31	15	18	4	1	0	5	1	3	0	0	2	0	0	0	0	0	1	0	0	0	0	0	0	0	0	0	0	7	217
1103	278.00	390	157	104	61	16	21	2	1	23	1	0	2	0	1	0	1	0	0	0	0	0	0	0	0	0	0	0	0	0	0	0	9	266
1108	279.50	450	184	117	79	32	15	6	1	1	2	3	0	3	2	1	4	0	0	0	0	0	0	0	0	0	0	0	0	0	0	0	6	307
1113	281.00	392	141	130	64	15	23	7	1	1	2	1	1	3	0	1	0	0	0	0	0	0	0	0	0	2	0	0	0	0	0	0	9	208
1118	282.50	492	226	149	54	17	7	12	4	0	6	8	1	1	4	2	1	0	0	0	0	0	0	0	0	0	0	0	0	0	0	0	11	269
1123	284.00	330	82	114	54	9	25	19	8	1	10	0	3	3	2	0	0	0	0	0	0	0	0	0	0	0	0	0	0	0	0	0	7	177
1128	285.50	392	134	113	52	19	27	18	4	0	2	5	2	6	2	3	1	0	0	4	0	0	0	0	0	0	0	0	0	0	0	0	1	251
1133	287.00	441	159	119	58	24	26	16	2	0	5	15	2	0	4	0	7	0	0	2	2	0	0	0	0	1	0	0	0	0	0	0	4	283
1138	288.50	471	149	146	69	26	27	21	3	0	4	8	1	3	1	0	11	1	0	0	0	0	0	1	0	0	0	0	0	0	0	0	9	246
1143	290.00	291	80	87	46	16	19	6	4	1	7	8	1	9	1	1	3	0	1	0	0	0	1	0	0	0	0	0	0	0	0	0	3	200
1148	291.50	343	108	128	59	16	8	12	2	0	3	2	1	0	2	0	1	1	0	0	0	0	0	0	0	0	0	0	0	0	0	0	7	200
1153	293.00	328	98	105	57	18	7	13	6	0	7	1	4	2	5	4	1	0	0	0	0	0	0	0	0	0	0	0	0	0	0	0	7	200
1158	294.50	306	108	90	41	25	14	7	0	1	2	5	1	4	4	2	1	0	0	1	0	0	0	0	0	0	0	0	0	0	0	0	2	178
1163	296.00	358	148	99	60	26	8	2	3	1	1	1	0	1	2	0	5	0	0	1	0	0	0	0	0	0	0	0	0	0	0	0	5	137
1168	297.50	388	155	114	44	32	13	4	1	4	5	1	1	3	3	3	2	2	0	0	0	0	0	1	0	0	0	0	0	0	0	0	4	145
1173	299.00	325	116	100	45	14	19	6	0	0	5	4	1	0	2	2	10	0	0	1	0	0	0	0	0	0	0	0	0	0	0	0	6	217
1178	299.85	317	155	90	16	11	11	5	2	0	14	2	2	1	1	3	2	0	0	2	0	0	0	0	0	0	0	0	0	0	0	0	9	218
1183	300.69	303	124	86	34	13	14	4	4	1	3	5	6	2	1	5	1	0	0	0	0	0	0	0	0	0	0	0	0	0	0	0	6	190
1188	301.54	349	115	122	58	22	9	7	1	6	5	0	2	1	0	0	1	0	0	0	0	0	0	0	0	0	0	0	0	0	0	0	9	203
1193	302.38	409	165	109	53	19	25	12	6	0	2	7	3	0	0	4	3	0	0	1	0	0	0	0	0	0	0	0	0	0	0	0	11	231
1198	303.23	340	105	101	44	14	26	12	3	0	13	8	2	0	3	2	5	0	2	0	0	0	0	0	0	0	0	0	0	0	0	0	12	202
1203	304.08	530	152	176	98	20	15	13	5	0	32	1	9	3	3	0	2	0	1	0	0	0	0	0	0	0	0	0	0	0	0	0	9	311
1208	304.92	429	160	119	55	17	29	12	3	7	3	2	4	9	5	0	0	0	2	1	0	0	0	0	0	1	0	0	0	0	0	0	3	354
1213	305.77	545	163	191	68	16	29	18	13	9	10	6	7	7	4	0	1	0	2	0	0	0	0	0	0	1	0	0	0	0	0	0	9	386
1218	306.62	447	164	102	73	52	12	10	9	7	1	4	4	0	1	0	0	1	6	0	0	0	0	0	0	1	0	0	0	0	0	0	7	418
1223	307.46	386	185	75	62	21	19	6	4	0	2	1	0	7	1	0	0	1	1	1	0	0	0	0	0	0	0	0	0	0	0	0	115	249
1228	308.31	391	175	62	91	17	16	6	0	7	3	4	3	3	1	0	0	0	2	1	0	0	0	0	0	0	0	0	0	0	0	0	8	266
1233	309.15	356	139	97	63	11	17	10	7	3	3	1	1	0	1	0	0	0	1	2	0	0	0	0	0	0	0	0	0	0	0	0	5	236
1238	310.00	546	188	108	97	61	19	15	1	14	4	16	3	16	0	0	0	0	2	0	1	1	0	0	0	0	0	0	0	0	0	0	7	385
1243	311.67	436	149	89	89	19	19	23	8	2	2	8	9	10	1	7	0	0	1	0	0	0	0	0	0	0	0	0	0	0	0	0	3	475
1248	313.33	416	135	86	71	21	16	15	5	7	3	7	10	17	1	10	0	0	6	1	1	1	0	3	0	0	0	0	0	0	0	0	2	341
1253	315.00	339	113	64	68	28	8	9	1	12	1	8	1	11	3	3	0	0	5	1	1	1	0	0	0	1	0	0	0	0	0	0	7	385
1258	316.67	420	138	108	63	22	18	9	11	18	3	8	3	5	8	0	0	1	3	1	1	0	0	0	0	0	0	0	0	0	0	0	9	451
1263	318.33	372	147	97	64	8	14	7	2	3	0	15	1	4	3	3	0	1	2	1	0	0	0	0	0	0	0	0	0	0	0	0	5	507
1268	320.00	437	189	117	49	7	14	8	4	13	3	5	3	11	5	7	0	0	2	0	0	0	0	0	0	0	0	0	0	0	0	0	6	507
1273	321.38	359	153	106	51	6	13	8	3	1	1	6	6	5	0	0	0	0	0	0	0	0	0	0	0	0	0	0	0	0	0	0	12	980
1278	322.75	517	198	136	70	20	17	9	3	7	2	8	1	16	4	12	3	1	6	1	2	0	0	0	0	0	1	0	0	0	0	0	4	619
1283	324.13	514	181	112	58	55	20	14	4	7	1	11	8	21	2	6	0	1	7	2	0	3	0	0	1	0	0	0	0	0	0	0	14	590
1288	325.50	495	176	117	49	44	16	15	5	13	0	11	10	14	3	3	4	2	8	1	3	1	0	0	0	0	0	0	0	0	0	0	3	359
1293	326.88	538	158	121	69	35	31	14	2	49	1	7	8	12	4	11	9	0	5	1	0	0	0	0	0	1	0	0	0	0	0	0	8	431
1298	328.25	492	184	93	68	38	22	15	5	22	3	12	5	11	1	3	4	0	1	2	1	0	0	1	0	0	1	0	0	0	0	0	11	364
1303	329.63	451	137	86	70	56	29	17	5	9	3	6	7	8	3	2	0	0	5	3	2	0	0	2	0	0	1	0	0	0	0	0	1	237
1308	331.00	422	117	73	78	42	18	26	2	9	10	3	12	12	4	2	1	1	3	3	1	0	0	2	1	0	2	0	0	0	0	0	8	228
1313	331.77	400	91	68	83	55	21	19	10	8	1	3	10	2	3	9	6	5	1	0	3	0	0	0	1	0	1	0	0	0	0	0	2	170
1318	332.54	518	112	97	123	85	34	0	7	19	2	3	11	1	6	9	3	0	4	1	0	0	0	0	0	1	0	0	0	0	0	0	3	237
1323	333.31	496	116	81	82	81	33	17	11	26	2	3	7	6	8	6	7	3	5	0	0	0	0	0	0	1	0	1	0	0	0	0	13	166
1328	334.08	388	81	84	84	49	28	15	8	11	1	0	11	5	4	0	0	0	3	0	0	0	0	4	0	0	0	0	0	0	0	0	5	183
1333	334.85	423	107	80	62	69	29	15	4	11	3	3	15	7	7	0	0	0	4	2	2	0	0	1	0	2	0	0	0	0	0	0	6	262
1338	335.62	494	169	117	63	61	27	12	4	6	5	4	7	4	6	1	1	1	4	1	0	0	0	1	0	0	0	0	0	0	0	0	6	282
1343	336.38	439	188	71	68	70	15	6	1	0	2	4	1	5	3	2	0	2	1	0	0	0	0	0	0	0	0	0	0	0	0	0	5	247

Cm below seafloor	Time (kyr)	Plk. total (not incl benthics)	N. pac (R)	Gr. inflata	Gg. bulloides	Ga. glutinata	Gs. ruber	Gr. truncatulinoides	N. dutertrei	N. pac (L)	O. universa	Gr. scitula	Gs. sacculifer	Gr. crassaformis	Ge. siphonifera	Gg. falconensis	Gg. quinqueloba	Gr. hirsuta	G. hexagona	Gr. menardii	Gg.rubescens	Gs. conglobatus	G. calida	Gs. tenellus	G. digitata	P. obliquiloculata	rubr(pk)	G. theyeri	Gr cavernula	Ga. uvula	Sphaer. dehiscens	Candeina nitid	Unknown	Benthics	Fragments
1348	337.15	425	178	92	64	41	16	7	4	0	8	0	1	5	4	1	2	0	0	0	0	0	0	2	0	0	0	0	0	0	0	0	5	298
1353	337.92	390	175	79	52	40	9	9	1	6	7	0	1	2	1	5	1	0	2	0	0	0	0	0	0	0	0	0	0	0	0	0	5	272
1358	338.69	336	125	82	64	40	2	2	2	3	2	2	2	0	2	6	1	0	1	0	0	0	0	0	0	0	0	0	0	0	0	0	8	252
1363	339.46	363	151	83	61	29	3	9	3	1	2	8	2	3	2	2	3	0	1	0	0	0	0	0	0	0	0	0	0	0	0	0	3	211
1368	340.23	348	136	96	72	11	6	9	1	0	1	1	6	1	2	1	1	3	0	0	1	0	0	0	0	0	0	0	0	0	0	0	11	329
1373	341.00	373	148	84	70	24	9	5	1	4	0	6	1	5	4	2	0	1	2	1	6	0	0	0	0	0	0	0	0	0	0	0	1	175
1378	341.82	351	153	76	42	19	7	7	2	1	3	1	2	0	2	14	8	3	2	1	0	7	0	0	0	0	0	0	0	0	0	0	2	203
1383	342.64	517	253	104	68	33	11	6	2	4	2	3	6	4	2	5	7	0	4	0	2	0	0	0	1	0	0	0	0	0	0	0	11	289
1393	344.27	423	216	73	53	33	9	4	2	5	5	2	0	4	0	8	8	0	0	0	1	0	0	0	0	0	0	0	0	0	0	0	3	183
1398	345.09	423	185	96	65	22	11	9	1	6	8	3	0	3	4	5	2	1	1	0	1	0	0	0	0	0	0	0	0	0	0	0	5	226
1403	345.91	511	252	133	48	26	11	12	0	4	6	1	5	0	4	4	1	4	0	0	0	0	0	0	0	0	0	0	0	0	0	0	4	203
1408	346.73	441	191	78	76	45	8	10	6	8	4	0	2	3	0	4	3	2	0	1	0	0	0	0	0	0	0	0	0	0	0	0	10	171
1413	347.55	404	154	79	101	30	4	5	1	3	7	1	1	3	0	6	6	1	2	0	0	0	0	0	0	0	0	0	0	0	0	0	2	170
1418	348.36	328	127	91	67	16	3	6	0	0	2	3	3	6	0	3	1	0	0	0	0	0	0	0	0	0	0	0	0	0	0	0	3	171
1423	349.18	324	136	76	49	16	4	8	2	6	2	2	0	1	3	7	7	1	2	1	1	0	0	0	0	0	0	0	0	0	0	0	8	136
1428	350.00	447	183	97	72	53	5	7	3	4	7	1	4	0	0	4	1	1	3	0	2	0	0	0	0	0	0	0	0	0	0	0	5	192
1433	350.82	335	125	97	55	30	8	0	1	3	5	2	2	1	1	2	3	0	0	0	0	0	0	0	0	0	0	0	0	0	0	0	4	160
1438	351.64	340	120	99	60	25	7	1	5	5	5	3	1	4	0	0	4	1	0	0	0	0	0	0	0	0	0	0	0	0	0	0	5	155
1443	352.29	339	156	111	3	34	4	14	1	1	1	1	3	1	1	2	0	1	1	2	0	0	0	0	1	1	0	0	0	0	0	0	9	238
1448	353.27	383	136	123	43	38	5	12	9	0	8	1	0	3	1	2	0	0	0	1	0	0	0	0	1	0	0	0	0	0	0	0	6	151
1453	354.09	451	139	155	86	27	9	10	5	4	3	4	1	1	4	1	0	0	0	2	0	0	0	0	0	0	0	0	0	0	0	0	8	192
1458	354.91	371	149	120	54	18	5	7	3	3	4	0	2	0	1	1	0	0	0	0	0	0	0	0	0	0	0	0	0	0	0	0	8	161
1463	355.73	388	153	125	49	25	5	6	4	6	7	1	2	0	0	2	0	0	1	1	0	1	0	0	0	0	0	0	0	0	0	0	7	142
1468	356.55	315	151	83	33	10	6	6	3	3	2	0	1	0	5	9	0	1	0	0	1	0	0	0	0	1	0	0	0	0	0	0	5	138
1473	357.36	515	214	110	77	49	7	4	8	6	14	2	0	0	3	9	1	4	2	2	2	1	0	0	0	0	0	0	0	0	0	0	8	216
1478	358.18	500	176	105	76	60	12	13	8	10	3	2	2	0	5	9	10	1	1	0	0	2	3	1	1	0	0	0	0	0	0	0	12	333
1483	359.00	420	155	90	77	31	15	5	5	2	6	5	2	11	1	7	6	1	0	1	0	0	0	0	0	0	0	0	0	0	0	0	9	249
1488	359.82	354	130	89	53	28	12	7	5	2	3	4	1	0	1	10	1	1	0	6	0	0	0	0	0	1	0	0	0	0	0	0	8	247
1493	360.64	466	174	145	52	27	4	9	8	10	15	2	0	1	0	7	4	0	1	4	0	2	0	1	0	0	0	0	0	0	0	0	8	378
1498	361.45	446	176	122	72	35	6	4	2	2	3	2	1	4	1	8	5	1	1	1	0	0	0	0	0	0	0	0	0	0	0	0	10	351
1503	362.27	344	125	89	62	27	7	8	8	4	4	0	1	4	1	1	2	0	0	1	0	0	0	0	0	0	0	0	0	0	0	0	5	262
1508	363.09	301	78	101	58	21	8	6	2	3	3	1	8	0	4	4	2	0	0	1	1	0	0	0	0	0	0	0	0	0	0	0	4	254
1513	363.91	318	121	92	41	21	11	7	3	1	4	1	3	2	2	3	0	0	4	1	0	0	0	0	1	0	0	0	0	0	0	0	11	411
1518	364.73	378	118	87	54	40	19	13	10	1	4	3	3	8	0	11	0	3	1	1	0	0	0	2	0	0	0	0	0	0	0	0	13	800
1523	365.55	333	105	106	44	33	8	16	5	1	1	3	2	3	1	1	0	1	3	0	0	0	0	1	0	0	0	0	0	0	0	0	19	508
1528	366.36	414	123	134	71	31	12	11	6	3	1	3	2	5	0	9	1	0	1	5	1	0	0	0	0	0	0	0	0	0	0	0	19	387
1533	367.18	448	136	83	84	39	21	25	12	6	9	2	7	7	1	7	0	5	1	0	2	0	1	0	0	0	0	0	0	0	0	0	9	374
1538	368.00	404	114	107	65	43	15	14	9	6	4	8	1	4	1	2	1	2	3	2	1	0	0	2	0	0	0	0	0	0	0	0	19	581
1543	371.50	326	84	142	31	24	5	7	4	12	3	2	4	2	0	1	0	1	1	3	0	0	0	0	0	0	0	0	0	0	0	0	19	401
1548	375.00	446	129	164	51	37	5	7	11	11	5	4	2	7	1	8	0	3	1	0	0	0	0	0	0	0	0	0	0	0	0	0	12	469
1553	376.76	325	78	119	43	23	9	14	3	6	3	5	5	3	1	6	0	1	5	1	0	0	0	0	0	0	0	0	0	0	0	0	12	554
1558	378.53	411	90	143	43	33	24	20	3	12	3	6	2	7	8	3	3	7	2	2	0	0	0	1	0	0	0	0	0	0	0	0	17	562
1563	380.29	314	64	87	40	23	15	30	7	4	7	9	4	9	1	4	0	1	5	2	0	0	0	1	0	0	0	1	0	0	0	0	8	326
1568	382.06	497	87	143	80	56	44	27	4	4	4	14	11	9	1	3	0	1	5	1	0	0	0	0	0	0	3	0	0	0	0	0	17	556
1573	383.82	316	59	74	43	50	41	15	1	0	5	10	1	4	1	4	1	1	4	0	0	0	0	1	0	0	0	0	0	0	0	0	5	450
1578	385.59	403	74	97	64	45	32	32	14	3	2	10	6	6	6	1	0	0	5	0	0	3	0	0	0	0	1	0	0	0	0	0	4	452
1583	387.35	459	82	94	89	36	44	39	16	4	4	13	6	14	3	1	0	1	7	5	1	0	0	0	0	0	0	0	0	0	0	0	7	469
1588	389.12	365	75	77	64	50	34	15	9	2	4	12	4	7	2	2	0	0	5	1	0	1	0	0	0	1	0	0	0	0	0	0	14	391
1593	390.88	387	70	111	51	34	26	33	10	6	4	8	10	12	5	1	0	1	3	0	1	0	0	0	0	0	0	0	0	0	0	0	9	437
1598	392.65	425	92	103	66	38	29	29	18	4	11	8	7	2	3	3	3	0	3	0	4	0	0	0	0	0	1	1	0	0	0	0	13	476
1603	394.41	375	88	117	57	27	18	23	4	7	4	7	6	8	2	2	2	0	0	2	1	0	0	0	0	0	0	0	0	0	0	0	13	454
1608	396.18	453	139	122	61	28	22	32	11	1	3	8	4	3	2	9	0	2	2	2	2	0	0	0	0	0	0	0	0	0	0	0	11	471
1613	397.94	377	102	92	57	24	28	30	13	2	0	7	5	0	0	6	1	0	3	1	5	1	0	0	0	0	0	0	0	0	0	0	9	342
1618	399.71	381	82	121	64	25	32	11	3	4	5	9	9	1	5	1	0	0	4	1	2	0	2	0	0	0	0	0	0	0	0	0	12	311
1623	401.47	370	116	88	55	27	26	26	7	1	4	7	1	0	4	5	1	0	0	1	1	0	0	0	0	0	0	0	0	0	0	0	2	395
1628	403.24	416	119	98	76	28	27	34	5	1	1	8	1	1	5	4	1	0	1	0	3	1	1	0	0	1	0	0	0	0	0	0	7	353
1633	405.00	428	111	100	67	25	30	39	5	5	2	7	7	7	1	3	1	1	0	2	12	1	0	0	1	0	1	1	0	0	0	0	6	363
1638	406.93	319	103	78	48	26	17	19	8	1	4	5	1	1	3	2	0	0	0	2	0	0	0	0	1	0	0	0	0	0	0	0	8	312
1643	408.87	405	124	96	71	33	26	20	12	2	1	6	6	2	1	0	1	0	1	0	2	0	0	0	1	0	0	0	0	0	0	0	9	273
1648	410.80	524	138	102	74	48	59	32	15	0	6	7	8	7	6	2	0	3	1	0	10	2	0	0	3	0	1	0	0	0	0	0	13	417
1653	412.73	322	109	60	46	26	15	15	9	1	15	5	10	1	3	0	0	0	3	0	1	0	0	0	0	0	3	0	0	0	0	0	6	160
1658	414.67	421	135	74	62	47	29	17	17	4	5	10	5	6	3	2	0	0	2	0	0	1	1	0	0	0	1	0	0	0	0	0	9	202
1663	416.60	439	134	79	93	42	26	18	5	0	7	10	5	10	2	4	0	2	0	1	0	0	0	0	1	0	0	0	0	0	0	0	9	293
1668	418.53	443	135	77	75	49	30	20	9	5	10	8	5	4	3	2	0	1	2	0	6	2	0	0	0	0	0	0	0	0	0	0	2	168
1673	420.47	553	163	79	95	56	55	21	30	1	7	10	11	8	5	6	1	0	4	0	1	0	0	0	0	0	0	0	0	0	0	0	4	191
1678	422.40	473	128	82	98	44	34	25	14	8	2	10	5	6	6	5	0	0	1	2	0	3	0	0	0	0	0	0	0	0	0	0	4	143
1683	424.33	546	149	70	157	86	34	0	11	3	3	10	8	2	2	0	0	0	2	3	2	2	1	0	0	0	1	0	0	0	0	0	3	229
1688	426.27	388	103	69	80	49	31	7	10	2	2	6	5	3	8	0	0	0	3	2	2	2	0	0	4	0	0	0	0	0	0	0	4	163
1693	428.20	345	140	61	48	39	15	4	3	4	4	4	6	4	2	5	0	0	2	0	1	0	1	0	2	0	0	0	0	0	0	0	2	205
1698	430.13	449	223	73	84	32	9	5	5	5	1	4	1	2	0	2	0	0	1	2	0	0	0	0	0	0	0	0	0	0	0	0	5	241
1703	432.07	424	222	71	73	24	10	1	5	4	4	5	1	0	1	3	0	0	0	0	0	0	0	0	0	0	0	0	0	0	0	0	7	264
1708	434.00	405	180	74	92	16	5	2	5	12	4	1	2	0	1	5	1	0	0	2	1	2	0	0	0	0	0	0	0	0	0	0	10	288
1713	436.85	418	171	100	82	23	10	4	4	3	4	2	1	3	1	4	2	1	0	3	0	0	0	0	0	0	0	0	0	0	0	0	9	284
1718	439.69	463	206	107	94	8	8	6	5	4	6	1	1	0	2	6	5	2	0	0	2	0	0	0	2	0	0	0	0	0	0	0	8	259
1723	442.54	406	165	95	92	9	13	3	1	10	4	1	1	1	3	4	0	0	0	0	0	2	0	0	2	0	0	0	0	0	0	0	5	207
1728	445.39	378	161	84	79	22	2	10	1	4	10	0	0	0	3	2	0	0	0	0	0	0	0	0	0	0	0	0	0	0	0	0	4	186
1733	448.23	466	191	91	101	30	12	3	4	3	8	1	3	0	5	5	9	0	0	0	0	0	0	0	0	0	0	0	0	0	0	0	4	309
1738	451.08	373	140	92	84	20	5	2	5	4	4	0	0	3	1	10	0	0	0	0	0	0	0	0	3	0	0	0	0	0	0	0	5	194
1743	453.92	410	155	105	89	15	5	3	6	25	0	0	0	0	0	5	2	0	0	0	0	0	0	0	0	0	0	0	0	0	0	0	3	294
1748	456.77	349	132	80	80	12	9	1	3	8	3	2	1	4	1	1	10	0	0	1	0	0	0	0	1	0	0	0	0	0	0	0	8	168
1753	459.62	427	168	115	51	42	5	2	7	7	3	5	4	1	4	1	10	2	0	0	0	0	0	0	0	0	0	0	0	0	0	0	2	228
1758	462.46	411	168	94	63	22	5	1	1	32	6	0	2	4	2	3	8	0	0	0	0	0	0	0	0	0	0	0	0	0	0	0	4	159
1763	465.31	451	157	136	69	10	8	4	3	44	0	2	0	3	0	5	9	1	0	0	0	0	0	0	0	0	0	0	0	0	0	0	5	216

Cm below seafloor	Time (kyr)	Plk. total (not incl benthics)	N. pac (R)	Gr. inflata	Gg. bulloides	Ga. glutinata	Gs. ruber	Gr. truncatulinoides	N. dutertrei	N. pac (L)	O. universa	Gr. scitula	Gs. sacculifer	Gr. crassaformis	Ge. siphonifera	Gg. falconensis	Gg. quinqueloba	Gr. hirsuta	G. hexagona	Gr. menardii	Gg.rubescens	Gs. conglobatus	G. calida	Gs. tenellus	G. digitata	P. obliquiloculata	rubr(pk)	G. theyeri	Gr cavernula	Ga. uvula	Sphaer. dehiscens	Candeina nitid	Unknown	Benthics	Fragments
1768	468.15	366	193	80	50	10	7	3	3	9	1	0	0	4	0	0	5	0	0	1	0	0	0	0	0	0	0	0	0	0	0	0	3	253
1773	471.00	360	144	82	64	15	5	7	3	16	2	2	3	1	2	2	10	0	0	2	0	0	0	0	0	0	0	0	0	0	0	0	1	120
1778	472.75	408	142	114	76	9	10	2	9	15	5	6	2	8	1	4	2	1	0	2	0	0	0	0	0	0	0	0	0	0	0	0	5	145
1783	474.50	439	160	136	57	14	3	2	5	35	8	0	4	3	0	2	10	0	0	0	0	0	0	0	0	0	0	0	0	0	0	0	6	235
1788	476.25	400	194	99	63	2	1	3	4	24	3	0	1	0	0	0	4	0	0	2	0	0	0	0	0	0	0	0	0	0	0	0	3	183
1793	478.00	399	156	103	62	8	5	8	3	34	8	0	0	3	0	0	6	0	0	0	0	0	0	0	0	0	0	0	0	0	0	0	8	192
1798	479.75	369	134	136	52	2	7	6	5	18	2	0	0	1	0	1	4	0	0	1	0	0	0	0	0	0	0	0	0	0	0	0	4	196
1803	481.50	419	157	153	49	3	0	7	7	30	3	0	2	4	1	0	3	0	0	0	0	0	0	0	0	0	0	0	0	0	0	0	11	316
1808	483.25	381	140	127	36	8	3	7	4	35	4	0	2	8	1	2	4	0	0	0	0	0	0	0	0	0	0	0	0	0	0	0	11	207
1813	485.00	392	174	108	42	14	1	11	4	30	3	0	3	0	1	0	0	0	0	1	0	0	0	0	0	0	0	0	0	0	0	0	7	288
1818	486.75	345	130	94	52	10	2	7	4	29	0	1	3	3	0	5	2	1	0	2	0	0	0	0	0	0	0	0	0	0	0	0	5	181
1823	488.50	423	165	91	66	20	13	11	5	29	3	3	2	6	0	1	6	0	0	0	0	1	0	0	1	0	0	0	0	0	0	0	8	238
1828	490.25	480	202	97	74	21	5	15	7	36	2	3	2	3	4	4	3	1	0	1	0	0	0	0	0	0	0	0	0	0	0	0	15	263
1833	492.00	418	170	102	40	35	2	19	8	13	7	3	2	4	3	4	0	3	0	3	0	0	0	0	0	0	0	0	0	0	0	0	15	225
1838	493.75	389	141	102	35	44	9	12	8	13	3	0	8	1	3	6	1	2	0	0	0	1	0	0	0	0	0	0	0	0	0	0	18	402
1843	495.50	305	107	76	59	18	4	10	3	7	1	2	1	2	2	2	6	1	0	1	1	0	1	0	0	1	0	0	0	0	0	0	18	404
1848	497.25	322	85	106	43	23	5	27	7	7	3	2	4	1	3	1	3	0	0	0	0	1	1	0	0	0	0	0	0	0	0	0	9	520
1853	499.00	373	146	124	40	12	7	21	4	8	2	0	0	1	3	2	2	0	0	0	0	0	0	0	0	0	0	0	1	0	0	0	22	455
1858	500.75	376	119	100	65	18	17	17	7	8	4	2	3	5	2	4	3	0	1	0	0	0	0	0	1	0	0	0	0	0	0	0	13	318
1863	502.50	418	148	110	53	26	11	20	6	14	0	9	2	3	4	1	7	1	1	0	0	2	0	0	0	0	0	0	0	0	0	0	30	503
1868	504.25	362	132	100	41	17	17	12	13	6	5	3	0	2	6	2	2	0	0	2	0	0	1	0	1	0	0	0	0	0	0	0	15	274
1873	506.00	437	145	114	66	33	16	12	8	10	1	3	5	8	6	2	4	0	0	2	0	0	0	0	0	1	0	0	0	0	0	0	8	342
1878	507.75	410	137	86	72	23	18	10	10	14	3	12	1	3	5	3	7	0	0	2	0	1	0	0	0	0	0	0	0	3	0	0	11	286
1883	509.50	392	150	98	53	20	14	15	6	9	2	6	3	5	1	4	3	1	0	1	0	0	0	0	0	0	0	0	0	1	0	0	13	238
1888	511.25	419	185	82	74	20	13	13	11	6	0	4	2	1	2	3	2	0	0	0	0	0	0	0	1	0	0	0	0	0	0	0	7	152
1893	513.00	381	173	62	60	28	10	15	3	8	2	4	2	1	4	1	4	2	0	2	0	0	0	0	0	0	0	0	0	0	0	0	6	247
1898	520.14	375	146	71	64	33	7	16	13	5	2	3	4	1	5	0	4	0	0	0	0	0	0	0	0	1	0	0	0	0	0	0	7	173
1903	527.29	400	175	69	62	33	16	5	7	5	0	3	4	5	3	7	4	0	2	0	0	0	0	0	0	0	0	0	0	0	0	0	3	273
1908	534.43	444	177	83	75	45	14	13	4	5	1	9	2	6	1	4	4	0	0	0	0	0	1	0	0	0	0	0	0	0	0	0	4	209
1913	541.57	318	134	50	49	23	10	8	5	7	3	3	6	6	3	3	5	2	0	0	0	1	0	0	0	0	0	0	0	0	0	0	5	151
1918	548.71	388	170	75	70	24	6	9	5	0	5	3	10	4	2	1	4	0	0	0	0	0	0	0	0	0	0	0	0	0	0	0	3	211
1923	555.86	476	223	82	68	42	11	6	8	8	4	6	1	7	3	1	5	0	0	1	0	0	0	0	0	0	0	0	0	0	0	0	10	251
1928	563.00	410	198	80	47	23	7	13	8	8	1	2	0	8	8	0	4	3	0	0	0	0	0	0	0	0	0	0	0	0	0	0	7	206
1933	564.10	392	159	82	63	27	5	11	2	7	5	3	6	5	5	4	4	1	1	0	0	0	0	0	2	0	0	0	0	0	0	0	5	183
1938	565.20	418	175	75	68	23	9	11	12	2	2	5	6	4	4	6	6	2	0	0	0	7	0	0	1	0	0	0	0	0	0	0	6	160
1943	566.30	308	146	78	25	19	2	10	7	8	4	0	0	0	0	4	3	1	0	1	0	0	0	0	0	0	0	0	0	0	0	0	5	153
1948	567.40	447	207	100	50	29	12	12	11	8	1	0	1	1	3	8	3	1	0	0	0	0	0	0	0	0	0	0	0	0	0	0	7	156
1953	568.50	346	148	79	38	23	12	8	11	5	0	1	1	5	5	3	6	0	0	1	0	0	0	0	0	0	0	0	0	0	0	0	7	183
1958	569.60	369	155	75	37	41	16	9	9	2	4	1	1	1	1	5	8	1	0	2	0	1	0	0	0	0	0	0	0	0	0	0	6	258
1963	570.70	348	172	102	28	8	13	5	4	1	3	0	5	3	0	3	0	0	0	1	0	0	0	0	0	0	0	0	0	0	0	0	8	235
1968	571.80	411	179	87	48	18	18	8	7	9	5	3	2	2	10	8	4	1	2	0	0	0	0	0	0	0	0	0	0	0	0	0	15	217
1973	572.90	370	193	80	31	14	12	3	11	5	4	0	3	2	2	2	7	1	0	0	0	0	0	0	0	0	0	0	0	0	0	0	0	234
1978	574.00	420	167	91	53	32	20	9	8	5	2	4	7	4	4	0	10	1	0	0	0	0	0	0	1	1	0	0	0	0	0	0	3	262
1983	579.38	378	132	57	69	39	24	12	9	6	5	4	4	2	3	3	8	1	0	0	0	0	0	0	0	0	0	0	0	1	0	0	7	170
1988	584.75	470	155	59	73	62	31	17	13	3	9	5	6	8	9	9	9	0	0	1	0	1	0	0	0	0	0	0	0	0	0	0	7	236
1993	590.13	380	189	45	38	20	14	6	14	10	10	1	7	1	3	5	8	2	3	2	0	0	0	0	1	0	0	0	1	0	0	0	7	111
1998	595.50	416	192	55	51	38	17	7	22	3	3	1	5	5	4	2	6	1	1	0	0	0	0	0	0	0	0	0	2	0	0	0	3	133
2003	600.88	426	208	53	48	37	22	4	13	3	13	1	2	2	2	0	4	3	4	2	0	0	0	0	5	0	0	0	0	0	0	0	8	146
2008	606.25	438	176	72	69	27	25	11	17	4	5	3	2	7	8	1	2	0	8	1	0	0	0	0	0	0	0	0	0	0	0	0	3	155
2013	611.63	366	134	82	65	17	6	11	21	1	7	3	5	1	1	5	1	3	1	2	0	0	0	0	0	0	0	0	0	0	0	0	9	111
2018	617.00	407	169	92	52	23	21	12	8	8	9	4	1	1	3	1	1	0	0	2	0	0	0	0	0	0	0	0	0	0	0	0	5	207
2023	618.83	416	176	95	53	32	12	7	6	7	5	1	1	3	7	2	4	1	1	2	0	0	0	0	0	1	0	0	0	0	0	0	11	183
2028	620.67	406	187	53	68	42	14	9	9	7	3	0	2	3	2	4	0	0	2	1	0	0	0	0	0	0	0	0	0	0	0	0	3	250
2033	622.50	355	147	75	58	27	11	10	8	2	4	2	2	4	1	1	1	0	1	1	0	0	0	0	0	0	0	0	0	0	0	0	10	231
2038	624.33	418	143	75	71	39	30	11	14	6	5	3	4	8	3	2	0	0	3	1	0	0	0	0	0	0	0	0	0	0	0	0	3	133
2043	626.17	456	160	77	86	50	16	9	3	4	3	5	3	16	6	5	4	2	4	0	0	2	0	0	0	1	0	0	0	0	0	0	8	99
2048	628.00	399	134	56	77	53	21	6	6	12	5	2	3	10	0	5	2	0	5	1	0	0	0	0	0	0	0	1	0	0	0	0	3	59
2053	631.00	419	129	87	92	49	5	4	3	13	7	4	1	10	6	0	8	1	0	0	0	0	0	0	0	0	0	0	0	0	0	0	2	40
2058	641.00	391	114	78	90	33	16	15	3	2	7	3	1	8	2	4	3	2	8	2	0	0	0	0	0	0	0	0	0	0	0	0	0	40
2073	668.00	413	176	87	81	19	5	11	2	5	5	1	3	5	4	4	2	1	0	2	0	0	0	0	0	0	0	0	0	0	0	0	1	98
2078	679.00	376	151	80	64	19	6	13	9	9	5	6	1	4	4	2	0	1	0	2	0	0	0	0	0	0	0	0	0	0	0	0	2	79
2083	681.50	403	140	91	82	30	4	9	5	5	3	1	2	19	4	2	3	3	0	0	0	0	0	0	0	0	0	0	0	0	0	0	1	92
2088	684.00	350	154	68	70	11	5	7	5	7	4	0	0	8	2	5	2	0	0	0	0	1	1	0	0	0	0	0	0	0	0	0	0	138
2093	689.00	391	133	86	87	25	9	16	2	9	3	5	3	9	1	2	0	0	0	1	0	0	0	0	0	0	0	0	0	0	0	0	4	141
2098	690.00	423	213	96	62	8	8	12	4	6	4	3	2	0	0	1	4	0	0	0	0	0	0	0	0	0	0	0	0	0	0	0	7	211
2103	691.00	381	132	126	67	15	2	12	6	4	3	1	1	5	1	0	4	1	1	0	0	0	0	0	0	0	0	0	0	0	0	0	2	119
2108	692.00	382	134	116	67	10	3	15	4	16	3	1	0	1	4	0	4	0	0	1	0	0	3	0	0	0	0	0	0	0	0	0	4	152
2113	693.00	372	135	122	47	12	9	18	1	15	2	1	0	4	0	1	1	3	0	1	0	0	0	0	0	0	0	0	0	0	0	0	3	163

APPENDIX 3.4

Diversity indices for the spliced Cape Basin record.

Age (k.y.)	Simple Diversity	Shannon Diversity:	Equitability
4.00	19	2.30	0.53
7.00	19	2.13	0.44
10.00	20	2.16	0.43
13.00	16	1.89	0.41
16.00	15	1.59	0.33
19.00	11	1.32	0.34
20.50	16	1.47	0.27
22.00	13	1.81	0.47
23.50	18	1.61	0.28
25.00	16	1.65	0.32
26.50	17	1.56	0.28
28.00	16	1.65	0.32
29.39	14	1.57	0.34
30.78	16	1.80	0.38
32.17	19	1.83	0.33
33.56	18	1.56	0.26
34.94	15	1.62	0.34
36.33	17	1.64	0.30
37.72	12	1.63	0.43
39.11	15	1.62	0.34
40.50	15	1.39	0.27
41.89	14	1.48	0.31
43.28	20	1.90	0.33
44.67	16	1.65	0.33
46.06	18	1.71	0.31
47.44	14	1.59	0.35
48.83	13	1.84	0.48
50.22	11	1.70	0.50
51.61	18	1.83	0.35
53.00	16	1.73	0.35
54.50	17	1.76	0.34
56.00	14	1.67	0.38
57.50	15	1.58	0.32
59.00	15	1.56	0.32
60.50	15	1.71	0.37
62.00	15	1.62	0.34
63.50	15	1.69	0.36
65.00	15	1.66	0.35
66.36	14	1.54	0.33
67.73	18	1.80	0.34
69.09	14	1.50	0.32
70.45	13	1.52	0.35
71.56	18	1.81	0.34
73.18	15	1.73	0.38
74.55	17	1.72	0.33
75.91	13	1.75	0.44
77.27	17	1.66	0.31
78.64	16	1.79	0.37
80.00	15	1.70	0.37
81.75	16	1.80	0.38
83.50	15	1.87	0.43
85.25	20	2.08	0.40
87.00	17	1.87	0.38
88.71	19	1.98	0.38
90.43	13	1.71	0.42
92.14	16	1.97	0.45
93.89	15	1.79	0.40
95.57	17	2.01	0.44
97.29	16	1.99	0.46
99.00	15	1.93	0.46
100.60	15	1.89	0.44
102.20	14	1.75	0.41
103.80	16	2.01	0.47
105.40	19	1.88	0.35
107.00	18	2.03	0.42
108.67	20	1.99	0.37
110.33	17	2.05	0.46
112.00	17	2.10	0.48
113.67	14	1.92	0.48
115.33	15	1.90	0.44
117.00	16	2.06	0.49
118.67	14	1.99	0.52
120.33	18	2.01	0.41
122.00	17	2.05	0.46
123.63	16	2.17	0.55
125.25	19	2.24	0.49
126.88	17	2.22	0.54
128.50	18	2.21	0.51
130.13	19	2.13	0.44
131.75	15	1.78	0.40
133.38	17	1.90	0.39
135.00	15	1.79	0.40
136.57	16	1.84	0.39
138.14	15	1.76	0.39
139.71	13	1.72	0.43
141.29	15	1.76	0.39
142.86	15	1.65	0.35
144.43	15	1.74	0.38
146.00	13	1.61	0.39
147.67	12	1.54	0.39
149.33	15	1.78	0.40
151.00	15	1.81	0.41
152.67	13	1.54	0.36
154.33	14	1.42	0.30
156.00	15	1.53	0.31
157.67	16	1.55	0.29
159.33	15	1.61	0.33
161.00	13	1.52	0.35
162.67	16	1.52	0.29
164.33	15	1.62	0.34
166.00	11	1.55	0.43
167.67	18	1.78	0.33
169.33	13	1.72	0.43
171.00	17	1.72	0.33
172.71	12	1.54	0.39
174.43	16	1.68	0.33
176.14	14	1.49	0.32
177.86	17	1.68	0.32
179.57	9	1.47	0.48
181.29	17	1.65	0.31
183.00	12	1.48	0.37
184.83	14	1.57	0.34
186.67	11	1.44	0.38
188.50	17	1.66	0.31
190.33	10	1.39	0.40
192.17	17	1.75	0.34
194.00	11	1.66	0.48
196.20	15	1.84	0.42
198.40	17	1.96	0.42
200.60	16	1.84	0.39
202.80	11	1.72	0.51
205.00	16	1.76	0.36
207.20	12	1.79	0.50
209.40	12	1.48	0.36
211.60	13	1.69	0.42
213.80	15	1.73	0.38
216.00	13	1.82	0.47
217.71	15	1.77	0.39
219.43	16	1.84	0.39
221.14	16	1.92	0.43
222.86	12	1.61	0.42
224.57	19	1.85	0.33
226.29	17	1.75	0.34
228.00	14	1.63	0.36
229.43	12	1.62	0.42
230.86	14	1.58	0.35
232.29	15	1.56	0.32
233.71	13	1.53	0.36
235.14	11	1.47	0.40
236.57	16	1.81	0.38
237.17	17	1.88	0.39
238.00	18	2.09	0.45
245.00	13	1.90	0.52
246.33	15	1.79	0.40
247.67	15	1.97	0.48
249.00	17	1.82	0.36
250.00	14	1.81	0.43
251.00	17	1.93	0.40
252.00	14	1.78	0.42
253.00	17	1.92	0.40
254.00	16	1.80	0.38
255.00	19	2.06	0.41
256.00	16	1.76	0.36
257.00	17	1.80	0.36
259.40	16	1.81	0.38
261.80	14	1.51	0.32
264.20	14	1.40	0.29
266.60	14	1.63	0.36
269.00	15	1.39	0.27
270.50	10	1.41	0.41
272.00	14	1.60	0.35
273.50	20	1.64	0.26
275.00	17	1.63	0.30
276.50	12	1.46	0.36
278.00	12	1.58	0.40
279.50	14	1.58	0.35
281.00	14	1.56	0.34
282.50	14	1.49	0.32
284.00	12	1.80	0.50
285.50	15	1.81	0.41
287.00	14	1.81	0.43
288.50	15	1.79	0.40
290.00	17	1.94	0.41
291.50	13	1.56	0.37
293.00	14	1.79	0.43
294.50	15	1.75	0.38
296.00	14	1.54	0.33
297.50	17	1.67	0.31
299.00	13	1.70	0.42
299.85	15	1.53	0.31
300.69	15	1.71	0.37
301.54	12	1.59	0.41
302.38	13	1.69	0.42
303.23	14	1.88	0.47
304.08	14	1.74	0.41
304.92	16	1.79	0.37
305.77	16	1.83	0.39
306.62	15	1.77	0.39
307.46	14	1.56	0.34
308.31	14	1.61	0.36
309.15	14	1.63	0.37
310.00	16	1.88	0.41
311.67	15	1.90	0.45
313.33	19	2.08	0.42
315.00	19	1.98	0.38
316.67	17	1.95	0.42
318.33	16	1.70	0.34
320.00	15	1.71	0.37
321.38	12	1.54	0.39
322.75	20	1.86	0.32
324.13	19	2.00	0.39
325.50	19	2.02	0.40
326.88	18	2.10	0.45
328.25	20	1.99	0.37
329.63	19	2.08	0.42
331.00	22	2.19	0.41
331.77	20	2.20	0.45
332.54	17	2.00	0.43
333.31	19	2.21	0.48
334.08	15	2.05	0.52
334.85	18	2.14	0.47
335.62	19	1.91	0.36
336.38	15	1.66	0.35
337.15	14	1.69	0.39
337.92	15	1.67	0.35
338.69	15	1.64	0.34
339.46	16	1.69	0.34
340.23	16	1.58	0.30
341.00	17	1.75	0.34
341.82	19	1.82	0.32
342.64	18	1.64	0.29
344.27	15	1.60	0.33
345.09	17	1.70	0.32
345.91	14	1.52	0.33
346.73	15	1.71	0.37
347.55	16	1.68	0.34
348.36	12	1.56	0.40
349.18	18	1.76	0.32
350.00	16	1.68	0.34
350.82	14	1.62	0.36
351.64	14	1.69	0.39
352.29	19	1.45	0.23
353.27	14	1.67	0.38
354.09	15	1.65	0.35
354.91	13	1.53	0.35
355.73	15	1.59	0.33
356.55	15	1.56	0.32
357.36	18	1.76	0.32
358.18	20	1.94	0.35
359.00	17	1.86	0.38

Age (k.y.)	Simple Diversity	Shannon Diversity:	Equitability
359.82	17	1.83	0.37
360.64	17	1.75	0.34
361.45	18	1.66	0.29
362.27	15	1.73	0.38
363.09	16	1.82	0.39
363.91	17	1.75	0.34
364.73	17	2.00	0.44
365.55	16	1.77	0.37
366.36	16	1.77	0.37
367.18	18	2.07	0.44
368.00	20	2.00	0.37
371.50	16	1.71	0.34
375.00	16	1.79	0.38
376.76	17	1.92	0.40
378.53	18	2.05	0.43
380.29	19	2.21	0.48
382.06	18	2.10	0.45
383.82	18	2.09	0.45
385.59	18	2.20	0.50
387.35	18	2.23	0.52
389.12	18	2.15	0.48
390.88	18	2.18	0.49
392.65	19	2.20	0.47
394.41	17	2.02	0.44
396.18	18	1.97	0.40
397.94	16	2.04	0.48
399.71	18	2.01	0.41
401.47	16	1.94	0.43
403.24	20	1.97	0.36
405.00	21	2.13	0.40
406.93	16	1.92	0.42
408.87	17	1.92	0.40
410.80	19	2.17	0.46
412.73	16	2.05	0.48
414.67	18	2.07	0.44
416.60	16	1.98	0.45
418.53	18	2.09	0.45
420.47	17	2.11	0.49
422.40	17	2.10	0.48
424.33	18	1.87	0.36
426.27	18	2.07	0.44
428.20	18	1.88	0.37
430.13	15	1.53	0.31
432.07	13	1.46	0.33
434.00	17	1.61	0.29
436.85	17	1.65	0.31
439.69	16	1.57	0.30
442.54	16	1.60	0.31
445.39	11	1.54	0.42
448.23	14	1.68	0.38
451.08	13	1.64	0.40
453.92	10	1.57	0.48
456.77	17	1.70	0.32
459.62	16	1.73	0.35
462.46	14	1.70	0.39
465.31	13	1.67	0.41
468.15	12	1.43	0.35
471.00	16	1.76	0.36
472.75	17	1.79	0.35
474.50	13	1.68	0.41
476.25	12	1.40	0.34
478.00	12	1.68	0.45
479.75	13	1.51	0.35
481.50	13	1.50	0.35
483.25	14	1.66	0.38
485.00	12	1.54	0.39
486.75	15	1.72	0.37
488.50	16	1.83	0.39
490.25	17	1.77	0.35
492.00	16	1.82	0.38
493.75	16	1.86	0.40
495.50	20	1.84	0.31
497.25	17	1.90	0.39
499.00	14	1.61	0.36
500.75	17	1.92	0.40
502.50	17	1.89	0.39
504.25	17	1.87	0.38
506.00	18	1.93	0.38
507.75	18	2.02	0.42
509.50	18	1.86	0.36
511.25	15	1.69	0.36
513.00	17	1.76	0.34
520.14	15	1.83	0.42
527.29	15	1.79	0.40
534.43	16	1.81	0.38
541.57	17	1.93	0.40
548.71	14	1.69	0.39
555.86	16	1.71	0.34
563.00	14	1.69	0.39
564.10	18	1.85	0.35
565.20	18	1.89	0.37
566.30	13	1.60	0.38
567.40	15	1.67	0.35
568.50	15	1.78	0.40
569.60	18	1.82	0.34
570.70	13	1.45	0.33
571.80	17	1.84	0.37
572.90	15	1.58	0.32
574.00	18	1.88	0.37
579.38	16	1.99	0.46
584.75	17	2.12	0.49
590.13	20	1.89	0.33
595.50	19	1.85	0.33
600.88	18	1.80	0.34
606.25	17	1.93	0.40
611.63	18	1.87	0.36
617.00	16	1.79	0.37
618.83	19	1.79	0.31
620.67	15	1.72	0.37
622.50	17	1.75	0.34
624.33	16	1.98	0.45
626.17	19	1.98	0.38
628.00	16	1.99	0.46
631.00	15	1.88	0.44
641.00	18	2.00	0.41
668.00	17	1.70	0.32
679.00	16	1.82	0.38
681.50	16	1.83	0.39
684.00	15	1.68	0.36
689.00	15	1.82	0.41
690.00	13	1.48	0.34
691.00	16	1.64	0.32
692.00	15	1.69	0.36
693.00	15	1.67	0.35

APPENDIX 4.1

Transfer function F81-25-5 for core GeoB 3603-2.

Depth (cmbsf)	Time (k.y.)	Commun-ality	Sest	West
8	4.00	0.958	21.45	17.65
13	7.00	0.956	20.38	17.18
18	10.00	0.975	20.58	16.48
23	13.00	0	17.89	14.09
28	16.00	0.991	21.05	17.15
33	19.00	0	20.18	16.08
38	20.50	0	19.38	15.88
43	22.00	0.972	21.43	17.83
48	23.50	0.979	20.70	16.70
53	25.00	0.993	20.96	17.06
58	26.50	0	21.20	17.40
63	28.00	0.986	21.39	18.19
68	29.39	0.983	21.51	17.41
73	30.78	0.983	21.21	17.41
78	32.17	0.974	22.96	19.06
83	33.56	0	21.76	17.66
88	34.94	0.988	22.73	19.23
93	36.33	0.987	21.80	18.20
98	37.72	0.975	21.08	17.08
103	39.11	0.976	19.35	15.25
108	40.50	0.987	19.83	16.33
113	41.89	0.987	20.87	17.27
118	43.28	0.982	22.78	18.78
123	44.67	0.983	22.84	19.64
128	46.06	0.987	20.15	16.25
133	47.44	0.98	19.30	15.20
138	48.83	0.981	20.03	15.93
143	50.22	0.98	20.39	16.89
148	51.61	0.984	20.78	17.18
153	53.00	0.978	21.00	17.00
158	54.50	0.975	20.75	16.85
163	56.00	0.98	21.78	17.98
168	57.50	0.987	19.34	16.14
173	59.00	0.991	20.52	16.42
178	60.50	0.981	21.96	18.16
183	62.00	0.981	17.58	13.68
188	63.50	0.981	20.49	16.39
193	65.00	0.984	20.85	17.35
198	66.36	0.987	19.95	16.35
203	67.73	0.958	21.36	17.36
208	69.09	0.98	20.76	17.56
213	70.45	0.98	20.71	16.61
218	71.56	0.973	22.07	18.27
223	73.18	0	24.87	20.97
228	74.55	0.981	21.46	17.36
233	75.91	0.975	19.55	16.05
238	77.27	0.979	21.26	17.66
248	80.00	0.969	21.15	17.65
253	81.75	0.915	20.49	16.69
258	83.50	0.978	19.63	16.43
263	85.25	0.972	19.66	15.56
268	87.00	0.97	21.03	17.23
273	88.71	0.974	19.29	15.39
278	90.43	0.985	20.58	16.48
283	92.14	0.964	19.94	16.44
288	93.89	0.979	18.52	14.92
293	95.57	0.979	19.21	15.11
298	97.29	0.981	19.17	15.67
303	99.00	0.978	19.28	15.68
308	100.60	0.955	20.02	16.02
313	102.20	0.979	20.30	16.40
318	103.80	0.974	20.75	16.95
323	105.40	0.976	19.46	16.26
328	107.00	0.951	21.76	17.66
333	108.67	0.978	21.38	17.58
338	110.33	0.962	19.86	15.76
343	112.00	0	18.45	14.35
348	113.67	0.966	22.43	18.33
353	115.33	0.985	20.24	16.74
358	117.00	0.971	20.61	17.01
363	118.67	0.973	19.33	15.33
368	120.33	0.984	20.67	16.77
373	122.00	0.985	20.76	16.96
378	123.63	0.977	20.79	17.59
383	125.25	0	21.92	17.82
388	126.88	0.942	22.68	18.88
393	128.50	0.956	22.36	18.46
398	130.13	0.973	21.89	17.79
403	131.75	0.986	22.15	18.05
408	133.38	0.978	20.40	16.90
413	135.00	0.99	20.69	17.09
418	136.57	0	16.55	12.55
423	138.14	0.984	20.51	16.61
428	139.71	0.978	19.86	16.06
433	141.29	0.986	20.45	17.25
438	142.86	0.979	21.65	17.55
443	144.43	0.989	19.63	15.83
448	146.00	0.992	20.08	16.18
453	147.67	0.993	21.72	17.62
458	149.33	0.986	21.11	17.61
463	151.00	0.99	21.69	18.09
468	152.67	0.993	21.42	17.42
473	154.33	0.989	20.22	17.02
478	156.00	0.989	21.86	17.76
488	159.33	0.986	20.35	16.45
493	161.00	0	22.10	18.00
498	162.67	0.987	20.99	17.49
503	164.33	0.989	22.25	18.65
508	166.00	0.988	21.95	17.95
513	167.67	0.975	20.21	16.31
518	169.33	0.989	19.40	15.30
523	171.00	0.991	20.68	17.18
528	172.71	0.981	21.51	17.91
533	174.43	0.984	21.02	17.02
538	176.14	0.982	19.96	16.76
543	177.86	0.991	20.34	16.24
548	179.57	0.99	19.97	16.17
553	181.29	0.985	18.43	14.53
558	183.00	0.98	17.74	13.64
563	184.83	0.988	20.79	16.79
568	186.67	0.99	21.66	17.76
573	188.50	0.996	21.73	17.93
578	190.33	0.993	21.04	17.84
583	192.17	0.989	19.50	15.40
588	194.00	0.994	20.01	16.21
593	196.20	0.979	21.04	17.14
598	198.40	0.975	18.84	14.74
603	200.60	0.98	20.33	16.83
608	202.80	0.985	20.73	17.13
613	205.00	0.983	19.09	15.09
618	207.20	0.975	18.84	14.94
623	209.40	0	17.96	14.16
628	211.60	0.978	21.86	18.66
633	213.80	0	17.49	13.39
638	216.00	0.981	23.39	19.59
643	217.71	9	18.92	14.82
648	219.43	0.98	19.76	15.66
653	221.14	0.982	21.54	18.04
658	222.86	0	17.89	14.29
663	224.57	0.987	20.03	16.03
668	226.29	0.984	20.89	16.99
673	228.00	0.986	19.78	15.98
678	229.43	0.976	19.46	16.26
683	230.86	0.983	18.49	14.39
688	232.29	0.985	18.30	14.50
693	233.71	0.989	21.37	17.47
698	235.14	0.984	21.29	17.19
703	236.57	0.986	20.87	17.37
708	238.00	0.978	20.66	17.06
713	239.57	0.975	20.84	16.84
718	241.14	0.964	21.65	18.15
728	244.29	0.983	19.41	15.41
733	245.86	0.985	20.61	16.71
738	247.43	0.986	21.21	17.41
743	249.00	0.981	20.52	17.32
748	250.67	0.976	20.26	16.16
753	252.33	0.974	20.74	16.94
758	254.00	0.977	21.27	17.37
763	255.67	0.989	21.26	17.16
768	257.33	0.992	21.41	17.91
773	259.00	0	17.87	14.27
778	260.67	0.989	19.17	15.17
783	262.33	0	17.36	13.46
788	264.00	0.995	20.71	16.61
793	265.67	0.993	20.27	16.77
798	267.33	0	21.11	17.51
803	269.00	0.995	21.64	17.64
808	270.50	0.99	21.28	18.08
813	272.00	0.975	20.57	16.47
818	273.50	0.995	21.05	16.95
823	275.00	0.995	20.85	17.35
828	276.50	0.992	20.07	16.47
833	278.00	0.99	19.93	16.43
838	279.50	0.984	19.65	16.05
843	281.00	0.995	20.77	16.77
848	282.50	0.989	21.75	18.55
853	284.00	0.977	21.04	16.94
858	285.50	0.978	21.30	17.20
863	287.00	0.993	19.28	16.08
868	288.33	0.985	21.24	17.14
873	289.67	0	19.11	15.01
878	291.00	0.993	21.28	17.48
883	292.33	0	16.88	12.98
888	293.67	0.994	20.07	15.97
893	295.00	0.989	20.67	17.17
898	296.33	0.993	19.68	16.08
903	297.67	0	17.41	13.41
908	299.00	0.991	19.53	16.33
913	300.10	0.989	18.22	14.12
918	301.20	0.988	19.57	15.77
923	302.30	0	18.36	14.46
928	303.40	0	19.12	15.02
933	304.50	0.986	19.66	16.16
938	305.60	0	19.31	15.71
943	306.70	0.995	21.32	17.32
948	307.80	0.991	20.92	17.72
953	308.90	0.98	20.86	17.06
958	310.00	0.989	19.87	15.97
968	313.00	0.991	22.13	18.63
973	314.50	0.976	18.06	14.56
978	316.05	0.983	20.68	17.08
983	317.50	0.977	19.89	15.89
988	319.00	0.988	19.20	16.00
993	320.50	0	17.15	13.65
998	322.00	0.993	19.62	15.82
1003	323.50	0	18.35	14.45
1008	325.00	0.986	19.30	15.20
1013	326.50	0.989	24.06	20.56
1018	328.00	0.984	21.36	17.26
1023	329.90	0.977	19.80	16.00
1028	331.00	0.986	21.31	17.41
1033	332.91	0.969	20.32	16.22
1038	334.07	0.982	22.25	18.75
1048	337.29	0.98	22.12	18.02
1053	338.86	0.958	21.45	17.65
1058	340.43	0.986	21.26	17.36
1063	342.00	0.987	23.00	18.90
1068	343.63	0.991	20.19	16.69
1073	344.93	0.987	21.61	17.61
1078	345.25	0.986	20.31	17.11
1083	348.50	0.983	20.24	16.74
1088	350.13	0.988	22.42	18.32
1093	351.75	0.985	20.51	17.01
1098	353.38	0.986	18.48	14.88
1103	355.00	0.993	21.18	17.18
1108	356.63	0.989	21.44	18.24
1113	358.25	0.991	21.89	18.69
1118	359.88	0.977	21.38	17.28
1123	361.50	0	21.09	16.99
1128	363.13	0.993	20.57	17.07
1133	364.75	0.984	21.63	18.03

APPENDIX 4.2

Transfer function F227-24-5 for core GeoB 3603-2.

Depth (cmbsf)	Time (k.y.)	Commun-ality	Sset	Wset	Asst
8	4.00	0.94	21.05	16.87	21.19
13	7.00	0.96	20.28	16.11	20.37
18	10.00	0.84	20.98	16.81	20.72
23	13.00	0.88	20.09	16.06	19.95
28	16.00	0	18.23	14.47	17.39
33	19.00	0	17.1	13.78	16.1
38	20.50	0	17.4	14	16.44
43	22.00	0	19.77	15.73	19.27
48	23.50	0	18.28	14.76	17.31
53	25.00	0	18.57	14.72	17.81
58	26.50	0	18.11	14.6	17.13
63	28.00	0	17.96	14.42	17.02
68	29.39	0	18.39	14.78	17.43
73	30.78	0	17.94	14.25	17.11
78	32.17	0	19.57	15.8	18.75
83	33.56	0	17.95	14.57	16.91
88	34.94	0	19.5	15.66	18.68
93	36.33	0	18.93	15.03	18.25
98	37.72	0	18.98	15.1	18.29
103	39.11	0	17.82	14.05	17.26
108	40.50	0	17.77	14.06	16.97
113	41.89	0	18.17	14.49	17.31
118	43.28	0	18.88	15.22	17.96
123	44.67	0	19.04	15.28	18.29
128	46.06	0	18.42	14.52	17.79
133	47.44	0	18.87	14.86	18.41
138	48.83	0	19.28	15.21	19.12
143	50.22	0	18.65	14.72	18.3
148	51.61	0	19.19	15.25	18.55
153	53.00	0	19.16	15.18	18.6
158	54.50	0	18.91	14.97	18.34
163	56.00	0	18.53	14.78	17.72
168	57.50	0	18.51	14.53	18.05
173	59.00	0	18.15	14.43	17.31
178	60.50	0	18.7	14.92	17.92
183	62.00	0	18.99	14.85	18.81
188	63.50	0	18.87	14.97	18.27
193	65.00	0	19.05	15.3	18.19
198	66.36	0	18.51	14.62	17.86
203	67.73	0	19.25	15.61	18.31
208	69.09	0	18.27	14.66	17.4
213	70.45	0	18.53	14.86	17.74
218	71.56	0	18.38	15.08	17.29
223	73.18	0	20.04	16.9	18.87
228	74.55	0	18.56	14.95	17.64
233	75.91	0	19.67	15.56	19.36
238	77.27	0	18.44	14.81	17.56
243	78.64	0	19.26	15.47	18.43
248	80.00	0	18.83	15.11	18.28
253	81.75	0	19.28	15.45	18.7
258	83.50	0.94	20.88	16.53	20.94
263	85.25	0.92	20.62	16.36	20.62
268	87.00	0	19.89	15.82	19.43
273	88.71	0.87	19.76	15.61	19.69
278	90.43	0	19.38	15.3	19
283	92.14	0.82	20.43	16.3	20.17
288	93.89	0.88	19.08	14.96	19.03
293	95.57	0.86	20.02	15.83	19.86
298	97.29	0.91	20.04	15.85	20.01
303	99.00	0.86	19.38	15.29	19.21
308	100.60	0.93	18.94	15.09	19.15
313	102.20	0	19.39	15.31	19.09
318	103.80	0.84	20.16	16.04	20.04
323	105.40	0	19.09	15.11	18.9
328	107.00	0	20.04	16.04	19.63
333	108.67	0	20.1	16.06	19.57
338	110.33	0.83	19.66	15.59	19.51
343	112.00	0.9	20.22	16.01	20.15
348	113.67	0	20.69	16.51	20.35
353	115.33	0	20.17	15.97	19.97
358	117.00	0.83	20.99	16.8	20.76
363	118.67	0.95	20.65	16.4	20.72
368	120.33	0.95	21.4	17.01	21.51
373	122.00	0.91	21.27	16.92	21.28
378	123.63	0.91	20.74	16.53	20.77
383	125.25	0.93	21.61	17.38	21.68
388	126.88	0.89	21.84	17.59	21.87
393	128.50	0.88	21.33	17.16	21.3
398	130.13	0	21.09	17.03	20.63
403	131.75	0	20.08	16.1	19.41
408	133.38	0.83	20.42	16.22	20.21
413	135.00	0	20.16	16.17	19.68
418	136.57	0.93	19.28	15.5	19.24
423	138.14	0	19.18	15.47	18.45
428	139.71	0.84	20.15	15.96	19.94
433	141.29	0	19.64	15.55	19.24
438	142.86	0	19.47	15.76	18.61
443	144.43	0	17.97	14.09	17.33
448	146.00	0	18.97	15.17	18.23
453	147.67	0	19.22	15.39	18.41
458	149.33	0	19.58	15.69	18.96
463	151.00	0	18.16	14.42	17.33
468	152.67	0	19.16	15.33	18.37
473	154.33	0	17.81	14.15	16.93
478	156.00	0	18.38	14.76	17.42
483	157.67	0	18.68	15.05	17.73
488	159.33	0	18.99	15.04	18.38
493	161.00	0	18.47	14.96	17.49
498	162.67	0	18.33	14.57	17.53
503	164.33	0	19.25	15.33	18.56
508	166.00	0	19.41	15.48	18.69
513	167.67	0	19.6	15.52	19.16
518	169.33	0	19.16	15.12	18.69
523	171.00	0	19.51	15.54	18.9
528	172.71	0	19.04	15.19	18.29
533	174.43	0	18.93	15.15	18.1
538	176.14	0	17.66	14	16.91
543	177.86	0	18.45	14.61	17.73
548	179.57	0	18.9	14.88	18.36
553	181.29	0	19.01	15.12	18.57
558	183.00	0	18.41	14.33	18.09
563	184.83	0	18.83	15.04	18.07
568	186.67	0	18.81	15.11	17.91
573	188.50	0	18.92	15.16	18.13
578	190.33	0	19.68	15.81	19.08
583	192.17	0	19.16	15.35	18.62
588	194.00	0	19.16	15.16	18.58
593	196.20	0	19.87	15.79	19.42
598	198.40	0.89	19.77	15.57	19.7
603	200.60	0	20.34	16.21	20
608	202.80	0	19.96	15.92	19.45
613	205.00	0	19.88	15.87	19.56
618	207.20	0	19.59	15.48	19.29
623	209.40	0	18.6	14.85	18.09
628	211.60	0	19.94	15.99	19.28
633	213.80	0.93	19.87	15.72	19.85
638	216.00	0	20.62	16.6	19.99
643	217.71	0.92	20.66	16.4	20.66
648	219.43	0.88	20.64	16.4	20.55
653	221.14	0.82	21.21	17	20.97
658	222.86	0.9	19.62	15.42	19.54
663	224.57	0	20	15.89	19.66
668	226.29	0	19.76	15.68	19.31
673	228.00	0	19.34	15.33	18.89
678	229.43	0	19.14	15.03	18.77
683	230.86	0	19.25	15.19	18.91
688	232.29	0	18.76	14.76	18.33
693	233.71	0	18.97	15.38	18.07
698	235.14	0	18.77	15	17.92
703	236.57	0	19.25	15.25	18.74
708	238.00	0	19.81	15.68	19.55
713	239.57	0.87	20.96	16.74	20.84
718	241.14	0.87	21.2	16.98	21.13
723	242.71	0	20.83	16.66	20.48
728	244.29	0	19.25	15.14	18.9
733	245.86	0	19.12	15.29	18.41
738	247.43	0	18.82	14.99	18.02
743	249.00	0	19.33	15.31	18.95
748	250.67	0	18.94	14.96	18.36
753	252.33	0	19.63	15.59	19.09
758	254.00	0	19.1	15.13	18.51
763	255.67	0	19.85	15.84	19.28
768	257.33	0	19.28	15.4	18.59
773	259.00	0	18.93	15.09	18.49
778	260.67	0	18.65	14.93	17.98
783	262.33	0	19.34	15.58	19.09
788	264.00	0	18.61	14.98	17.75
793	265.67	0	18.66	14.99	17.89
798	267.33	0	17.95	14.47	16.95
803	269.00	0	18.53	14.79	17.66
808	270.50	0	18.35	14.66	17.45
813	272.00	0	19.06	15.34	18.22
818	273.50	0	18.59	15	17.72
823	275.00	0	19.07	15.13	18.38
828	276.50	0	18.55	14.73	17.82
833	278.00	0	19.3	15.35	18.72
838	279.50	0	18.66	14.67	18.17
843	281.00	0	18.69	14.97	17.89
848	282.50	0	18.98	15.2	18.2
853	284.00	0	19.7	15.92	19
858	285.50	0	19.7	15.81	19.04
863	287.00	0	19.6	15.66	19.21
868	288.33	0	20.04	16.15	19.46
873	289.67	0	19.89	15.95	19.6
878	291.00	0	19.86	15.88	19.24
883	292.33	0.88	19.52	15.6	19.39
888	293.67	0	18.76	15.1	18.03
893	295.00	0	19.27	15.38	18.61
898	296.33	0	18.66	14.8	17.97
903	297.67	0	18.75	14.96	18.38
908	299.00	0	18.99	15.15	18.41
913	300.10	0	17.22	13.62	16.6
918	301.20	0	19.19	15.38	18.62
923	302.30	0	19.04	15.26	18.56
928	303.40	0	18.78	15.11	18.28
933	304.50	0	20.08	16.05	19.81
938	305.60	0	19.81	15.87	19.44
943	306.70	0	19.16	15.45	18.38
948	307.80	0	18.25	14.49	17.47
953	308.90	0	18.56	14.79	17.76
958	310.00	0	18.66	14.87	17.96
963	311.50	0	19.53	15.72	19.35
968	313.00	0	19.47	15.74	18.64
973	314.50	0.92	18.7	14.64	18.61
978	316.05	0	19.75	15.76	19.35
983	317.50	0.84	19.03	15.09	18.76
988	319.00	0	19.1	15.15	18.57
993	320.50	0.89	19.01	15.21	18.87
998	322.00	0	19.03	15.22	18.4
1003	323.50	0.86	19.75	15.68	19.57
1008	325.00	0	18.7	14.87	18.17
1013	326.50	0	19.17	15.37	18.41
1018	328.00	0	18.71	14.79	18.07
1023	329.90	0.81	19.75	15.62	19.48
1028	331.00	0	19.76	15.68	19.28
1033	332.91	0.95	19.01	15.24	19.14
1038	334.07	0	20.47	16.38	20.05
1043	335.71	0.77	20.52	16.48	20.18
1048	337.29	0	20.66	16.55	20.17
1053	338.86	0	20.24	16.19	19.87
1058	340.43	0	19.53	15.52	18.93
1063	342.00	0	19.72	15.81	19
1068	343.63	0	18.14	14.43	17.28
1073	344.93	0	18.65	14.8	17.94
1078	345.25	0	19.08	15.07	18.54
1083	348.50	0	19.81	15.75	19.37
1088	350.13	0	19.74	15.74	19.21
1093	351.75	0	19.22	15.22	18.66
1098	353.38	0	18.92	14.81	18.62
1103	355.00	0	19.79	15.73	19.29
1108	356.63	0	19.33	15.35	18.71
1113	358.25	0	18.58	14.98	17.62
1118	359.88	0	18.71	14.81	18.06
1123	361.50	0	17.99	14.6	16.95
1128	363.13	0	18.11	14.47	17.19
1133	364.75	0	19.92	15.92	19.32

APPENDIX 4.3

Transfer function F279-24-5 for core GeoB 3603-2.

Depth (cmbsf)	Time (k.y.)	Commun-ality	Sest	West	Aest
8	4.00	0.95	22.2	17.82	20.1
13	7.00	0.95	20.96	16.89	19.09
18	10.00	0.85	21.85	17.33	19.89
23	13.00	0.87	20.97	16.84	19.34
28	16.00	0	18.63	14.97	17.56
33	19.00	0	15.8	14.05	15.64
38	20.50	0	16.48	14.52	16.21
43	22.00	0.72	20.83	16.44	19.18
48	23.50	0	18.05	15.38	17.44
53	25.00	0.6	19.15	15.3	17.98
58	26.50	0	17.71	15.1	17.14
63	28.00	0	17.25	14.65	16.66
68	29.39	0	18.5	15.26	17.66
73	30.78	0.54	18.15	14.5	17.02
78	32.17	0.54	19.66	15.92	18.42
83	33.56	0	17.08	14.61	16.52
88	34.94	0	19.87	16.01	18.64
93	36.33	0.63	19.4	15.47	18.11
98	37.72	0.6	19.17	15.44	18.02
103	39.11	0.61	17.63	14.46	16.73
108	40.50	0	17.47	14.53	16.76
113	41.89	0	17.84	14.84	17.07
118	43.28	0.49	18.93	15.42	17.84
123	44.67	0.57	19.1	15.35	17.86
128	46.06	0.65	18.78	15.01	17.62
133	47.44	0.75	19.5	15.34	18.12
138	48.83	0.85	20.17	15.96	18.65
143	50.22	0.79	19.41	15.24	17.93
148	51.61	0.66	19.94	15.82	18.56
153	53.00	0.69	19.68	15.58	18.33
158	54.50	0.68	19.33	15.36	18.05
163	56.00	0.56	18.66	14.94	17.5
168	57.50	0.73	19.17	15.22	17.89
173	59.00	0	18.74	15.03	17.67
178	60.50	0.56	18.7	15.07	17.59
183	62.00	0.87	19.5	15.51	18.16
188	63.50	0.65	19.23	15.45	18.02
193	65.00	0	19.94	16.15	18.75
198	66.36	0.62	18.76	15.15	17.69
203	67.73	0	19.49	16.06	18.37
208	69.09	0	17.59	14.99	16.99
213	70.45	0	17.95	15.13	17.17
218	71.56	0	18.21	15.82	17.7
223	73.18	0	20.28	17.61	19.44
228	74.55	0	18.02	15.29	17.35
233	75.91	0.81	20.48	16.18	18.9
238	77.27	0	17.85	15.14	17.19
243	78.64	0.55	19.63	15.83	18.39
248	80.00	0.6	18.35	15.19	17.36
253	81.75	0.63	19.64	15.7	18.25
258	83.50	0.93	20.82	16.65	19.12
263	85.25	0.93	20.72	16.56	19.01
268	87.00	0.76	20.42	16.07	18.88
273	88.71	0.89	20.73	16.44	19.04
278	90.43	0.77	20.08	15.88	18.63
283	92.14	0.83	20.91	16.56	19.19
288	93.89	0.9	19.93	15.83	18.45
293	95.57	0.87	20.78	16.5	19.11
298	97.29	0.93	20.92	16.66	19.16
303	99.00	0.87	20.17	15.98	18.49
308	100.60	0.95	20.63	16.42	18.96
313	102.20	0.82	20.23	15.96	18.65
318	103.80	0.87	21.24	16.79	19.43
323	105.40	0.84	20.19	15.98	18.57
328	107.00	0.75	20.87	16.43	19.18
333	108.67	0.73	21.01	16.57	19.33
338	110.33	0.86	20.72	16.39	19.03
343	112.00	0.89	20.76	16.6	19.11
348	113.67	0.79	21.56	16.93	19.73
353	115.33	0.85	20.88	16.53	19.21
358	117.00	0.84	21.4	16.97	19.62
363	118.67	0.94	20.95	16.86	19.13
368	120.33	0.95	21.23	17.05	19.34
373	122.00	0.92	21.37	17.07	19.51
378	123.63	0.93	21.84	17.39	19.84
383	125.25	0.93	21.95	17.89	19.86
388	126.88	0.91	23.09	18.37	20.82
393	128.50	0.9	22.56	17.95	20.41
398	130.13	0.75	21.97	17.33	20.1
403	131.75	0.66	20.97	16.6	19.38
408	133.38	0.85	21.08	16.67	19.35
413	135.00	0.74	21.11	16.75	19.52
418	136.57	0.9	19.86	16.1	18.51
423	138.14	0.62	20.56	16.46	19.19
428	139.71	0.85	20.61	16.34	19
433	141.29	0.78	20.41	16.1	18.86
438	142.86	0.55	20.39	16.44	19.15
443	144.43	0.65	18.58	14.74	17.4
448	146.00	0.61	20.01	16.1	18.8
453	147.67	0	19.96	16.05	18.74
458	149.33	0.68	20.56	16.2	19.03
463	151.00	0.6	18.79	14.71	17.51
468	152.67	0.58	19.89	15.99	18.7
473	154.33	0	17.84	14.82	17.09
478	156.00	0	18.21	15.17	17.43
483	157.67	0	18.57	15.44	17.73
488	159.33	0.66	19.64	15.67	18.34
493	161.00	0	17.75	15.26	17.17
498	162.67	0	18.33	15.04	17.43
503	164.33	0.63	19.79	15.7	18.42
508	166.00	0.61	19.9	15.89	18.61
513	167.67	0.75	20.31	16.05	18.82
518	169.33	0.74	19.89	15.81	18.58
523	171.00	0.68	20.51	16.28	19.07
528	172.71	0.57	19.19	15.53	18.07
533	174.43	0	19.39	15.74	18.32
538	176.14	0	16.88	14.16	16.24
543	177.86	0.63	19.14	15.18	17.9
548	179.57	0.7	19.57	15.58	18.33
553	181.29	0.75	19.97	16	18.73
558	183.00	0.8	19.12	15.24	17.93
563	184.83	0.6	19.63	15.72	18.46
568	186.67	0	19.44	15.79	18.39
573	188.50	0.6	19.75	15.62	18.43
578	190.33	0.67	20.68	16.48	19.31
583	192.17	0.71	20.21	16.05	18.8
588	194.00	0.69	20.02	15.93	18.65
593	196.20	0.77	20.46	16.08	18.86
598	198.40	0.9	20.41	16.24	18.83
603	200.60	0.81	21.02	16.66	19.37
608	202.80	0.73	20.79	16.47	19.27
613	205.00	0.8	20.63	16.46	19.16
618	207.20	0.82	20.25	16.1	18.8
623	209.40	0.7	19.79	16.01	18.72
628	211.60	0.66	20.82	16.52	19.34
633	213.80	0.91	20.11	16.17	18.71
638	216.00	0.67	21.36	16.77	19.66
643	217.71	0.91	20.51	16.39	18.95
648	219.43	0.89	20.85	16.6	19.2
653	221.14	0.83	21.55	17.06	19.74
658	222.86	0.9	20.03	16.01	18.61
663	224.57	0.81	20.76	16.44	19.14
668	226.29	0.76	20.48	16.15	18.94
673	228.00	0.75	20.12	15.95	18.73
678	229.43	0.79	19.73	15.6	18.36
683	230.86	0.8	19.85	15.76	18.49
688	232.29	0.76	19.56	15.59	18.32
693	233.71	0	20.05	16.37	18.99
698	235.14	0	19.12	15.6	18.13
703	236.57	0.73	20.01	15.72	18.49
708	238.00	0.83	20.66	16.3	18.99
713	239.57	0.88	21.36	17	19.47
718	241.14	0.89	22.36	17.73	20.23
723	242.71	0.79	21.62	17.04	19.77
728	244.29	0.79	20.12	15.9	18.63
733	245.86	0.64	20.02	15.99	18.73
738	247.43	0.57	19.34	15.59	18.2
743	249.00	0.77	20.04	15.86	18.57
748	250.67	0.68	19.7	15.7	18.39
753	252.33	0.71	20.29	16.04	18.85
758	254.00	0.68	19.73	15.64	18.36
763	255.67	0.7	20.66	16.36	19.18
768	257.33	0.64	20.17	16	18.8
773	259.00	0.74	20.02	16.11	18.83
778	260.67	0.63	19.85	16.06	18.77
783	262.33	0.81	20.34	16.45	19.1
788	264.00	0	19.64	16.06	18.67
793	265.67	0.59	19.88	16.01	18.73
798	267.33	0	17.8	15.21	17.27
803	269.00	0	19.09	15.31	17.97
808	270.50	0	18.79	15.25	17.82
813	272.00	0.56	19.95	16.13	18.81
818	273.50	0	19.64	16	18.63
823	275.00	0.63	19.82	15.82	18.56
828	276.50	0.61	19.35	15.54	18.25
833	278.00	0.69	20.12	16.03	18.83
838	279.50	0.72	19.22	15.25	17.95
843	281.00	0	19.64	15.83	18.54
848	282.50	0.6	19.76	15.64	18.43
853	284.00	0.64	20.78	16.63	19.42
858	285.50	0.66	20.52	16.27	19.1
863	287.00	0.77	20.49	16.33	19.06
868	288.33	0.7	21.08	16.69	19.48
873	289.67	0.81	20.5	16.36	19.04
878	291.00	0.68	20.72	16.43	19.24
883	292.33	0.86	20.19	16.29	18.88
888	293.67	0.61	19.97	16.12	18.84
893	295.00	0.66	20.16	16.04	18.83
898	296.33	0.63	19.59	15.75	18.47
903	297.67	0.77	19.83	15.99	18.68
908	299.00	0.69	20.05	16.03	18.78
913	300.10	0.67	18.28	14.47	17.18
918	301.20	0.69	20.27	16.2	18.97
923	302.30	0.73	20.27	16.32	19.04
928	303.40	0.71	19.96	15.97	18.7
933	304.50	0.83	20.57	16.36	18.99
938	305.60	0.78	20.66	16.51	19.24
943	306.70	0	20.27	16.34	19.08
948	307.80	0.61	19	15.01	17.78
953	308.90	0.54	18.63	15.19	17.64
958	310.00	0.63	19.66	15.78	18.52
963	311.50	0.84	20.45	16.55	19.13
968	313.00	0.57	20.48	16.4	19.16
973	314.50	0.92	18.8	14.9	17.32
978	316.05	0.79	20.31	15.99	18.68
983	317.50	0.85	19.25	15.18	17.66
988	319.00	0.72	19.97	15.95	18.7
993	320.50	0.87	19.65	15.79	18.26
998	322.00	0.66	20.19	16.21	18.97
1003	323.50	0.86	20.22	16.17	18.78
1008	325.00	0.72	19.65	15.59	18.34
1013	326.50	0.66	19.8	15.34	18.14
1018	328.00	0.69	19.3	15.08	17.87
1023	329.90	0.83	20.49	16.18	18.87
1028	331.00	0.74	20.46	16.17	18.96
1033	332.91	0.96	20.49	16.39	18.7
1038	334.07	0.77	21.4	16.82	19.56
1043	335.71	0.8	21.53	16.93	19.61
1048	337.29	0.73	21.4	16.83	19.67
1053	338.86	0.78	21.18	16.66	19.32
1058	340.43	0.68	20.22	16.02	18.81
1063	342.00	0.61	20.26	16.09	18.82
1068	343.63	0	18.37	15.2	17.61
1073	344.93	0.6	18.93	15.15	17.76
1078	345.25	0.7	19.74	15.69	18.41
1083	348.50	0.77	20.54	16.24	19
1088	350.13	0.72	20.47	16.07	18.86
1093	351.75	0.69	19.96	15.85	18.57
1098	353.38	0.81	19.6	15.56	18.28
1103	355.00	0.74	20.54	16.19	19
1108	356.63	0.66	20	15.89	18.64
1113	358.25	0	18.59	15.57	17.84
1118	359.88	0.68	19.3	15.08	17.88
1123	361.50	0	17.92	15.27	17.32
1128	363.13	0	18.26	15.26	17.57
1133	364.75	0.69	20.75	16.37	19.15

APPENDIX 4.4

Transfer function F221-24-5 for the spliced Cape Basin record.

Depth (cmbsf)	Time (k.y.)	Commun-ality	Sast	West	Aast
8	4	0.9	22.21	17.71	20.05
13	7	0.88	21.79	17.22	19.6
18	10	0.9	21.62	17.17	19.5
23	13	0.84	21.29	16.87	19.24
28	16	0.84	19.01	14.97	17.29
33	19	0.78	17.81	13.84	16.27
38	20.5	0.84	18.31	14.51	16.78
43	22	0.83	20.67	16.45	18.77
48	23.5	0.81	19.47	15.48	17.8
53	25	0.84	18.95	14.93	17.27
58	26.5	0.83	19.05	15.05	17.41
63	28	0.82	19.07	14.93	17.35
68	29.39	0.81	19.07	15	17.45
73	30.78	0.84	19.01	14.88	17.18
78	32.17	0.86	20.43	16.22	18.55
83	33.56	0.79	19.27	14.96	17.43
88	34.94	0.84	19.8	15.81	18.11
93	36.33	0.85	19.64	15.56	17.87
98	37.72	0.81	19.04	15.11	17.49
103	39.11	0.8	19.15	15.13	17.48
108	40.5	0.84	18.09	14.37	16.64
113	41.89	0.82	18.82	14.85	17.18
118	43.28	0.84	20.21	15.92	18.29
123	44.67	0.84	19.76	15.56	17.92
128	46.06	0.88	18.61	14.82	17.09
133	47.44	0.82	18.7	14.64	17.03
138	48.83	0.87	19.48	15.58	17.94
143	50.22	0.82	19.1	14.95	17.35
148	51.61	0.88	19.92	15.85	18.12
153	53	0.83	19.14	15.16	17.55
158	54.5	0.86	19.28	15.28	17.7
163	56	0.82	19.17	15.04	17.39
168	57.5	0.87	18.9	15.04	17.31
173	59	0.84	18.5	14.53	16.87
178	60.5	0.82	19.36	15.18	17.63
183	62	0.85	18.54	14.77	17.06
188	63.5	0.85	19.8	15.78	18.07
193	65	0.86	20.03	15.94	18.25
198	66.36	0.86	18.34	14.7	16.94
203	67.73	0.89	20.76	16.44	18.78
208	69.09	0.84	19.18	15.36	17.64
213	70.45	0.88	20.01	15.87	18.19
218	71.56	0.87	20.44	16.28	18.68
223	73.18	0.78	21.94	17.47	19.83
228	74.55	0.85	19.86	15.89	18.18
233	75.91	0.85	20.14	16.02	18.32
238	77.27	0.83	19.75	15.71	18.05
243	78.64	0.86	20.48	16.21	18.53
248	80	0.86	20.15	16.1	18.39
253	81.75	0.81	20.01	15.79	18.14
258	83.5	0.91	20.75	16.68	18.97
263	85.25	0.87	21.2	16.88	19.24
268	87	0.84	20.05	15.82	18.29
273	88.71	0.87	20.86	16.6	18.91
278	90.43	0.87	19.32	15.49	17.8
283	92.14	0.85	20.75	16.45	18.79
288	93.89	0.87	19.79	15.83	18.12
293	95.57	0.89	20.81	16.57	18.87
298	97.29	0.95	20.47	16.44	18.65
303	99	0.86	20.38	16.04	18.37
308	100.6	0.86	20.59	16.41	18.82
313	102.2	0.85	19.85	15.76	18.06
318	103.8	0.91	20.9	16.74	19.02
323	105.4	0.89	20.73	16.38	18.71
328	107	0.89	20.69	16.52	18.84
333	108.67	0.89	20.75	16.52	18.82
338	110.33	0.87	20.95	16.72	19.02
343	112	0.84	21.19	16.89	19.3
348	113.67	0.85	21.08	16.81	19.21
353	115.33	0.88	20.39	16.3	18.59
358	117	0.85	21.37	17.07	19.39
363	118.67	0.91	21.31	16.91	19.23
368	120.33	0.93	21.23	17	19.29
373	122	0.93	20.96	16.9	19.15
378	123.63	0.92	21.68	17.31	19.6
383	125.25	0.91	22.02	17.45	19.82
388	126.88	0.93	21.97	17.54	19.84
393	128.5	0.91	21.98	17.54	19.86
398	130.13	0.89	21.76	17.37	19.68
403	131.75	0.87	20.73	16.5	18.8
408	133.38	0.89	20.8	16.61	18.91
413	135	0.88	20.49	16.35	18.62
418	136.57	0.83	20.67	16.36	18.7
423	138.14	0.87	20.5	16.26	18.58
428	139.71	0.87	20.38	16.21	18.57
433	141.29	0.86	20.06	15.93	18.26
438	142.86	0.86	19.83	15.91	18.19
443	144.43	0.83	18.19	14.25	16.61
448	146	0.84	19.72	15.7	18
453	147.67	0.83	19.97	15.9	18.21
458	149.33	0.83	20.27	15.97	18.35
463	151	0.85	18.24	14.08	16.56
468	152.67	0.84	19.3	15.42	17.73
473	154.33	0.81	18.99	14.99	17.32
478	156	0.84	19.37	15.3	17.68
483	157.67	0.82	19.32	15.29	17.63
488	159.33	0.87	19.76	15.77	18.04
493	161	0.77	19.58	15.39	17.82
498	162.67	0.84	19.23	15.31	17.62
503	164.33	0.83	19.67	15.52	17.89
508	166	0.82	19.44	15.46	17.81
513	167.67	0.84	19.94	15.89	18.23
518	169.33	0.87	19.4	15.54	17.86
523	171	0.86	20.42	16.27	18.57
528	172.71	0.82	19.52	15.55	17.88
533	174.43	0.85	19.06	15.26	17.54
538	176.14	0.8	18.16	14.22	16.62
543	177.86	0.87	18.93	14.92	17.2
548	179.57	0.85	18.41	14.76	17.05
553	181.29	0.87	18.96	15.21	17.48
558	183	0.83	17.32	13.96	16.21
563	184.83	0.83	18.7	14.79	17.18
568	186.67	0.86	18.89	15.1	17.39
573	188.5	0.88	18.8	14.68	17.15
578	190.33	0.84	19.18	15.31	17.7
583	192.17	0.89	20.04	15.83	18.14
588	194	0.92	19.67	15.73	17.97
593	196.2	0.87	19.75	15.66	18.02
598	198.4	0.91	20.53	16.49	18.74
603	200.6	0.89	20.38	16.35	18.6
608	202.8	0.86	20.38	16.29	18.57
613	205	0.86	19.93	15.92	18.2
618	207.2	0.85	19.77	15.86	18.13
623	209.4	0.79	18.28	14.57	16.94
628	211.6	0.84	19.81	15.89	18.18
633	213.8	0.89	19.6	15.76	18.02
638	216	0.85	20.21	16.08	18.45
643	217.71	0.87	20.15	16.06	18.49
648	219.43	0.88	20.41	16.36	18.65
653	221.14	0.88	20.91	16.78	19.08
658	222.86	0.91	19.62	15.76	18
663	224.57	0.88	20.6	16.37	18.68
668	226.29	0.87	20.21	16.08	18.42
673	228	0.84	18.83	14.89	17.26
678	229.43	0.82	19.17	15.13	17.59
683	230.86	0.83	18.83	14.92	17.26
688	232.29	0.88	18.41	14.77	17.02
693	233.71	0.8	19.51	15.57	17.9
698	235.14	0.81	18.85	15.07	17.38
703	236.57	0.86	19.85	15.66	17.99
983	237.17	0.88	19.67	15.44	17.75
988	238	0.88	21.46	17.04	19.4
993	245	0.87	21.18	16.95	19.27
998	246.33	0.85	19.87	15.8	18.1
1003	247.67	0.86	21.09	16.83	19.17
1008	249	0.87	20.15	15.94	18.27
1013	250	0.87	20.12	16.12	18.45
1018	251	0.86	20.92	16.68	19.05
1023	252	0.85	20.31	16.2	18.56
1028	253	0.83	20.67	16.36	18.72
1033	254	0.84	20.61	16.42	18.83
1038	255	0.87	20.56	16.35	18.72
1043	256	0.87	20.29	16.22	18.5
1048	257	0.86	20.34	16.1	18.42
1053	259.4	0.88	20.47	16.33	18.63
1058	261.8	0.86	19.22	15.4	17.7
1063	264.2	0.83	18.37	14.46	16.8
1068	266.6	0.85	19.97	15.98	18.3
1073	269	0.66	18.1	13.92	16.33
1078	270.5	0.78	20	15.88	18.28
1083	272	0.83	20.24	16.03	18.37
1088	273.5	0.87	19.82	15.74	18.04
1093	275	0.87	19.82	15.79	18.11
1098	276.5	0.82	19.95	15.92	18.26
1103	278	0.86	17.24	13.23	15.5
1108	279.5	0.84	19	15.03	17.39
1113	281	0.83	19.51	15.46	17.83
1118	282.5	0.85	18.62	14.97	17.24
1123	284	0.85	20.69	16.45	18.76
1128	285.5	0.86	20.68	16.53	18.84
1133	287	0.83	20.44	16.26	18.61
1138	288.5	0.83	19.76	15.72	18.07
1143	290	0.87	20.19	16.03	18.34
1148	291.5	0.85	19.07	15.25	17.54
1153	293	0.88	20.12	16.12	18.38
1158	294.5	0.84	20.11	15.89	18.32
1163	296	0.85	18.88	14.95	17.24
1168	297.5	0.85	19.31	15.15	17.55
1173	299	0.83	19.86	15.76	18.15
1178	299.85	0.81	20.04	16.04	18.35
1183	300.69	0.87	20.32	16.17	18.49
1188	301.54	0.85	18.41	14.37	16.7
1193	302.38	0.86	20.2	16.16	18.45
1198	303.23	0.85	20.52	16.4	18.71
1203	304.08	0.84	20.13	16.03	18.33
1208	304.92	0.84	20.08	15.77	18.14
1213	305.77	0.87	20.12	15.84	18.15
1218	306.62	0.84	19.55	15.35	17.66
1223	307.46	0.82	19.76	15.75	18.05
1228	308.31	0.82	18.89	14.71	17.08
1233	309.15	0.87	19.76	15.62	17.92
1238	310	0.82	18.76	14.5	16.93
1243	311.67	0.85	20.33	16.15	18.48
1248	313.33	0.87	20.07	15.77	18.17
1253	315	0.86	18.26	14.04	16.46
1258	316.67	0.88	19.21	15.05	17.29
1263	318.33	0.86	19.04	15.02	17.37
1268	320	0.86	18.49	14.37	16.74
1273	321.38	0.82	19.39	15.4	17.71
1278	322.75	0.88	19.06	14.93	17.34
1283	324.13	0.84	20.27	15.9	18.34
1288	325.5	0.85	19.52	15.21	17.61
1293	326.88	0.89	17.67	13.42	15.87
1298	328.25	0.87	18.77	14.58	16.9
1303	329.63	0.86	20.66	16.26	18.65
1308	331	0.84	20.67	16.25	18.66
1313	331.77	0.86	20.48	16.11	18.5
1318	332.54	0.88	19.7	15.48	17.77
1323	333.31	0.87	19.51	15.26	17.61
1328	334.08	0.85	20.5	16.15	18.5
1333	334.85	0.85	21.05	16.66	19.04
1338	335.62	0.85	20.61	16.23	18.61
1343	336.38	0.79	20.03	15.87	18.28
1348	337.15	0.84	20.14	16.06	18.37
1353	337.92	0.83	18.91	14.71	17.18
1358	338.69	0.85	18.45	14.49	16.84
1363	339.46	0.85	18.68	14.84	17.15
1368	340.23	0.84	19.2	15.3	17.61
1373	341	0.83	19.14	14.96	17.37
1378	341.82	0.84	19.59	15.49	17.94
1383	342.64	0.84	19.17	15.05	17.44
1393	344.27	0.83	18.35	14.28	16.73
1398	345.09	0.86	18.69	14.6	17.02
1403	345.91	0.82	19.28	15.12	17.58
1408	346.73	0.86	18.72	14.65	16.97
1413	347.55	0.85	17.9	14.06	16.41
1418	348.36	0.84	18.21	14.52	16.86
1423	349.18	0.87	17.94	13.92	16.34
1428	350	0.83	18.99	14.93	17.29
1433	350.82	0.85	18.9	14.83	17.16
1438	351.64	0.88	18.33	14.4	16.63
1443	352.29	0.68	19.94	15.56	18.18
1448	353.27	0.84	19.17	15.4	17.66
1453	354.09	0.88	18.9	14.93	17.22
1458	354.91	0.86	18.5	14.63	16.92
1463	355.73	0.86	18.38	14.43	16.74
1468	356.55	0.86	19.15	15.12	17.51

Depth (cmbsf)	Time (k.y.)	Commun-ality	Ssst	Wsst	Assst
1473	357.36	0.86	19.11	15.07	17.38
1478	358.18	0.87	19.2	14.99	17.38
1483	359	0.88	19.7	15.62	17.92
1488	359.82	0.88	20.27	16.08	18.41
1493	360.64	0.87	18.2	14.26	16.56
1498	361.45	0.86	18.56	14.68	17.02
1503	362.27	0.88	19.17	15.11	17.38
1508	363.09	0.89	20.03	15.79	18.11
1513	363.91	0.87	20.24	16.11	18.42
1518	364.73	0.87	20.66	16.5	18.82
1523	365.55	0.83	19.74	15.68	18.02
1528	366.36	0.88	19.31	15.3	17.64
1533	367.18	0.86	20.52	16.2	18.56
1538	368	0.87	19.85	15.62	17.95
1543	371.5	0.86	18.55	14.45	16.72
1548	375	0.88	18.41	14.42	16.71
1553	376.76	0.87	19.61	15.36	17.76
1558	378.53	0.87	19.71	15.36	17.8
1563	380.29	0.85	20.86	16.5	18.88
1568	382.06	0.85	21.23	16.8	19.21
1573	383.82	0.83	21.33	16.97	19.43
1578	385.59	0.84	21.54	17.09	19.46
1583	387.35	0.85	21.61	17.12	19.49
1588	389.12	0.86	21.44	17.01	19.37
1593	390.88	0.85	21.14	16.71	19.1
1598	392.65	0.86	21.3	16.86	19.22
1603	394.41	0.87	20.08	15.77	18.14
1608	396.18	0.86	20.68	16.53	18.84
1613	397.94	0.84	20.94	16.63	19
1618	399.71	0.88	20.99	16.6	18.97
1623	401.47	0.86	20.75	16.56	18.89
1628	403.24	0.84	20.55	16.34	18.74
1633	405	0.82	20.91	16.47	18.93
1638	406.93	0.86	20.79	16.55	18.87
1643	408.87	0.84	20.86	16.51	18.86
1648	410.8	0.84	21.88	17.49	19.82
1653	412.73	0.85	22.14	17.53	19.93
1658	414.67	0.86	21.23	16.79	19.15
1663	416.6	0.85	20.85	16.65	18.96
1668	418.53	0.84	20.99	16.59	18.97
1673	420.47	0.86	21.83	17.36	19.7
1678	422.4	0.87	20.8	16.41	18.78
1683	424.33	0.84	21.41	16.88	19.27
1688	426.27	0.86	21.72	17.19	19.57
1693	428.2	0.85	20.43	16.09	18.48
1698	430.13	0.84	18.76	14.75	17.05
1703	432.07	0.85	18.81	14.84	17.13
1708	434	0.89	17.71	13.82	16.03
1713	436.85	0.88	19.13	15.12	17.4
1718	439.69	0.89	18.23	14.45	16.7
1723	442.54	0.87	17.99	13.96	16.3
1728	445.39	0.84	17.22	13.5	15.86
1733	448.23	0.87	19.36	15.28	17.58
1738	451.08	0.88	18.17	14.37	16.66
1743	453.92	0.91	15.52	11.89	14.05
1748	456.77	0.89	17.66	13.78	15.98
1753	459.62	0.86	18.71	14.66	16.93
1758	462.46	0.88	15.58	11.81	14
1763	465.31	0.91	14.41	10.71	12.94
1768	468.15	0.86	16.91	13.15	15.38
1773	471	0.89	17.13	13.23	15.44
1778	472.75	0.92	17.85	13.95	16.11
1783	474.5	0.9	15.29	11.76	13.81
1788	476.25	0.89	14.19	11	13.01
1793	478	0.89	14.97	11.31	13.51
1798	479.75	0.89	15.84	12.24	14.41
1803	481.5	0.89	14.16	10.93	12.96
1808	483.25	0.89	15.15	11.49	13.65
1813	485	0.85	15.82	12.13	14.3
1818	486.75	0.89	15.57	11.83	14.02
1823	488.5	0.88	16.86	12.95	15.17
1828	490.25	0.88	16.49	12.64	14.85
1833	492	0.83	18.58	14.49	16.83
1838	493.75	0.85	19.52	15.23	17.61
1843	495.5	0.88	18.05	14.04	16.34
1848	497.25	0.85	19.25	15.07	17.42
1853	499	0.85	18.04	14.04	16.44
1858	500.75	0.89	19.35	15.18	17.5
1863	502.5	0.85	18.35	14.2	16.56
1868	504.25	0.88	20.05	15.81	18.12
1873	506	0.89	19.64	15.4	17.7
1878	507.75	0.9	18.92	14.79	17.04
1883	509.5	0.88	19.06	14.91	17.24
1888	511.25	0.87	19.16	15.08	17.38
1893	513	0.84	19.12	14.91	17.27
1898	520.14	0.85	19.85	15.62	17.93
1903	527.29	0.86	19.76	15.53	17.89
1908	534.43	0.85	19.28	15.11	17.51
1913	541.57	0.86	19.56	15.32	17.65
1918	548.71	0.84	19.98	15.89	18.19
1923	555.86	0.86	18.98	14.88	17.17
1928	563	0.83	18.56	14.52	16.84
1933	564.1	0.85	18.93	14.77	17.14
1938	565.2	0.86	20.05	15.9	18.21
1943	566.3	0.84	17.64	13.75	16.08
1948	567.4	0.86	19.03	14.93	17.28
1953	568.5	0.86	19.67	15.48	17.8
1958	569.6	0.85	20.32	16.1	18.45
1963	570.7	0.84	19.86	15.82	18.13
1968	571.8	0.87	19.57	15.34	17.7
1973	572.9	0.86	19.48	15.33	17.63
1978	574	0.85	20.27	15.94	18.28
1983	579.38	0.86	20.29	15.96	18.3
1988	584.75	0.85	21.3	16.89	19.26
1993	590.13	0.85	20.26	15.93	18.25
1998	595.5	0.85	20.84	16.45	18.8
2003	600.88	0.83	20.96	16.54	18.91
2008	606.25	0.87	20.77	16.39	18.73
2013	611.63	0.9	20.25	16.08	18.38
2018	617	0.86	19.88	15.63	17.95
2023	618.83	0.87	19.5	15.31	17.62
2028	620.67	0.85	19.84	15.58	17.92
2033	622.5	0.87	19.98	15.82	18.13
2038	624.33	0.87	20.81	16.41	18.75
2043	626.17	0.85	19.96	15.69	18.08
2048	628	0.86	19.44	15.18	17.52
2053	631	0.86	17.75	13.79	16.02
2058	641	0.87	20.02	15.85	18.2
2073	668	0.87	18.77	14.74	17.07
2078	679	0.87	18.92	14.84	17.11
2083	681.5	0.88	18.53	14.57	16.85
2088	684	0.89	17.76	13.92	16.2
2093	689	0.86	18.65	14.52	16.87
2098	690	0.85	17.8	13.98	16.27
2103	691	0.88	17.44	13.79	16.03
2108	692	0.88	16.62	12.84	15.07
2113	693	0.85	17.16	13.07	15.52

APPENDIX 4.5

Alkenone SSTs for core GeoB 3603-2.

Depth (cmbsf)	Time (k.y.)	SST Uk'37
8	4.00	21.1
13	7.00	20.8
18	10.00	20.3
23	13.00	20.3
28	16.00	19
33	19.00	18.4
38	20.50	18
43	22.00	19.1
48	23.50	18.4
53	25.00	18.6
58	26.50	18.1
63	28.00	18.5
68	29.39	19
73	30.78	19
78	32.17	18.5
83	33.56	19.2
88	34.94	18.8
93	36.33	18.6
98	37.72	18.9
103	39.11	18.9
108	40.50	18.6
113	41.89	18.2
118	43.28	18.5
123	44.67	19.1
128	46.06	19.2
133	47.44	18.9
138	48.83	19.5
143	50.22	19.2
148	51.61	20.4
153	53.00	20.7
158	54.50	20.5
163	56.00	21.2
168	57.50	20.6
173	59.00	20.3
178	60.50	20.1
183	62.00	20.2
188	63.50	20.3
193	65.00	19.5
198	66.36	19.3
203	67.73	19.7
208	69.09	20.1
213	70.45	19.9
218	71.56	19.5
223	73.18	20
228	74.55	20.6
233	75.91	20.3
238	77.27	20.4
243	78.64	20.9
248	80.00	21.3
253	81.75	22.2
258	83.50	21.5
263	85.25	20.9
268	87.00	20.2
273	88.71	20.7
278	90.43	20.8
283	92.14	21
288	93.89	21.2
293	95.57	21.1
298	97.29	21.6
303	99.00	21.8
308	100.60	21.2
313	102.20	21.3
318	103.80	21
323	105.40	21
328	107.00	21.2
333	108.67	20.8
338	110.33	20.4
343	112.00	20.9
348	113.67	20.9
353	115.33	21.7
358	117.00	22.5
363	118.67	22.3
368	120.33	22.9
373	122.00	22.6
378	123.63	23.2
383	125.25	23.5
388	126.88	23.5
393	128.50	23.3
398	130.13	21.7
403	131.75	21.3
408	133.38	20.8
413	135.00	19.5
418	136.57	19.8
423	138.14	20.7
428	139.71	20.4
433	141.29	18.9
438	142.86	19.3
443	144.43	19.2
448	146.00	19.3
453	147.67	19.6
458	149.33	19.5
463	151.00	18.9
468	152.67	18.1
473	154.33	18.2
478	156.00	19.5
483	157.67	19.2
488	159.33	19.4
493	161.00	19.2
498	162.67	18.7
503	164.33	19.2
508	166.00	19.8
513	167.67	19.8
518	169.33	20
523	171.00	20.2
528	172.71	19.4
533	174.43	19.2
538	176.14	20
543	177.86	20.2
548	179.57	19.8
553	181.29	19.4
558	183.00	19.1
563	184.83	19.1
568	186.67	19.5
573	188.50	20.5
578	190.33	21
583	192.17	20.7
588	194.00	20.6
593	196.20	20.9
598	198.40	21.1
603	200.60	20.9
608	202.80	20.4
613	205.00	20.1
618	207.20	19.9
623	209.40	20
628	211.60	20.5
633	213.80	20.6
638	216.00	20.8
643	217.71	20.9
648	219.43	20.8
653	221.14	20.5
658	222.86	20.1
663	224.57	19.6
668	226.29	19.8
673	228.00	19.9
678	229.43	20.4
683	230.86	20.4
688	232.29	20.1
693	233.71	20.5
698	235.14	20.6
703	236.57	21.6
708	238.00	22
713	239.57	22.2
718	241.14	23.2
723	242.71	22
728	244.29	20.5
733	245.86	19.9
738	247.43	17.9
743	249.00	17.8
748	250.67	17.7
753	252.33	18.2
758	254.00	18.4
763	255.67	18.4
768	257.33	18.4
773	259.00	18.6
778	260.67	19
783	262.33	19.1
788	264.00	18.8
793	265.67	18.8
798	267.33	18.4
803	269.00	18.4
808	270.50	18.5
813	272.00	18.5
818	273.50	18.8
823	275.00	18.6
828	276.50	18.9
833	278.00	19.2
838	279.50	19.6
843	281.00	19.4
848	282.50	19.3
853	284.00	19.1
858	285.50	19.3
863	287.00	19.8
868	288.33	19.8
873	289.67	19.3
878	291.00	19.3
883	292.33	18.7
888	293.67	17.9
893	295.00	18.5
898	296.33	18.5
903	297.67	18.4
908	299.00	18.6
913	300.10	19.2
918	301.20	19
923	302.30	18.7
928	303.40	18.9
933	304.50	19.3
938	305.60	19.7
943	306.70	19.4
948	307.80	19
953	308.90	19.5
958	310.00	19.7
963	311.50	20.1
968	313.00	20.3
973	314.50	21
978	316.05	21
983	317.50	20.3
988	319.00	20.5
993	320.50	
998	322.00	20.9
1003	323.50	21.6
1008	325.00	21.6
1013	326.50	21.5
1018	328.00	21.5
1023	329.90	21.9
1028	331.00	
1033	332.91	22.7
1038	334.07	22.2
1043	335.71	22.2
1048	337.29	21.1
1053	338.86	21.3
1058	340.43	20.2
1063	342.00	19.3
1068	343.63	18.4
1073	344.93	17.5
1078	345.25	17.8
1083	348.50	18.1
1088	350.13	17.9
1093	351.75	17.9
1098	353.38	17.9
1103	355.00	18.5
1108	356.63	18.8
1113	358.25	18.5
1118	359.88	19
1123	361.50	18.3
1128	363.13	18.7